Functional impact of Kir4.1 channels in hippocampal NG2 glia on neuronal plasticity and behavior

Dissertation

Zur

Erlangung des Doktorgrades (Dr. rer. nat.)

der

Mathematisch-Naturwissenschaftlichen Fakultät

der

Rheinischen Friedrich-Wilhelms-Universität Bonn

vorgelegt von

Aline Timmermann

aus

Gelsenkirchen

Bonn, 2020

Angefertigt mit Genehmigung der Mathematisch-Naturwissenschaftlichen Fakultät der Rheinischen Friedrich-Wilhelms-Universität Bonn

1. Gutachter:	**Prof. Dr. Christian Steinhäuser** Institut für Zelluläre Neurowissenschaften Universität Bonn
2. Gutachter:	**Prof. Dr. Walter Witke** Institut für Genetik Universität Bonn

Tag der Promotion: 07.07.2020

Erscheinungsjahr: 2020

Acknowledgements

First of all, I would like to thank my supervisor **Prof. Dr. Christian Steinhäuser** for giving me the opportunity to work on this great project with all these various techniques over the past years. Sharing the enthusiasm of the "other cells" in the brain, I became part of the glial cell family and the IZN. I am very thankful for his guidance and support (scientifically and beyond).

I am grateful to **Prof. Dr. Walter Witke, Prof. Dr. Karl Schilling** and **Prof. Dr. Irmgard Förster** for accepting my request to be part of the examination committee and for their time and efforts in reviewing my thesis.

My sincere thanks go to **PD Dr. Gerald Seifert** for all his support and guidance during my time at the IZN. Teamed up not only for daily consumption of black tea and hours in the animal facility, but together we were trying to understand the role of grey matter NG2 glia.

I also would like to thank **PD Dr. Ronald Jabs** for his constant support and help. Guiding me through the jungle of statistics and providing me with Igor tools, he kept smiling despite me entering his office for the 6th time of the day and answering all kind of questions throughout the years.

Further, I would like to thank **Prof. Dr. Christian Henneberger** for fruitful scientific discussions and scientific advice.

Thomas Erdmann deserves many thanks for his organizational support and his patience, enduring the daily sound of the water cooker.

I also would like to express my gratitude to my collaborators **Dr. Andras Bilkei-Gorzo, Prof. Dr. Andreas Zimmer** and **Dr. Anne Boehlen** for all their time, efforts and great contributions to my project.

My special thanks got to the whole **IZN family**!!! I really enjoyed spending these years with you and I am grateful for all your help, advice and support (even in filling out vacations sheets for me) each and every day. We celebrated carnival with Pfannkuchen (aka Berliner), brought Christmas flair to the lab, incl. decorations, "Schrott", Glühwein and Pottrum (and hot apple juice!) and we spent time together while biking, hiking, paddling, bowling and "escaping" on our works outing days. And despite being frustrated of winning the holy grail of the IZN kicktipp only once, I would always take up the challenge again!

… to be continued on the next page…

Alberto P (*Italian connection, banana spray*); **Björn B** (*a fisher man´s friend, Bang Boom Bang, pink socks*); **Catia D** (*Mrs. Microscope, „so cute" and joyful, a heart for chocolate brownies and muffins*); **Camille P** (*kindred spirit,* walks and talks, *dinner-dates, avocado*); **Charlotte** (*Pottperle*); **Daniel M** (*Mr. intracellular solution, master confectioner*); **Dario T** (*NG2 glia team,* (not) *a quiet Mafiosi*); **Delaware K** (*Pakistani wraps, hairdryer*); **Dmitry F** (*Tea Bro, very creative DiY expert*); **Ines N**, now H (*mensa fries, guided more than the first steps of a lot IZN PhD students*); **Julia M**. (*1live, patch-buddy, tonic GABA currents*); **Katharina H** (*queens Victoria sponge cake, connected to the world*); **Kirsten B** (*statistic genius, support & help wherever you go & whatever you do*); **Linda P** (*Dr. NG2, GABA, StarWars*); **Lukas H** (*„a coffee a day…", God of "R"*); **Magda S** (*CPEBs, polish flag vodka*); **Michel H** (*New Zealand, shorts & shirts*) ; **Monika P** (*aka microglia, yoga, pink coffee mug sister*); **Nehal G** (*NG2 glia team, chocolate & cake & cookies - IZN catering*); **Paula B** (*3D paint!, riding on ski – kite – and the U16/18)*; **Petr U** (my IZN *seminar seat neighbor*); **Steffi G** (*Mars, Bike, hike*); **Steffi S,** now H (*penicillin, advices for lab, live and love*); **Stefan H** (*Dr. NG2, AMPA receptors, rowing*); **Stefan P** (*aka Podolksi, FC Kölle, Mr. NG2 who taught me everything*); **Tushar D** (*phosphorylation, connexins, mensa Couscous*); **Peter B** (*Romanian gangster, fries, coffee, "aber das E ist stumm"*); **Silke K** (*always a nice story to tell, "Silke´s shop"*); **Zhou W** (*Green tea expert, panda cookies*)

My deepest thanks are devoted to my "**Ice Cream team**". Thank you for standing by my site all the years; for comforting me, helping me, laughing with me, for being with me. Thank you for pushing me and pulling me along the way and giving me courage. You are in more than one way two great and impressive friends.

I also would like to express my gratitude towards the people outside the IZN. My beloved friends, every one of you has my deepest thanks for all the unconditional support and sympathy you were providing me. For all the time we spend together until now and all the joy, jokes and happiness - Ruhrpottperlen, Sonnenscheinpfad, Schlemkrampen, Murmannsfeld, TKS… - I am really grateful to call you my friends.

Aus tiefstem Herzen möchte ich euch, meiner wunderbaren Familie, danken. Meiner Schwester und meinen Eltern für die unentwegte und unermüdliche Unterstützung, euer Verständnis und dafür, dass ihr immer für mich da wart (und seid!).

THANKS. **grazie**

Danke

Merci. спасибо

obrigado **谢谢**

podziękować **شكرا**

Glück auf!

Table of Contents

Abbreviations **9**

1 Introduction **12**

1.1 The Hippocampus 12

1.2 The Cerebellum 16

1.3 Synaptic transmission 18

1.3.1 AMPA receptors 18

1.3.2 Short-term plasticity 20

1.3.3 Long-term plasticity 21

1.4 Glial cells 22

1.4.1 NG2 glia 24

1.5 Myelin 26

1.6 Kir channels 28

1.6.1 Kir4.1 channels 29

2 Aim of the Study **31**

3 Materials **33**

3.1. Devices 33

3.2 Software 36

3.3 Chemicals 36

3.4 Antibodies 38

3.4.1 Primary Antibodies 38

3.4.2 Secondary Antibodies 38

3.5 Solutions 38

3.5.1 Extracellular solution 38

3.5.2 Intracellular solution 40

3.5.3 Other 41

4 Methods 42

4.1 The Cre/loxP system 42

4.2 Mouse models 43

4.2.1 NG2-EYFPki 43

4.2.2 NG2-CreER^{T2} x Rosa26-EYFP 44

4.3 Tamoxifen administration 45

4.4 Electrophysiology 46

4.4.1 Preparation of acute brain slices 46

4.4.2 Electrophysiological setup 46

4.4.3 Whole cell patch-clamp recordings 47

4.4.4 Passive membrane properties 47

4.4.6 Paired pulse stimulation 49

4.4.7 Field potential recordings 50

4.4.7.1 Setup 50

4.4.7.2 Long-term potentiation 51

4.4.8 Application techniques 52

4.4.8.1 Bath application 52

4.4.8.2 Focal pressure application 52

4.5 Molecular Analysis 54

4.5.1 FAC sorting 54

4.5.2 Semiquantitative qPCR 55

4.5.3 Single cell RT PCR 56

4.6 Immunohistochemistry 59

4.6.1 Tissue fixation 59

4.6.2 Preparation of brain sections 59

4.6.3 Antibody labeling of free-floating brain sections 59

4.5.4 Confocal Imaging 60

4.6.5 Microscopic analysis and quantification 60

4.7 Behavioral experiments 61

4.7.1 Object location recognition test 61

4.7.2 Partner recognition test 62

4.7.3 Y-Maze labyrinth 62

4.7.4 Beam walk test 63

4.8 Statistics 63

5 Results 64

5.1 Inducible knockout of Kir4.1 in NG2 glia 64

5.1.1 Knockout efficiency in Kir4.1 fl/fl; NG2-CreER^{T2} mice 64

5.1.2 Establishment of an efficient tamoxifen protocol 68

5.2 Role of Kir4.1 in regulating passive membrane properties 73

of NG2 glia 73

5.3 Consequences of Kir4.1 deletion on NG2 glia excitability 76

5.4 Effect of Kir4.1 on NG2 glia proliferation 81

5.5 Effect of Kir4.1 on NG2 glia differentiation into oligodendrocytes 83

5.6. Impact of Kir4.1 on hippocampal myelination 86

5.7 Short-term synaptic plasticity at the Schaffer collateral - NG2 glia 88

synapse 88

5.8 Long-term potentiation in Kir4.1 deficient mice 91

5.9 Behavioral analysis of mice lacking Kir4.1 95

5.9.1 Novel object location recognition test 95

5.9.2 Partner recognition test 96

5.9.3 Y-Maze test 99

5.10 NG2 glia specific knockout of Kir4.1 in the cerebellum 99

5.10.1 Transcript analysis of CreER^{T2} mediated knockout of Kir4.1 100

5.10.2 Passive membrane properties of NG2 glia in the cerebellar 101

molecular layer 101

5.10.3 Short-term plasticity at the climbing fiber - NG2 glia synapse 103

5.10.4 Effect of Kir4.1 ko on NG2 glia proliferation in the cerebellar cortex 105

5.10.5 Effect of Kir4.1 on NG2 glia differentiation into oligodendrocytes in the cerebellar cortex 108

5.10.6 Beam walk paradigm 111

5.11 AMPA receptor knockout in NG2 glia: Triple GluA flox mice 112

5.11.1 Passive membrane properties of triple GluA flox NG2 glia in the hippocampus 112

5.11.2 Characterization of kainte induced currents in hippocampal 114

NG2 glia of triple GluA flox mice 114

5.11.3 Single-cell TR-PCR analysis of AMPA receptor subunits of triple 117

GluA flox NG2 glia 117

5.12 AMPA receptor knockout in NG2 glia: Quadruple GluA flox mice 118

6 Discussion **120**

6.1 Kir4.1 determines NG2 glia properties 120

6.2 Increased release probability at neuron-NG2 glia synapses in Kir4.1 flox mice 124

6.3 Deletion of Kir4.1 in NG2 glia favors myelination 127

6.4 Altered memory performance in mice lacking Kir4.1 in NG2 glia 132

6.5 NG2 glia driven deletion of Kir4.1 in the cerebellum 137

6.6 Deletion of AMPA receptors in hippocampal NG2 glia 139

7 Summary **141**

8 Perspectives **143**

References **145**

Abbreviations

A	ampere
aCSF	artificial cerebrospinal fluid
AMPA	α-amino-3-hydroxy-5-methyl-4-isoxazolepropionic acid
as	antisense
ATP	adenosine triphosphate
$BaCl_2$	barium chlorid
BAPTA	1,2-bis(o-aminophenoxy)ethane-N,N,N',N'-tetraacetic acid
bp	base pairs
°C	degree Celsius
Ca^{2+}	calcium
CA	Cornu Ammonis
$CaCl_2$	calcium chlorid
CC	corpus callosum
CCD	charge-coupled device
cDNA	cyclic deoxyribonucleic acid
Cm	membrane capacitance
CNP	cyclic nucleotide phosphodiesterase
CNS	central nervous system
Cre	cyclization recombination (enzyme)
C_T	threshold cycle
DEPC	diethyl pyrocarbonate
DG	dentate gyrus
DIC	differential interference contrast
DNA	deoxyribonucleic acid
dNTP	deoxynucleotide triphosphate
DTT	dithiothreitol
EDTA	ethylenediaminetetraacetic acid
EGTA	ethylene glycol tetraacetic acid
EPSC	excitatory postsynaptic current
EPSP	excitatory postsynaptic potential
ER	estrogen receptor
ER^{T2}	estrogen receptor variant 2
EYFP	enhanced yellow fluorescent protein
FACS	fluorescence Activated Cell Sorting
fEPSP	Field exitatory postsynaptic potentials
Fig	figure
fl/fl	floxed (loxP sites) on both allels
g	conductance
GABA	γ-aminobutyric acid
$GABA_A$ receptor	ionotropic GABA receptor
GFAP	glial fibrillary acidic protein
GFP	green fluorescent protein
GluA	AMPA receptor subunit
GSTpi	glutathione S-transferases
h	hour
HBSS	Hanks' Balanced Salt Solution

HEPES	4-(2-hydroxyethyl)-1-piperazineethanesulfonic acid
HRB	hormone binding domain
Hz	Hertz
I	current
IFC	Interface chamber
I-V	current-voltage
kHz	kilo Hertz
Kir	inwardly-rectifying
ko	knock-out
loxP	locus of crossing over P
LSM	laser scanning microscope
LTP	long-term potentiation
MAG	myelin associated glycoprotein
MBP	myelin basic protein
mEPSP	miniature exitatory postsynaptic potential
mg	miligram
Mg^{2+}	magnesium
min	minute
mM	milimolar
mOhm	mega Ohm
mRNA	messenger ribonucleic acid
ms	millisecond
mV	milli volt
N	number of mice
n	number of cells
Na_v	voltage gated sodium channels
NBQX	2,3-Dioxo-6-nitro-1,2,3,4-tetrahydrobenzo[f]quinoxaline-7-sulfonamide
NG2	nerve/glia antigen 2, a chondroitin sulfate proteoglycan
NGS	Normal goat serum
NMDA	N-methyl-D-aspartic acid
OHT	4-hydroxytamoxifen
OPC	oligodendrocyte precursor cell
p	postnatal day
PBS	Phosphate buffered saline
PCR	polymerase chain reaction
PDGFRα	platelet-derived growth factor receptor α
pF	picofarad
PLP	proteolipid protein
pmol	picomol
PPR	paired-pulse ratio
psi	pound-force per square inch
Q	charge
Rosa26	Rosa 26 promoter
Rm	membrane resistance
RMP	resting membrane potential
RNA	ribonucleic acid
Rs	series resistance
RT	room temperture
RT-PCR	reverese transcription PCR

SD	standard deviation
se	sense
sec	second
slm	stratum lacunosum moleculare
sm	stratum moleculare of the dentae gyrus
sr	stratum radiatum
Tab	table
TBS	theta burst stimulation
TEA	Tris-acetate-EDTA
TTX	tetrodotoxin
U	enzyme unit (µmol/min)
µ	micro
V	volt
Vhold	holding potential
wpi	weeks post injection
wt	wild type
YFP	yellow fluorescent protein

1 Introduction

The brain is the main control center of our body receiving, processing and proceeding various kinds of information. Coded in electrical signals of different frequency and strength, information is transmitted through a network of neurons. In the end these signals can translate for instance into movements, sensory perception and the formation of memory. But there is more needed than just neurons to preserve brain functions and plasticity. Research of the past years proved that a family of non-neuronal cells called glia (G*reek* for "glue") build not only a structural unit to keep neurons together (Virchow, 1856**)**. These cells are able to actively support and modulate neuronal function. But there is still more to understand about glial cells and their impact on brain function in health and disease.

In the present study the most recently discovered member of the glial cell family will be introduced and further characterized: NG2 glia. These glial cells represent the 4th member of the glial cell family. Knowledge about their role in the brain and the impact of the unique relationship between neurons and NG2 glia are still nebulous.

1.1 The Hippocampus

The hippocampus is a grey matter region in the brain that belongs to the limbic system. It is structured in a laminar manner, comprising different hippocampal layers that receive well defined inputs. The hippocampus can be subdivided into the regions CA1, CA2 and CA3. Each of these regions is composed of distinct layers, namely stratum oriens, stratum pyramidale, stratum radiatum and stratum lacunosum moleculare (Fig. 1.1 A, B.). Together with the dentate gyrus, subiculum, pre-subiculum, para-subiculum and the entorhinal cortex the hippocampus forms a functional unit, called the hippocampal formation. These six brain areas are connected with each other by unidirectional projections of excitatory neurons (Andersen et al., 2006). Starting at the entorhinal cortex, neurons from layer II and III send axons to the dentate gyrus and the hippocampus. These fiber tracts form the perforant path that provides the main input to both subregions (Fig. 1.1 A, C). Layer II axons project to the

granule cells of the dentate gyrus and to pyramidal cells located in the CA3 region of the hippocampus. Those axons of layer III send projections to dendrites of hippocampal pyramidal cells located in the stratum lacunosum moleculare of the CA1 region. CA3 neurons that additionally receive input from granule cells via mossy fibers, forward the information via the Schaffer collaterals likewise to CA1 pyramidal cells. Here, synapses between dendrites located in the stratum oriens and stratum radiatum are formed. CA1 pyramidal neurons project finally back to the entorhinal cortex. Between the hippocampus of the left and right hemisphere, information is shared via commissural projections that arise from the granule cells of the dentate gyrus that send their axons to the CA3 and CA1 region of the other hemisphere (Andersen et al., 2006; Fröhlich, 2016; Neves et al., 2008)**.** This loop circuit is further modulated by the highly diverse anatomically and functional population of interneurons that make up 10% of all neurons in the hippocampus (Andersen et al., 2006). Besides the entorhinal cortex, the hippocampus receives direct input from other brain regions like perirhinal and postrhinal cortex, the medial septum or amygdala. The output of the hippocampus is also not only straight to the entorhinal cortex but targets additionally the amygdala and prefrontal cortex (Knierim, 2015).

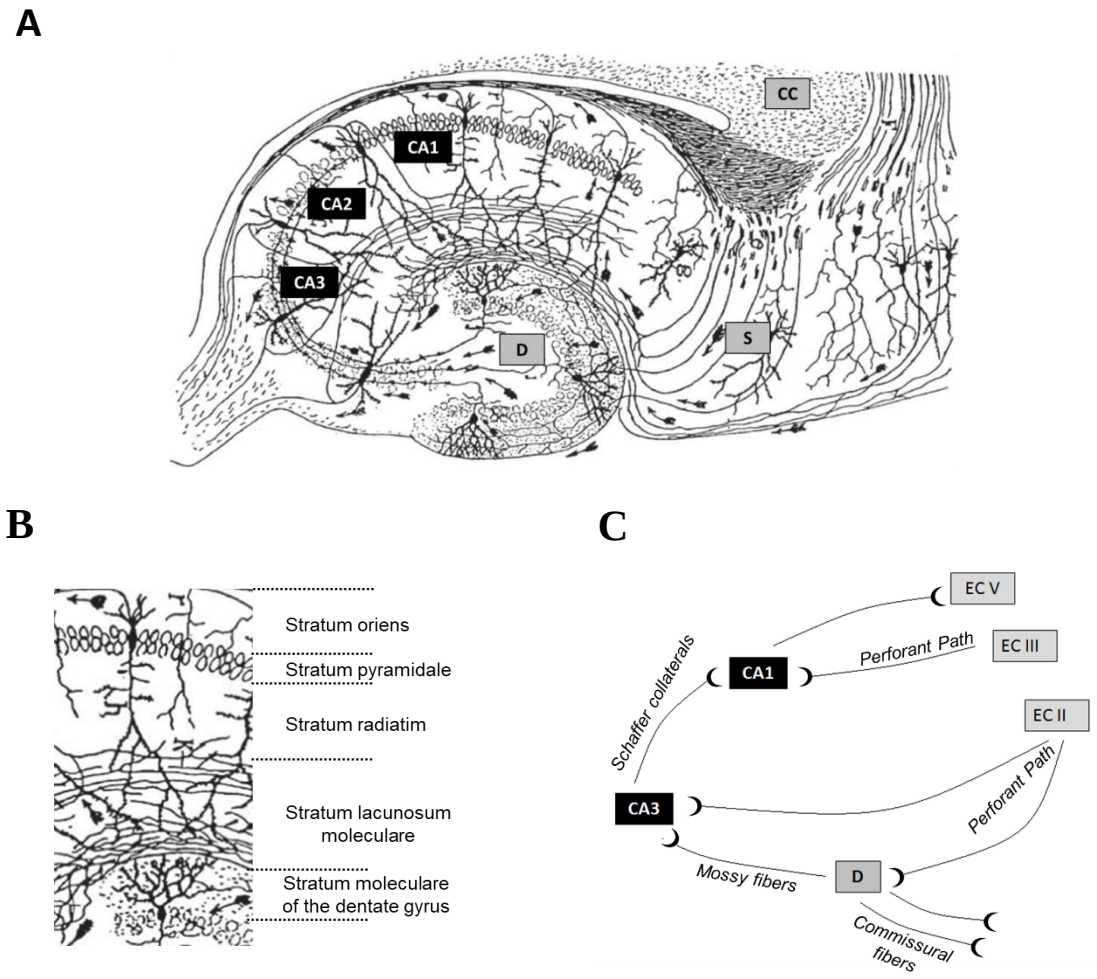

Figure 1.1: Hippocampal circuity. A) Drawing of a hippocampal slice displaying different structures like dentate gyrus (D), the ammons´ horn (Cornu Amonis, CA1, CA2, CA3) and neuronal connections. Modified from Ramón y Cajal, 1909. **B)** Laminar structure of the hippocampal CA1 region. Modified from Ramón y Cajal, 1909. **C)** Circuity of the hippocampal formation. Synaptic connections transmit the information from the entorhinal cortex to the hippocampus and the dentate gyrus and back to the entorhinal cortex. Modified from Neves et al., 2008. CC, corpus callosum; S, Subiculum; D, Dentate gyrus; CA, cornus ammonis (1-3); EC, entorhinal cortex (layer II, III, V).

The hippocampus was shown to play a central role for learning and memory. The importance of the hippocampus in the recall of memories became evident with the publication of the case study from Scoville in 1957. Here the patient H.M who suffered from temporal lobe epilepsy underwent an operation in which the hippocampus and adjacent structures of the temporal lobe were bilaterally resected. Despite a reduction in seizure development, further tests revealed a loss of short-term memory. While general intelligence and early memories like childhood events were not affected the patient was not able to remember the recently introduced hospital stuff neither was he able to find the bathroom (Scoville and Milner, 1957). Years later Timothy Bliss and Terje Lømo detected a promising cellular mechanism linking

memory with the hippocampal formation. They detected that in the dentate gyrus neuronal activity can be strengthened for several hours after high frequency stimulation of the performant path. The authors postulated that this potentiation could be the basis for memory storage (see section 1.3.3) (Bliss and Lømo, 1973). Nevertheless, one should keep in mind that memory consolidation is a complex process that also involves other brain regions to a different extend. Depending on the type of information and the way the information is processed, *memory* can be classified into either explicit (declarative) or implicit (non-declarative) memory. Declarative memory describes the active recall of facts (semantic memory) and events (episodic memory) and is "*the memory*" that people have in mind when they remember the past (Squire, 2004; Squire and Dede, 2015) (Fig. 1.2). It is a conscious way of retrieving former information and mainly requires the hippocampus, the entorhinal cortex, perirhinal cortex, and parahippocampal cortices (Squire and Zola-Morgan, 1991). Non-declarative memory includes all other memories existing and comprises rather an intuitive recollection of the past that results in a reaction. Here the attack of a dog might result in a (nondeclarative) fear (phobia) of dogs, whereas the attack itself can be recalled and vividly described to others (declarative memory). Thus, despite the independency of these memory systems, they can work in parallel (Squire, 2004).

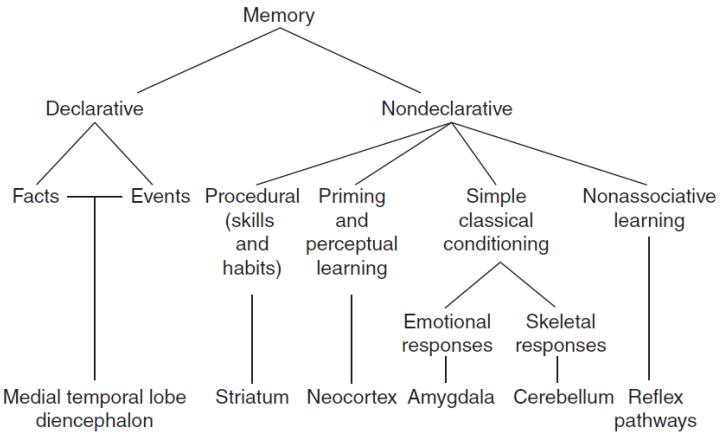

Figure 1.2. Long-term memory systems. Long-term memory can be grouped into declarative and nondeclarative memory. Depending on the type of memory, different brain areas are involved. Adapted from (Squire and Dede, 2015).

1.2 The Cerebellum

Despite a volume of only 10% of the total brain volume, the cerebellum comprises more than half of the entire neuronal cell population in the brain. These neurons are placed in three different layers of the cerebellar cortex namely granule cell layer, molecular layer and Purkinje cell layer (Fig 1.3). The core of the cerebellar cortex is the white matter, containing myelinated axons providing input to the cerebellar cortex and carrying the processed signal out of the cerebellum (Kandel et al., 2000). Information that is processed in the cerebellum is coming from different brain regions. Signals from the spinal cord, cerebral cortex and vestibular system are forwarded via mossy fibers to the granule cells in the granule cell layer. Granule cell axons project to the molecular layer where they branch into parallel fibers. These fibers are forming synapses on the massive dendritic tree of Purkinje cells which is extended into the molecular layer. Additionally, Purkinje cells receive input from climbing fibers that arise from the inferior olive of the brain stem. Each climbing fiber twines along the soma and dendritic tree of Purkinje cells creating various contact sites. Each climbing fiber is making multiple contacts with several Purkinje cells, whereas one Purkinje cell is innervated only by a single climbing fiber (Raymond et al., 1996; Purves et al., 2001).

Purkinje cells are the only output source of the cerebellar cortex. Depending on the input, either via climbing fibers or through the mossy fiber/climbing fiber pathway, different firing patterns are generated. Beside simple spikes evoked upon parallel fiber input, a more complex activity pattern (complex spikes) characterized by a strong depolarization followed by a high frequency burst of smaller discharges, occurs upon climbing fiber input (Eccles et al., 1966; Thach, 2017). Internal loop systems involving the action of inhibitory neurons further modulate the activity of mossy fibers and Purkinje cells and thus the output of the cerebellar cortex. The information is transmitted by Purkinje cells and sent out to different brain areas that are, among others, involved in conducting movements like the vestibular nuclei or cerebral cortex (via the thalamus) (Marr, 1969; Purves et al., 2003). The cerebellum is a control center that monitor and adjust movements if necessary. Due to the input from cortical areas and sensory systems, intended movements and actual movements can be compared and corrected if an “error” occurs (Purves et al., 2001). This correction happens instantaneously but can also be learned (“motor learning”) and stored as memory. This use-dependent adaptation is thought to be based on the interplay between mossy fiber/parallel fibers and climbing fibers and (long-lasting) changes of synaptic strength at the Purkinje cell (Albus, 1971; Ito and Kano, 1982; Lee et al., 2015; Marr, 1969; Purves et al., 2001). Nevertheless, the impact of neuronal plasticity at the Purkinje cell synapse in memory formation and the contribution of plasticity taking place elsewhere in cerebellar circuity is the subject of current

research (D'Angelo et al., 2016; Gao et al., 2012; Lee et al., 2015; Luque et al., 2016; Schonewille et al., 2011).

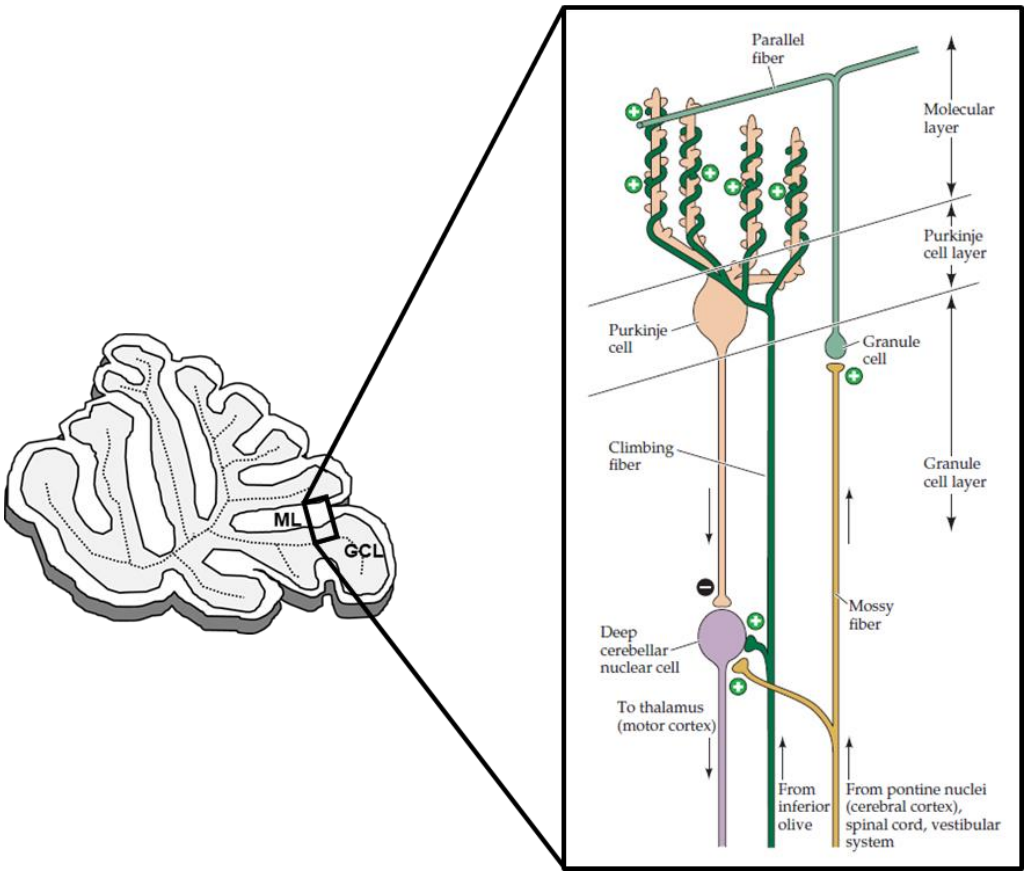

Figure 1.3: Cerebellar circuity. Left: Scheme of a cerebellar section. Right: Magnified area of the section (black square) displaying synaptic connections within the cerebellar circuity. Information from different brain regions arrive in the cerebellum via climbing fibers and mossy fibers. Climbing fibers innervate Purkinje cells directly, whereas mossy fibers first synapse onto granule cells before the signal is transmitted to Purkinje cells via parallel fibers, the axons of granule cells. + indicates excitatory input, - inhibitory input. ML, molecular layer; GCL, granule cell layer. Modified from Purves et al., 2001.

1.3 Synaptic transmission

Neurons receive and integrate incoming signals and pass it to another neuron. The transmission of the signal can thereby be either electrically or chemically. Electric synapses are formed by channels called gap junctions that tightly connect pre- and postsynapse and allow ions and metabolites to pass (Pereda, 2014). At chemical synapses the information is carried in a more indirect way via neurotransmitters. Neurotransmitters are stored in vesicles in the terminal of the presynapse. Some of them (1 - 2% of all vesicles) are already docked to the presynaptic membrane, ready for being released (readily releasable pool of vesicles). Other vesicles (10 - 20%) diffuse within the synapse (recycling pool of vesicles), not contacting the membrane until the readily releasable pool is depleted. After vesicles of the recycling pool released their neurotransmitters, this pool is refilled by recycling vesicles that diffuse again before the cycle restarts (Denker and Rizzoli, 2010; Heuser and Reese, 1973; Rizzoli and Betz, 2005). Most of the vesicles (80 - 90%) represent the reserve pool that is being recruited to the plasma membrane during intense or long-lasting stimulation when the other two pools are exhausted (Denker and Rizzoli, 2010; Rizzoli and Betz, 2005). When an action potential reaches the bouton, the subsequent depolarization leads to an opening of voltage gated Ca^{2+} channels. Ca^{2+} can enter the cell and trigger the final fusion of vesicles with the membrane, leading to a release of neurotransmitters into the synaptic cleft. The transmitters diffuse to the adjacent postsynapse and bind to receptors on the postsynaptic site. Dependent on the receptor type that is activated the electrochemical gradient between the intracellular and extracellular space, excitation or inhibition takes place in the postsynaptic neuron, affecting the further transmission of the signal.

1.3.1 AMPA receptors

The neurotransmitter glutamate activates different metabotropic and ionotropic receptors of the glutamate receptor family. Activation of metabotropic receptors lead to excitation or inhibition of the postsynaptic cell, activation of ionotropic receptors is in contrast, always excitatory. Together with kainate receptors and NMDA (N-methyl-D-aspartate) receptors, AMPA (a-amino-3-hydroxy-5-methylisoxazole-4-propionic acid) receptors belong to ionotropic glutamate receptors (Kandel et al., 2000),

AMPA receptors channels are tetramers that are formed by the GluA1, GluA2, GluA3 and/or GluA4 subunits (Hollmann, 1994). In the hippocampal CA1 region about 80% of the pyramidal neurons express heteromeric channels, formed mainly by Glu1/GluA2 and to a

lower levels by GluA2/GluA3 (Lu et al., 2009). Depending on the subunits composition, Na^+, Ca^{2+} and K^+ can pass the pore. A critical role for the AMPA receptor channel function is ascribed to the GluA2 subunit. It determines the receptors permeability for Ca^{2+} (Geiger et al., 1995; Hollmann et al., 1991), the single channel conductance (Swanson et al., 1997) and sensitivity to be blocked by polyamines in a voltage dependent manner (Donevan and Rogawski, 1995; Kamboj et al., 1995a; Koh et al., 1995). These characteristics are defined by the structure of the GluA2 subunit. Each AMPA receptor subunit is composed of 3 transmembrane domains (TMDs) and a pore lining membrane segment (M2 loop) (Kandel et al., 2000) (Fig. 1.4). Due to a negative electrostatic potential in the channel pore, divalent cations are attracted and pass through the channel (Kuner et al., 2001; Wright and Vissel, 2012). In presence of the GluA2 subunit this negative potential is neutralized, suppressing Ca^{2+} influx. This Ca^{2+} impermeability relies on the post-transcriptional modification of a single amino acid residue located in the M2 segment of the GluA2 subunit (Fig. 1.4). During this process of RNA editing (Q/R editing), the uncharged amino acid glutamine (Q) is replaced by a positively charged arginine (R), neutralizing the negative potential and preventing Ca^{2+} to permeate (Hume et al., 1991; Kuner et al., 2001; Sommer et al., 1991; Verdoorn et al., 1991; Wright and Vissel, 2012). Even though AMPA receptors with unedited GluA2 subunits exist, allowing Ca^{2+} to pass, 99% of AMPA receptors contain the edited GluA2 subunit, making these AMPA receptors Ca^{2+} - impermeable (Wright and Vissel, 2012).

Not only Q/R editing at the GluA2 subunit affect the channel function. Also other modifications of AMPA receptor subunits take place that alter channel properties like kinetics, pharmacology or even trafficking of AMPA receptors. These posttranscriptional and translational modifications involve R/G editing, alternative splicing (flip/flop splice variants), glycosylation and phosphorylation (Palmer et al., 2005). Additionally, the interaction of AMPA receptors with regulatory proteins like TARPS (transmembrane AMAPA regulatory proteins) and cornichon homologs 2 and 3 (CNIH2, CNIH3) can further determine AMPA receptor function and assembly (Milstein et al., 2007; Schwenk et al., 2009; Tomita et al., 2003; Traynelis et al., 2010).

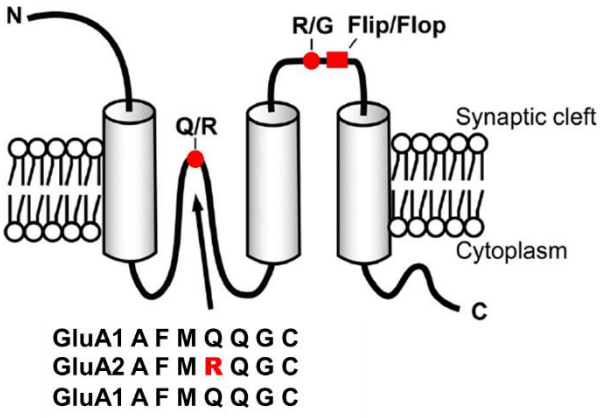

Figure 1.4. Molecular structure of AMPA receptor subunits. A single AMPA receptor subunit consists of 3 TMD´s and a pore forming membrane segment. Sites for posttranscriptional modification are indicated in red. Q/R editing at the pore lining segment of GluA2 subunit replaces the uncharged glutamine (Q) by a positively charged arginine (R) that alters the Ca^{2+} permeability of the channel. Modified from Wright and Vissel, 2012.

1.3.2 Short-term plasticity

Synaptic transmission is not a static process but can adapt to changes of neuronal activity. This plasticity includes mechanisms on the pre- and postsynaptic site lasting between ms to minutes (short term plasticity) or even hours to days (long term plasticity) resulting in a decrease or increase of synaptic strength (Abbott and Regehr, 2004).

Short term plasticity describes modulations (strengthening or weakening) of synaptic efficacy that persists only on a short time scale and reflects a change in the probability that neurotransmitters are released from the presynapse (Abbott and Regehr, 2004; Zucker and Regehr, 2002). As the release is a Ca^{2+}- dependent process, a main mechanism to modulate neurotransmitter release is the change of the intracellular Ca^{2+} concentration in the presynapse. Ca^{2+} that is entering the synapse upon an incoming action potential remains in the bouton for several hundred milliseconds. If a successive second action potential arrives, Ca^{2+} entering the synapse on this second signal is added to the remaining Ca^{2+}. This rise of the intracellular Ca^{2+} concentration triggers the fusion of a larger fraction of vesicles with the membrane. This second response being larger than the first one is called paired pulse facilitation and reflects the initially low probability of a synapse to release neurotransmitters (Debanne et al., 1996; Katz and Miledi, 1968). However, if most vesicles were already released upon the first stimulus, the second stimulus will evoke the release of only a smaller number of vesicles. This paired pulse depression with the second response being smaller than the first one takes place at synapses showing a high release probability (Debanne et al., 1996). Given these characteristics synapses represent filter systems that let signals of certain frequencies pass more likely than others: Facilitating synapses function as high pass filters, able to transmit high frequency discharges. Synapses showing depression act

as low pass filters and transmit low frequency signals more efficient. In different synapses of a single neuron both, facilitation and depression can occur. Transition of facilitation to depression can take place even in thr same synapse. Thus, the predominant form of release probability or filter system being activated at a synapse influences the information processing within the neuronal network (Debanne et al., 1996; Zucker, 1989).

1.3.3 Long-term plasticity

Long term plasticity describes a long-lasting modulation of neurotransmission at the synapse and is thought to build the basis of learning and memory (Kandel, 2001). That responses in the neuronal network were able to remain potentiated for several hours after high frequency stimulation (HFS) was first shown in the dentate gyrus (Bliss and Lømo, 1973) and a few years later in the CA1 region of the hippocampus (Schwartzkroin and Wester, 1975). According to the time course of potentiation, this strengthening of synaptic transmission can be subdivided into three phases: Post tetanic potentiation (PTP) that occurs after the high frequency burst, followed by a fast and transient component described as short-term potentiation (STP). STP then finally passes into a long-lasting increase of synaptic strength, called long-term potentiation (LTP) (Volianskis et al., 2013) (Fig. 1.5).

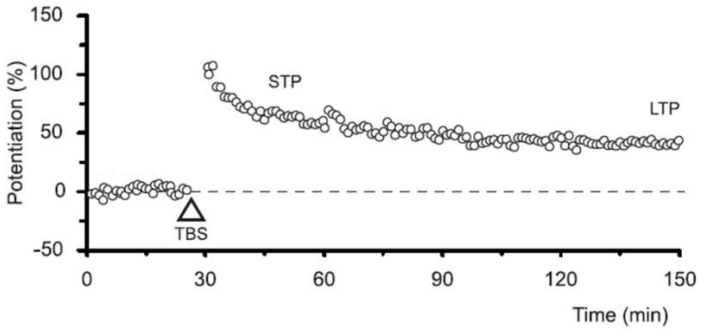

Figure 1.5: Phases of potentiation after high frequency stimulation. Post tetanic potentiation (PTP), short-term potentiation (STP) and long-term potentiation (LTP) were induced after application of a theta-burst protocol (TBS, triangle) to hippocampal slices. TBS, theta burst. Modified from (Volianskis et al., 2013).

At hippocampal CA3 – CA1 synapses the formation of LTP is an NMDA receptor depend mechanism (Collingridge et al., 1983; Lynch et al., 1983). Mg^{2+} that initially blocks the NMDA receptor channel pore is removed upon a strong depolarizing signal, allowing Ca^{2+} to pass into the post-synapse (Macdermott et al., 1986; Mayer et al., 1984; Nowak et al., 1984). The increase in Ca^{2+} concentration leads to the activation of different kinases like the Ca^{2+}/calmodulin-dependent kinase II (CaMKII) and protein kinase A (PKA) (Abel et al., 1997; Fukunaga et al., 1993; Kandel, 2001, Malinow et al., 1989; Silva et al., 1992a, 1992b).

During the first few hours of LTP (early phase of LTP, E-LTP) already existing proteins are modified by CaMKII. This includes the phosphorylation of the AMPA receptor subunit GluA1 that results in an increase of the receptor´s single channel conductance and, thus enhancing the postsynaptic response (Barria et al., 1997; Benke et al., 1998; Derkach et al., 1999). Additionally, new AMPA receptors are inserted into the postsynaptic membrane that are either recruited from an intracellular AMPA receptor pool or redistributed by lateral diffusion within the plasma membrane (Penn et al., 2017; Shi et al., 1999). To maintain LTP on a longer timescale, changes on transcriptional and translational levels are necessary. For the late phase of LTP (L-LTP) these changes require the activity of cAMP dependent PKA that affect the expression of genes and protein synthesis (Abel et al., 1997; Frey et al., 1988; Frey et al., 1993; Kandel, 2001; Nguyen et al., 1994). As LTP can persist in living animals for a month or longer, it is thought to provide the cellular basis for memory storage (Douglas and Goddard, 1975; Lisman et al., 2012). Pharmacological blockage of NMDA receptors and hence NMDA receptor mediated LTP, blocked memory formation (Morris et al., 1986). Likewise, it was shown that in transgenic mice expressing dysfunctional PKA, the expression of L-LTP was impaired and accompanied by deficits in long-term memory formation (Abel et al., 1997). Whitlock et al. (2006) could further prove that learning - induced plasticity is similar to the plasticity seen after HFS that induced LTP in the hippocampus (Whitlock, 2006).

1.4 Glial cells

Glial cells are non-neuronal cells present in the CNS and PNS. In the CNS they are grouped into microglial cells, astrocytes, oligodendrocytes and NG2 glia. The name glia was first set by Virchow in the 19th century who recognized these cells as *Nervenkitt* – a kind of "glue" responsible for keeping neurons together (Virchow, 1856**).** But over time the view of glial cells as solely being a structural unit in the brain became different. They are active players in different brain functions:

MICROGLIA (Fig. 1.6 A) represent the resident immune defense of the brain. With motile processes they are constantly scanning their vicinity and phagocytose unnecessary cell debris that accrue in the brain (Nimmerjahn et al., 2005). In case the brain is invaded by pathogens, microglia become active and release substances with pro-and anti-inflammatory effects to eliminate the intruders and if needed to induce tissue remodeling or repair (Czeh et al., 2011; Wang et al., 2015). Further they are able to fine tune neuronal excitability by pruning synapses (Paolicelli, 2011; Schafer et al., 2012; Weinhard et al., 2018).

Neuronal excitability and function is also affected by **ASTROCYTES** (Fig. 1.6 B). With their fine processes they are ensheathing about 140 000 synapses, forming, together with the pre- and postsynapse, the so called tripartite synapse (Allen and Barres, 2009; Bushong et al., 2002). During neuronal transmission astrocytes are able to remove and recycle neurotransmitters that were released into the synaptic cleft (Rothstein et al., 1996; Tani et al., 2014). In addition astrocytes are themselves able to release neuromodulatory substances (gliotransmitters) like D-serine, allowing an active interference with neuronal communication (Henneberger et al., 2010; Volterra and Meldolesi, 2005). Being coupled with other astrocytes via gap junctions, they are forming a network that allows the uptake and redistribution of K^+ (spatial buffering) to ensuring ion homeostasis during neuronal activity (Orkand et al., 1966; Wallraff et al., 2006). As they are further contacting blood vessels, they are not only modulating the blood brain barrier but also control blood flow (Attwell et al., 2010; Janzer and Raff, 1987; Kacem et al., 1998; Rivera et al., 2016; Rouach et al., 2008; Takano et al., 2006). In addition, metabolites can be imported from the blood stream and delivered to neurons. Thus, astrocytes are an important energy source for the energetically demanding process of of action potential propagation (Pellerin and Magistretti, 1994; Rouach et al., 2008)**.**

OLIGODENDROCYTES (Fig. 1.6 C) are the myelin forming cells in the brain that are mainly located in white matter regions (Dimou et al., 2008). Formation of myelin is crucial to enable fast and efficient propagation of axon potentials along the neuronal axon (see section 1.5) (Nave, 2010a). Besides their role in myelination, oligodendrocytes were shown to transport metabolites in addition to astrocytes**.** It is hypothesized that these cells import glucose from the extracellular space via the glucose transporter GluT1 or receive glucose from astrocytes via gap junctions. Glycose can then be metabolized to lactate and pyruvate (Fünfschilling et al., 2012). As oligodendrocytes are in direct contact with neurons via myelin they are able to shuttle these metabolites to neurons, thus, maintaining axonal function (Fünfschilling et al., 2012; Lee et al., 2012; Meyer et al., 2018; Nave, 2010b).

NG2 GLIA (Fig. 1.6 D) represent the 4th type of glial cells and will be introduced in more detail in the following section.

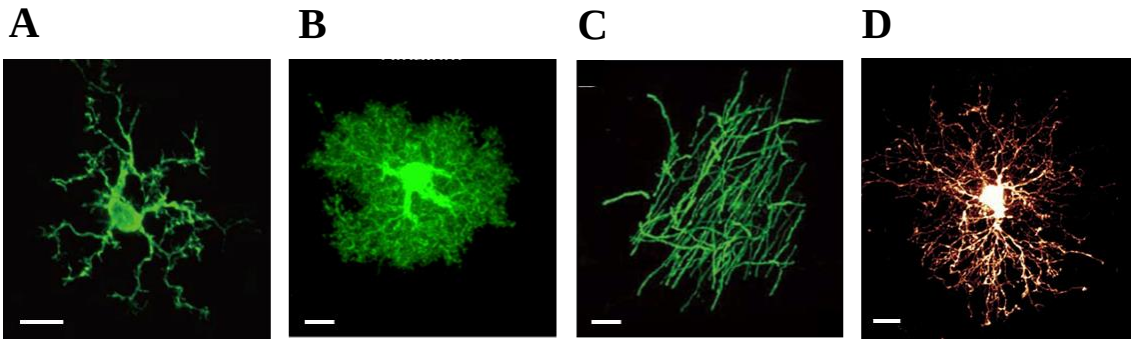

Figure 1.6: Glial cells in the CNS. Example images of **A)** a cortical microglia cell, **B)** an astrocyte of the Striatum, **C)** an oligodendrocyte from the somatosensory cortex and of **C)** a NG2 glia of the hippocampus. Depending on the brain region and activity state, morphological differences within one glial cell type can be detected. Scale bar, 10 µm. Modified from Chai et al., 2017; Haberlandt et al., 2011; Mei et al., 2013; Takayama et al., 2016.

1.4.1 NG2 glia

The name NG2 glia originate from the expression of the chondroitin sulphate proteoglycan NG2 (neuron-glia factor 2) on the cell membrane that was detected by an antiserum supposed to target cells with neuronal (N) and glial (G) characteristics (Stallcup, 1981; Wilson et al., 1981). These cells represent the largest proliferative cell population in the postnatal CNS outside the neurogenic niches, accounting to 70 - 90% of all proliferating cells (Nishiyama, 2013). Throughout life, they populate grey and white matter regions of the CNS. However, grey and white matter NG2 glia display a profound difference: While in grey matter most NG2 glia retain their NG2 phenotype, the majority of NG2 glia in white matter differentiate into oligodendrocytes, thus, representing a pool of oligodendrocyte precursor cells (OPCs) (Bergles et al., 2010; Dimou et al., 2008). The transition to a mature myelinating oligodendrocytes entails drastic changes for these cells: AMPA receptors, NMDA receptors and voltage gated Na^+ channels are downregulated; the cells resting potentials become more positive; the cell capacitance increases, different cell surface marker like NG2 and PDGFRα are lost while other antigens like MBP are upregulated (De Biase et al., 2010; Kukley and Dietrich, 2009; Nishiyama et al., 2009).

NG2 glia express a variety of ion channels including voltage gated Na^+, Ca^{2+} and K^+ channels and inwardly rectifying Kir4.1 channels that lead to a rather complex current pattern that can be elicited upon de- and hyperpolarizing voltage steps (Steinhäuser et al., 1994). Even though this set of ion channels is similar to those of neurons, NG2 glia do not fire action potentials. The density of voltage gated Na^+ channels in the membrane is too low and the expression level of K^+ channels too high to allow to elicit action potentials (Bergles et al., 2000; De Biase et al., 2010; Sontheimer et al., 1996). Intriguingly, NG2 glia receive direct synaptic input

from GABAergic and glutamatergic neurons, a characteristic unique among glial cells (Bergles et al., 2000; Jabs et al., 2005; Lin and Bergles, 2004a). The synapses established between neurons and NG2 glia resemble in structure classical neuronal synapses. This includes a post synaptic density (PSD) on the site of NG2 glia and docked and free moving vesicles on the neuronal side (Haberlandt et al., 2011) (Fig. 1.7). In turn, processes of a single NG2 glia can contact multiple synapses of different neurons (Butt et al., 2005). The release of neurotransmitters from neurons like glutamate and GABA lead to the activation of AMPA and $GABA_A$ receptors that are expressed by NG2 glia, resulting in a depolarization of the glial cell (Bergles et al., 2000; Jabs et al., 2005; Lin and Bergles, 2004a).

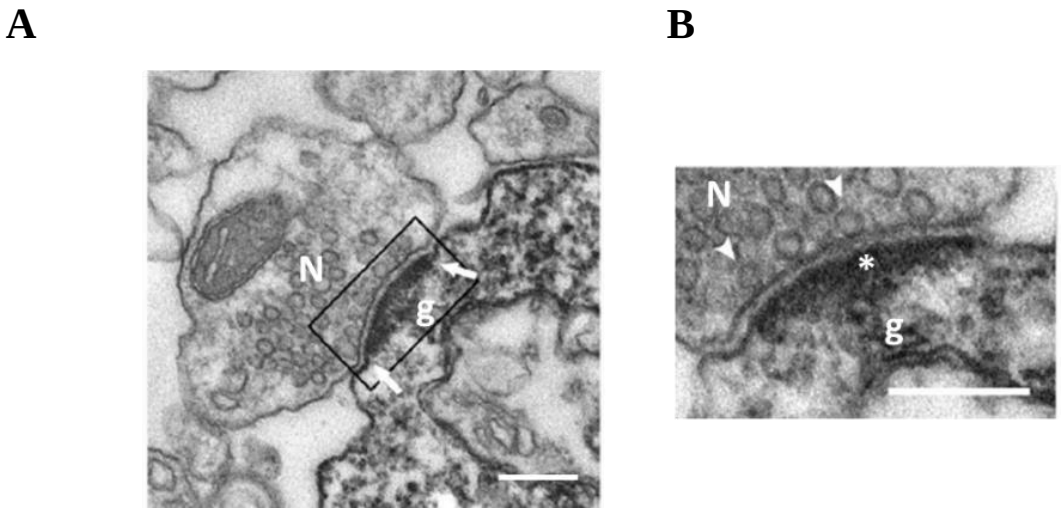

Figure 1.7: Synaptic connectivity between neurons and NG2 glia. Electron microscopic images of cells in hippocampal slices from juvenile (p9–12) hGFAP-EGFP mice. **A)** A synapse (arrows) between a neuron (N) and NG2 glia (g). Black square encircles the area depicted in **B).** The neuron - NG2 glia synapse displays characteristics of a synapse typically established between neurons: Docked vesicles (arrowheads) at the presynapse and a post synaptic density (star) on the post-synaptic site. Scale bar 200 nm each. Modified from Haberlandt et al., 2011.

Neuron - NG2 glia synapses are established in the 1st postnatal week or even before, at a prenatal state as recently observed in the spinal cord (Mangin et al., 2008; Osterstock et al., 2018). During NG2 glia proliferation these synaptic connections are transferred to the daughter cells, but get lost upon if NG2 glia differentiation into oligodendrocytes (Ge et al., 2009; Kukley et al., 2010). For white matter NG2 glia neuronal activity was shown to affect NG2 glia proliferation and differentiation with consequences on myelination (Gibson et al., 2014; Li et al., 2010; Mitew et al., 2018). But in grey matter regions like the hippocampus, the physiological impact of the neuronal innervation of NG2 glia is still not clear.

1.5 Myelin

Myelin represents the enlarged plasma membrane of oligodendrocytes that stretch out their processes to wrap up to 100 layers of their membrane around neuronal axons (Fields, 2014; Peters, 1964). The thickness of this multilamellar structure is thereby correlated with the axonal diameter, with larger axons being myelinated to a larger extend (Waxman and Sims, 1984). Myelin sheaths are composed of different lipids (75%) and proteins (25%) (Williams et al., 1993) (Fig. 1.8). Myelin basic protein (MBP) plays a central role for the myelin structure. Located in the cytoplasm, MBP pulls opposing cytoplasmic bilayers together, thus keeping myelin in a compact shape (Aggarwal et al., 2013; Min et al., 2009; Readhead et al., 1987). Myelin functions as an electric insulator, shielding the axon from the extracellular space (Baumann and Pham-Dinh, 2001). Only those axonal segments where myelin is absent, called nodes of Ranvier, are exposed to the extracellular space, enabling channel - mediated flow of ions across the membrane. At these sites, large densities of voltage gated Na^+ channels are present (Kaplan et al., 1997). Opening of these channels upon a depolarizing signal allows Na^+ to enter the axon and to promote propagation of action potentials along the axon. As nodes of Ranvier are distributed over the entire axon, electrical signals propagate from node to Node in a saltatory fashion (Tasaki, 1939). This signal propagation can be up to 100-fold faster than in unmyelinated axons and is less energy demanding (Nave, 2010a). Nevertheless, the limited access to the extracellular space also limits the access to extracellular glucose that can be taken up by neurons via the glucose transporter GLUT3 and be used as energy source (Nagamatsu et al., 1993; Nave, 2010b). To ensure the continuous supply of energy, myelin is used as road to shuttle metabolites from oligodendrocytes to the axon (see section 1.4), thus compensating for this self-imposed limitation (Fünfschilling et al., 2012; Lee et al., 2012).

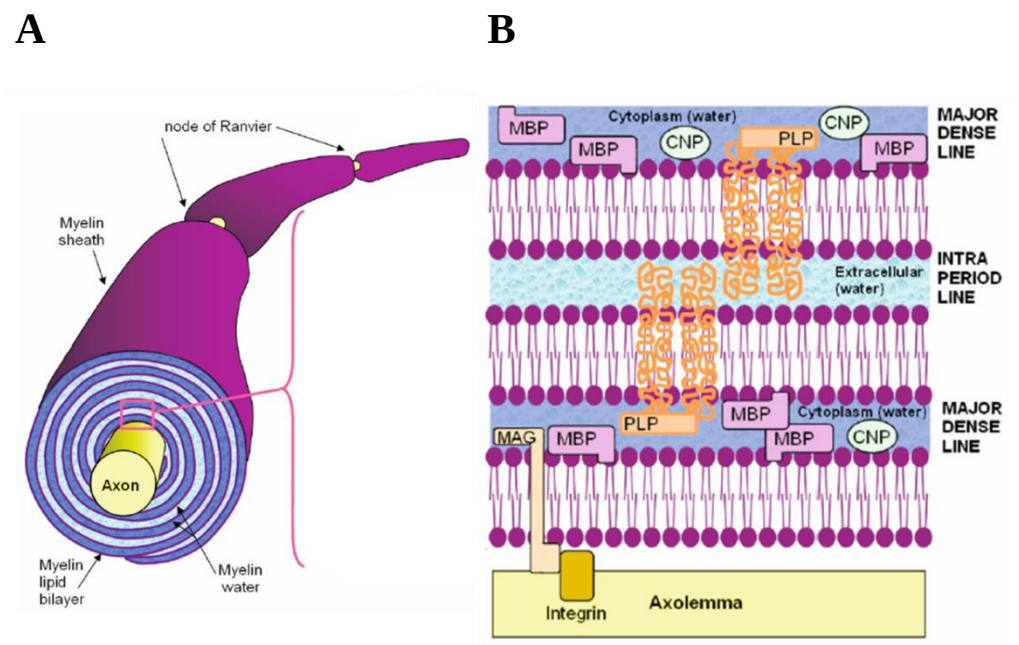

Figure 1.8 Structure of the CNS myelin sheath.
A) The plasma membrane of oligodendrocytes processes is wrapped in a spiral fashion around neuronal axons. **B)** Within this structure different myelin proteins are located. The major dense line is the compact cytoplasmic space of the oligodendrocyte process; the intraperiod line represents the compact extracellular space that is formed between two opposing membrane layers (Laule et al., 2007, Williams et al., 1993). PLP, proteolipid protein (50% of all myelin proteins); MBP, myelin basic protein (30%); CNP, cyclic nucleotide phosphodiesterase (4%); MAG, myelin-associated glycoprotein (1%). Modified from Laule et al., 2007.

Myelin is not a uniform structure. Across brain regions and between axons but also along axons, myelin sheath thickness and the size and number internodes can differ. This affects the speed of signal conduction and hence the timing and synchronicity of impulse transmission (Ford et al., 2015; Glasser and Van Essen, 2011; Salami et al., 2003; Tomassy, 2014). For instance, within the auditory system, variation in myelination and axon diameter allows the fine tuning of information processing, providing the basis for sound localization (Ford et al., 2015).

In mice, myelination starts at birth and continues throughout life until age-related degradation starts (Baumann and Pham-Dinh, 2001; Hill et al., 2018; Hughes et al., 2018). Once myelin structures are formed they remain highly stable, only a minority of internodes are retracted or expanded (Hill et al., 2018). This innate myelination can, however, be modulated upon external stimuli and neuronal activity (Mount and Monje, 2017). In vivo studies showed that enhanced neuronal activity artificially induced by optogenetic tools or naturally occurring during physical exercises like wheel running led to an increased myelination (Gibson et al., 2014; McKenzie et al., 2014). Inhibition of neuronal activity negatively affected myelination

(Etxeberria et al., 2016; Fields, 2014b; Wake et al., 2015). These modulations that led to an increased or decreased conduction of neurotransmission thus allow a dynamic influence on neuronal circuit function (Baraban et al., 2016; Etxeberria et al., 2016; Fields, 2014b; Wake et al., 2015). In this regard myelination can adapt to changes in neuronal network activity, similarly to what has been described for synapses that adapt during changes of short and long-term memory. Thus, plasticity of the neuronal network does not only rely on changes on the synaptic side but as well on the side of myelination.

1.6 Kir channels

Kir channels are a channel family with 7 sub-families (Kir1.0-Kir7.0), with at least 4 members each (Hibino et al., 2010). A channel is formed by four subunits (tetrameric complex) each consisting of two transmembrane domains (TMD1, TMD2) (Fig. 1.10). Both, the N- and C terminus are directed to the intracellular side whereas the selectivity filter, enabling K^+ ions to pass, is formed by the extracellular loop (H5 or P-loop) (Hibino et al., 2010; Hille, 2001). This selectivity filter is common to all K^+ channels (including voltage gated K^+ channels) and is characterized by a so called signature sequence, a certain amino acid sequence containing -thr-X-X-thr-X-gly-tyr-gly-glu, with X being undetermined amino acids (Hille, 2001). Kir channels can exist as homomers containing four subunits of the same type or are heteromeric if the channel is composed of two different isoforms (Hibino et al., 2010). Heteromeric channels are generally formed from subunits of the same family but can also be formed from subunits of different families (Hibino et al., 2010). Kir channels are voltage dependent, showing a high open probability around the K^+ equilibrium potential. At more positive potentials, the conductance is reduced. Favoring influx of K^+ at negative voltages and limiting efflux at more depolarized potentials, coined the term “inward rectifying” for this channel family (Hille, 1992). Determinants for this inward rectifying current - voltage (I-V) relationship are intracellular polyamines like spermine and spermidine and Mg^{2+}, which block the channel pore at positive potentials (Fig. 1.9). The block vanishes at potentials close to the K^+ equilibrium potential, allowing K^+ to pass the pore (Fakler et al., 1995; Lopatin et al., 1994; Matsuda et al., 1987; Oliver et al., 2000). Whether a channel is strong or weakly rectifying relies on the amino acid composition at the TMD2 site. In strong rectifying channels (like Kir2.x channels), negative charged amino acids like aspartate or glutamate are present, favoring a strong interaction with polyamines or Mg^{2+}. Weak rectifying channels (like Kir1.x channels) exhibit an uncharged amino acid at this position (Glowatzki et al., 1995; Hibino et al., 2010; Oliver et al., 2000). Across Kir subfamilies, the degree of

rectification but also other biophysical properties like sensitivity to ATP, pH or G-proteins, additionally affect channel conductance. The expression of heteromeric channels further increases the functional variety of Kir channels (Hibino et al., 2010). Kir channels are expressed in various cell types. In Cardiac myocytes they are responsible to set the heart rate. In neurons they are needed to control repolarization. In glial cells like astrocytes they were shown to be required for the regulation of ion homeostasis (Butt and Kalsi, 2006; Ishii et al., 1997; Kofuji et al., 2000; Krapivinsky et al., 1995; Takahashi, 1990; Williams et al., 1988)

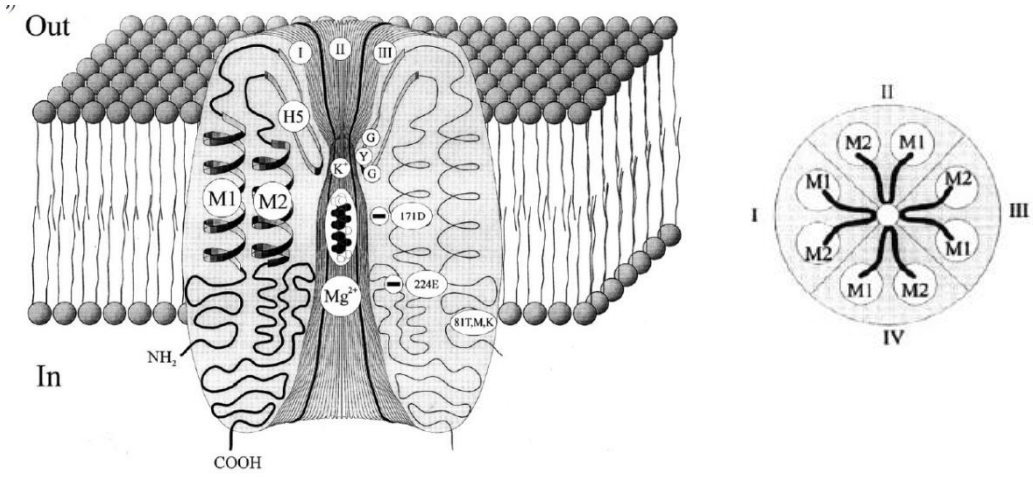

Figure 1.9: Kir channel structure. Kir channel subunits are composed of 2 TMDs (M1, M2) that are connected via a loop structure (P-loop, H5) that forms the selectivity filter for K^+. Kir channels are tetramers built of 4 subunits (I, II, III, IV). Residues in the TMD2 determine the affinity for Mg^{2+} and polyamine and thus the degree of rectification. Modified from Nichols and Lopatin, 2002.

1.6.1 Kir4.1 channels

The Kir channel subtype Kir4.1 is expressed throughout the entire CNS (Higashi et al., 2001). This channel is glia - specific as it was only found in Bergmann glia cells, Müller cells, astrocytes, oligodendrocyte and NG2 glia (Higashi et al., 2001; Ishii et al., 1997; Kofuji et al., 2000; Poopalasundaram et al., 2000). In NG2 glia, regional and developmental differences in Kir4.1 expression exist. In white matter, juvenile NG2 glia showed a higher expression of Kir4.1 than grey matter NG2 glia (Chittajallu et al., 2004). During postnatal development inwardly rectifying K+ currents are upregulated in NG2 glia (Kressin et al., 1995) (Fig. 1.10). The expression of this subunit has a strong influence on the membrane properties of glial cells as it determines their resting membrane potential. Thus, glial cells expressing high levels of Kir4.1 are characterized by a low membrane resistance and a membrane resting potential close to the K^+ equilibrium potential at (Kressin et al., 1995; Neusch et al., 2001; Seifert et al., 2009). The role of Kir4.1 in glial cells seems mainly to be closely associated with its

subcellular distribution: In astrocytes it is located at the end-feet/processes close to the synapses, nodes of Ranvier and blood vessels (Higashi et al., 2001; Schirmer et al., 2018). This allows astrocytes to regulate K^+ concentration in the extracellular space ("spatial buffering", see section 1.4) and to control neuronal excitability (Djukic et al., 2007; Higashi et al., 2001; Kofuji and Newman, 2004; Tong et al., 2014). In oligodendrocytes the subcellular distribution is different. Here, Kir4.1 is mainly found in the soma and at the inner tongue of myelin that is produced by this type of glia cells (Kalsi et al., 2004; Poopalasundaram et al., 2000; Schirmer et al., 2018). The functional implication for this expression pattern is not clear yet. According to different ko models (see below), Kir4.1 seems to play a role in oligodendrocyte maturation (Neusch et al., 2001). Data obtained from the barrel cortex suggest a role of Kir4.1 in NG2 glia in sensing local K^+ concentrations, allowing NG2 glia to monitor neuronal activity (Maldonado et al., 2013).

Kir4.1 is crucial for proper brain function. Indeed, in mice lacking Kir4.1, oligodendrocytes remain immature, unable to form compact myelin, followed by hypomyelination, axonal degeneration and motor impairment. Vacuolization in the spinal cord and brain stem was detected in Kir4.1 ko mice leading to death by p24 (Neusch et al., 2001). In a study from Djukij and colleagues, Kir4.1 deletion was restricted to the *gfap* promoter, thus mainly affecting astrocytes. Due to its role in K^+ buffering and glutamate transport, this ko resulted in hyperexcitability of neurons, generation of seizures and impaired survival rates (Djukic et al., 2007).

Animal models allowing an inducible deletion of Kir4.1 in a specific type of glia cells at restricted timepoints are crucial to unmask the role of Kir4.1 in different glia cells (Butt and Kalsi, 2006; Higashi et al., 2001; Kalsi et al., 2004; Poopalasundaram et al., 2000).

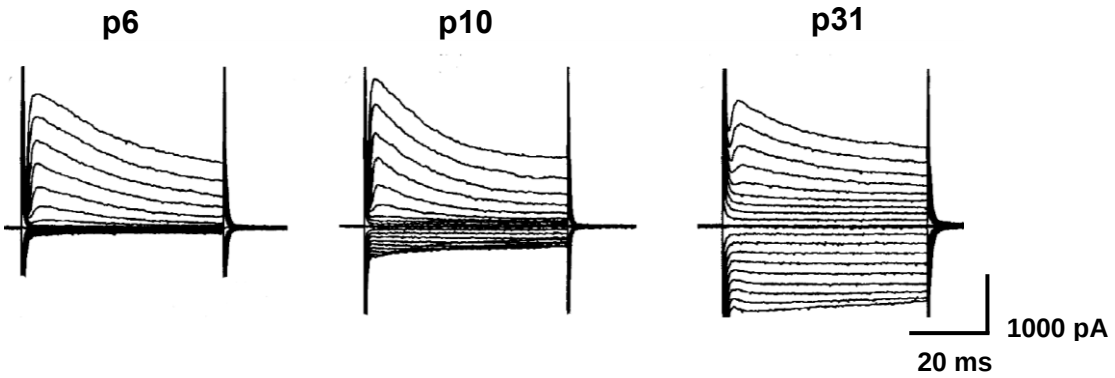

Figure 1.10: Expression inwardly rectifying K^+ channels in NG2 glia. The current pattern of NG2 glia, elicited by de- and hyperpolarizing voltage steps, at different time points of postnatal development (p6, p10 and p31). Modified from Kressin et al. , 1995.

2 Aim of the Study

NG2 glia are unique among other CNS glial cells as they receive direct synaptic input from GABAergic and glutamatergic neurons. The physiological role of NG2 glia, especially in grey matter and the impact of this neuron – NG2 glia signaling are, however, still not understood. As NG2 glia and neurons express a similar set of ion channels, a specific manipulation of NG2 glia function through pharmacological intervention is difficult. Thus, I decided for a genetic approach that specifically targets a signaling molecule in the NG2 glia membrane. Based on the Cre/LoxP system, a mouse line was generated that allows deletion of the inwardly rectifying K^+ channel Kir4.1 specifically in adult NG2 glia upon tamoxifen injection. The following study aimed to characterize the consequences of a NG2 glia-targeted deletion of Kir4.1 on the cellular and behavioral level in order to understand the enigmatic role of these glial cells and their interactions with neurons.

To this end, the following questions were asked and investigated in detail in adult $CreER^{T2}$ x Kir4.1 flox mice with a focus on the hippocampus and associated functions:

i. Does NG2-CreER^{T2} mediated recombination successfully delete Kir4.1 in NG2 glia?

The successful induction of Kir4.1 ko in NG2 glia, is the first critical step that is required before consequences of a NG2 glia-targeted deletion of Kir4.1 can be investigated. A high efficiency of $CreER^{T2}$ mediated depletion of Kir4.1 is necessary to provoke pronounced and detectable effects of dysfunctional NG2 glia on the cellular and behavioral level. The first goal of the present study is to estimate recombination efficiency.

ii. ***Does the deletion of Kir4.1 affect NG2 glia properties?***

Adult NG2 glia are characterized by a resting membrane potential close to the K^+ equilibrium potential and a low membrane resistance, both determined by the expression of Kir4.1 channels (Karram et al., 2008; Kressin et al., 1995). Throughout life these glial cells are proliferating and populate the entire CNS (Bergles and Richardson, 2016; Degen et al., 2012; Young et al., 2013). However, NG2 glia of grey and white matter display a fundamental difference: The majority of white matter NG2 glia differentiate into myelinating oligodendrocytes, thereby losing the neuronal input and other NG2 glia characteristics (De Biase et al., 2010; Fröhlich et al., 2011; Kukley et al., 2010; Nishiyama et al., 2009). Most of grey matter NG2 glia, in contrast, retain their NG2 phenotype throughout life (Bergles et al., 2010; Dimou et al., 2008). To understand the consequences of ablation of Kir4.1 from hippocampal NG2 glia, NG2 glia properties need to be evaluated on functional and molecular levels.

iii. ***Do dysfunctional NG2 glia affect neuronal function and animal behavior?***

That NG2 glia receive direct synaptic input from GABAergic and glutamatergic neurons is a phenomenon observed throughout the entire brain (Balia et al., 2015; De Biase et al., 2010; Lin and Bergles, 2004b). Theses synapses are established directly after birth and are preserved until adulthood (Mangin et al., 2008; Passlick et al., 2016). Neurotransmitters that are released from the neuronal presynapse induce receptor mediated inward currents in the postsynaptic NG2 glial cell (Balia et al., 2015; Bergles et al., 2000; Jabs et al., 2005; Mangin et al., 2008; Passlick et al., 2016). The impact of the constant neuronal input on NG2 glia, but also the consequences for the innervating neuron, are still not understood. Whether/how NG2 glia can in turn affect neuronal activity and brain function, is a question that has been addressed in the present study.

3 Materials

3.1. Devices

Devices	Company
A/D converter	ITC-16 (HEKA Elektronik, Lambrecht, Germany)
Amplifier (Patch-clamp)	EPC-800 (HEKA Elektronik, Lambrecht, Germany)
Amplifier (Field potential recordings)	EXT-02B (highpass 0.1 Hz, lowpass 20 kHz;) (npi electronic GmbH, Tamm, Germany)
Bath chamber/shifting table	Base plate 500B, shifting table V240, bridge 500 with control units SM-5 and -6 (Luigs & Neumann, Ratingen, Germany)
CCD camera	VX45 (Optronis, Kehl, Germany)
current stimulator	DS3 (Digitimer Ltd, Hertfordshire, UK)
Differential amplifier	DPA-2FS (npi electronic GmbH, Tamm, Germany)
Data acquisition system (Field potential recordings)	USB-6221 (National Instruments, Austin, USA)
Electrophoresis	E0763 (Sigma-Aldrich, Munich, Germany)
Flow cytometer	FACSAriaIII, 70 µm nozzle (BD Biosciences, Heidelberg, Germany)
Fluorescence illumination system	Polychrome II, 75W xenon lamp (Till Photonics, Martinsried, Germany)
Glass pipettes	Borosilicate glass GB150F-10 (Science Products, Hofheim, Germany)

Devices	Company
Heating system	Temperature controller (Luigs & Neumann, Ratingen, Germany)
Interface-type recording chamber (IFC)	custom-made by AG Prof. Dr. Heinemann (Charité, Berlin, Germany)
Laser scanning microscope	SP8 (Leica Microsystems, Wetzlar, Germany)
LEGO bricks	(LEGO, Billund, Denmark)
Magnet stirrer	RCT basi (IKA Labortechnik, Staufen, Germany)
Magnet stirrer, heating	ARE F20520162 (VELP Scientifica, Usmate, Italy)
Micromanipulators	Micromanipulator 6540 R094 with control unit 5171 (Eppendorf, Hamburg, Germany) LN mini 25 (Luigs & Neumann, Ratingen, Germany)
Micropipette Puller	P-87 (Sutter Instrument, Novato, USA)
Microscope	Stereo microscope Stemi 2000 (Zeiss, Oberkochen, Germany)
Microscope (Patch-Clamp)	Axioskop FS2 (Zeiss, Oberkochen, Germany)
Noise eliminator	HumBug 50/60 Hz noise eliminator (Quest Scientific Instruments Inc, North Vancouver, BC, Canada)
Objectives	CP-Achromat (5x; NA: 0.12) (Zeiss, Oberkochen, Germany) LUMPlan FI/IR (60x; NA: 0.90) (Olympus, Tokio, Japan)
Oscilloscope	HM 507 (Hameg, Mainhausen, Germany)
Osmometer	Vapor Pressure Osmomoter 5520 (Wescor Vapro, Logan, USA)
PCR-Cycler	PTC-200 (Biozym, Hessisch Oldendorf, Germany)
PCR-Cycler (RT-PCR)	CFX 384 (Biorad, Munich, Germany)

Devices	Company
pH meter	766 Laboratory pH Meter (Knick, Berlin, Germany)
Pressure application system	Octaflow (ALA Scientific Instruments, Farmingdale, USA)
Sonificator	Transonic 5520 (Elma-Ultrasonic, Singen, Germany)
Stimulation electrode, concentric bipolar	CBARC75 (FHC, Bowdoin, USA)
Syringe pump	SP-22012 (Braun, Melsungen, Germany); (WPI, Saraota, USA)
Tubing pump	ISM 930C (Ismatec/Idex, Wertheim, Germany)
UV-light Cabinet	Multi Image light cabinet (Alpha innotec, Kasendorf, Germany)
Vortexer	Model 444-1372 (VWR, Darmstadt, Germany)
Vibration isolation platform	Vision Isostation VIS-3036 (Newport, Irvine, USA)
Vibratome	VT1000 S ; VT1200 S (Leica Microsystems, Wetzlar, Germany) Model 7000smz-2 (Campden Instruments, Barrow upon Soar, UK)
Water bath	Model-1003 (Gesellschaft für Labortechnik (GFL), Burgwedel, Germany)
Weighing scale (miligram balance)	VIC-412 (Acculab vicon, Bradford,USA)
Weighing scale (micro balance)	BP121S (Sartourius, Göttingen, Germany)

3.2 Software

Software	Company
EthoVision tracking system	Noldus, Wageningen, Netherlands
IGOR Pro 7	WaveMetrics, Lake Oswego, USA
ImageJ	NIH, Maryland, USA
LAS AF	Leica Microsystems, Wetzlar, Germany
Office 2010+2016	Microsoft, Redmond, USA
Origin Pro 9	OriginLab, Northampton, USA
pClamp 10	Molecular Devices, Union City, USA
Prism 5	Graphpad, San Diego, USA
TIDA 5	HEKA Elektronik, Ludwigshafen, Germany
R	R Core Team , General Public License

3.3 Chemicals

Chemicals	Company
Acetic acid	Roth, Karlsruhe, Germany
Agarose	Invitrogen, Darmstadt, Germany
BAPTA	Sigma-Aldrich, Munich, Germany
BaCl2	Sigma-Aldrich, Munich, Germany
$CaCl_2.6H_2O$	AppliChem GmbH, Darmstadt, Germany
Carbogen	Linde, Pullach, Germany
CO_2/O_2 (50%/50%)	Linde, Pullach, Germany
DMSO	Sigma-Aldrich, Munich, Germany
dNTPs	Applied Biosystems, Darmstadt, Germany
DTT	Thermo Fisher, Waltham, USA
Dynabeads Oligo $(dT)_{25}$	Invitrogen, Darmstadt, Germany
EDTA Na_2	Sigma-Aldrich, Munich, Germany
EGTA	Sigma-Aldrich, Munich, Germany
Ethanol 99%	AppliChem GmbH, Darmstadt, Germany
Ethanol abs.	Roth, Karlsruhe, Germany
Ethidiumbromid	Roth, Karlsruhe, Germany
First-Strand Buffer	Invitrogen, Darmstadt, Germany
Glucose	AppliChem GmbH, Darmstadt, Germany
glue	Superglue, Uhu, Bühl, Germany
HEPES	AppliChem GmbH, Darmstadt, Germany
Hoechst 33342	Molecular Probes, Eugene, USA
Isofluran	Piramal Healthcare, Morpeth, UK
Kainate	WDT, Garbsen, Germany

Chemicals	Company
KCl	AppliChem GmbH, Darmstadt, Germany
K-Gluconat	Sigma-Aldrich, Munich, Germany
Ketamin (10%)	WDT, Garbsen, Germany
Low Molecular Weight DNA Ladder	New England BioLabs, Ipswich, USA
lysis/binding buffer	Invitrogen, Darmstadt, Germany
Mounting Medium	Aqua-Poly/Mount, Polyscience).
Na2-ATP	Sigma-Aldrich, Munich, Germany
Na-Azide	Sigma-Aldrich, Munich, Germany
NaCl	AppliChem GmbH, Darmstadt, Germany
Na2HPO4.2H2O	Sigma-Aldrich, Munich, Germany
NaH2POH4	AppliChem GmbH, Darmstadt, Germany
NaHCO3	AppliChem GmbH, Darmstadt, Germany
NBQX	Tocris Bioscience, Bristol, UK
Neural Dissociation Kit	Miltenyi, Germany
NGS	Merck Millipore, Darmstadt, Germany
MgSO4.7H2O	AppliChem GmbH, Darmstadt, Germany
MinElute PCR Purification Kit	Qiagen, Hilden, Germany
oligo-dT_{24}-primer	Eurogentec, Lüttich, Belgien
PCR Buffer	Thermo Fisher, Waltham, USA
Picrotoxin	Ascent (now: Abcam), Cambridge, UK
PFA	AppliChem GmbH, Darmstadt, Germany
Platinum® Taq Polymerase	Thermo Fisher, Waltham, USA
Quinine	Sigma-Aldrich, Munich, Germany
Random Hexamer Primer	Roche Applied Science, Mannheim,Germany
RNasin® RNase Inhibitor	Promega, Madison, USA
Sucrose	AppliChem GmbH, Darmstadt, Germany
Sunflower seed oil from Helanthius annus	Sigma-Aldrich, Munich, Germany
Superscript® III Reverse Transcriptase	Invitrogen, Darmstadt, Germany
Takyon real-time PCR mastermix	Eurogentec, Lüttich, Belgien
tamoxifen	Sigma-Aldrich, Munich, Germany
Taq DNA Polymerase	Thermo Fisher, Waltham, USA
Taqman primer/probe mix	Applied Biosystems, Darmstadt, Germany
Tris	AppliChem GmbH, Darmstadt, Germany
TritonX-100	Sigma-Aldrich, Munich, Germany
TTX	Abcam, Cambridge, UK
Xylazine hydrochloride	Sigma-Aldrich, Munich, Germany

3.4 Antibodies

3.4.1 Primary Antibodies

Epitope	Species	Dilution	Company
GFP	chicken	1:500	Abcam
GSTpi	mouse	1:500	BD Bioscience
Ki67	rabbit	1:500	Novocastra
MBP	rabbit	1:250	Millipore
PDGFRα	rabbit	1:200	Thermo Fisher

3.4.2 Secondary Antibodies

Antibody	Dilution	Company
Anti-chicken-A488	1:500	Molecular Probes
Anti-rabbit-A647	1:500	Molecular Probes
Anti-rabbit-A594	1:500	Molecular Probes
Anti-mouse-A647	1:500	Molecular Probes

3.5 Solutions

3.5.1 Extracellular solution

Solutions were adjusted for the pH (7.35-7.4) by carbogen supply (95% CO_2 / 5% O_2).

Preparation solution

Substance	mM
NaH_2PO_4	1,25
NaCl	87
KCl	2.5
$MgCl_2$	7
$CaCl_2*6H_2O$	0.5
Glucose	25
$NaHCO_3$	26
Sucrose	61.3

aCSF for RT

Substance	mM
NaH_2PO_4	1,25
NaCl	126
KCl	3
$MgSO_4$*7 H_20	2
$CaCl_2$*6H_2O	2
Glucose	10
$NaHCO_3$	26

aCSF for RT + $MgCl_2$

Substance	mM
NaH_2PO_4	1.25
NaCl	126
KCl	3
MgCl2.6H20	2
$CaCl_2$*6H_2O	2
Glucose	10
$NaHCO_3$	26

aCSF for 35°C

Substance	mM
NaH_2PO_4	1.25
NaCl	132
KCl	3
MgCl2.6H20	2
$CaCl_2$*6H_2O	2
Glucose	10
$NaHCO_3$	20

aCSF for 35°C
(extracellular field recordings)

Substance	mM
NaCl	131
KCl	2,5
$CaCl_2$	2
$MgSO_4$*7H_20	1,3
NaH_2PO_4	1,25
$NaHCO_3$	21
Glucose	10

3.5.2 Intracellular solution

Solutions were adjusted for the pH (7.28) with HCl/KOH.

KCl- based
Intracellular solution

Substance	mM
KCl	130
MgCl2	2
CaCl2	0.5
BAPTA	5
HEPES	10
Spermine	3

K-gluconate- based
Intracellular solution

Substance	mM
K-gluc	125
MgCl2	2
EGTA	0.5
Hepes	10
KCl	20
NaCl	3
Na2-ATP	*3*

3.5.3 Solutions for immunohistochemistry

PBS (10x)

Substance	mM
NaH_2PO_4	17
$Na_2HPO_4*2H_2O$	3
NaCl	1.5

pH (7.4) adjusted with NaOH/HCl

PBS with sodium azide

Substance	Conc.
NaN_3	0.01% (w/v)
PBS	1x

pH (7.4) adjusted with NaOH/HCl

Paraformaldehyde

Substance	Conc.
PFA	4% (w/v)
PBS	1x

pH (7.4) adjusted with NaOH/HCl

Blocking solution

Substance	Conc.
NGS	10% (v/v)
Triton X-100	0.5% (v/v)
PBS	1x

Antibody solution

Substance	Conc.
NGS	5% (v/v)
Triton X-100	0.1% (v/v)
PBS	1x

3.5.3 Other

TAE (10x)

Substance	mM
Tris	40
Acetic acid	20
EDTA Na_2	1

4 Methods

4.1 The Cre/loxP system

The Cre/lox P system allows regional and temporal modulation of the genome. This system originally expressed in bacteriophage 1 includes an enzyme of the integrase family, called Cre (**c**yclization **re**combination). This enzyme specifically recognizes two 34 bp sequences called lox P sites (**l**ocus **o**f **X**-over of **P**1) and catalyzes recombination of a DNA sequence flanked by these sites (Hoess et al., 1982; Metzger et al., 1995; Sternberg and Hamilton, 1981). Each loxP site consists of two palindromic sequences with a 8 bp core sequence in between (Fig.4.1). Cre mediated excision of a gene takes place when both loxP sites flanking the gene are oriented in the same direction; inversion if the loxP sites are in inverted orientation (Sauer, 1998). To restrict Cre mediated recombination to a certain cell line or region, Cre expression can be limited to a cell or tissue specific promoter (Gu et al., 1992; Tsien et al., 1996).

Fig. 4.1: LoxP site structure. One LoxP site consists of two 13 bp sequences flanking an 8 bp core (grey box). Modified from (Sauer, 1998).

To be able to control Cre activity in a temporal manner, an inducible Cre system was established. Therefore, a modified hormone binding domain (HBD) of the human **e**strogen **r**eceptor (**ER^{T2}**) was fused to the **Cre** enzyme creating the fusion protein **CreER^{T2}** (Feil et al., 1997). Due to the property of HBDs to associate with heat shock proteins, CreER^{T2} is initially sequested in the cytosol and not able to enter the nucleus and to mediate recombination (Fig. 4.2) (Picard, 1994; Scherrer et al., 1993)**.** Solely in presence of synthetic ligands like tamoxifen or its derivate OHT, the heat shock protein disassembles from CreER^{T2}, allowing the enzyme to enter the nucleus and induce the knockout (ko) of the gene flanked by the loxP sites. Endogenous estrogen fails to induce CreER^{T2} activity as mutations

of three different amino acid residues (G400V/M543A/L540A) makes CreER^{T2} insensitive to endogenous estrogen (Feil et al., 1997).

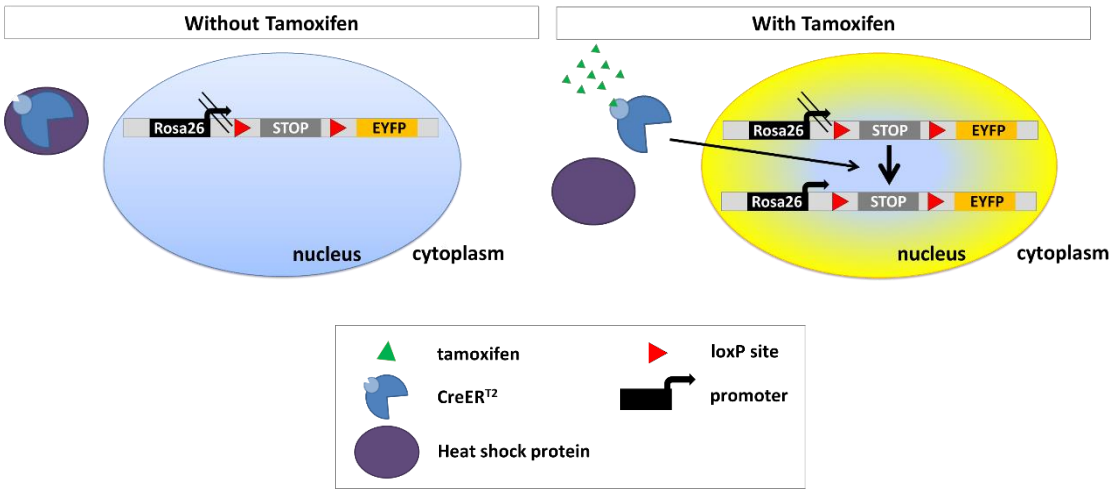

Fig. 4.2: Induction of a CreER^{T2} mediated recombination
A) In absence of tamoxifen, CreER^{T2} is trapped in the cytosol by heat shock proteins. **B)** In presence of tamoxifen, steric inhibition of CreER^{T2} is removed and the recombinase can enter the nucleus to mediate recombination of genes flanked by loxP sites. Here, expression of the reporter protein EYFP is initially blocked by a stop codon flanked by loxP sites. CreER^{T2} mediated recombination excise the stop sequence allowing EYFP to be expressed. Modified from Cox et al., 2012; Greco and Guo, 2010.

4.2 Mouse models

In the present study four different mouse lines were used: NG2-EYFPki mice, control mice (NG2-CreER^{T2} x Rosa26EYFP mice), Kir4.1 flox mice (Kir4.1 fl/fl; NG2-CreER^{T2}xRosa26EYFP mice) and GluA flox mice (GluA fl/fl; NG2-CreER^{T2}xRosa26EYFP mice). All animals were kept in a 24h day-night cycle in the „Haus für experimentelle Tiertherapie“ (HET) at the University Clinic Bonn and treated according to the European and local governmental regulations.

4.2.1 NG2-EYFPki

Mice of the NG2-EYFPki line were used as a control in the experiments mentioned in section 5.1.2 (FACS), section 5.8 (LTP) and section 5.11 (AMPA receptor ko mice). This mouse line based on a C57Bl/6N background was generated by Khalad Karram in 2008 using homologous recombination to insert EYFP (enhanced yellow fluorescent protein) cDNA into exon 1 of the NG2 gene. EYFP expression driven by the endogenous NG2 promoter allows

identification of NG2 glia by intrinsic yellow fluorescence (Karram et al., 2008). Because of the knock-in of the EYFP into the coding region of the NG2 protein, this mouse model can be further considered as a NG2 ko model, hence homozygous breeding resulted in a total loss of the NG2 protein (Karram et al., 2008; Passlick et al., 2016).

4.2.2 NG2-CreER^{T2} x Rosa26-EYFP

In the present study a mouse line was used in which expression of the CreER^{T2} recombinase is driven specifically by the NG2 promoter. This NG2 glia CreER^{T2} mouse line (NG2-CreER^{T2}) is based on the Cre/loxP system and was first characterized by Huang et al. in 2014 (Huang et al., 2014). CreER^{T2} is a fusion protein of the Cre enzyme, mediating a recombination induced gene ko, and a mutated human estrogen receptor (ER^{T2}), allowing Cre activity to be controlled by the presence of estrogen analogues like tamoxifen (Feil et al., 1997; Huang et al., 2014). In this mouse line, the CreER^{T2} sequence was introduced to the exon 1 of the NG2 gene, restricting CreER^{T2} expression to the NG2 promoter. To monitor CreER^{T2} activity this mouse line was further crossbred with the reporter line TgH(Rosa26-floxed-stop-EYFP) (Rosa26-EYFP). Here, EYFP expression is controlled by the ubiquitously expressed Rosa 26 promoter. As the expression of EYFP is initially blocked by the presence of a floxed stop codon, CreER^{T2} entering the nucleus can mediate recombination to remove the stop sequence, allowing EYFP to be expressed. Thus, all NG2 expressing cells with an active CreER^{T2} recombinase are supposed to be EYFP fluorescent (Huang et al., 2014; Srinivas et al., 2001). Animals of this NG2-CreER^{T2} x Rosa26-EYFP mouse line were used as a control and are hereinafter referred to as **control mice**. Both, CreER^{T2} expression and the expression of the reporter gene EYFP were either homo- or heterozygous in these mice.

To specifically induce a ko of the K^+ channel Kir4.1 in NG2 glia, mice carrying the floxed Kir4.1 gene (Kir4.1 fl/fl) were crossbred with the above mentioned control line. These mice (Kir4.1 fl/fl; NG2-CreER^{T2} x Rosa26-EYFP) were bred homozygous for the Kir4.1 floxed gene and homo- or heterozygous for the expression of CreER^{T2}. Animals of this mouse line were termed **Kir4.1 flox mice.**

A mouse line with a NG2 glia specific deletion of the AMPA receptor subunits GluA1, GluA2 and GluA4 and one with a targeted deletion of all four AMPA receptor subunits (GluA1, GluA2, GluA3, GluA4) were generated by crossbreeding the control line with mice having the corresponding genes of the AMPA receptor subunits flanked by the loxP sites. The obtained **triple GluA flox mice** (NG2-CreER^{T2} x GluA1fl/fl; GluA2fl/fl; GluA4fl/fl x

Rosa26-EYFP) or **quadruple GluA flox mice** (NG2-CreER^{T2} x GluA1fl/fl; GluA2fl/fl; GluA3fl/fl; GluA4fl/fl x Rosa26-EYFP) were part of the experiments mentioned in section 5.11. In these experiments, mice being homozygous for the floxed AMPA receptor subunits and homo- or heterozygous for the expression of CreER^{T2} were used.

All four mouse lines that are based on the NG2-CreER^{T2}x Rosa26EYFP construct (control, Kir4.1 flox, triple GluA flox, quadruple GluA flox) were treated with tamoxifen (see section 4.3) to induce CreER^{T2} activity. In mice of the control line CreER^{T2} activity only resulted in the expression of the reporter gene EYFP, whereas in Kir4.1 flox mice the Kir4.1 channel and in triple/quadruple AMPA receptor mice three or four AMPA receptor subunits were additionally deleted. NG2-EYFPki mice were not injected with tamoxifen.

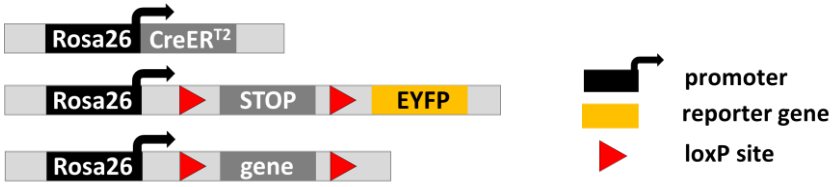

Fig. 4.3: Scheme of the genetic modification of the NG2-CreER^{T2} x Rosa26-EYFP based mouse models. The expression of the enzyme CreER^{T2} is controlled by the NG2 promoter. To monitor CreER^{T2} activity, a gene construct coding for EYFP was used as reporter. Expression of EYFP by the artificial Rosa26 promoter was initially prevented by a stop codon. Active CreER^{T2} recognizes the loxP sites flanking the stop codon, enabling EYFP expression after mediating recombination at these sites. In Kir4.1 flox mice the gene coding for the Kir4.1 channel (k*cnj10*) and in GluA flox mice the genes coding for the AMPA receptor subunits (*gria1 - 4)* were additionally floxed. P, promoter.

4.3 Tamoxifen administration

The tamoxifen injection protocol used was established to reach a high recombination rate of the gene of interest with minimally necessary injection. Mice of either sex of the control, Kir4.1 flox and quadruple GluA flox mouse line were intraperitoneally injected with 1.5 mg tamoxifen once per day for 3 consecutive days. Mice of the triple GluA flox line received injections of 1 mg tamoxifen per injection and were injected twice a day for five consecutive days. Tamoxifen was dissolved freshly each day in ethanol absolute and sunflower seed oil in a ratio of 1:10. Electrophysiological analysis was performed 3-4 weeks post injection (wpi) in all mice and immunohistochemistry 8 wpi in control and Kir4.1 flox mice. For behavioral experiments, animals of the control and Kir4.1 flox mouse line were introduced into the tasks starting from the third week after injection.

4.4 Electrophysiology

4.4.1 Preparation of acute brain slices

Mice were anesthetized by O_2/CO_2 (50%/50%) or isoflurane before decapitation. The brain was rapidly removed and flushed with ice cold preparation solution. For horizontal sections of the hippocampus, the cerebellum and a part of the frontal brain were removed. A part of the dorsal brain was further cut to create an even plane on which the brain was finally glued to the specimen holder. The plate was transferred into the buffer tray of the vibratome surrounded by ice and filled with ice cold preparation solution.

For miniature excitatory postsynaptic potential recordings (section 5.3), stimulation experiments (section 5.7) and extracellular field potential recordings (section 5.8) 300 µm thick sections were cut. For other experiments (application of $BaCl_2$, section 5.1.1; application of kainate, section 5.11.2 and 5.12) 200 µm thick sections were used. For cerebellar slices both cerebellar hemispheres were cut and the vermis was fixed on the specimen holder. Sections of 250 µm thickness were sliced as mentioned for hippocampal sections and treated as mentioned before. After sectioning, hippocampal/cerebellar brain slices were incubated for 15 min at 35°C in preparation solution before either being stored in aCSF at RT (field potential recordings) or in aCSF pre-warmed to 35°C, slowly cooling down to RT (patch-clamp recordings), until use. Slices were allowed to recover for at least 1 h before being used for experiments. All solutions were constantly gassed by O_2/CO_2 (95%/5%) to maintain a pH of 7.4.

4.4.2 Electrophysiological setup

For whole cell patch-clamp experiments an upright microscope was used. The microscope was placed on a vibration isolated table and shielded for electromagnetic waves by a faraday cage. A bath chamber was fixed on a motorized stage, allowing movements in x and y direction. A motorized focus was used to adjust the focal plane with either a dry 5x objective or a 60x immersion objective. The image of the slice was captured by a CCD camera and displayed on the computer monitor. Differential interference contrast (DIC) optics allowed enhanced contrast of all tissue structures. A fluorescence illumination system was used to visualize cells with intrinsic fluorescence. All incoming electrical signals were detected by a teflon coated silver wire with a chlorinated tip and enhanced by a pre-amplifier (head-stage) before being transmitted to the main amplifier EPC800. Signals were further processed by a

differential amplifier (DPA-2FS) and converted to a digital signal by a A/D converter and finally displayed by the patch-clamp software Tida. A silver pellet placed in the bath chamber and connected to the head stage was used as grounding. A heating system connected to the holder of the bath chamber allowed measurements at 35°C (mEPSCs recordings, section 4.4.5 and 5.3; Schaffer collateral stimulation, section 4.4.6 and 5.7; cerebellar recordings 5.10.2 and 5.10.3).

4.4.3 Whole cell patch-clamp recordings

Whole cell patch-clamp recordings from NG2 glia were performed to measure ionic currents passing over the entire membrane of the cell. The brain slice was placed in a bath chamber and fixed by a platinum wire with nylon threads. As recording electrode, a glass pipette of 2-5 MOhm resistance was pulled from a borosilicate glass filament with a horizontal puller. The pipette was filled with solution resembling the cytoplasm of the cell (intracellular solution) and fixed to the head stage. A small but constant overpressure applied via a tubing system provoked an outflow of intracellular solution, preventing the pipette tip to be plugged. Under optical control, using the 60x immersions objective, the pipette was carefully moved with electric micromanipulators close to cell of interest. When the overpressure was released, the cell membrane flipped to the pipette generating a tight seal. The cell was then clamped to -80 mV, if not stated otherwise. To establish the whole cell configuration small pulses of negative pressure were applied, rupturing the cell membrane beneath the pipette. To keep the cell at -80 mV, the head stage hosts an operational amplifier that compares the desired holding potential (V_{hold} = -80 mV) to the actual resting membrane potential (RMP) of the cell. If the RMP differs from V_{hold} the difference is counterbalanced by injection of a current (I), forcing the cell to adapt to the desired potential V_{hold}. While switching from the voltage clamp mode to the current-clamp mode, this feedback loop that enforces the cell to stay at a certain potential is inactive and the actual membrane potential can be measured.

4.4.4 Passive membrane properties

The passive membrane properties of a cell were calculated by considering the properties of a cell equivalent to an electrical circuit (Fig. 4.4 A). The cell membrane, a lipid bilayer, can be considered as a capacitor as it separates charged ions of the extracellular and intracellular space, generating an electric field. The amount of charge (Q) that can be stored by the capacitor (membrane capacitance, Cm), is proportional to its size (here membrane surface area). Ion channels that are embedded in the membrane function as resistors, allowing

charged ions to cross the membrane. This membrane resistance (Rm) depends on the type and amount of open ion channels in the cell membrane. During whole-cell patch-clamp recordings, the transition between the patch pipette and the cytoplasm represent another resistor that is added in series to Cm and Rm. The series resistance (Rs) depend on the access to the cell interior and the composition of pipette solution and cytoplasm and diffusion parameters (Sherman-Gold, 2012).

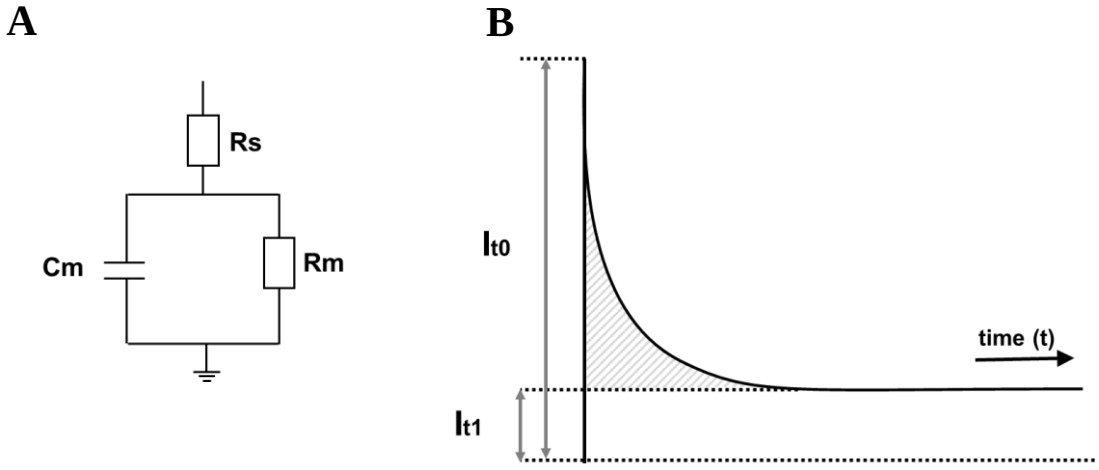

Fig. 4.4: Determining Passive membrane properties of a cell
A) Electrical circuit in a whole-cell configuration. Cm (membrane capacitance), determined by the size of the lipid bilayer; Rm (membrane resistance), determined by ion channels embedded in the membrane; Rs (series resistance), determined at the transition between patch-pipette and the intracellular space. **B)** Current response of a cell to a Δ10 mV depolarizing voltage step. I_{t0}, capacitive current at the beginning of recharging the membrane (time point t0); I_{t1} steady state current after recharging the capacitor. The change of charge (ΔQ) is represented by the integral under the capacitive current. Adapted from (Sherman-Gold, 2012).

To determine Rs, Rm and Cm, the cell was repetitively (10 times) depolarized by 10 mV (ΔV = 10 mV) for 50 ms and the current responses (Fig. 4.2 B) were averaged. The applied voltage leads to a recharge of the capacitor, resulting in a capacitive current (I_{t0}). When the capacitor is fully recharged, the current reaches a steady state I_{t1}. I_{t0} and I_{t1} are used to determined Rs and Rm according to Ohm´Law (equation 1 and 2). Cm is defined by the change of charge (ΔQ) between I_{t0} and I_{t1} (equitation 3). Calculations were performed by using IGOR Pro macros custom-written by Ronald Jabs.

$$Rs = \frac{\Delta V}{I_{t0}} \quad (1)$$

$$Rm = \frac{\Delta V}{I_{t1}} - Rs \quad (2)$$

$$Cm = \frac{\Delta Q}{\Delta V} - Rs \quad (3)$$

4.4.5 Miniature EPSPs

Miniature excitatory post synaptic potentials (mEPSPs) were recorded in recombined NG2 glia in the CA1 region of the stratum radiatum. To prevent spontaneous activity of neurons, aCSF was supplemented with TTX (0.5 mM), a blocker for voltage gated Na^+ channels. For some recordings NBQX (10 µM) and/or picrotoxin (150 µM) were applied via the perfusion system to distinguish between glutamatergic and GABAergic input. mEPSPs were recorded for 8 min with a K-gluconate based intracellular solution. Recordings were sampled at 6 kHz and filtered at 1 kHz. For analysis, events were identified by using a template-based search with pClamp and either retained or discarded after visual inspection. Cells with less than 3 events detected were rejected and not taken into analysis. Amplitudes, kinetics (rise- and decay time) and frequencies of mEPSPS were analyzed by a custom-written macro with IGOR Pro Software. The rise time was determined between 20% and 80% of the rising phase of the event (Fig. 4.5). The decay time (τ) was determined by a monoexponential fit of the mEPSP decay.

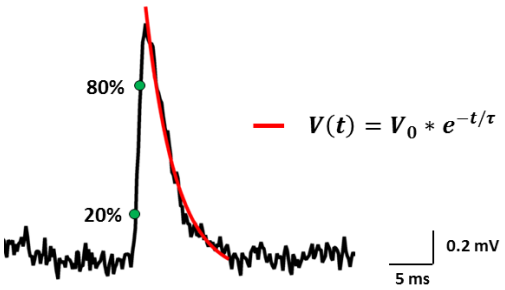

Fig. 4.5: Analysis of rise time and decay time.
Example of a mEPSP. The rise time was determined between 20% and 80% (green circles) of the rising phase; the decay time was determined by a monoexponential fit of the mEPSP decay (red).

4.4.6 Paired pulse stimulation

Excitatory postsynaptic currents (EPSCs) of hippocampal NG2 glia were evoked by stimulating Schaffer collaterals with a monopolar stimulation electrode. The electrode, consisting of a chlorinated silver wire inside an aCSF filled borosilicate glass pipette (< 1 MOhm resistance), was placed in the stratum radiatum of the CA1 region of the hippocampus. For recording EPSCs of cerebellar NG2 glia the stimulation pipette was placed in the granule cell layer where climbing fiber traverse and innervate NG2 glia of the molecular layer. Biphasic stimulation pulses of 150 µs were applied via a pulse generator and the stimulus intensity was adjusted to stimulate single or few presynaptic fibers (minimal stimulation). For paired pulse recordings, two stimulation pulses with an inter-stimulus interval of 50 ms were

applied 40 to 120 times in a 15 s interval. A KCl-based intracellular solution was used for recording evoked excitatory postsynaptic currents (eEPSCs) of recombined NG2 glia in the hippocampal CA1 region of the stratum radiatum or in the cerebellar molecular layer. In some recordings glutamatergic input was separated from GABAergic input by application of the GABA receptor blocker picrotoxin (150 µM) via the perfusion system. Recordings were sampled at 10 kHz, filtered at 1 kHz and analyzed by a custom-written macro in the IGOR Pro Software. Kinetic properties of eEPSCs were calculated for responses evoked upon the first stimulus pulse. As for mEPSPs, the rise time was determined at 20% to 80% of the rising phase and the decay time constant τ by a monoexponential fit (equation 1).

$$I(t) = I_0 * e^{-t/\tau} \qquad (4)$$

Stimuli that did not elicit a response, called failures, were excluded from analysis of rise and decay time. A stimulus was considered a failure if the amplitude of the response was less than 2-times the full width at half maximum of the baseline current.

To estimate the release probability at the neuron - NG2 glia synapse, the paired pulse ratio (PPR) was determined. Here, the ratio of the mean amplitude (including failures) upon the second pulse (I_{amp2}) to the mean amplitude evoked upon the first pulse (I_{amp1}) was calculated (equation 5). At synapses with a ratio of > 1 facilitation takes place, at synapses with a PPR of < 1, depression.

$$PPR = \frac{I_{amp2}}{I_{amp1}} \qquad (5)$$

4.4.7 Field potential recordings

Field potential recordings and their analysis were performed by Dr. Anne Bohlen (Institute of Cellular Neurosciences, University of Bonn, Bonn).

4.4.7.1 Setup

Slices were transferred to an interface-type recording chamber (IFC) under a Leica microscope. In the IFC, the slice is placed on filter paper and is continuously perfused by low levels of aCSF (34°C). Field potentials were recorded with an aCSF filled glass pipette (resistance 3-8 MΩ) and sampled at 10 kHz. Signals were amplified and filtered by an Ext-02B amplifier. Noise of 50 /60 Hz was removed by a HumBug noise eliminator. Data was acquired with the NI USB-6221 system and displayed by the software WinWCP (version 4.6.1).

4.4.7.2 Long-term potentiation

Field excitatory postsynaptic potentials (fEPSPs) in the stratum radiatum of the hippocampal CA1 region were evoked by a concentric bipolar stimulation electrode placed at the border of CA2/CA3. The stimulus intensity was adjusted by an isolated current stimulator and the half-wave pulse duration was set to 100 µs. To determine the excitability of the slice (input-output relationship) and the maximal possible amplitude of the fEPSP, increasing stimulation intensities from 20 µA to 500 µA were delivered 3 times and the fEPSP slope and amplitude averaged accordingly. The stimulus intensity used for the experiments was adjusted to receive 50% of the maximal evoked fEPSP amplitude. The slope of the fEPSP was used as an indication for neuronal network activity before, during and after induction of long-term potentiation (LTP) and analyzed by calculating the linear rising phase of the fEPSP between two manually set points and normalized to baseline.

LTP was induced by a theta burst stimulation (TBS) protocol containing trains of 8 stimuli at 5 Hz, each stimulus consisting of 4 pulses at 100 Hz. These 8 trains of stimuli were repeated 3 times with an inter-stimulus interval of 1 min (Fig. 4.6). For baseline recordings stimulation pulses with an interval of 15 s were applied 10 min before (40 pulses in total) and for 30 min after (120 pulses in total) application of the TBS protocol. The generated fEPSP slopes were normalized to the mean fEPSP slope during baseline recordings. Recordings that showed more than 10% fEPSP slope variability during baseline recording were excluded.

To determine the release probability before and after TBS induced LTP, paired stimulation pulses with an inter-stimulus interval of 50 ms were applied every 15 s for 10 min. The PPR was calculated by dividing the second fEPSP slope by the first (equation 6).

$$PPR = \frac{slope\ 2}{slope\ 1} \qquad (6)$$

Input-output curves were obtained with increasing stimulation intensities (20 µA to 500 µA). Each stimulus intensity was delivered 3 times, mean values were calculated and the initial slope of the fEPSPs was evaluated. All field potential recordings were analyzed with pClamp.

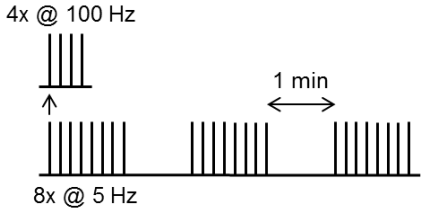

Fig.4.6: Schematic illustration of the TBS protocol.
LTP was induced by a theta burst protocol composed of 8 trains of stimuli applied with an inter-stimulus interval of 0.2 s (5 Hz). Each stimulus, consisting of 4 stimulation pulses, was applied with a 0.01 s interval (100 Hz). These 8 trains were repeated 3 times with an inter-train interval of 1 min.

4.4.8 Application techniques

4.4.8.1 Bath application

The application of different substances via the perfusion system was used during Schaffer collateral stimulation and mEPSPs. To guarantee a uniform distribution of aCSF supplemented with picrotoxin (150 µM), TTX (0.5 µM) and/or NBQX (10 µM) and to ensure global effect of the substances on the brain slice, the blocker solutions were applied for several minutes prior to recording.

4.4.8.2 Focal pressure application

The application of substances dissolved in aCSF via the focal pressure application system Octaflow was used to validate the ko of either the K^+ channel Kir4.1 (section 5.1.1) or AMPA receptors (section 5.11.2 and 5.12) in recombined NG2 glia of Kir4.1 flox mice or triple/quadruple GluA flox mice, respectively. The Octaflow system consists of 8-12 valves, with one teflon tube per valve that converge into a combined quartz pipette with a diameter of 100 µm. Upon an electrical signal that is triggered by the Octaflow software, individual channels open, allowing an immediate application of substances. To prevent leakage of substances from the quartz pipette, aCSF is continuously flushing out of the pipette via gravitation until a valve opens. To exclude responses upon the applied pressure itself, aCSF was applied for 3 ms prior to the application of agonists and antagonists. Cells responding to aCSF were excluded from analysis. All solutions used were saturated with carbogen before being filled into the system to ensure a stable pH. The application of the substances with a pressure of 3 psi (equals 20.7 kPa) was performed with carbogen. Whole-cell patch-clamp recordings were performed with a KCl-based intracellular solution.

The existence of Kir4.1 mediated currents in recombined NG2 glia of Kir4.1 flox mice was proven by focal application of aCSF supplemented with the Kir channel blocker $BaCl_2$ (100 µM). The amplitude of Kir4.1 mediated currents was determined at a potential of -130 mV, a voltage where Kir channels show inward rectification. The membrane conductance (g) was determined before and after $BaCl_2$ (equation 7). For these experiments aCSF with $MgCl_2$ was used to prevent precipitation of $BaCl_2$ in presence of $MgSO_4$.

$$g\ at-130\ mV\ \left(\frac{pA}{mV}\right) = \frac{I_{amp}\ at-130\ mV\ (pA)}{(-130\ mV - Vm\ (mV))} \qquad (7)$$

To test for the presence of AMPA receptors in recombined hippocampal NG2 glia of triple and quadruple GluA flox mice, the AMPA/kainate receptor agonist kainate (250 µM) was used. aCSF supplemented with quinine (200 µm), TTX (0.5 µM) and picrotoxin (100 µM) was focally applied for at least 3 min to block K^+ channels, Na_v channels and $GABA_A$ receptors, respectively. The blockers were supposed to unmask the pure AMPA receptor mediated responses upon kainate application (solved in the blocker solution mentioned; applied for 15 s). The current density was calculated by normalizing receptor currents to the membrane capacitance (Cm) (equation 8)

$$current\ density\ \left(\frac{pA}{pF}\right) = \frac{I_{amp}\ (pA)}{Cm\ (pF)} \qquad (8)$$

The rectification of the AMPA receptor mediated current was estimated by calculating the rectification index. During patch-clamp recordings the cell was continuously clamped every 3 s to different voltages (-40/-20/0/20/40/80/100/-100 mV), each voltage step lasting for 100 ms. The voltage evoked currents before kainate application were subtracted from those during kainate application with respect to the individual voltage step applied. After normalization to the smallest current measured during the voltage step protocol (mainly at -100 mV), the relation between current and voltage (I-V relationship) was displayed. The reversal potential (V_{rev}), meaning the voltage at which the receptor current reverses direction was read out from the curve. V_{rev} and the peak amplitude (I_{amp}) during kainate application at a voltage of +40 mV and -70 mV were used to calculate the rectification index (equation 9).

$$Rectification\ index = \frac{I_{amp}at+40\ mV\ (pA)}{(40\ mV - V_{rev}(mV)} \ / \ \frac{I_{amp}at-70\ mV\ (pA)}{(70\ mV - V_{rev}(mV))} \qquad (9)$$

The rectification index reflects the relation of inward and outward directed currents, determined at voltages negative and positive to the reversal potential (here, -70 mV and +40 mV). A rectification index < 1 is ascribed to receptors that exhibit more inward than outward currents, displayed by an inwardly rectifying I-V relation. A rectification index >1 characterizes receptor currents that favor outward over inward directed currents, displayed by an outwardly rectifying I-V relation.

4.5 Molecular Analysis

The existence and amount of certain mRNA expressed in NG2 glia was assessed by molecular analysis including semi quantitative real-time PCR (qPCR) of FAC sorted cells and single cell reverse transcription PCR (RT-PCR) of cell harvested from the slice. Experiments and analysis were performed by Dr. Gerald Seifert (Institute of Cellular Neurosciences, Bonn).

4.5.1 FAC sorting

The level of mRNA (Kir4.1, MBP, MAG) in hippocampal NG2 glia was quantified by semi quantitative RT- PCR (see below). For this purpose, NG2 glia were isolated from brain tissue of NG2-EYFPki mice (p60), control and Kir4.1 flox mice (both 3-4 weeks after tamoxifen injection, p50-60) by fluorescence activated cell sorting (FACS). Mice of both sexes were anesthetized with isoflurane and decapitated. The brains were dissected and whole hippocampi were isolated under microscopic control. The tissue was mechanically ruptured and digested in papain for 15 min 37 °C. To degrade the DNA the tissue was incubated for 10 more minutes with DNAse and further dissociated by Pasteur pipettes and filtered through a 70 µm cell strainer. After adding 10 ml HBSS (Hanks' Balanced Salt Solution) supplemented with Ca^{2+} and Mg^{2+}, the solution was centrifuged for 10 min (300 x g) and the respective pellet re-suspended in 1 ml HBSS without Ca^{2+} and Mg^{2+}.

As NG2 cells of all three mouse lines were expressing the fluorescence protein (E)YFP either under control of the NG2 promoter (in NG2-EYFPki mice) or driven by the artificial Rosa26 promoter after Cre mediated recombination (in control and Kir4.1 flox mice), NG2 glia could be identified and sorted according to the EYFP specific emission at 527 nm by a flow cytometer (70 µm nozzle). Sorted cells were collected in HBSS (without Ca^{2+} and Mg^{2+}) and the solution centrifuged for 10 min (2000 x g). The supernatant was discarded and the cells were re-suspended in 200 µl lysis/binding buffer. Samples were frozen in liquid nitrogen and stored at -80 °C before use.

4.5.2 Semiquantitative qPCR

Samples containing the FAC-sorted NG2 glia were incubated in lysis/binding buffer to extract the mRNA from the cells. To specifically isolate the mRNA, the samples were incubated with polymer particles covered with an oligo dT sequence (oligo(dT)25-linked Dynabeads). Here, the poly A-tale of the mRNA binds to the oligo dT sequence and can be separated from the rest of the solution via a magnet. For first strand synthesis, these beads with the adherent mRNA were suspended in DEPC-treated water (20 µl) and incubated with first strand buffer supplemented with the chemicals listed in table 1.1. The first strand synthesis was induced at 50 °C for 1h.

Table 1.1: Reaction mixture for the first strand synthesis. Total reaction volume of 40 µl used, including 20 µl mRNA suspended in DEPC-treated water.

Component	Concentration
first strand buffer	1x
DTT	10 mM
dNTPs	250 µM
oligo-dT_{24}-primer	5 µM
RNAse inhibitor RNAsine)	80 U
SuperscriptIII reverse transcriptase	400 U

Table 1.2: Reaction mixture for qPCR. Reaction volume of 12.5 µl (based on injection water), including 1 µl of cDNA.

Component	Concentration
Reaction mix Tycon	1x
Primer/Probe mix	1x

To assess the mRNA quantity, 1 µl of the first strand synthesis product was added to the *Tycon* reaction mix and a primer/probe mix (table 1.2) and the PCR program for qPCR started (Table 1.3). The Taq probe in the mixture is an oligonucleotide labelled with a fluorescent reporter at the 5´end and a second fluorescent dye at the 3´end. When the reporter dye is excited with the appropriate wavelength, energy is transferred between both dyes: The reporter dye emitting energy and the other dye absorbing it, thus, acting as a fluorescent quencher. During the amplification process of the PCR, the DNA polymerase cleaves the probe and disrupts the energy transfer. The energy, that was supposed to be absorbed, is now emitted as light and can be detected by the qPCR detection system CFX 384 (Holland et al., 1991; Livak et al., 1995; Seifert et al., 2002). Per PCR cycle the emission accumulates and can be measured in real time. The fluorescence intensity is increasing exponentially until a

plateau phase is reached. In the exponential phase the threshold cycl (CT) can be determined and used to calculate the amount of RNA that was initially used (Fink et al., 1998; Seifert et al., 2002). The relative quantification of the gene expression ratio of the target gene and ß-actin, a housekeeping gene serving as reference, was determined by comparing both CT and was calculated as followed:

$$X_{target} / X_{ß\text{-}actin} = E_{ß\text{-}actin}^{CT\ ß\text{-}actin} / E_{target}^{CT\ target} \qquad (10)$$

with **X** being the input copy number, **E** the efficiency of amplification and $\mathbf{C_T}$ the threshold cycle. The amplification efficiency was assessed by serial dilutions of mRNA and was 1.93 for Kir4.1, 1.94 for ß-actin, 1.91 for MAG and 1.89 for MBP. Water was used as a negative control.

Table 1.3: PCR program for qPCR.

	Temp (°C)	Time (min)	Cycles
	50	2:00	1x
Denaturation	95	10:00	1x
Denaturation	95	0:15	50x
Hybridization	60	0:60	
Elongation	60		

4.5.3 Single cell RT PCR

4.5.3.1 Harvesting single cells

The presence or absence of mRNA in single NG2 glia was assessed by single cell RT-PCR. NG2 glia that were electrophysiologically characterized by the patch-clamp technique were isolated from brain tissue when the cell was still attached to the patch pipette. The pipette with the cell attached was lifted carefully above the slice and the isolated cell aspirated into the pipette. The pipette was removed and the intracellular solution of the pipette including the cell expelled into a thin walled Eppendorf tube with 3 µl DEPC water (RNAse and DNA free) and frozen in liquid nitrogen. Cells were stored until use at -20°C.

4.5.3.2 Single cell RT PCR

To reveal the presence or absence of mRNA in a single cell, a two-step reverse transcription PCR (RT-PCR) was performed. In the first step mRNA was transcribed into cDNA. Therefore, each cell collected was treated for 1 h at 37°C with a buffer composed of the

chemicals mentioned in table 1.4. As negative control DEPC water was used. RNA isolated from the whole mouse brain served as positive control.

Table 1.4: Reaction mixture for the first step of single cell RT-PCR.
Total reaction volume of 10 µl, including 3 µl DEPC-treated water containing a single cell.

Component	Concentration
first strand buffer	1x
DTT	10 mM
dNTPs	250 µM
Random hexamer Primer	50 µM
RNAse inhibitor (RNAsine)	20 U
SuperscriptIII reverse transcriptase	100 U

In the second step a two-round multiplex PCR was performed to identify specific cDNA sequences. For the first round 10 µl of the cDNA were added to the substances listed in table 1.5 before the PCR reaction was started (45 cycles, 51°C, 2,5 h; table 1.6). Here primers were used that recognize the cDNA of the either the K^+ channel subunit Kir4.1 or the AMPA receptor subunits GluA1, GluA2, GluA3 and GluA4. To reassure the origin of the cDNA to be NG2 glia specific, primers binding to the sequence of the NG2 glia marker PDGFRα were additionally used.

Table 1.5: Reaction mixture for the first round of the two-round multiplex PCR. Total reaction volume of 50 µl (injection water based), including 10 µl of the PCR product.

Component	Concentration
PCR Buffer*	1x
$MgCl_2$	2.5 mM
Sense primer	200 nM
Antisense primer Kir	200 nM
dNTPs	4*50 µM
Taq Polymerase	2 U

Table 1.6: PCR program for the 1st part of a two-round multiplex PCR

	Temp [°C]	time	cycles
	94	3:00	1x
Denaturation	94	0:25	5x
Hybridization	51	2:00	
Elongation	72	1:00	
Denaturation	94	0:25	40x
Hybridization	51	0:45	
Elongation	72	1:00	
	72	7:00	1x

For the second-round nested primers were used that bind within a specific sequence of the PCR product obtained from the reaction before. 2 µl of the PCR product were added to the substances mentioned in table 1.7 and amplified in a PCR reaction (35 cycles, 54°C, 2,5 h; table 1.8).

Table 1.7: Reaction mixture for the second round of the two-round multiplex PCR.
Total reaction volume of 50 µl (injection water based), including 2 µl of the PCR product from the first round of the multiplex PCR.

Component	Concentration
PCR Buffer*	1x
$MgCl_2$	2,5 mM
dNTPs	50 µM
sense primer nested	200 nM
antisense primer nested	200 nM
Platinum Taq Polymerase	2.5 U

Table 1.8: PCR program for the 2nd part of a two-round multiplex PCR

	Temp (°C)	Time (min)	Cycles
	94	3:00	1x
Denaturation	94	0:25	5x
Hybridization	54	2:00	
Elongation	74	0:25	
Denaturation	94	0:25	30x
Hybridization	54	0:45	
Elongation	72	0:25	
	72	7:00	1x

4.5.3.3 Agarose gel electrophoresis

To finally assess the presence or absence of certain mRNA in single cells, agarose gel electrophoresis was performed. A 1.5% agarose gel (agarose dissolved in Tris-acetate-EDTA (TAE) buffer) was supplemented with 20 µL ethidiumbromid (1 mg/ml) to visualize the PCR products under UV-light. In TAE-buffer the gel was loaded with 10 µl PCR product mixed with 2 µL loading dye. Samples were separated in an electric field (240 V for 40-45 min) by their size and charge. A low molecular weight DNA ladder, was used to indicate molecular size and to identify cDNA.

4.6 Immunohistochemistry

To quantify the recombination efficiency in control and Kir4.1 flox mice, brain tissue was fixed by paraformaldehyde (PFA) and brain sections were stained for the NG2 glia specific marker PDGFRα and the reporter protein EYFP. Proliferation and differentiation of recombined NG2 glia was assessed by immunostainings for Ki67 and GSTpi. Hippocampal myelination was revealed by staining for the myelin basic protein (MBP).
For immunohistochemistry mice 8 weeks post tamoxifen injection were prepared as mentioned in the following.

4.6.1 Tissue fixation

Mice were deeply anesthetized by intraperitoneal injection of 75 to 100 µl of xylaxine (2%)/ketamine (100 mg/ml) in a ratio of 1:3. Mice were intracardially perfused with ice cold phosphate buffered saline (PBS) solution followed by 4% PFA, 5 ml/min each. Brains were dissected and post fixed overnight in 4% PFA at 4°C before being transferred into PBS until sectioning.

4.6.2 Preparation of brain sections

For immunohistochemistry, coronal sections of the hippocampus or parasagittal slices of the cerebellar vermis were used. For coronal sections, the cerebellum and a part of the frontal brain were removed and the brain frontally glued to the specimen holder. For sagittal sections, the vermis was cut as described before (section 4.4.1). The specimen holder was transferred into the buffer tray surrounded by ice and containing PBS. Sections of 40 µm thickness, obtained with a vibratome, were stored until use in a 24 well plate in PBS supplemented with sodium azide.

4.6.3 Antibody labeling of free-floating brain sections

Free floating brain sections stored in PBS with sodium acid were washed three times with PBS prior to antibody treatment. To permeabilize the brain tissue and to block unspecific binding sites, sections were incubated for 2h at RT in PBS containing 0.5% triton and 10% normal goat serum (NGS). Primary antibodies were diluted in PBS with 0.1% triton and 5% NGS and were applied to the brain sections for at least 12 h at 4°C. Before adding the corresponding fluorescent secondary antibody (diluted in in PBS with 0.1% triton and 5% NGS) for 2 h at RT, sections were washed three times with PBS. Cell nuclei were stained

with Hoechst 33342 (1:100 in dH_2O) for 10 min. Before and after Hoechst treatment, brain sections were again washed three times with PBS. Sections were mounted on cover slips with mounting medium.

4.5.4 Confocal Imaging

Images of 1024 x 1024 pixels (581.25 µm x 581.25 µm) were captured with a confocal laser scanning microscope using a 20x immersions objective. Images represent Z-stack images of 4 µm depths with a step size of 1 µm. Laser intensity was adjusted according to the signal intensity to avoid oversaturation. Images were recorded and processed with LAS software from Leica. Based on the fluorescently labeled secondary antibody (section 3.4.2) and fluorescent dye used, excitation wavelength was set to 415 - 449 nm (Hoechst 33342), 500 - 600 nm (Alexa 488), 589 - 696 nm (Alexa 597) and 652 - 749 nm (Alexa 647). Images were analyzed with Fiji software.

4.6.5 Microscopic analysis and quantification

Immunostainings were evaluated from stratum radiatum, stratum lacunosum moleculare and stratum moleculare of the dentate gyrus from at least 3 mice per genotype with 3 slices per mouse. NG2 glia recombination, proliferation and differentiation were assessed by staining for PDGFRα - a marker for NG2 glia**,** Ki67 - a marker for dividing cells and GSTpi - a marker for mature oligodendrocytes. Recombined NG2 glia expressing EYFP were labeled with anti-GFP antibodies. For evaluation, confocal images of GSTpi, Ki67 and PDGFRα stainings were displayed with maximum intensity projections and cell populations counted as followed: Recombination efficiency was determined as the proportion of cells being positive for the reporter ($EYFP^+$) and the NG2 glia marker PDGFRα ($PDGFR\alpha^+$) among all NG2 glia ($EYFP^+$ $PDGFR\alpha^+$/$PDGFR\alpha^+$ cells). For differentiation, the proportion of recombined ($EYFP^+$) cells being positive for GSTpi ($GSTpi^+$) among all recombined cells was evaluated ($EYFP^+$ $GSTpi^+$/$EYFP^+$ cells). The population of proliferative cells was calculated from the number of $EYFP^+$ and $Ki67^+$ cells ($EYFP^+$ $Ki67^+$/$EYFP^+$ cells).

For quantification of myelination, sections were immunolabeled for the myelin basic protein (MBP) and the mean intensity projection was analyzed. To reduce variations within the staining procedure, fixed brain slices of control and Kir4.1 flox mice were stained and imaged in parallel. For the intensity analysis a threshold intensity was determined to distinguish between the MBP signal and background of the image. The threshold value was chosen by comparing the signal intensities between images and set accordingly for optimal signal

detection in all images. The intensity values of grey levels were determined per hippocampal area and normalized to the intensity recorded in the stratum lacunosum moleculare of Kir4.1 flox mice.

4.7 Behavioral experiments

Memory performance of control and Kir4.1 flox was assessed in different behavior paradigms in collaboration with Dr. Andras Bilkei-Gorzo and Prof. Dr. Andreas Zimmer (Department of Molecular Psychiatry, University of Bonn, Bonn). At least 1 week prior to experiments, mice were housed in a reversed 12h day/night cycle and experiments were performed during the dark phase when mice are active. Behavioral tests were conducted on groups of either sex in a dimly illuminated and sound isolated room. Experiments were performed as mentioned before (Albayram et al., 2016; Bilkei-Gorzo et al., 2017). In brief:
For the object location recognition test and partner recognition test an open field arena (44 cm x 44 cm) was covered with 1 cm sawdust. During the experimental phase sawdust was not changed to saturate it with the odor of the animals. Mice were separated to different arenas according to their sex to prevent any bias due to olfactory cues. During the habituation phase, mice were placed into the center of the arena and were allowed to explore the environment for 5 min for 3 consecutive days. The activity of each mouse during the test phase of the object location recognition test, partner recognition test and Y-maze paradigm was tracked by Noldus Ethovision XT software.

4.7.1 Object location recognition test

For the object location recognition test, three identical objects (LEGO bricks with different colors) were placed next to each other on one site of the arena. Mice were allowed to explore the enriched environment for 6 min (trial 1) and the time they spent on investigating the objects was recorded. After trial 1, the mouse was removed from the arena for 30 min until trial 2 started. In trial 2 one of the objects was rebuilt and moved within the arena. The mouse was placed back and the activity of the mouse was recorded for 3 min once the mouse began to interact with the new object. The preference (**P**) for the relocated object was calculated as percentage of the time spent exploring the moved object ($\mathbf{T_a}$) relative to the total exploration time on the moved and the other two remaining objects ($\mathbf{T_a}$, $\mathbf{T_b}$, $\mathbf{T_c}$) (equation 11). Novelty preference (**NP**) was calculated by the preference (P) of the mouse in trial 1 (P_{t1}) and trial 2 (P_{t2}) (equation 12).

$$P = \frac{T_a}{T_a + T_b + T_c} * 100 \qquad (11)$$

$$NP = \frac{(P_{t1} - P_{t2})}{P_{t1}} * 100 \qquad (12)$$

4.7.2 Partner recognition test

For the partner recognition test, mice were habituated as mentioned before (3 days, 5 min per day). On the test day a partner mouse of the same sex as the test mouse (but from a different cage) was placed in a metal grid cage and the cage positioned in one corner of the open field arena 6-7 cm from the walls. An object of the same size, shape and material (here a metal can) was placed in opposite of the grid cage with the same distance from the wall. The behavior of the test mouse was recorded for 9 min (trial 1). In trial 2, following 1 h, 2 h, 4 h or 8 h after trial 1, the object was replaced by another partner mouse in a grid cage and the test mouse was placed back into the arena. Subsequently, after the first interaction with the new partner the activity of the test mouse was recorded for 3 min. The different time intervals between trial 1 and trial 2 were carried out on consecutive days. Thus, each inter-trial interval represents a new experiment including different partner mice. The ability to distinguish between the new and the old partner was defined by the novelty preference. The novelty preference was calculated from the time spent with the novel partner mouse ($\mathbf{T_a}$) and the time spent with the remaining partner ($\mathbf{T_b}$) (equation 13).

$$NP = \frac{(T_a - T_b)}{T_b} * 100 \qquad (13)$$

4.7.3 Y-Maze labyrinth

In the Y-maze paradigm mice were placed for 10 min in a Y-shaped arena, each of the three arms being 20 cm long and 15 cm high. The time spent in each arm was recorded and the number and sequence of arm entries were analyzed. To determine working memory the total number of spontaneous alternations (**SA**; entering 3 different arms consecutively) relative to the total number of arm entries (**TA**) minus 2 was calculated (equation 14): SA/TA-2 *100. The maze was thoroughly cleaned using detergent between the animals to avoid odor cues.

$$NP = \frac{SA}{(TA - 2)} * 100 \qquad (14)$$

4.7.4 Beam walk test

The beam walk paradigm was used to assess motor performance in control and Kir4.1 flox mice. Here a 1 m rod was fixed to a shelf at the height of 70 cm. A dark plastic chamber (7 x 10 x 10 cm^3, the ground covered with saw dust) was placed at the end of the rod, serving as a getaway spot for the mouse balancing on the beam. On the first day, mice were placed onto the free end of a 28 mm diameter rod and were allowed to climb into the chamber. Mice, which fell down were placed back to the original position until the chamber was reached. The test was repeated 2 additional times. At the end of this train period each animal was able to quickly walk from the start position to the goal chamber. On the second day (trial day), the test was carried out again as described above. This time all animals were tested in the order of the thickest (28 mm diameter) rod first, followed by the middle sized (14 mm) and finally the thinnest (8 mm) rod. The time from starting on the rod until entering the goal chamber with all 4 legs (latency) was measured.

4.8 Statistics

The data was analyzed with Igor Pro, Origin, Prism and R software. Normal (Gaussian) distribution of data was analyzed with the Shapiro–Wilk test. Parametric and non-parametric tests were used to determine statically differences. Non-paired data sets were analyzed with student's t-test or Mann-Whitney U test with or without Welch correction for equal or diverse variances. Paired data sets were analyzed with either paired t-test or Wilcoxon Rank test. For group analysis Kruskal-Wallis test with post-hoc Dunn´s test, 1-way ANOVA with post-hoc Tukey test or 2-way ANOVA followed by Bonferronis t-test were applied. Significance level was set to $p < 0.05$.

5 Results

5.1 Inducible knockout of Kir4.1 in NG2 glia

The role of NG2 glia especially in grey matter and the impact of receiving direct synaptic input from GABAergic and glutamatergic neurons stays elusive since the discovery of NG2 glia and their unique neuronal connection (Bergles et al., 2000). In the present study a mouse line was established to induce a knockout (ko) of the K^+ channel Kir4.1 specifically in NG2 glia. This mouse line that is based on the Cre/loxP system was generated by breeding the NG2-CreER^{T2} x Rosa26-EYFP mouse line (**control mice**) with mice carrying the gene for the K^+ channel Kir4.1 flanked by two recognition sites for the Cre recombinase (Kir4.1 fl/fl; NG2-CreER^{T2} x Rosa26-EYFP mice; **Kir4.1 flox mice**). In this system a modified version of the Cre enzyme is fused to the human estrogen receptor and is specifically expressed under the NG2 promoter. This construct not only allows Cre expression to be restricted to cells owning the NG2 promoter but further to control the timing of Cre mediated recombination by the addition of estrogen analogues. In this study CreER^{T2} mediated recombination was induced by intraperitoneal application of the estrogen analogue tamoxifen. NG2 glia in which CreER^{T2} was active and able to mediate recombination were identified by the expression of the reporter protein EYFP (enhanced yellow fluorescent protein) and termed recombined NG2 glia.

The efficiency of recombination and the concomitant ko of Kir4.1 were assessed by combining different molecular and electrophysiological methods and is described in the following sections.

5.1.1 Knockout efficiency in Kir4.1 fl/fl; NG2-CreER^{T2} mice

Both mouse lines, Kir4.1 flox and the control were treated with the tamoxifen protocol described by Huang and colleagues in 2014 who generated the NG2-CreER^{T2} mouse line (Huang et al., 2014): Adult mice were injected twice a day for five consecutive days with the estrogen analogue tamoxifen. Per mouse and per injection 1 mg tamoxifen was solved in sunflower seed oil and ethanol absolute before injecting the substance intraperitoneally. Three weeks after the last injection whole-cell patch-clamp recordings were performed in the CA1

region of the stratum radiatum of hippocampal brain slices of tamoxifen treated mice. In recombined NG2 glia of control mice, in which CreER^{T2} activity only induced the expression of the reporter gene while keeping the Kir4.1 gene intact, application of de- and hyperpolarizing voltage steps elicited current responses typical for this type of glia cells (Fig. 5.1): Depolarizing NG2 glia led to transient K^+ outward currents mediated by A-type K^+ channels (Fig. 5.1-1) and sustained K^+ currents through delayed rectifying K^+ channels (Fig. 5.1-2). The activity of other voltage gated channels like Na_v channels are thereby masked by the pronounced K^+ flow. Voltages hyperpolarizing the cell evoked currents known to be mediated by Kir4.1 channels (Fig. 5.1-3) (Kressin et al., 1995; Steinhäuser et al., 1994).

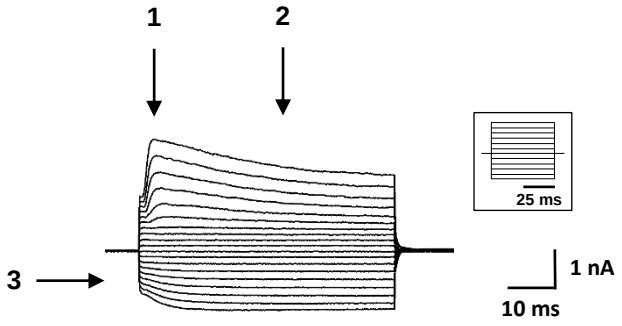

Fig. 5.1: Current pattern of recombined NG2 glia in control mice.
Example of the whole-cell current pattern of recombined NG2 glia evoked by de- and hyperpolarizing voltage steps between -160 mV and +20 mV lasting for 50 ms (holding potential of -70 mV; inset describes voltage commands). Depolarization of NG2 glia led to the opening of A-type K^+ channels (-**1**- transient K^+ current) and delayed rectifying K^+ channels (-**2**- sustained K^+ current). Kir4.1 mediated currents (-**3**-) were evoked by applying hyperpolarizing voltage steps.

To identify the proportion of Kir4.1 mediated currents in recombined NG2 glia of control and Kir4.1 flox mice the Kir channel blocker $BaCl_2$ was applied to the cells by using a focal pressure application system (Haberlandt et al., 2011; Larson et al., 2018; Passlick et al., 2016; Seifert et al., 2009). In presence of $BaCl_2$ currents evoked by voltages hyperpolarizing the cell were drastically reduced. The conductance of the Kir4.1 channel measured at -130 mV was diminished from 14.03 ± 4.33 pA/mV to 1.78 ± 0.86 pA/mV (n = 11) (Fig. 5.2). As in Kir4.1 flox mice CreER^{T2} activity was supposed to mediate recombination and subsequent ko of the Kir4.1 channel recombined NG2 glia of this mouse line should be insensitive to $BaCl_2$. Unexpectedly, when analyzing recombined NG2 glia of Kir4.1 flox mice two populations of recombined NG2 glia were identified: i) Despite CreER^{T2} activity indicated by EYFP fluorescence some recombined NG2 glia showed a channel conductance at -130 mV of 13.52 ± 5.26 pA/mV that could be reduced to 1.61 ± 0.94 pA/mV upon $BaCl_2$ application (n = 35) (Fig. 5.3 A). As these characteristics were similar to those of recombined NG2 glia in control

mice these cells were termed Kir4.1 wild-type cells (Kir4.1 wt cells). ii) Those NG2 glia that showed a Kir conductance less than 6 pA/mV already before $BaCl_2$ application (1.46 ± 1.03 pA/mV, n = 49) were defined as Kir4.1 ko cells and termed Kir4.1 ko cells (Fig. 5.3 B). Nevertheless, even in these Kir4.1 ko cells $BaCl_2$ reduced the channel conductance measured at -130 mV to a small (1.00 ± 0.52 pA/mV, n = 49) but statistically significant extent.

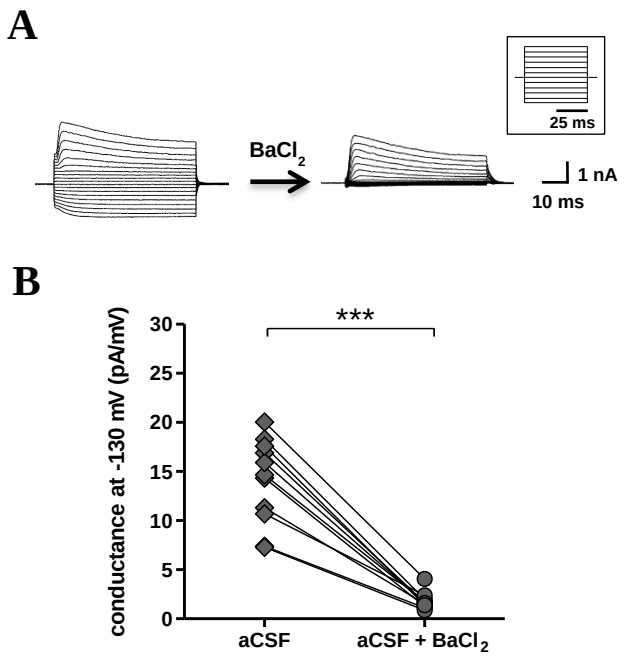

Fig. 5.2: Pharmacological and electrophysiological characterization of recombined NG2 glia in control mice.

A) Whole-cell current pattern of recombined NG2 glia evoked by de- and hyperpolarizing steps between -160 mV and +20 mV lasting for 50 ms before and after focal pressure application of the Kir channel blocker $BaCl_2$ (100 µM) (holding potential of -70 mV). Kir4.1 mediated currents evoked by applying hyperpolarizing voltage steps to -160 mV could be blocked by $BaCl_2$. **B)** The conductance of Kir4.1 channel activity decreased by 87% to less than 2 pA/mV in presence of $BaCl_2$. Wilcoxon rank test. n = 11. *** $p<0.001$.

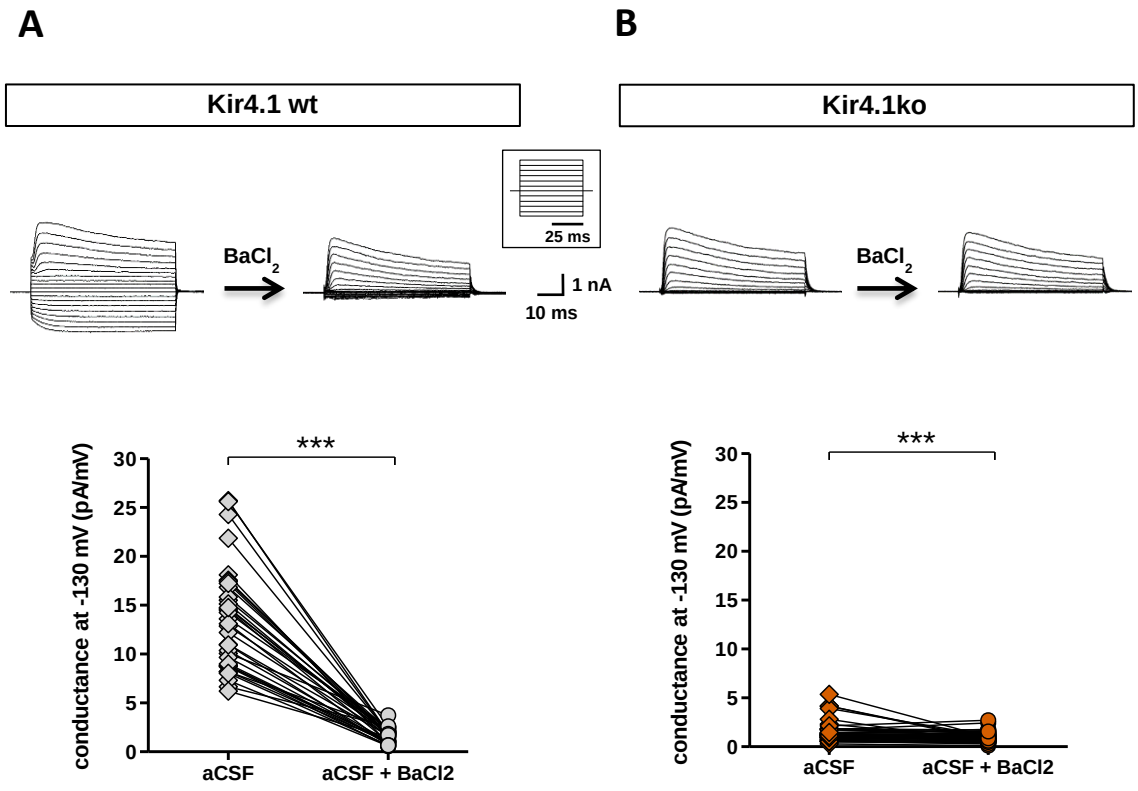

Fig. 5.3: Pharmacological and electrophysiological characterization of recombined NG2 glia in Kir4.1 flox mice.
Whole-cell current pattern of recombined NG2 glia evoked by de- and hyperpolarizing steps between -160 mV and +20 mV before and after application of the Kir channel blocker $BaCl_2$ (100 µM) (holding potential of -70 mV). **A**) Recombined NG2 glia showing a conductance of > 6 pA/mV at -130 mV were termed Kir4.1 wild-type (wt) cells (n = 35). **B)** Recombined NG2 glia with a conductance < 6 pA/mV were defined as Kir4.1 ko cells (n = 49). Wilcoxon rank test. *** p<0.001.

To further assess the presence (Kir4.1 wt cells) or absence (Kir4.1 ko cells) of Kir4.1 mRNA in recombined NG2 glia, cells were harvested from hippocampal slices to perform reverse transcription PCR (RT-PCR) from single cells (done by Dr. Gerald Seifert) (Fig. 5.4). Indeed, molecular analysis proved the presence of Kir4.1 mRNA in cells showing a conductance of more than 6 pA/mV (Kir.4.1 wt cells; 8/8 cells) and its absence in cells with less than 6 pA/mV conductance (Kir4.1 ko cells; 15/16 cells). These data demonstrated an incomplete ko of the Kir4.1 gene in Kir4.1 flox mice after $CreER^{T2}$ induced recombination by tamoxifen application.

For the following experiments recombined NG2 glia of Kir4.1 flox mice were categorized to either Kir4.1 ko or Kir4.1 wt cells according to their conductance at -130 mV (Kir4.1 ko cells < 6 pA/mV > Kir4.1 wt cells). All three groups (control, Kir4.1 wt and Kir4.1 ko cells) were treated separately for analysis in each experiment performed in this study.

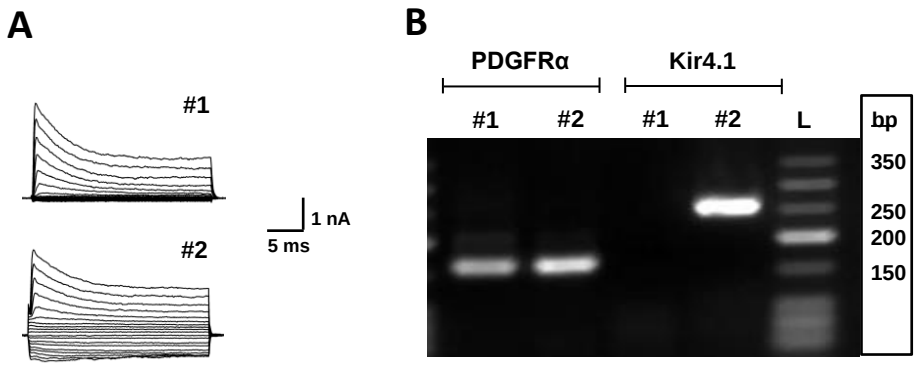

Fig. 5.4: Molecular analysis of recombined NG2 glia in Kir4.1 flox mice.
A) Whole-cell current pattern of two recombined NG2 glia that were harvested from slices of Kir4.1 flox mice and used for single-cell RT-PCR. **B)** Agarose gel of the products from the single-cell RT-PCR performed on cells shown in A). In NG2 glia defined as Kir4.1 ko cells (cell #1; conductance of < 6 pA/mV), the absence of Kir4.1 mRNA could be confirmed. In Kir4.1 wt cells (cell #2; conductance of > 6 pA/mV) the presence of Kir4.1 mRNA was proven. The identity of NG2 glia was verified by the presence of mRNA coding for the NG2 glia marker PDGFRα. L, low molecular weight DNA ladder; bp, base pairs.

5.1.2 Establishment of an efficient tamoxifen protocol

The efficiency of the tamoxifen protocol used (two injections of 1 mg tamoxifen per day for 5 consecutive days) to induce a ko of the K^+ channel Kir4.1 specifically in NG2 glia was evaluated electrophysiologically by the number of recombined NG2 glia showing a conductance of less than 6 pA/mV at a potential of -130 mV (Kir4.1 ko cells) among the total number of recombined NG2 glia (indicated by expressing EYFP fluorescence) patched in brain slices of one animal. In Kir4.1 flox mice injected at the age of p76 (N = 3) less than 20% of the cells characterized were lacking Kir4.1 (Fig. 5.5). Injection of younger mice (p25, N = 4; p35, N = 5) revealed a ko efficiency of up to 60%. Nevertheless, the variation of the ko efficiency between mice treated with the same protocol was evident. Keeping the time point of, other parameters of the tamoxifen protocol were optimized: Changes of the frequency of injections (once or twice per day for three or 10 consecutive days), the amount of tamoxifen used (1.5 - 2 mg) or the time period before experiments were conducted (three days up to five weeks after the last injection). The most promising protocol to achieve a high ko efficiency in parallel with a reduced stress level for the mice was a three days injection of 1.5 mg tamoxifen once per day (N = 3). Here, 76.67 ± 8.51% of all recombined NG2 glia were lacking Kir4.1 mediated currents.

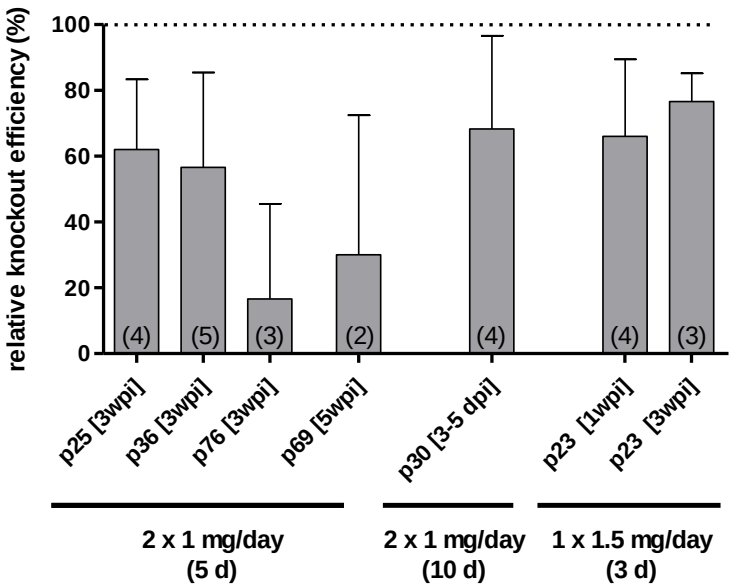

Fig. 5.5: Relative ko efficiency of different tamoxifen protocols applied.
Ko efficiency was assessed by the number of Kir4.1 ko cells (less than 6 pA/mV conductance at -130 mV) among all recombined NG2 glia patched per mouse. Mice were injected at different ages (p25-76) and analyzed three to five days post injection (dpi) or one up to five weeks post injection (wpi). The dose of tamoxifen varied between 1 mg tamoxifen twice a day (2 x 1 mg/day) for five or 10 consecutive days (5 d, 10 d) and 1.5 mg once a day for three consecutive days (1 x 1.5 mg/day (3 d). In all protocols, ko efficiency varied between mice. Number of mice is given in the bar graphs.

The patch-clamp technique allowed the evaluation of the tamoxifen induced ko on functional level in single cells. To further assess the ko of Kir4.1 on transcript level Dr. Gerald Seifert quantified the amount of Kir4.1 mRNA in recombined NG2 glia of the entire hippocampus with semiquantitative PCR. Three weeks after tamoxifen injection the hippocampus of control and Kir4.1 flox mice was dissected and hippocampal cells sorted by fluorescence activated cells sorting (FACS). Recombined NG2 glia were distinguishable from other cells by expression of the reporter protein EYFP (Fig.5.6 A). The fluorescence intensity detected at the EXFP specific wavelength of 527 nm was at least 10 times higher than backround fluorescence. To confirm the specificity of the sorted cell population representing recombined NG2 glia, semiquantitative PCR was performed. The sorted cells were tested for the presence of mRNA specifically expressed in NG2 glia (PDGFRα), neurons (Rbfox3), microglia cells (Aif1) and astrocytes (Aldh1L1) (Fig. 5.6 B). Less than 3% of the mRNA content was positive for the non-NG2 glia markers (Rbfox3: 0.79 ± 1.57%; Aif1: 1.11 ± 2.14%; AldH1L1: 0.12 ± 0.21%; N = 9 mice), identifying the sorted cells as being purely NG2 glia. Finally, the mRNA level of Kir4.1 was determined in these cells. Compared to recombined NG2 glia of control mice (n = 11) the mRNA level of Kir4.1 was reduced by 86.7% in Kir4.1 flox mice (N = 8) (Fig. 5.6 C).

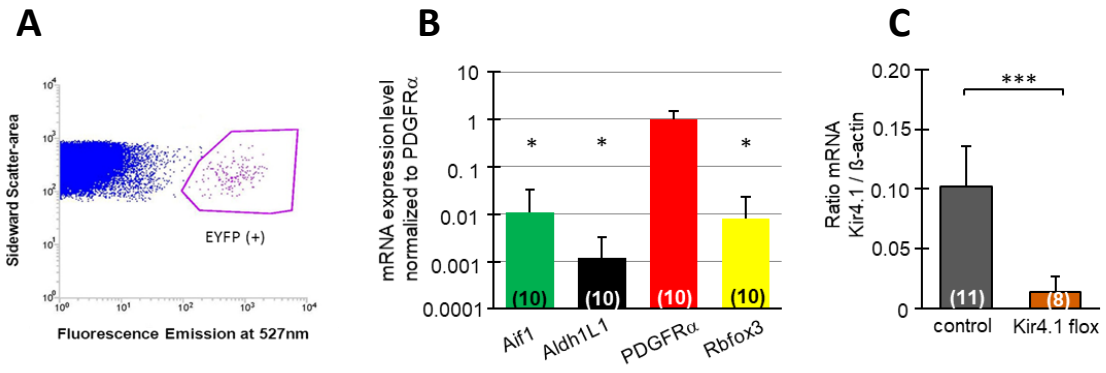

Fig. 5.6: Kir4.1 mRNA level in hippocampal NG2 glia.
A) Sideward scatter plot obtained from the FAC sorter. FAC sorted EYFP-positive cells from the hippocampus of Kir4.1 flox mice are indicated by the boxed area. Cells were sorted according to their fluorescence emission at 527 nm. **B)** Semiquantitative PCR confirmed specificity of FAC sorted cells being NG2 glia by detecting a high level of mRNA coding for the NG2 glia marker PDGFRα. Transcripts for astrocytes (Aldh1L1), neurons (Rbfox3) and microglia cells (Aif1) were almost absent. **C)** The ratio of Kir4.1 mRNA found in recombined NG2 glia and the housekeeping gene ß-actin (serving as internal standard) revealed a significant downregulation of Kir4.1 transcripts in recombined NG2 glia of Kir4.1 flox mice. t-test. Mean ± SD. Number of mice is given in parenthesis.

The recombination efficiency in control and Kir4.1 flox mice was investigated 4 and 8 weeks after tamoxifen injection by immunohistochemistry. Mouse tissue was fixed by intracardial perfusion with paraformaldehyde. Brains were cut with a vibratome into 40 µm thick coronal sections before being stained for the reporter protein EYFP and the NG2 glia marker PDGFRα (Fig. 5.7 A). The number of NG2 glia expressing the reporter gene EYFP and being positive for the NG2 glia marker PDGFRα were identified as recombined NG2 glia ($PDGFR\alpha^+EYFP^+$ cells) and were compared to the total number of NG2 glia ($PDGFR\alpha^+$ cells) in the hippocampal brain slice. Recombination 4 and 8 weeks after tamoxifen injection took place in 60-85 % of NG2-glia cells in both control and Kir4.1 flox mice (Fig. 5.7 B; Table 2). 2-way ANOVA, comparing genotype, time point of analysis and interaction of those, did not reveal any significant differences.

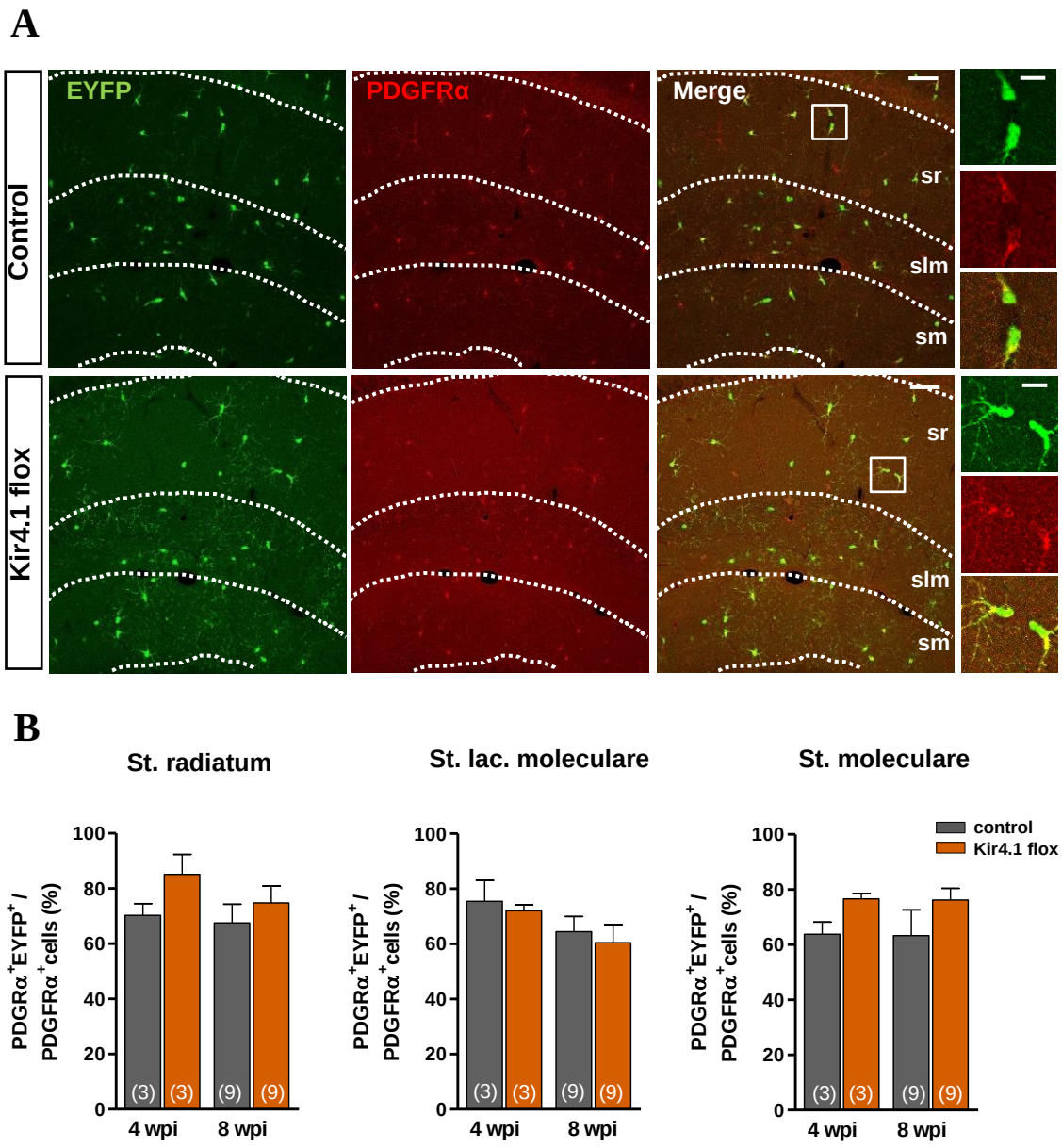

Fig. 5.7: Recombination efficiency in control and Kir4.1 flox mice.
A) Immunostainings for EYFP (green) and the NG2 glia marker PDGFRα (red) in coronal slices of the hippocampus of control and Kir4.1 flox mice. Boxed areas are shown at higher magnification on the right. Scale bar 60 µm and 15 µm (insets). **B)** Recombination efficiency is represented by the proportion of $EYFP^+PDGRa^+/PDGR\alpha^+$ cells 3 weeks and 8 weeks post injection (wpi) of tamoxifen. Recombination efficiency varied between 60-85%. Mean ± SEM. 2-way ANOVA with post-hoc Tukey test. sr, stratum radiatum; slm, stratum lacunosum moleculare; sm, stratum moleculare of the dentate gyrus. Number of mice is given in parenthesis in the bar graphs.

Table 2: Recombination efficiency in control and Kir4.1 flox mice.
Recombination efficiency was calculated by determining the number of cells positive for the reporter protein EYFP and the NG2 glia marker PDGFRα ($EYFP^+PDGR\alpha^+$ cells) among all NG2 glia ($PDGR\alpha^+$ cells) in the hippocampal slice. Mean ± SEM. 2-way ANOVA with post-hoc Tukey test. sr, stratum radiatum; slm, stratum lacunosum moleculare; sm, stratum moleculare of the dentate gyrus. wpi, weeks post injection. N, number of mice.

	Quantification	Mouse line	sr	slm	sm	N
4 wpi	**$PDGFR\alpha^+EYFP^+$/ $PDGFR\alpha^+$ cells (%)**	Control	70.31 ± 3.48	75.46 ± 6.19	63.78 ± 3.65	3
		Kir4.1 flox	85.14 ± 5.88	72.01 ± 1.83	76.61 ± 1.59	3
8 wpi	**$PDGFR\alpha^+EYFP^+$/ $PDGFR\alpha^+$ cells (%)**	Control	67.58 ± 6.33	64.43 ± 5.22	63.30 ± 8.78	9
		Kir4.1 flox	74.76 ± 5.76	60.48 ± 6.17	76.17 ± 4.05	9

Possible consequences of the Kir4.1 deletion on the density of hippocampal NG2 glia were assessed by counting the number of PDGFRα positive cells per area (mm^2) (Fig. 5.8; table 3). Indeed, comparing the NG2 glia population 4 and 8 weeks after tamoxifen injection revealed a time dependent decrease of PDGFRα positive cells in control mice in all three hippocampal subregions analyzed. The number of NG2 glia decreased at 8 wpi from 104.58 ± 2.00 cells per mm^2 in the stratum radiatum and 121.15 ± 6.03 cells per mm^2 in the stratum moleculare of the dentate gyrus to 60% in both subregions ($p = 0.008$ and $p = 0.005$, respectively). In the stratum lacunosum moleculare the decrease was about 55% ($p = 0.033$). In Kir4.1 flox mice a significant reduction to 78% was observed in the stratum moleculare of the dentate gyrus at the same time point of analysis ($p = 0.023$). Comparing the density of NG2 glia between control and Kir4.1 flox mice revealed no differences neither 4 wpi nor 8 wpi. These results indicate a developmental reduction of the NG2 glia density under normal (control) conditions that seemed to be attenuated in mice lacking the Kir4.1 channel in NG2 glia. A change in the proliferative activity of NG2 glia that could explain these observations 8 wpi was further investigated in chapter 5.4.

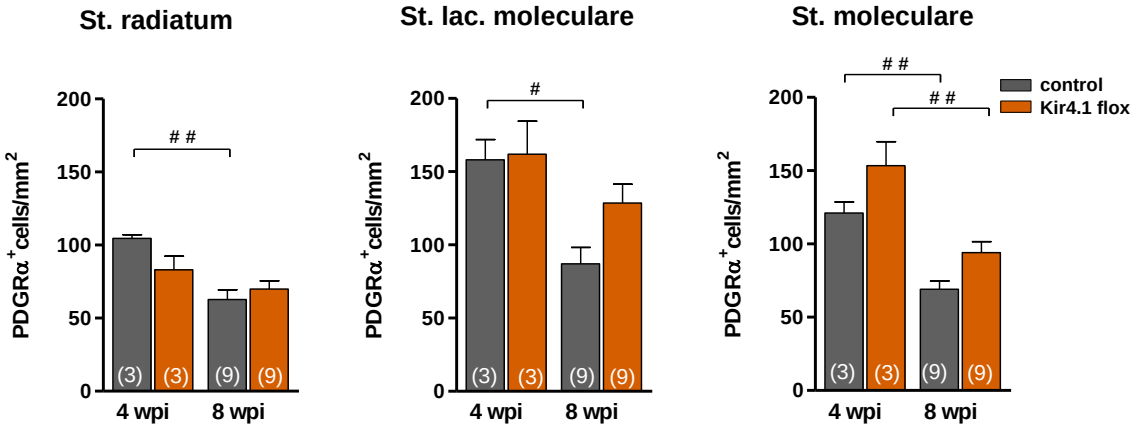

Fig. 5.8: NG2 glia populations in control and Kir4.1 flox mice.
The density of NG2 glia in the hippocampus of control and Kir4.1 flox mice was analyzed 4 and 8 weeks post tamoxifen injection and calculated by determining the number of cells being positive for the NG2 glia marker PDGRα per area (mm^2). Mean ± SEM. St., stratum; lac. lacunosum; St. moleculare, stratum moleculare of the dentate gyrus. 2-way ANOVA with post-hoc Tukey test. Number of mice is given in parenthesis in the bar graphs.

Table 3: NG2 glia population in control and Kir4.1 flox mice per mm^2.
Hippocampal NG2 glia population quantified by determingin the number of cells being positive for the NG2 glia marker PDGRα per area (mm^2). Control and Kir4.1 flox mice were analyzed 4 and 8 weeks post tamoxifen injection. Mean ± SEM. N, number of mice. wpi, weeks post injection. sr, stratum radiatum; slm, stratum lacunosum moleculare; sm, stratum moleculare of the dentate gyrus. 2-way ANOVA with post-hoc Tukey test. Double crosses (#) indicate statistical significant difference at different timepoints of analysis (4 wpi vs 8 wpi) within one group.

	Quantification	Mouse line	Sr	slm	sm	N
3 wpi	**PDGFRα⁺cells/ mm^2**	Control	104.58 ± 2.00#	158.01 ± 11.39#	121.15 ± 6.03#	3
		Kir4.1 flox	83.01 ± 7.62	161.86 ± 18.35	153.36 ± 13.38#	3
8wpi	**PDGFRα⁺ cells/ mm^2**	Control	62.69 ± 6.30	87.05 ± 10.56	69.05 ± 5.45	9
		Kir4.1 flox	69.86 ± 5.31	128.55 ±12.17	94.01 ± 7.06	9

5.2 Role of Kir4.1 in regulating passive membrane properties of NG2 glia

Kir4.1 channels are crucial to determine the membrane resistance and the membrane potential of NG2 glia. Blocking Kir channel activity in NG2 glia pharmacologically by $BaCl_2$ in rat hippocampal slices and the induction of a NG2 glia specific ko of Kir4.1 in a PDGFRα-CreER^{T2} mouse line revealed an increased membrane resistance and a depolarized membrane potential in NG2 glia (Chan et al., 2013a; Larson et al., 2018). To investigate if similar changes occur in the NG2-CreER^{T2} mouse line used in this study, membrane properties were compared between recombined NG2 glia of control and Kir4.1 flox mice. Therefore whole-cell patch-clamp recordings were performed on recombined NG2 glia 3-4 weeks post

tamoxifen injection. The presence or absence of Kir4.1 mediated currents and thus, the identification of a recombined NG2 glia being wild-type for Kir4.1 (Kir4.1 wt cells) or a ko cell (Kir4.1 ko cells) was determined by calculating the channel conductance at a voltage of -130 mV as described in section 5.1.1.

Recombined NG2 glia of control mice and Kir4.1 wt cells had a channel conductance of 10 to 23 pA/mV that was significantly higher compared to a conductance of less than 6 pA/mV determined in Kir4.1 ko cells (Fig. 5.9 A, B; table 4). According to the membrane potential that is dependent on the type and number of ions being able to pass the membrane, Kir4.1 wt cells (n = 55) and NG2 glia of control mice (n = 82) had a similar resting membrane potential (RMP) of about -80 to -90 mV, close to the K^+ equilibrium potential (Fig. 5.9 B; table 4). The membrane resistance (Rm) that reflects the density of open channels in the cell membrane was determined between -70 mV and -60 mV (holding potential of -70 mV) or between -80 mV and -70 mV (holding potential of -80 mV) and ranged between 30 and 115 MOhm (Fig. 5.9 C; Table 4). However, in NG2 glia lacking Kir4.1 channels (Kir4.1 ko cells, n = 128) these membrane properties were dramatically changed: The resting membrane potential was depolarized to -61 mV (Fig. 5.9 B, C; Table 4) and the membrane resistance was increased, reaching values above 1000 MOhm. Nevertheless, due to to technical limitations, the appropriate calculation of the membrane resistance of these high Ohmic cells was impossible. Thus Kir4.1 ko cells with an estimated membrane resistance of more than 3000 MOhm (10 out of 128 cells) were excluded from the analysis. The membrane capacitance (Cm) reflecting the size of the cell membrane was with 23 to 38 pF and not different between groups (Fig. 5.9 D; Table 4). These results are in line with previous studies, supporting the role of Kir4.1 in determining the membrane resistance and membrane potential of NG2 glia (Djukic et al., 2007; Kressin et al., 1995; Larson et al., 2018).

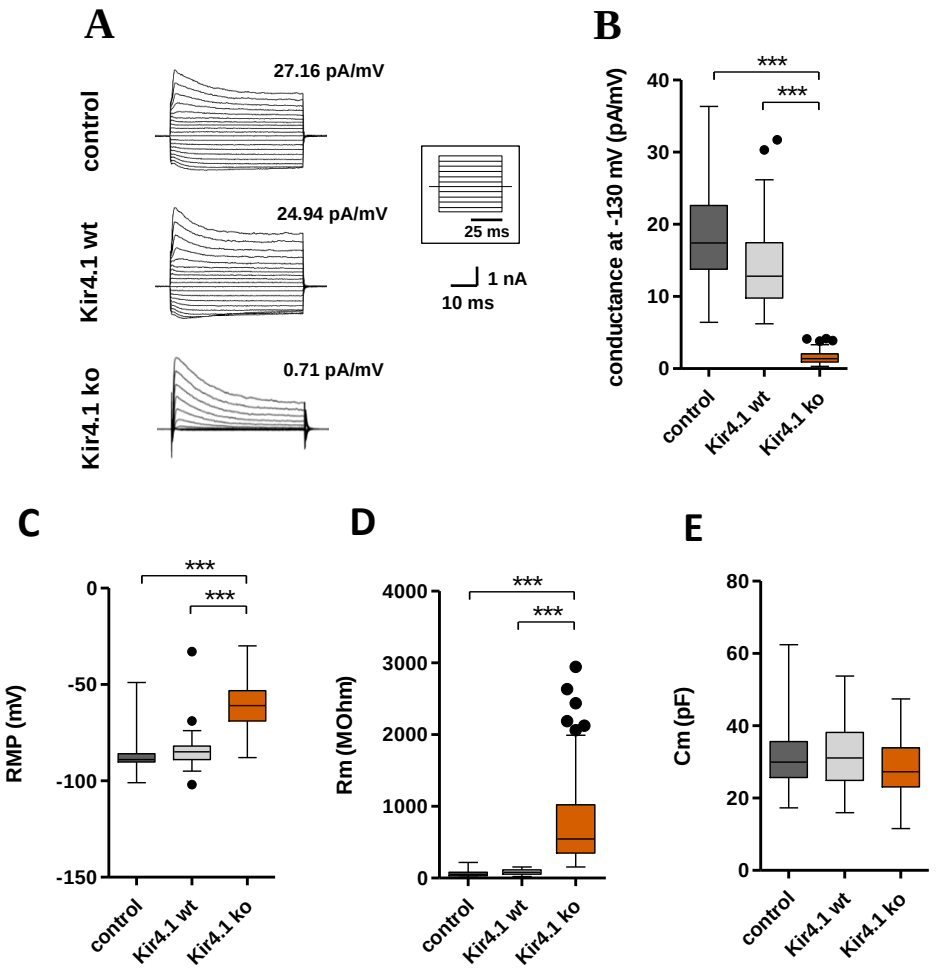

Fig. 5.9: Kir4.1 channels determine passive membrane properties of NG2 glia.
A) Representative whole-cell current patterns of recombined NG2 glia of control (control) and Kir4.1 flox mice (Kir4.1 wt, Kir4.1 ko) elicited by voltage steps ranging from -160 to +20 mV. The channel conductance at -130 mV is mentioned obove the respective current. **B)** NG2 glia of Kir4.1 flox mice showing less than 6 pA/mV conductance at -130 mV were considered as Kir4.1 ko cells, above as Kir4.1 wt cells. **C)** In the absence of the Kir4.1 channels the resting membrane potential (RMP) of NG2 glia was depolarized by about 20 mV and **D)** the membrane resistance (Rm) was 3 to 30-fold higher. **E)** The membrane capacitance (Cm) was indistinguishable between control and recombined NG2 glia of Kir4.1 flox mice. Kir4.1 ko cells: n = 128 (n = 118 for Rm); Kir4.1 wt cells: n = 55; control cells: n = 82. Kruskal-Wallis test with post-hoc Dunn´s test. Data is presented as tukey box-plots with median (central line), quartiles (25% and 75%; box) and percentiles (1.5 times the interquartile range). Outliers are shown as dots.

Table 4: Passive membrane properties of recombined NG2 glia of control and Kir4.1 flox mice.
RMP, resting membrane potential; Rm, membrane resistance; Cm, membrane capacitance. Data is given as median and interquartile range (quartile 25% – quartile 75%). Number of cells is given in square brackets.

	control	Kir4.1 wt	Kir4.1 ko
Conductance at -130 mV (pA/mV)	17.42 (13.78 – 22.62) [82]	12.81 (9.77 – 17.46) [55]	1.40 (0.93 – 2.05) [128]
RMP (mV)	-89 (-90 – -86) [82]	-85 (-89 – -82) [55]	-61 (-69 – -53) [128]
Rm (MOhm)	50.75 (32.69 – 81.75) [82]	81.22 (56.56 – 115.17) [55]	546.10 (348.94 – 1022.90) [118]
Cm (pF)	29.98 (25.68 – 35.66) [82]	31.09 (24.92 – 38.16) [55]	27.28 (23.09 – 33.89) [128]

5.3 Consequences of Kir4.1 deletion on NG2 glia excitability

In immature dentate granule cells (DGCs) Kir channels are expressed at very low levels resulting in a membrane resistance higher than in mature DGCs, subsequently causing an increased excitability upon neuronal input (Mongiat et al., 2009). To test if Kir4.1 similarly determines the excitability of NG2 glia, miniature postsynaptic potentials (mEPSPs) were recorded in recombined glia cells of control and Kir4.1 flox mice. mEPSPs represent responses upon single vesicular release of neurotransmitters from the pre-synapse. This release occurs by spontaneous fusion of single vesicles with the pre-synaptic membrane in the absence of an action potential and the subsequent influx of Ca^{2+} (Vautrin and Barker, 2003). In presence of TTX that prevents the opening of voltage gated Na^{+} channels and with that the generation of action potentials, whole-cell patch-clamp recordings were performed in recombined NG2 glia. In the current clamp mode, that records the physiological response upon neurotransmitter release as a shift in membrane potential, the shape and properties of mEPSP were highly different between Kir4.1 ko cells compared to Kir4.1 wt and control cells (Fig. 5.10; Table 5). In NG2 glia lacking the Kir4.1 channel, depolarizations of 1.37 to 2.24 mV were detected that were lasting up to 39 ms (n = 27) (Fig. 5.10 A-C, $p < 0.001$). In recombined NG2 glia showing Kir4.1 channel mediated K^{+} influx (control and Kir4.1 wt cells; n = 13 and n = 22, respectivly) mEPSPs only lasted about 2.8 - 4 ms and reached only half the magnitude. This is in line with experiments in which Kir4.1 channels where blocked with $BaCl_2$ (Chan et al., 2013). In presence of $BaCl_2$, mEPSPs of NG2 glia in the stratum radiatum of the CA1 region showed an increased amplitude and prolonged time constant of

voltage decay. Concomitantly, the rise time of mEPSPs measured in Kir4.1 ko cells was increased to 2.7 ms, compared to a rise time of around 0.8 - 1.1 ms in control and Kir4.1 wt cells (Fig. 5.10 D, $p < 0.001$). Thus, the Kir4.1 channel strongly influences the excitability of NG2 glia upon synaptic input.

To further estimate the number of synaptic contacts in control, Kir4.1 wt and Kir4.1 ko cells, the time interval between events (inter-event interval) was taken as a measure. Taking the number of events per time instead would be another method to determine the connectivity of NG2 glia. This approach, however, is more susceptible to the recording duration and might be less appropriate for NG2 glia in which the occurrence of events is rather small (Bergles et al., 2000; Lemon, 2016; Passlick et al., 2016). Interestingly the inter-event interval was significantly higher in Kir4.1 ko cells (40.03 s) compared to Kir4.1 wt cells (5.27 s). This observation indicates differences in connectivity between neurons and NG2 glia in Kir4.1 flox mice, with a lower number of synapses being established between neurons and in NG2 glia lacking Kir4.1 channels.

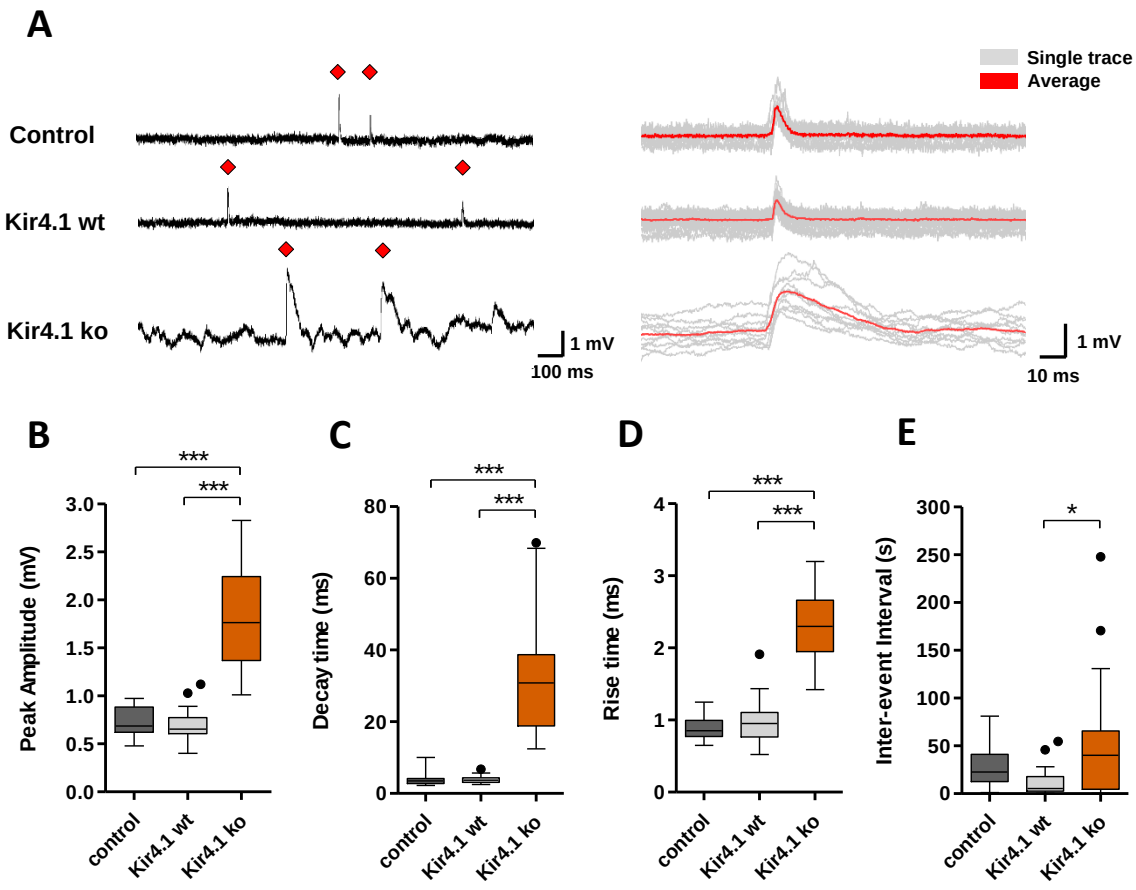

Fig. 5.10: Properties of mEPSPs in in recombined NG2 glia
A) Example traces of mEPSPs of control (top), Kir4.1 wt (middle) and Kir4.1 ko (bottom) cells (holding potential of -73 mV, liquid junction potential (LJP) corrected). Red diamonds indicate depolarizations upon single vesicular release. On the right: Corresponding superimposed single (grey) and average mEPSP traces (red; average of 10-29 events). **B-D)** In Kir4.1 ko cells peak amplitude, decay and rise time were increased compared to Kir4.1 wt and control cells. **E)** The inter-event interval of mEPSPs was higher in Kir4.1 ko cells compared to Kir4.1 wt cells. Control, n = 13; Kir4.1 wt cells, n = 22; Kir4.1 ko cells, n = 27. Kruskal-Wallis test with post-hoc Dunn´s test. Data is presented as tukey box-plots with median (central line), quartiles (25% and 75%; box) and percentiles (1.5 times the interquartile range). Outliers are shown as dots.

Table 5: Characteristics of miniature EPSPs in control, Kir4.1 wt and Kir4.1 ko cells.
Data is given as median and interquartile range (quartile 25% – quartile 75%). Number of cells is given in square brackets.

	control	Kir4.1 wt	Kir4.1 ko
Peak Amplitude (mV)	0.69 (0.62 – 0.88) [13]	0.65 (0.61 – 0.77) [22]	1.76 (1.37 – 2.24) [27]
Rise time (ms)	0.85 (0.77 – 0.99) [13]	0.95 (0.76 – 1.11) [22]	2.30 (1.94 – 2.66) [27]
Decay time (ms)	3.49 (2.80 – 4.18) [13]	3.68 (3.11 – 4.39) [22]	30.84 (18.80 – 38.68) [27]
Inter-event Interval (s)	22.71 (12.64 – 41.05) [13]	5.27 (2.74 – 17.86) [22]	40.03 (4.68 – 65.71) [27]

Both glutamatergic as well as GABAergic input result in a depolarization of NG2 glia (Jabs et al., 2005; Lin and Bergles, 2004a). To separate the glutamatergic input from GABAergic input, aCSF was supplemented with the GABA receptor blocker picrotoxin (150 µM) and applied to hippocampal brain slices of control and Kir4.1 flox mice via the perfusion system. Peak amplitude, decay time constant and rise time of mEPSPs recorded in recombined NG2 glia were not altered in the presence of picrotoxin (Fig. 5.11, Table 6). However, in Kir4.1 wt cells the inter-event interval of mEPSPs recorded in aCSF supplemented with picrotoxin was surprisingly reduced from around 10 s to 2 s, indicating an increase in mEPSP frequency in these cells. The inter-event interval and the frequency of mEPSPs in Kir4.1 ko cells and control cells was not affected by picrotoxin. Application of both picrotoxin and NBQX (10 µM), a blocker for AMPA and kainate receptors, fully abolished (Fig. 5.12).

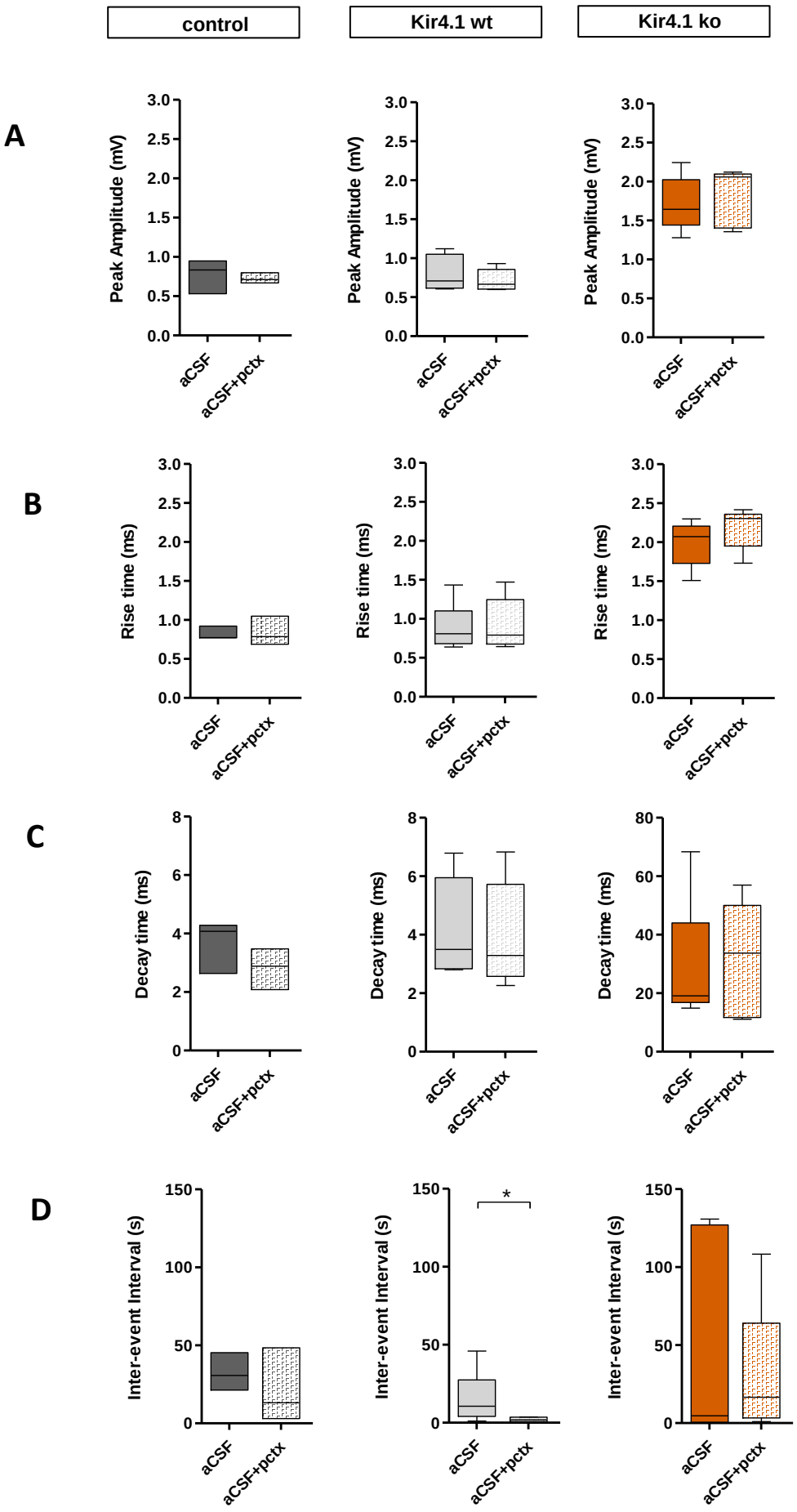
control
Kir4.1 wt
Kir4.1 ko
A
Peak Amplitude (mV)
B
Rise time (ms)
C
Decay time (ms)
D
Inter-event Interval (s)
*
aCSF
aCSF+pctx

Fig. 5.11: Characteristics of mEPSPs in presence or absence of GABA receptor blocker picrotoxin
In control, Kir4.1 wt and Kir4.1 ko cells **(A)** peak amplitude, rise **(B)** and decay time **(C)** of mEPSPs did not change in the presence of the GABA receptor blocker picrotoxin (150 µM). **D)** The inter-event interval of mEPSPs was reduced in the presence of picrotoxin in Kir4.1 wt cells (holding potential of -73 mV, LJP corrected). Mann-Whitney U-Test. control, n = 3; Kir4.1 wt cells, n = 6; Kir4.1 ko cells, n = 5. Data is presented as tukey box-plots with median (central line), quartiles (25% and 75%; box) and percentiles (1.5 times the interquartile range).

Table 6: Characteristics of mEPSP of recombined NG2 glia in control and Kir4.1 flox mice in the presence or absence of the GABA receptor blocker picrotoxin.
+ pctx, aCSF supplemented with picrotoxin (150 µM). Data is given as median and interquartile range (quartile 25% – quartile 75%). n, number of cells.

	Control		Kir4.1 wt		Kir4.1 ko	
	aCSF	**+ pctx**	**aCSF**	**+ pctx**	**aCSF**	**+ pctx**
Peak Amplitude (mV)	0.83 (0.53 - 0.95)	0.71 (0.67 -0.79)	0.71 (0.62 - 1.05)	0.67 (0.60 - 0.86)	1.64 (1.44 - 2.02)	2.06 (1.40 - 2.10)
Rise time (ms)	0.77 (0.77 - 0.92)	0.79 (0.69 - 1.05)	0.81 (0.68 - 1.10)	0.79 (0.68 -1.25)	2.07 (1.73 - 2.21)	2.3 (1.95 - 2.36)
Decay time (ms)	4.08 (2.64 - 4.28)	2.89 (2.09 - 3.48)	3.5 (2.78 - 5.95)	3.29 (2.58 - 5.72)	19.13 (16.84 - 44.02)	33.67 (11.69 - 50.06)
Inter-event Interval (s)	30.72 (21.36 - 45.32)	13.17 (3.01 - 48.42)	10.60 (4.03 - 27.42)	2.00 (0.85 - 3.56)	4.68 (0.54 - 127.10)	16.54 (3.37 - 64.10)
n	3		6		5	

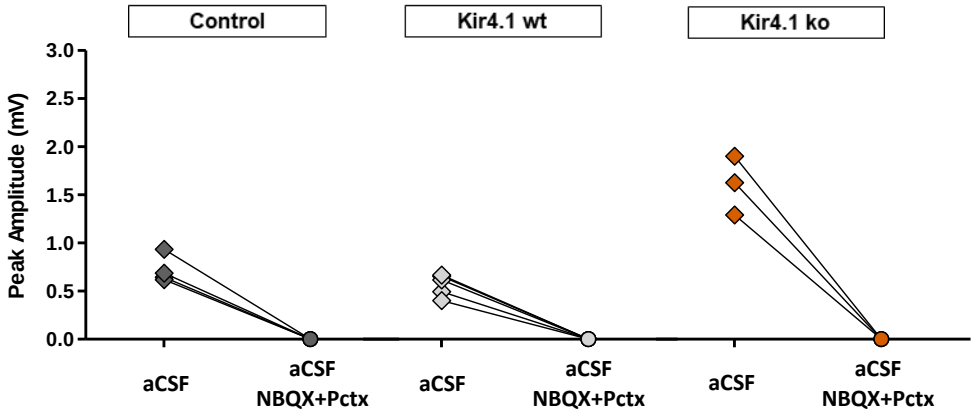

Fig. 5.12: Supression of mEPSPs by blocking AMPA -, kainate - and GABA receptors
Blocking AMPA and kainate receptors with NBQX (10 µM) and GABA receptors with picrotoxin (150 µM) abolished mEPSPs in control, Kir4.1 wt and Kir4.1 ko cells (holding potential of -73 mV, LJP corrected). control, n = 2; Kir4.1 wt cells, n = 3; Kir4.1 ko cells, n = 3. Each symbol represents the mean of all events detected in a cell.

5.4 Effect of Kir4.1 on NG2 glia proliferation

NG2 glia represent the largest proliferative cell population outside the neurogenic niches in the adult brain. With increase in age the expression level of the K^+ channel Kir4.1 increases concomitantly with a decline of the proliferative activity of these cells, extending cell cycle times from a few hours to days (Knutson et al., 1997; Kressin et al., 1995; Simon et al., 2011). If the deletion of Kir4.1 affected NG2 glia proliferation, immunostainings for the nuclear antigen Ki67 and for the reporter protein EYFP were performed 8 weeks after tamoxifen induced deletion of Kir4.1 (Fig. 5.12 A). Ki67 is present in all phases of the cell cycle except the resting state G0, thus representing an ideal marker to identify proliferative cells (Gerdes et al., 1984). When comparing the proportion of recombined proliferating NG2 glia being proliferative active ($Ki67^+EYFP^+$ cells) among all recombined cells ($EYFP^+$ cells), no difference between control mice and mice lacking Kir4.1 in NG2 glia (Kir4.1 flox mice) could be detected (Fig. 5.13 B; Table 7). Up to 8.8% of all recombined NG2 glia were proliferativing in the hippocampus of both mouse lines. In control mice, however, the proportion of $Ki67^+EYFP^+$/ $EYFP^+$ cells was reduced from 8.80 ± 1.98% to 2.31 ± 0.84% ($p = 0.037$) between stratum radiatum and stratum lacunosum moleculare. Interestingly, the total number of $Ki67^+$ cells per mm^2 ($Ki67^+$ cells/mm^2) in these mice was more than doubled in the stratum lacunosum moleculare compared to the stratum radiatum ($p = 0.038$). In Kir4.1 flox mice, the density of proliferating cells between hippocampal subregions was similar. Compared to control, however, the number of $Ki67^+$ cells per mm^2 was increased in Kir4.1 flox mice (12.60 ± 1.47 cells per mm^2 vs 8.00 ± 1.04 cells per mm^2, $p = 0.038$) (Fig. 5.12 B; Table 7).

These results imply that the loss of Kir4.1 in NG2 glia do not play a dominant role in regulating the proliferative activity of NG2 glia. However, the differences between stratum radiatum and stratum lacunosum moleculare as observed in control mice seem to be compensated in Kir4.1 flox mice.

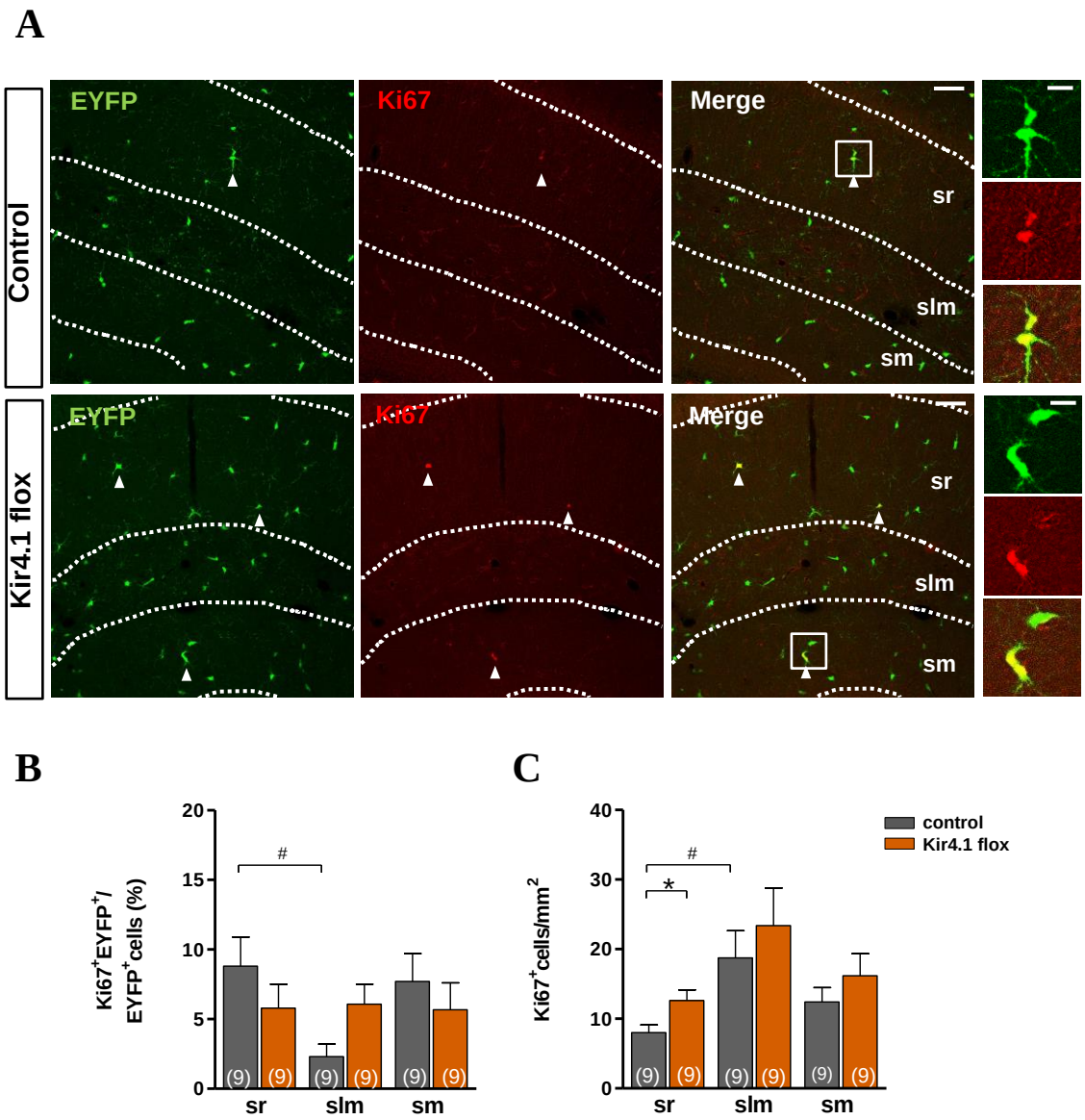

Fig. 5.13: Proliferation of NG2 glia is not affected in Kir4.1 flox mice.
A) Coronal sections of the hippocampus of control and Kir4.1 flox mice immunostained with EYFP (green) and nuclei antibody Ki67 (red). Double labeling of $EYFP^+$ and $Ki67^+$ cells is indicated by arrowheads. Boxed areas are shown at higher magnification on the right. Scale bar 60 µm and 15 µm (insets). **B)** Number of $Ki67^+EYFP^+$ cells among all $Ki67^+$ cells was similar in control and Kir4.1 flox mice, whereas in control mice a statistically significant reduction in the slm compared to the sr was observed. **C)** The total number of $Ki67^+$ cells was increased in the sr of Kir4.1 flox mice compared to control mice and in control mice compared to slm and sr. Mean ± SEM. Statistically significant differences are indicated as follows: * between genotypes within one hippocampal subregion (Mann-Whitney U Test); # between hippocampal subregions within one genotype (Kruskal-Wallis test with post-hoc Dunn´s test). sr, stratum radiatum; slm, stratum lacunosum moleculare; sm, stratum moleculare of the dentate gyrus. Number of mice is given in parenthesis in the bar graphs.

Table 7: Number of proliferative active cells in the hippocampus of control and Kir4.1 flox mice.
Percentage of all recombined cells proliferating ($Ki67^+EYFP^+$ cells) among all recombined NG2 glia ($EYFP^+$ cells). The total amount of proliferating cells was determined per mm^2. Mean ± SEM. Significant differences are indicated as follows: * between genotypes within one hippocampal subregion (Mann-Whitney U Test); # between hippocampal subregions within one genotype (Kruskal-Wallis test with post-hoc Dunn´s test). sr, stratum radiatum. slm, stratum lacunosum moleculare. sm, stratum moleculare of the dentate gyrus. N, number of mice.

Quantification	Mouse line	sr	slm	sm	N
$Ki67^+EYFP^+$/ $EYFP^+$cells (%)	Control	8.08 ± 1.98#	2.31 ± 0.84#	7.71 ± 1.89	9
	Kir4.1 flox	5.79 ± 1.62	6.07 ± 1.35	5.67 ± 1.83	9
$Ki67^+$ cells/mm^2	Control	8.00 ± 1.04*#	18.74 ± 3.68#	12.42 ± 1.93	9
	Kir4.1 flox	12.60 ± 1.47	23.37 ± 5.12	16.19 ± 2.97	9

5.5 Effect of Kir4.1 on NG2 glia differentiation into oligodendrocytes

After birth most NG2 glia in white matter differentiate into myelinating oligodendrocytes that wrap axons with myelin sheaths, allowing signal transduction to be fast and efficient (Baumann and Pham-Dinh, 2001; Dimou et al., 2008). How differentiation of NG2 glia into oligodendrocytes is triggered is not clear. To test if the ability of NG2 glia to differentiate into oligodendrocytes was affected in the hippocampus upon deletion of Kir4.1 at 8 weeks after tamoxifen induced ko, coronal sections of fixed brains were stained for the oligodendrocyte marker GSTpi and the reporter protein EYFP (Fig. 5.14 A). The proportion of oligodendrocytes originating from recombined NG2 glia ($GSTpi^+EYFP^+$ cells) among all cells positive for GSTpi was analyzed. Within the stratum radiatum and the stratum lacunosum moleculare no difference between control mice and mice lacking Kir4.1 in NG2 glia was observed (Fig. 5.14 B; Table 8). The proportion of double positive cells ($GSTpi^+EYFP^+$ cells) for both genotypes was between 5 and 10% in the stratum radiatum and 24 to 37% in the stratum lacunosum moleculare. Only in the stratum moleculare of the dentate gyrus the proportion of recombined NG2 glia being positive for $GSTpi^+$ was significantly increased comparing in Kir4.1 flox mice vs control (27.00 ± 2.84% vs 15.94 ± 2.72%; $p = 0.022$). The total number of oligodendrocytes in the stratum radiatum, stratum lacunosum moleculare and stratum moleculare of the dentate gyrus was unaltered between genotypes (Fig. 5.14 C, Table 8). However, between hippocampal subregions differences in both, the number of $GSTpi^+EYFP^+$ cells among all $GSTpi^+$cells and the total number of $GSTpi^+$ cells per area were detected in both genotypes. In the stratum lacunosum moleculare the proportion of recombined NG2 glia being positive for $GSTpi^+$ (control: $p = 0.04$; Kir4.1 flox: $p = 0.03$) and the density of $GSTpi^+$ cells per area (control and Kir4.1 flox: $p < 0.001$) was several fold higher compared to the stratum radiatum in both mouse lines. A significant upregulation of

double positive NG2 glia ($GSTpi^+EYFP^+$ cells/$GSTpi^+$cells; p = 0.023) in Kir4.1 flox mice and the density of $GSTpi^+$cells in both, Kir4.1 flox (p = 0.012) and control mice (p = 0.041) were observed in the stratum moleculare of the dentate gyrus compared to stratum radiatum. These results suggest that differentiation of NG2 glia into oligodendrocytes was not dependent on the presence of their Kir4.1 gene.

To exclude unspecific binding of the oligodendrocyte marker GSTpi to undifferentiated NG2 glia, fixed brain slices of NG2-EYFPki mice were stained. In this mouse line the expression of EYFP is driven by the NG2 promoter (Karram et al., 2008). After differentiation into oligodendrocytes and the concomitant downregulation of NG2 promoter activity, EYFP expression declines. However, in contrast to the NG2-EYFPki mouse line, the expression of the reporter protein EYFP in NG2 glia of Kir4.1 flox and control mice can be used to track the fate of recombined NG2 glia. Once $CreER^{T2}$ was able to mediate recombination the expression of the reporter protein EYFP under the control of the Rosa 26 promoter is constantly driven, independent of the differentiation state of the recombined cell (Huang et al., 2014). Oligodendrocytes originating from recombined NG2 glia are EYFP positive as shown in this study (Fig. 5.14). Indeed, in slices of NG2-EYFPki mice, co-localization of both EYFP and the oligodendrocyte marker GSTpi was not detected (Fig. 5.15). These results confirm the specificity of the GSTpi antibody for oligodendrocytes and approve the NG2-$CreER^{T2}$ mouse line as a reliable tool to track the fate of NG2 glia.

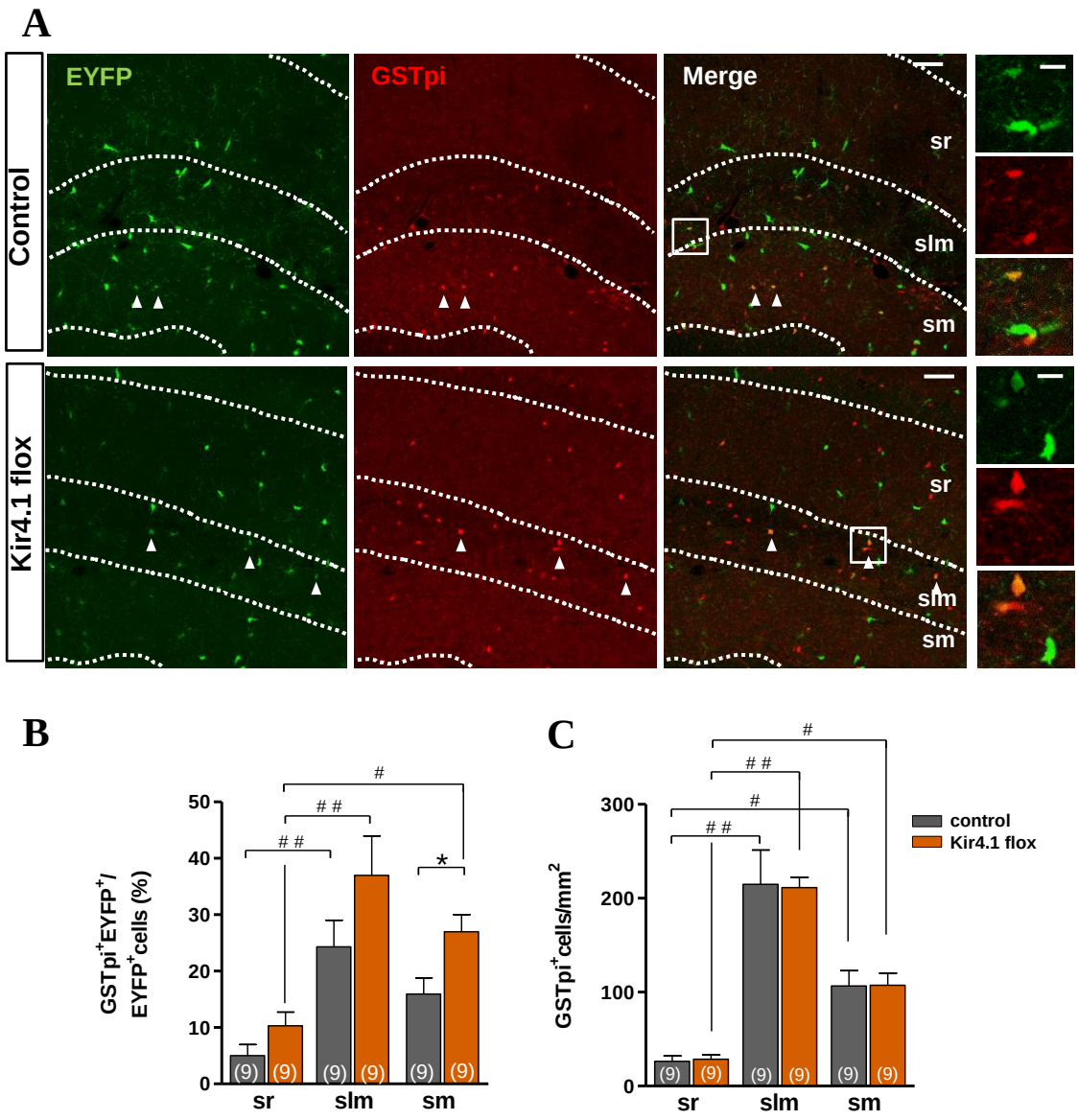

Fig. 5.14: In Kir4.1 flox mice, differentiation of recombined NG2 glia into oligodendrocytes was increased in the stratum moleculare of the dentate gyrus.
A) Coronal sections of the hippocampus of control and Kir4.1 flox mice were immunostained for EYFP (green) and the oligodendrocytic marker GSTpi (red). Double labeling of $EYFP^+$ and $GSTpi^+$ cells is indicated by arrowheads. Boxed areas are shown at higher magnification on the right. Scale bar 60 µm and 15 µm (insets). **B)** The proportion of recombined NG2 glia ($EYFP^+$) that differentiate into oligodendrocytes ($EYFP^+$ $GSTpi^+$cells) was increased in sm but not in sr and slm**. C)** The density of $GSTpi^+$ cells was not different between genotypes and hippocampal subregions. Mean ± SEM. Significant differences are indicated as follows: * between genotypes (Mann-Whitney U Test); # between hippocampal subregions within one genotype (Kruskal-Wallis test with post-hoc Dunn´s test). sr, stratum radiatum. slm, stratum lacunosum moleculare. sm, stratum moleculare of the dentate gyrus. Number of mice is given in parenthesis in the bar graphs.

Table 8: Density of hippocampal GSTpi$^+$ oligodendrocytes of control and Kir4.1 flox mice.
Percentage of recombined NG2 glia (EYFP$^+$) that differentiated into oligodendrocytes (GSTpi$^+$EYFP$^+$ cells) among all recombined NG2 glia. The desntiy of oligodendrocytes was determined per mm^2. Mean ± SEM. Significant differences are indicated as follows: * between genotypes (Mann-Whitney U Test); # between hippocampal subregions within one genotype (Kruskal-Wallis test with post-hoc Dunn´s test). sr, stratum radiatum. slm, stratum lacunosum moleculare. sm, stratum moleculare of the dentate gyrus. N, number of mice.

Quantification	Mouse line	sr	slm	sm	N
GSTpi+EYFP+/ EYFP+cells (%)	Control	5.01 ± 1.84$^{\#}$	24.32 ± 4.43$^{\#}$	15.94 ± 2.72*	9
	Kir4.1 flox	10.30 ± 2.31$^{\#}$	36.99 ± 6.58$^{\#}$	27.00 ± 2.84$^{\#}$	9
GSTpi+ cells/mm2	Control	26.44 ± 5.43$^{\#}$	214.92 ± 34.27$^{\#}$	106.67 ± 15.37$^{\#}$	9
	Kir4.1 flox	28.50 ± 4.65$^{\#}$	211.44 ± 10.22$^{\#}$	107.48 ± 11.86$^{\#}$	9

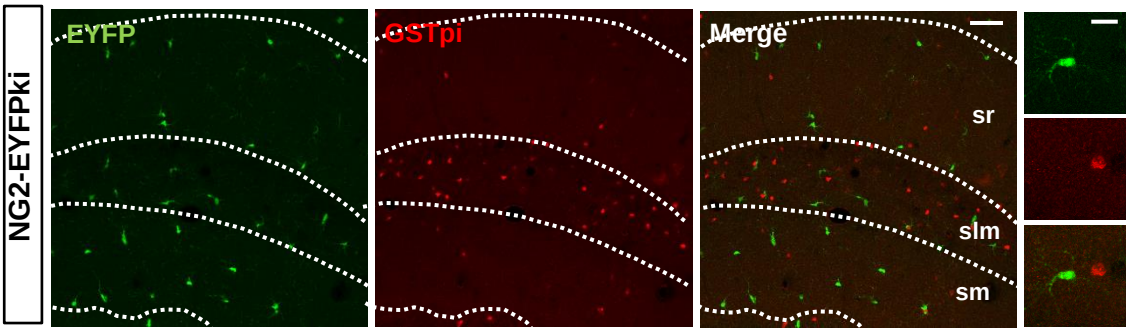

Fig. 5.15: Specificity of the oligodendrocyte marker GSTpi.
Coronal sections of the hippocampus of a NG2-EYFPki mouse were stained for EYFP (green) and the oligodendrocyte marker GSTpi (red). Boxed areas are shown at higher magnification on the right. Scale bar 60 µm and 15 µm (insets). No-colocalization of undifferentiated NG2 glia (EYFP$^+$) with the oligodendrocyteic marker GSTpi (EYFP$^+$ GSTpi$^+$cells) was detected. sr, stratum radiatum. slm, stratum lacunosum moleculare. sm, stratum moleculare of the dentate gyrus. N = 1, n = 2 slices

5.6. Impact of Kir4.1 on hippocampal myelination

Next, the efficiency of myelination was quantified in mice missing Kir4.1, 8 weeks post tamoxifen injection. The immunoreactivity of hippocampal brain slices for myelin basic protein (MBP) antibody was used as an indication for the amount of myelin produced as this protein represents one of the major myelin proteins that is responsible for the compaction of myelin (Baumann and Pham-Dinh, 2001; Readhead et al., 1987). To reduce variability within the staining procedure, fixed brain slices of control and Kir4.1 flox mice were stained and imaged in parallel. Intensity values of grey levels were divided by the analyzed area in each hippocampal subregion and normalized to the intensity recorded in the stratum lacunosum moleculare of Kir4.1 flox mice. Surprisingly, in mice lacking Kir4.1 in NG2 glia, MBP immunoreactivity was significantly increased in all 3 hippocampal subregions analyzed, compared to control mice. In strata radiatum and moleculare of the dentate gyrus this increase

was about 3-fold, in the stratum lacunosum moleculare abou 2.5-fold ($p < 0.001$) (Fig. 5.16). In both, control and Kir4.1 flox mice the highest MBP immunoreactivity was detected in the stratum lacunosum moleculare. These observations indicate that the deletion of Kir4.1 in NG2 glia affected the expression of MBP by oligodendrocytes. It needs to be considered that MBP is only expressed by oligodendrocytes on the protein level but can be found on the transcript level in NG2 glia (Ye et al., 2003). The same applies to the myelin associated glycoprotein (MAG). This protein, which is thought to be involved in initiation and maintenance of myelination, exists in NG2 glia only on the transcript level (Diers-Fenger et al., 2001; Ye et al., 2003). To evaluate possible changes on the amount of MBP and MAG mRNA in recombined NG2 glia of Kir4.1 flox mice, semiquantitative PCR was performed by Dr. Gerald Seifert, three weeks after injection of tamoxifen. Recombined NG2 glia of both control and Kir4.1 flox mice were FAC sorted according to their expression of the reporter protein EYFP that was indicating CreER^{T2} activity. Semiquantitative PCR revealed an upregulation of MBP (54%) and MAG (32%) transcripts in cells lacking Kir4.1, compared to recombined NG2 glia of control mice (Fig. 5.17). These findings indicate that in NG2 glia, the expression level of MAG and MBP mRNA is affected by Kir4.1 channel expression. Further it seems that Kir4.1 in NG2 glia plays a role in regulating myelination.

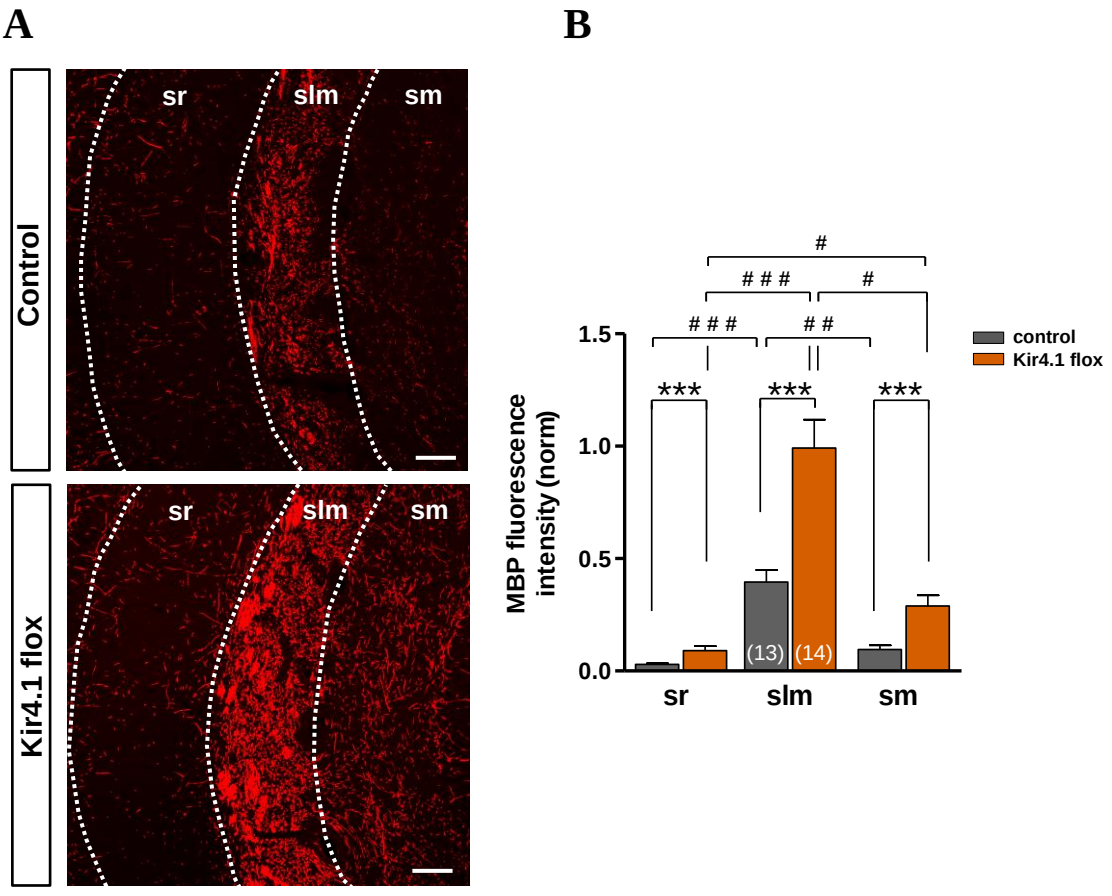

Fig. 5.16: Myelination in the hippocampus of control and Kir4.1 flox mice.
A) Coronal sections of the hippocampus of control and Kir4.1 flox mice were immunostained for MBP (myelin basic protein, red) 8 weeks post tamoxifen injection. **B)** MBP staining intensity was quantified and normalized to the MBP intensity detected in the slm of Kir4.1 flox mice. In sr, slm and sm, the MBP intensity was increased in Kir4.1 flox mice compared to control. Comparing all 3 hippocampal subregions revealed the highest MBP immunoreactivity in the slm in both mouse lines. Mean ± SEM. Significant differences are indicated as follows: * between genotypes within one hippocampal subregion (t-test); # between hippocampal subregions within one genotype (1-way ANOVA with post-hoc Tukey test). sr, stratum radiatum; slm, stratum lacunosum moleculare; sm, stratum moleculare of the dentate gyrus. Number of mice is given in parenthesis in the bar graphs.

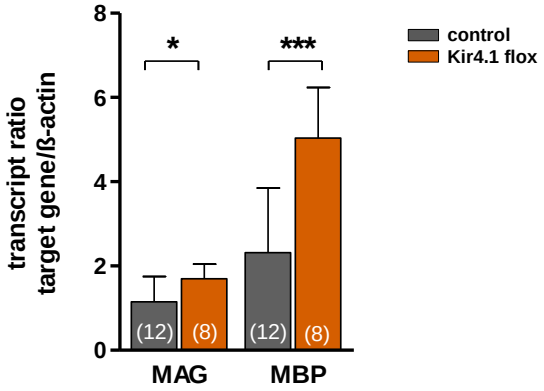

Fig. 5.17: Upregulation of MAG and MBP transcripts in recombined NG2 glia of Kir4.1 flox mice.
Semiquantitative PCR of FAC sorted NG2 glia revealed an upregulation of gene transcript for MAG and MBP. Transcript levels are normalized to the housekeeping gene ß-actin (serving as an internal standard). Mean ± SEM. t-test. MAG, myelin associated protein. MBP, myelin basic protein. sr, stratum radiatum. slm, stratum lacunosum moleculare. sm, stratum moleculare of the dentate gyrus. Number of mice is given in parenthesis in the bar graphs.

5.7 Short-term synaptic plasticity at the Schaffer collateral - NG2 glia synapse

Synaptic transmission is a dynamic process that is influenced by different mechanisms on short- and long-time scales. Changes on short time scales, called short term plasticity, include changes of the probability of neurotransmitters to be released into the synaptic cleft (Abbott and Regehr, 2004). To investigate if the release probability at the neuron-NG2 glia synapse is affected in absence of Kir4.1 in NG2 glia, paired pulse recordings were performed in hippocampal brain slices. Minimal stimulation of Schaffer collaterals with a monopolar electrode evoked excitatory postsynaptic currents (eEPSCs) in recombined NG2 glia of control and Kir4.1 flox mice (Fig. 5.18 A). The mean eEPSC amplitudes evoked upon two consecutive stimulation pulses were used to calculate the paired pulse ratio (amplitude 2/amplitude 1) that is indicative for the release probability at a synapse (Abbott and Regehr, 2004; Zucker and Regehr, 2002). The mean eEPSC amplitudes thereby represent the average

response of a cell to a stimulus pulse, including stimulations without eliciting a response (called “failures”). At synapses of neuron - recombined NG2 glia in control and Kir4.1 flox mice, a paired pulse ratio of > 1 was determined (paired pulse facilitation), indicative of a low release probability at these synapses (Fig. 5.18 B; Table 9). Nevertheless, at both, Kir4.1 ko and Kir4.1 wt synapses of Kir4.1 flox mice, paired pulse facilitation was, with a paired pulse ratio of 1.49 to 1.67, significantly lower as compared to the facilitation observed in recombined NG2 glia of control mice with a paired pulse ratio of 2.65 ($p = 0.008$ and $p = 0.037$, respectively). These results imply a slightly increased release probability at neuron-NG2 glia synapses in Kir4.1 flox mice. Interestingly when GABAergic input was blocked by picrotoxin (150 µM), the release probability was similar in control and Kir4.1 flox mice. Comparing the kinetic properties of EPSCs evoked in control, Kir4.1 wt and ko cells did not reveal differences between groups, neither in presence nor in absence of the GABA receptor blocker. The rise time varied between 0.28 ms and 0.58 ms and the decay time constant between 0.54 ms and 2.66 ms (Fig. 5.18 C, D; Table 9). This led to the assumption that in Kir4.1 flox mice the degree of facilitation and hence the release probability at the neuron-NG2 glia synapse might be influenced by GABAergic input. However, this input is weaker compared to the glutamatergic input as the decay time constant was not significantly different in presence or absence of the GABA receptor blocker picrotoxin. In light of previous experiments done in our and other labs the decay time constant highly differs between AMPA receptors (1-5 ms) and GABA receptor (around 20 ms) mediated currents, making AMPA or GABA receptor mediated input distinguishable from one another (Jabs et al., 2005; Lin and Bergles, 2004a).

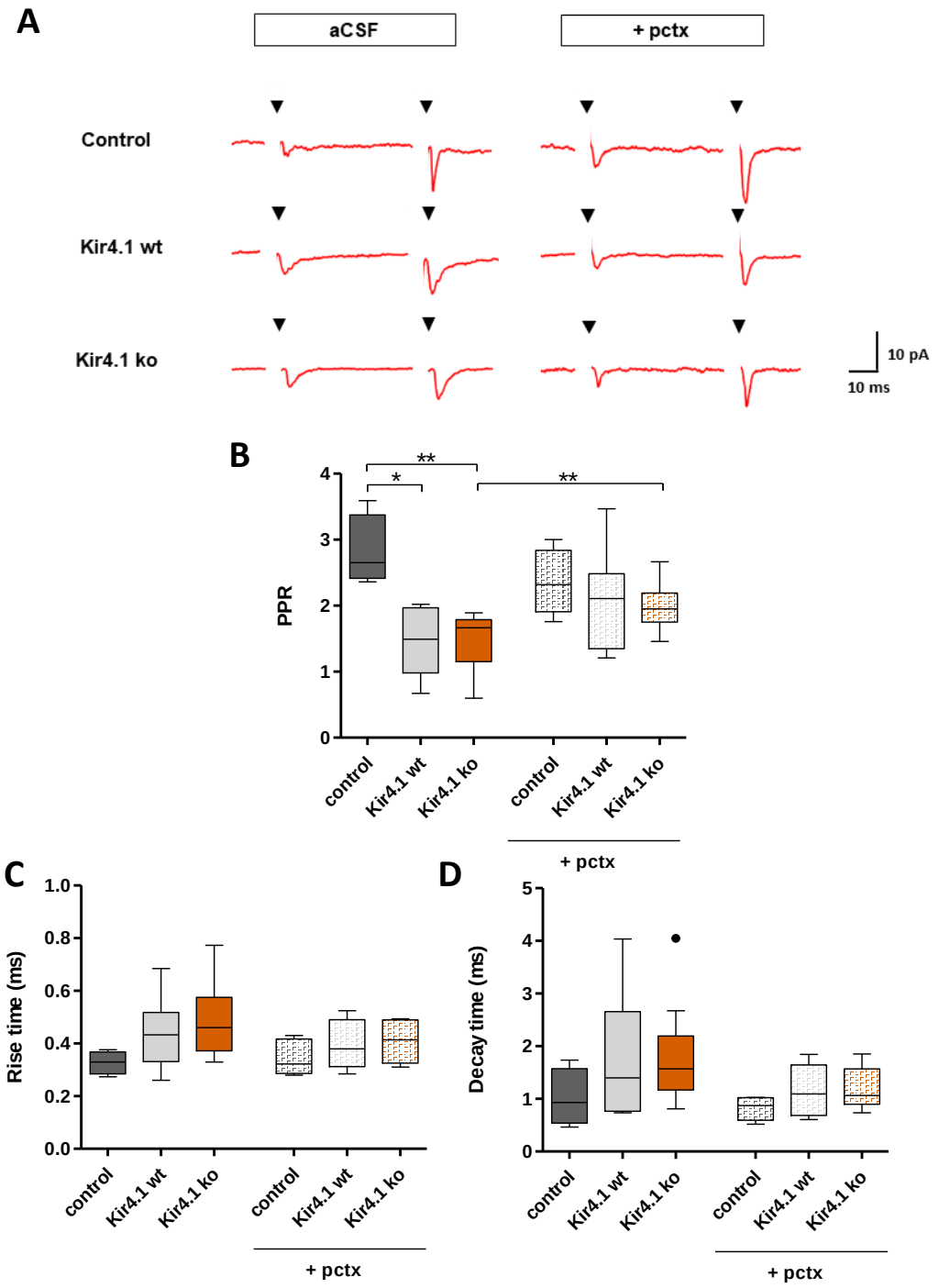

Fig.5.18: Characteristics of eEPSCs in recombined NG2 glia during Schaffer collateral stimulation
A) Average time course of current responses from recombined NG2 glia of control (control) and Kir4.1 flox mice (Kir4.1 wt, Kir4.1 ko) to paired pulse stimulation of Schaffer collaterals (inter-stimulus interval of 50 ms) in absence and presence of the GABA receptor blocker picrotoxin (150 µM; +pctx) (holding potential of -80 mV). Stimulation pulse is indicated by black triangles. **B)** Paired pulse ratio (PPR) was decreased in Kir4.1 flox mice compared to control mice. In presence of picrotoxin no difference was detected between groups. **C)** The rise time and **D)** decay time of eEPSCs evoked in recombined NG2 glia did not change, neither in presence or in the absence of picrotoxin nor between control and Kir4.1 flox mice. Kruskal-Wallis test with post-hoc Dunn´s test (between groups), Mann-Whitney U Test (aCSF vs aCSF + pctx). aCSF: control, n = 4; Kir4.1 wt cells, n = 6; Kir4.1 ko cells, n = 12. aCSF + picrotoxin: control, n = 5; Kir4.1 wt cells, n = 8; Kir4.1 ko cells, n = 7. Data is presented as tukey box-plots with median (central line), quartiles (25% and 75%; box) and percentiles (1.5 times the interquartile range).

Table 9: Properties of Schaffer collateral induced EPSCs in recombined NG2 glia in the absence or presence of picrotoxin.
PPR, paired pulse ratio. + pctx, aCSF supplemented with picrotoxin (150 µM). Data is given as median and interquartile range (quartile 25% – quartile 75%). n, number of cells.

	control		Kir4.1 wt		Kir4.1 ko	
	aCSF	**+ pctx**	**aCSF**	**+ pctx**	**aCSF**	**+ pctx**
PPR	2.65 (2.41 – 3.38)	2.32 (1.90 – 2.84)	1.49 (0.98 – 1.97)	2.11 (1.35 – 2.48)	1.67 (1.15 – 1.79)	1.95 (1.75 – 2.19)
Rise time (ms)	0.33 (0.28 – 0.42)	0.32 (0.29 – 0.41)	0.43 (0.33 – 0.52)	0.38 (0.31 – 0.49)	0.46 (0.37 – 0.58)	0.41 (0.33 – 0.49)
Decay time (ms)	0.93 (0.54 – 1.57)	0.87 (0.59 – 1.02)	1.39 (0.77 – 2.66)	1.09 (0.69 – 1.56)	1.57 (1.17 – 2.19)	1.07 (0.90 – 1.57)
n	4	5	6	8	12	7

5.8 Long-term potentiation in Kir4.1 deficient mice

As NG2 glia lacking Kir4.1 showed drastic changes in their membrane properties and were highly excitable upon neuronal input, the role of NG2 glia within the neuronal network might be emphasized in Kir4.1 flox mice. To investigate possible changes of neuronal network activity, field excitatory postsynaptic potentials (fEPSPs) were recorded in the CA1 region of the stratum radiatum of the hippocampus (experiments performed by Dr. Anne Boehlen). Schaffer collaterals were stimulated by a bipolar stimulation electrode and fEPSP were recorded with an aCSF filled recording electrode (Fig. 5.19 A). The excitability of hippocampal slices of control and Kir4.1 flox mice were assessed by analyzing the initial slope of the fEPSP upon increasing stimulation intensities between 20 and 500 µA (Fig. 5.19 B, C). No difference in the input- output relation between slices of control and Kir4.1 flox mice were detected. The stimulus intensity to evoke half-maximum of a fEPSP was similar between slices of control (52.69 ± 4.7 µA; n = 13 slices) and Kir4.1 flox mice (48.43 ± 3.1 µA; n = 35 slices) (Fig. 5.19 D). Thus, a ko of Kir4.1 in NG2 glia seemed not to affect neuronal excitability in the stratum radiatum of the hippocampus. For the following experiments the stimulation intensity was individually set to 50% of the stimulation intensity needed to induce maximal fEPSPs amplitudes.

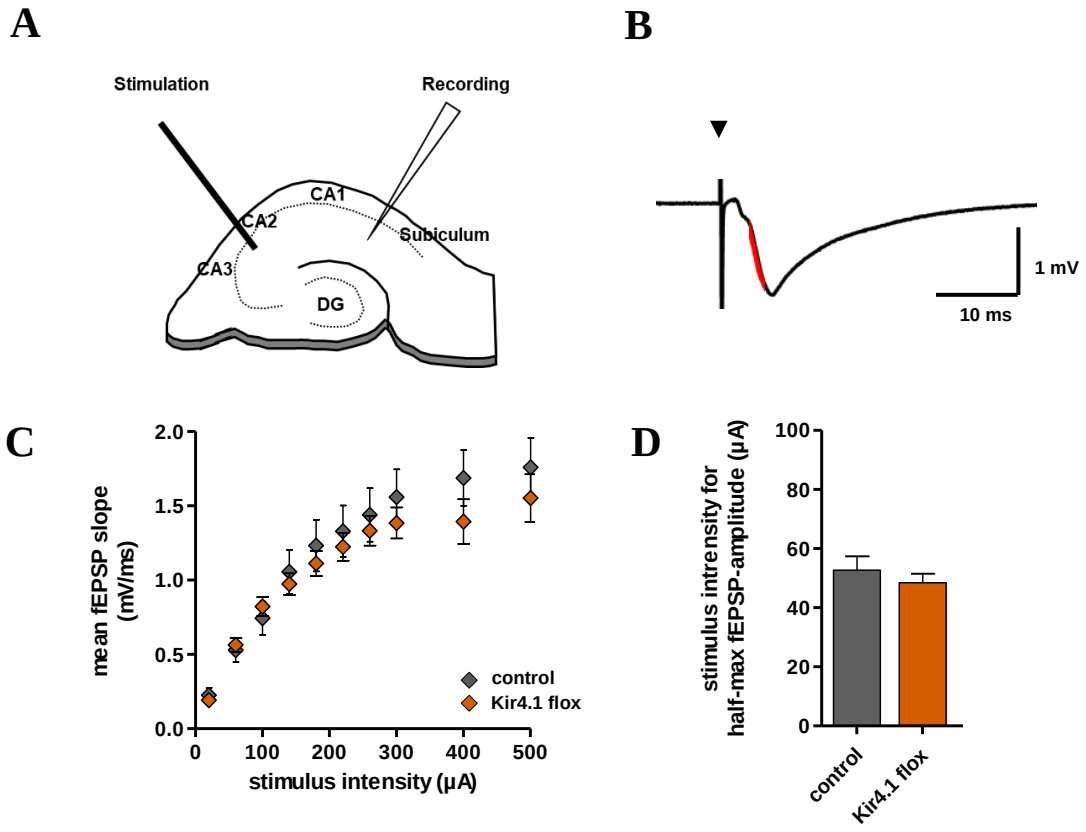

Fig. 5.19: Stimulus-response relation at CA3-CA1 synapses.
A) Position of stimulation and recording electrode in hippocampal slices. The dentate gyrus (DG), the three cornu ammonis areas (CA1-CA3) and the subiculum are labeled. **B)** Example of a fEPSP measured in the CA1 region of the stratum radiatum. The slope was determined at the linear rising phase (red) of the fEPSP. Stimulation pulse is indicated by black triangle. **C)** Mean of fEPSP slopes evoked by different stimulation intensities (input-output curve). Sensitivity to electrical stimulation was similar between slices of control and Kir4.1 flox mice. **D)** The stimulation intensity to elicit half-maximum fEPSP amplitudes was not different between genotypes. control: n = 13 slices; Kir4.1 flox: n = 35 slices. Mean ± SEM. t-test.

To investigate possible changes of synaptic plasticity at the CA3-CA1 synapses in control and Kir4.1 flox mice, Schaffer collaterals were stimulated and long-term potentiation (LTP) was induced. LTP was induced by theta burst stimulation (TBS), a high frequency stimulation protocol resembling discharges of hippocampal neurons that occur during learning and exploration (O'Keefe and Nadel, 1978). In figure 5.20 B the time course of fEPSPs before and after TBS induced LTP is shown. In slices of both control and Kir4.1 flox mice responses to Schaffer collateral stimulation were potentiated after LTP induction. The potentiation was not different between control (223.08 ± 31.75 %) and slices of Kir4.1 flox mice (166.42 ± 9.63%) within the first 3 min after the theta burst was applied (Fig. 5.20 C). Surprisingly, after 25-30 min, when LTP was established, slices of Kir4.1 flox mice showed considerably less potentiation (17%; p = 0.014) than controls. Thus, in mice lacking the Kir4.1 channel

specifically in NG2 glia neuronal activity was impaired after high frequency stimulation. These observations led to the assumption that NG2 glia do influence neuronal network activity and might be essential for proper synaptic transmission.

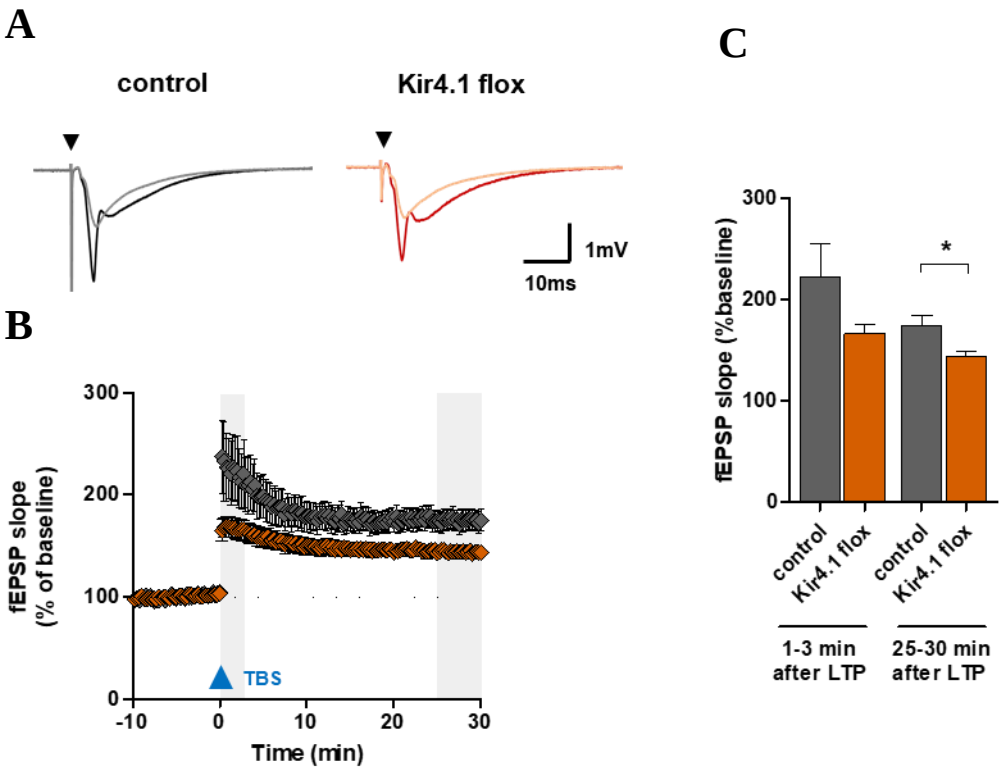

Fig. 5.20: TBS induced LTP in the hippocampus was impaired in Kir4.1 flox mice.
A) Representative fEPSPs from control and Kir4.1 flox mice recorded in the CA1 region of the stratum radiatum before (grey, orange) and 25-30 min after (black, red) induction of LTP by three trains of theta burst stimulation (TBS) of Schaffer collaterals. Stimulation pulse is indicated by black triangle. **B)** Time-course of fEPSP slopes before and after TBS (blue triangle) induced LTP. Grey bars highlight time points of analysis (see C; 1-3 min and 25-30 min after LTP induction). **C)** Analysis of fEPSP slopes revealed significant differences 25-30 min after TBS. Control n = 9 slices; Kir4.1 flox n = 30 slices. Mean ± SEM. Mann-Whitney U Test.

A possible reason for an impaired LTP might be a change in the release probability of neurotransmitters at neuronal synapses. To investigate if presynaptic release probability was altered in Kir4.1 flox mice, the paired pulse ratio (PPR) of fEPSPs was analyzed. A series of two stimuli with 50 ms interval were applied before (baseline) and after TBS induced LTP. The time course of the paired pulse ratio (PPR) calculated by the mean fEPSP slope of the 2nd pulse divided by the fEPSP slope of the 1st pulse, is displayed in Fig.5.21 A. During baseline conditions and after LTP induction PPR was similar between control and Kir4.1 flox mice (Fig. 5.21 B). The transient drop in PPR after TBS reflects an increase of release probability that is known to occur after LTP induction (Frey et al., 2009; Kleschevnikov et al., 1997; McNaughton, 1982; Sokolov et al., 1998). These observations indicate that the

release probability at CA3-CA1 synapses was not altered in mice lacking Kir4.1 in NG2 glia, leading to the conclusion that impaired LTP was not mediated by presynaptic mechanisms, rather by changes on postsynaptic side.

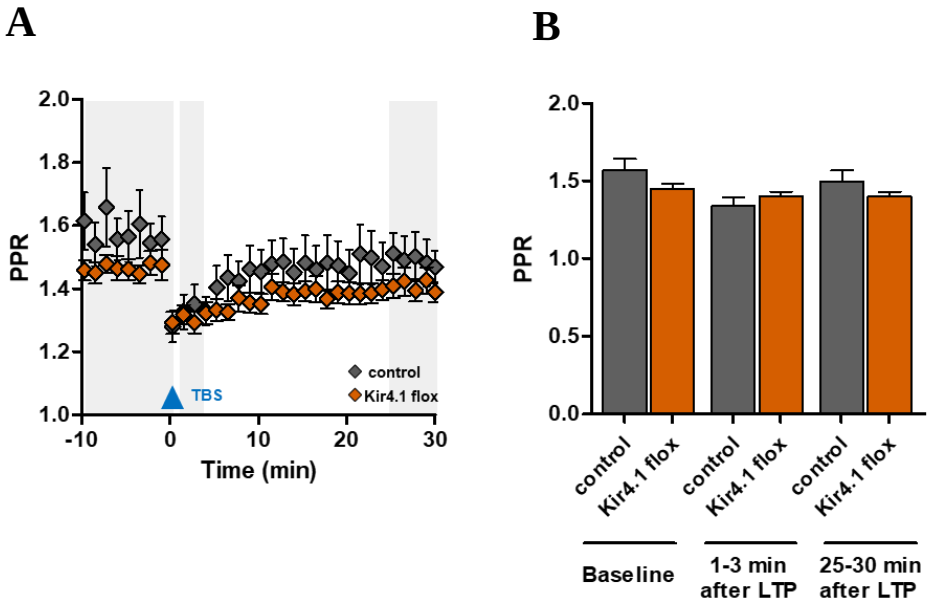

Fig. 5.21: Release probability before and after LTP induction was not different between control and Kir4.1 flox mice

A) Time course of the paired pulse ratio (PPR) of fEPSPs recorded in slices of control (n = 9) and Kir4.1 fox mice (n = 24). A transient decrease of the PPR occurred during post-tetanic potentiation in both groups. Grey bars highlight time points of analysis (see B; baseline, 1-3 min and 25-30 min after LTP induction). **B)** Analysis of the paired pulse ratio between slices of control (n = 9, black) and Kir4.1 flox mice (n = 24) during baseline conditions, 1-3 min and 25-30 min after TBS. PPR was not different between slices of control and Kir4.1 flox mice (2-sample t-test).

Both mouse lines, control and Kir4.1 flox, were generated by Huang et al. (2014) by homologous recombination to introduce the recombinase CreER^{T2} into exon 1 of the NG2 allel (Huang et al., 2014) (see section 4.2). As this knock-in strategy ablate the expression of the proteoglycan NG2 on the allele, mice expressing CreER^{T2} on one allele were heterozygous for the NG2 protein; those expressing CreER^{T2} on both alleles were homozygous, unable to express NG2. For the present study mice, homo- and heterocygous for Cre, were used. To investigate if the deletion of the NG2 proteoglycan had an impact on the impaired LTP observed in Kir4.1 flox mice, the LTP experiments were repeated in hippocampal slices of NG2-EYFPki mice. In this mouse line, the fluorescent protein EYFP was likewise inserted into exon 1 of the NG2 gene leading to a NG2 ko if expressed on both alleles (Karram et al., 2008). LTP was induced by the same TBS protocol used for control and Kir4.1 flox mice in slices of NG2-EYFPki mice being wild-type for the proteoglycan NG2 (wt), heterozygote (+/-) or even completely lacking NG2 (-/-). All three genotypes tested

in the present study were not statistically different from one another neither 1-3 min nor 25-30 min after LTP induction (Fig. 5.22). These results support the finding that the impaired LTP observed in Kir4.1 flox mice was related to the ko of Kir4.1 in NG2 glia and not due to the ko of the proteoglycan NG2.

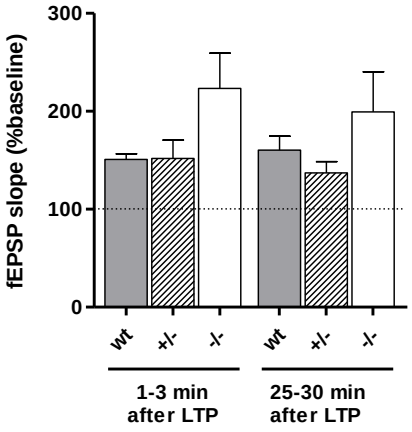

Fig. 5.22: The proteoglycan NG2 did not influence hippocampal LTP
A) fEPSP slopes recorded in hippocampal slices of NG2-EYFPki mice of three different genotypes. fEPSP slopes were not statistically different between mice being wt, +/- or -/- for the NG2 proteoglycan. wt, mice being wild-type for the NG2 protein (n = 5 slices); +/-, mice being heterozygous for the NG2 protein (n = 10 slices); -/-, mice lacking the NG2 protein (ko mice, n = 8 slices). Mean ± SEM. Kruskal-Wallis test with post-hoc Dunn´s test.

5.9 Behavioral analysis of mice lacking Kir4.1

LTP is considdered to be an important cellular mechanism for in learning and memory (Bliss and Lømo, 1973; Lynch, 2004). The impairment of theta burst induced hippocampal LTP suggested that learning and memory formation in mice might be altered upon deletion of Kir4.1 in NG2 glia. As the hippocampus is known to be involved in declarative, working and social memory appropriate behavior paradigms were conducted on control and Kir4.1 flox mice to assess possible consequences on behavioral function (Albayram et al., 2016; Lynch, 2004). Data was analyzed by 2-way ANOVA comparing genotype, sex and interaction of those.

5.9.1 Novel object location recognition test

Declarative memory is a form of long-term memory that allows the comparison of facts or events (Squire, 2004; Squire and Dede, 2015). To evaluate declarative memory in mice lacking the Kir4.1 channel in NG2 glia, the novel object location recognition test was

performed. In this test mice were exposed to three identical objects in an arena (Fig. 5.23 A). During the test phase, 1 h after habituation, one object was removed and substituted by a different object placed to another position. The time the mouse spends with this new object and the remaining objects was analyzed. Remarkably, Kir4.1 flox mice tlacking the Kir4.1 channel in NG2 glia showed a higher preference for the new, relocated object than control mice (38.50 ± 10.73% vs 3.66 ± 9.02%; p = 0.012) (Fig. 5.23 B). Sex of the animals or interaction between sex and genotype did not influence novel object location recognition. These results indictaed an improvement of declarative memory in mice lacking Kir4.1 in NG2 glia.

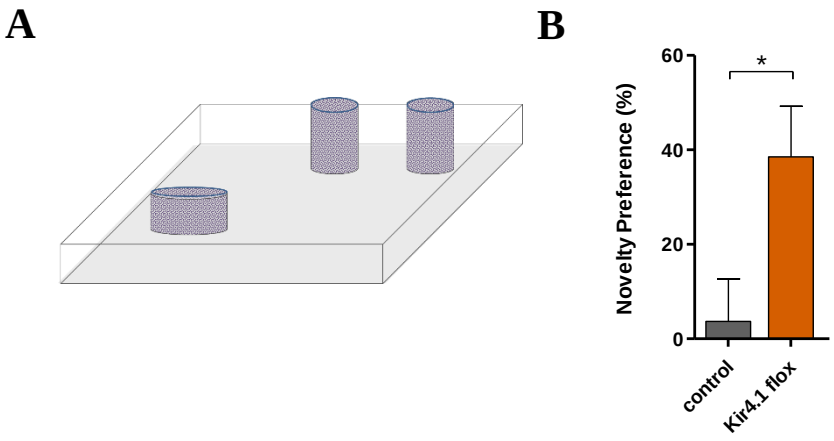

Fig. 5.23: Novel object location recognition test
A) Scheme of the novel object location recognition paradigm. Three identical objects were placed in an arena. One object was removed and a different object was placed to another position. The preference for this new relocated object was evaluated. **B)** Increased preference for the relocated object in Kir4.1 flox mice. control, 14 mice; Kir4.1 flox, 14 mice. Mean ± SEM.

5.9.2 Partner recognition test

The partner recognition test is another behavioral paradigm to assess long-term memory in terms of social memory performance (Bilkei-Gorzo et al., 2014, 2017). In this paradigm mice of either the Kir4.1 flox or control group were exposed to a partner mouse and an object (trial 1), before (trial 2) the object was repelaced by second, new partner mouse 1, 2, 4 or 8 h after trial 1 (Fig. 5.24 A). The time spend with the new partner (N) compared to the time spend with the remaining partner mouse (R) from trial 1 was evaluated. In this social assay the ability to distinguish between a previous, known partner and a new partner is critically dependent on the hippocampus and other areas of the limbic system (Bilkei-Gorzo et al., 2014).

In the first set of experiments a new partner mouse was introduced to either a control or Kir4.1 flox mouse, 1 h after trial 1. The preference for the new partner mouse was similar for control and Kir4.1 flox mice (54.77 ± 21.04% and 58.84 ± 17.75%, resepectivly) (Fig. 5.24 B). However, the sex of the mice affected the partner recognition, as female mice showed in general a higher preference for the new partner than male mice (Fig. 5.24 C; $p = 0.007$). An interaction of sex and genotype could be excluded.

In the second set of experiments the time before the new partner was presented after trial 1 was increased (2 up to 8 h). A time period of 2 h in between trials was already sufficient to remove the gender specific difference observed 1 h after trial 1. As before, the preference for the new partner was similar for Kir4.1 and control mice (Fig. 5.24 B). No interaction of sex and genotype was detected either. The same applies to the novelty preference evaluated after longer intervals (4 and 8 h after trial 1). The preference for the new partner remained indistinguishable between control and Kir4.1 flox mice and between male and female mice.

These observations indicate that mice lacking the K^+ channel Kir4.1 in NG2 glia have a similar social memory as control mice. Social deficits that could influence the interaction with the partner mouse could be excluded, as both control and Kir4.1 flox mice, independent of the gender, showed a high preference for the partner mouse compared to the object presented in trial 1 (Fig. 5.24 D).

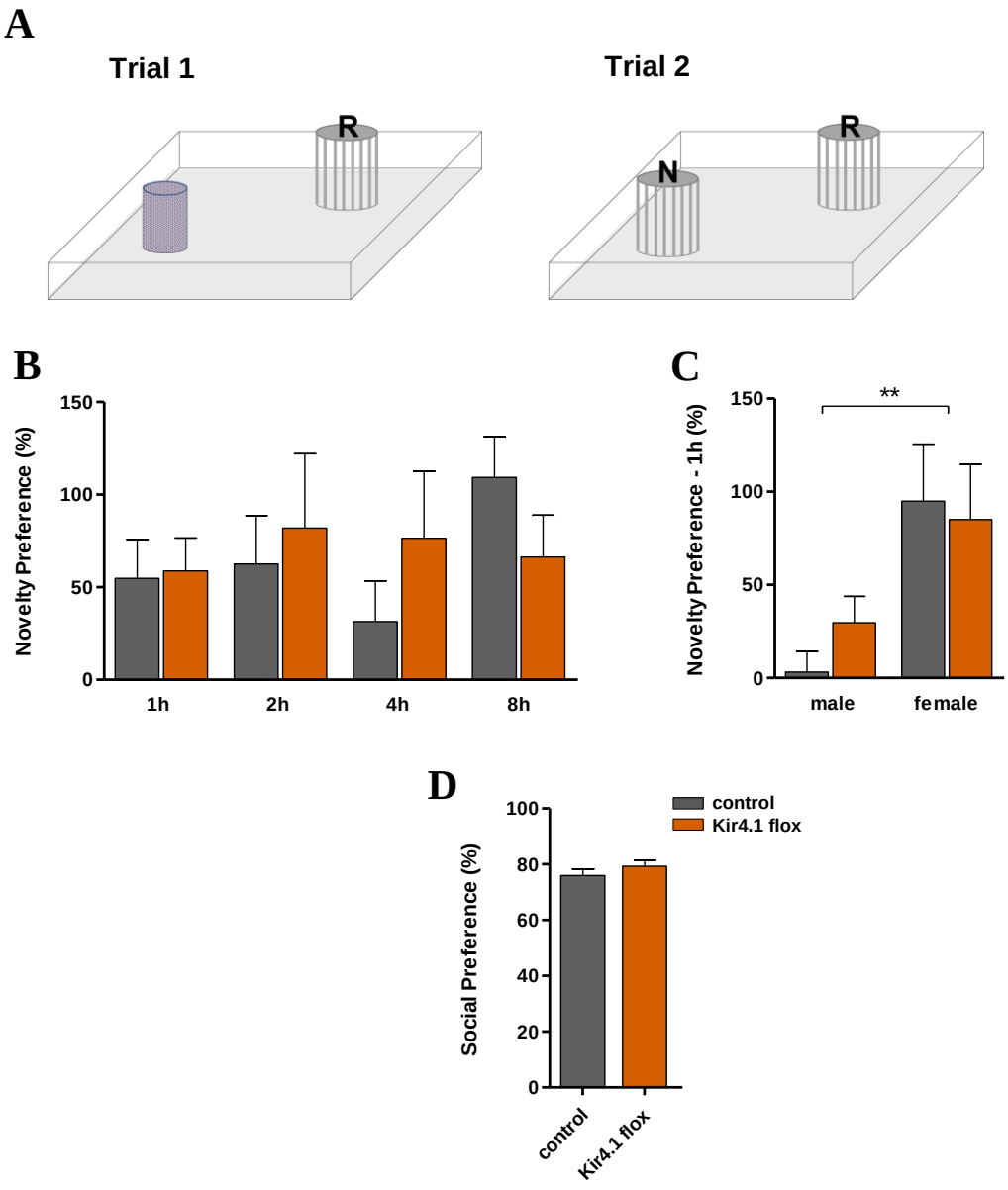

Fig. 5.24: Partner recognition test.
A) Scheme of the experimental settings for the partner recognition test. In **trial 1** the test mouse was exposed to an object (cylinder) and a partner mouse in a metal grid cage (R). In **trial 2** (1 h up to 8 h after trial 1) the object was replaced by another, new partner mouse (N). The time spent with the previous, remaining partner from trial 1 (R) and the new partner mouse (N) was compared. **B)** No difference between control and Kir4.1 flox mice was detected. **C)** Sex differences were detected 1 h after trial 1 ($p = 0.007$). **D)** Social preference was identical in control and Kir4.1 flox mice. Control, 16 mice (7 males, 9 females); Kir4.1 flox, 19 mice (9 males, 10 females). Mean ± SEM.

5.9.3 Y-Maze test

A Y-maze paradigm was used to investigate working memory, a form of short-term memory that requires the activity of the hippocampus and prefrontal cortex (Albayram et al., 2016; Lynch, 2004). In this behavior task mice were placed in a 3-armed arena and their natural preference to explore always a new arm instead of repetitively one and the same arm was evaluated (Fig. 5.25 A). The number of alternating arm entries that is indicative for the strength of working memory was not different between control and Kir4.1 flox mice. Analysis of possible sex specific effects revealed no differences between male or female mice of control or Kir4.1 flox mice (Fig. 5.25 B). Moreover, no interaction between sex and genotype was found. Thus, working memory was not altered in mice lacking Kir4.1 in NG2 glia.

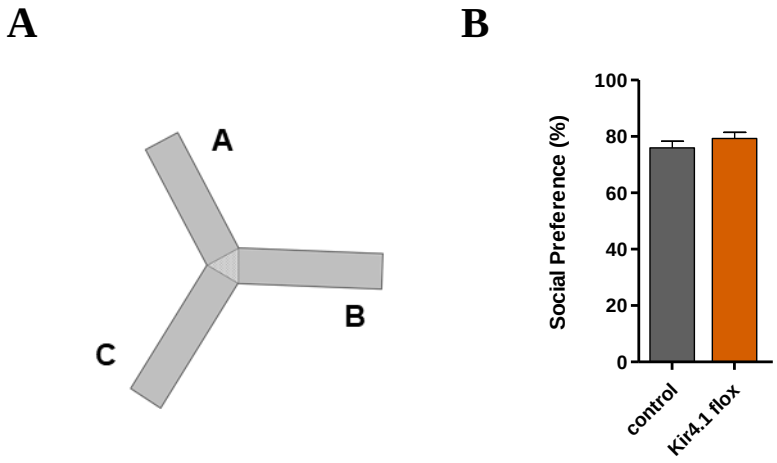

Fig. 5.25: Y-maze paradigm.
A) Scheme of the Y-maze paradigm. Mice were placed in the Y-shaped maze and their entries into the three arms (A, B, C) tracked and analyzed. **B)** Control and Kir4.1 flox mice similarly visited all three arms in an alternating fashion (A-B-C-A-B…) independent of their gender. Control, 17 mice; Kir4.1 flox, 19 mice. Mean ± SEM.

5.10 NG2 glia specific knockout of Kir4.1 in the cerebellum

Intrinsic properties of NG2 glia like ion channel expression, differentiation and proliferation can differ among the NG2 glia population depending on developmental state and the brain region where they reside (Chittajallu et al., 2004; Dimou et al., 2008; Kressin et al., 1995; Young et al., 2013). This heterogeneity does not only concern grey versus white matter NG2 glia but is also present between regions within either of these structures. Thus, in NG2 glia of white matter regions short cell cycle lengths of about 9 days in the corpus callosum and 15 days in the spinal cord were observed in adult mice. In grey matter regions the cycle was shown to be prolonged, varying between 27 days in the spinal grey matter and 36 days in the

cortex (Young et al., 2013). In terms of differentiation, most of the white matter NG2 glia differentiate into oligodendrocytes, whereas grey matter NG2 glia mainly keep their NG2 phenotype throughout adulthood (Dimou et al., 2008; Kang et al., 2010). Interestingly, the responsiveness towards neuronal input can also differ between NG2 glia of different brain regions. In the hippocampus neuronal stimulation induced inward currents of only a few pA whereas in the cerebellum amplitudes of several 100 pA were detected (Jabs et al., 2005; Lin et al., 2005; Passlick et al., 2016). The consequences of a NG2 glia specific ko of the K^+ channel Kir4.1 on the above mentioned paramaters was addressed in the following study.

5.10.1 Transcript analysis of CreER^{T2} mediated knockout of Kir4.1

The efficiency of the tamoxifen induced deletion of Kir4.1 in cerebellar NG2 glia was determined by semiquantitative PCR (performed by Dr. Gerald Seifert). As described for the hippocampus (section 5.1.2) the cerebellum was isolated 3 weeks after tamoxifen injection from both control (NG2-CreERT2x Rosa26-EYFP) and Kir4.1 flox mice (Kir4.1 fl/fl; NG2-CreER^{T2} x Rosa26EYFP). Based on the expression of the reporter protein EYFP, recombined NG2 glia were sorted from the entire cerebellar tissue by FACS. To assess the level of Kir4.1 transcripts in the sorted cell populations, semiquantitative PCR was performed. The analysis revealed that the tamoxifen induced ko of Kir4.1 in Kir4.1 flox mice reduced Kir4.1 mRNA by 84% ($p = 0.04$) (Fig. 5.26).

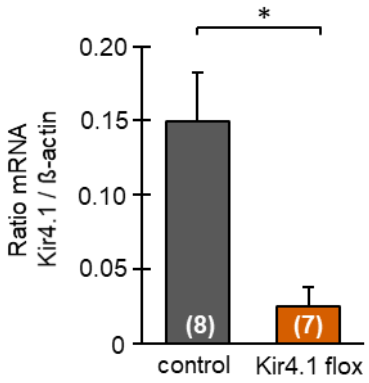

Fig. 5.26: Kir4.1 mRNA level in cerebellar NG2 glia.
Semiquantitive PCR of FAC sorted recombined NG2 glia revealed a downregulation of Kir4.1 transcripts in these cells as the ratio of Kir4.1 mRNA and the housekeeping gene ß-actin (serving as internal standard) was significantly decreased. t-test. Mean ± SD. Number of mice is given in parenthesis.

5.10.2 Passive membrane properties of NG2 glia in the cerebellar molecular layer

In the hippocampus the selective deletion of the K^+ channel Kir4.1 from NG2 glia induced massive changes in the passive membrane properties of these cells as displayed by a more positive resting membrane potential and an increased membrane resistance (section 5.2). To evaluate the effect of the ko on cerebellar NG2 glia, whole-cell patch-clamp recordings were performed in the cerebellar molecular layer 3-4 weeks after tamoxifen injection. Sagittal sections from the vermis were prepared from tamoxifen treated Kir4.1 flox mice and from NG2-EYFPki mice (untreated). NG2 glia of the NG2-EYFPki mouse line constantly express EYPF under the NG2 glia promoter (section 4.2.1) and served in this experiment as control. In regard of the incomplete ko of Kir4.1 described before (section 5.1), recombined NG2 glia of Kir4.1 flox mice were defined as Kir4.1 wt or Kir4.1 ko cells based on the residual conductance of the Kir4.1 channel measured at -130 mV (Kir4.1 ko cells < 6 pA/mV at -130 mV > Kir4.1 wt). Overall the conductance of Kir4.1 ko cells was significantly reduced (2.03 pA/mV) compared to Kir4.1 wt cells (10.76 pA/mV, $p < 0.001$) and NG2 glia of NG2-EYFPki mice (23.24 pA/mV, $p < 0.001$) (Fig. 5.27 A, B; Table 10). As expected, in NG2 glia lacking Kir4.1 mediated currents the membrane potential was more depolarized (-69 mV) than in NG2-EYFPki cells (-88 mV; $p < 0.001$) and Kir4.1 wt cells (- 84 mV; $p = 0.025$) (Fig. 5.27 C; Table 10). The deletion of this channel further resulted in a 3- to 10-fold increase of the membrane resistance ($p < 0.001$) that was determined by voltage steps from -80 mV to -70 mV (Fig. 5.27 D; Table 10). Kir4.1 wt cells and NG2 glia of the NG2-EYFPki mouse line were indistinguishable from one another according to membrane potential, membrane resistance and channel conductance at -130 mV. Comparing the membrane capacitance of all three groups, ranging between 22 pF and 28 pF, did not reveal any difference (Fig. 5.27 E; Table 10). These results confirm the importance of Kir4.1 channels in determining the membrane resistance and membrane potential of NG2 glia.

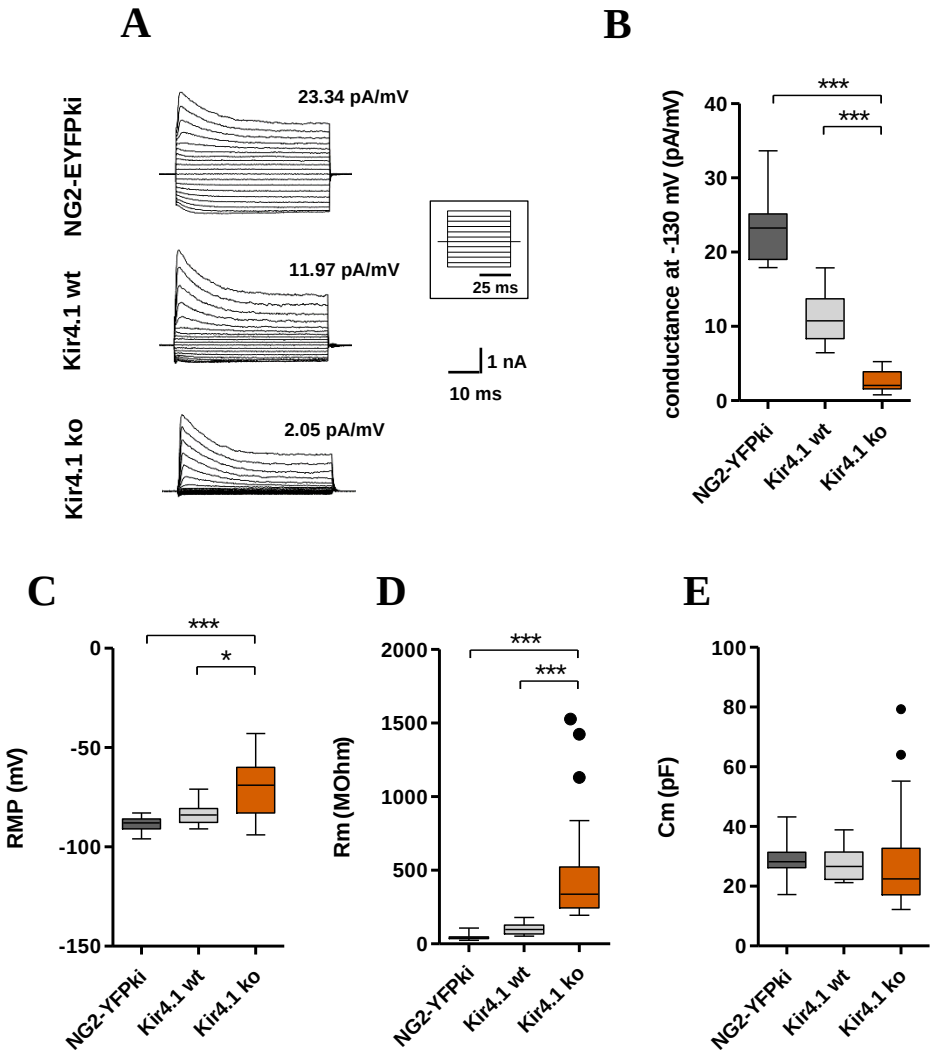

Fig. 5.27: Kir4.1 channels determine passive membrane properties of cerebellar NG2 glia.
A) Representative whole-cell current patterns of NG2 glia of NG2-EYFPki mice and recombined NG2 glia of Kir4.1 flox mice (Kir4.1 wt, Kir4.1 ko) located in the cerebellar molecular layer. Currents were elicited by voltage steps ranging from -160 to +20 mV. The channel conductance at -130 mV is mentioned obove the respective current. Recombined NG2 glia of Kir4.1 flox mice with a conductance less than 6 pA/mV were considered as Kir4.1 ko cells, above as Kir4.1 wt cells. **B)** In Kir4.1 ko cells the channel conductance was significantly lower compared to NG2 glia expressing Kir4.1. **C)** In the absence of Kir4.1 channels the resting membrane potential (RMP) of NG2 glia was depolarized by about 20 mV and **D)** the membrane resistance (Rm) was 3 to 30-fold higher. **E)** The membrane capacitance (Cm) was indistinguishable between NG2 glia of NG2-EYFPki mice and recombined NG2 glia of Kir4.1 flox mice. Kir4.1 ko cells: n = 32; Kir4.1 wt cells: n = 12; NG2-EYFPki cells: n = 26. Kruskal Wallis ANOVA with Dunn´s correction. Data is presented as tukey box-plots with median (central line), quartiles (25% and 75%; box) and percentiles (1.5 times the interquartile range). Outliers are shown as dots.

Table 10: Passive membrane properties of cerebellar NG2 glia of NG2-EYFPki mice (NG2-EYFPki) and recombined NG2 glia of Kir4.1 flox mice (Kir4.1 wt, Kir4.1 ko).
RMP, resting membrane potential; Rm, membrane resistance; Cm, membrane capacitance. Data is given as median and interquartile range (quartile 25% – quartile 75%). Number of cells is given in square brackets.

	NG2-EYFPki	Kir4.1 wt	Kir4.1 ko
Conductance at -130 mV (pA/mV)	23.24 (19.02 – 25.15) [16]	10.76 (8.33 – 13.71) [12]	2.03 (1.60 – 3.89) [32]
RMP (mV)	-88 (-91 – -86) [16]	-84 (-88 – -81) [12]	-69 (-83 – -60) [32]
Rm (MOhm)	39.61 (35.59 – 47.31) [16]	97.50 (66.98 – 128.27) [12]	337.73 (244.57 – 523.14) [32]
Cm (pF)	28.34 (26.20 – 31.37) [16]	26.66 (22.28 – 31.44) [12]	22.42 (17.16 – 32.74) [32]

5.10.3 Short-term plasticity at the climbing fiber - NG2 glia synapse

To investigate the role of Kir4.1 channels on the release probability at the CF - NG2 glia synapses, paired pulse recordings were obtained from NG2 glia in the molecular layer of the cerebellum. A monopolar stimulation electrode was positioned in the cerebellar granule cell layer (GCL) where climbing fibers traverse towards Purkinje cells and NG2 glia (Fig. 5.28 A). The mean amplitudes of excitatory postsynaptic currents (eEPSCs) evoked upon two consecutive stimulation pulses were used to calculate the paired pulse ratio (amplitude 2/amplitude 1). Stimulation of climbing fibers induced eEPSCs of several 100 pA in NG2 glia of NG2-EYFPki mice and recombined NG2 glia of Kir4.1 flox mice (Lin et al., 2005) (Fig. 5.28 B). The stimulus induced response was highly reliable and as every stimulus elicited a response (no failures). During the application of 2 consecutive stimuli a strong paired pulse depression was observed in NG2 glia of both mouse lines. However, the degree of paired pulse depression mirrored by the paired pulse ratio was not different between NG2-EYFPki cells, Kir4.1wt cells and Kir4.1 ko cells (0.48, 0.43 and 0.35, respectively) (Fig. 5.28 C; Table 11). The kinetic properties of the first stimulus induced EPSC were also similar between groups (Fig. 5.28 D, Table 11). These observations suggest that in the cerebellum the presence of Kir4.1 does not play a role in forming the release probability at the cerebellar CF - NG2 glia synapse.

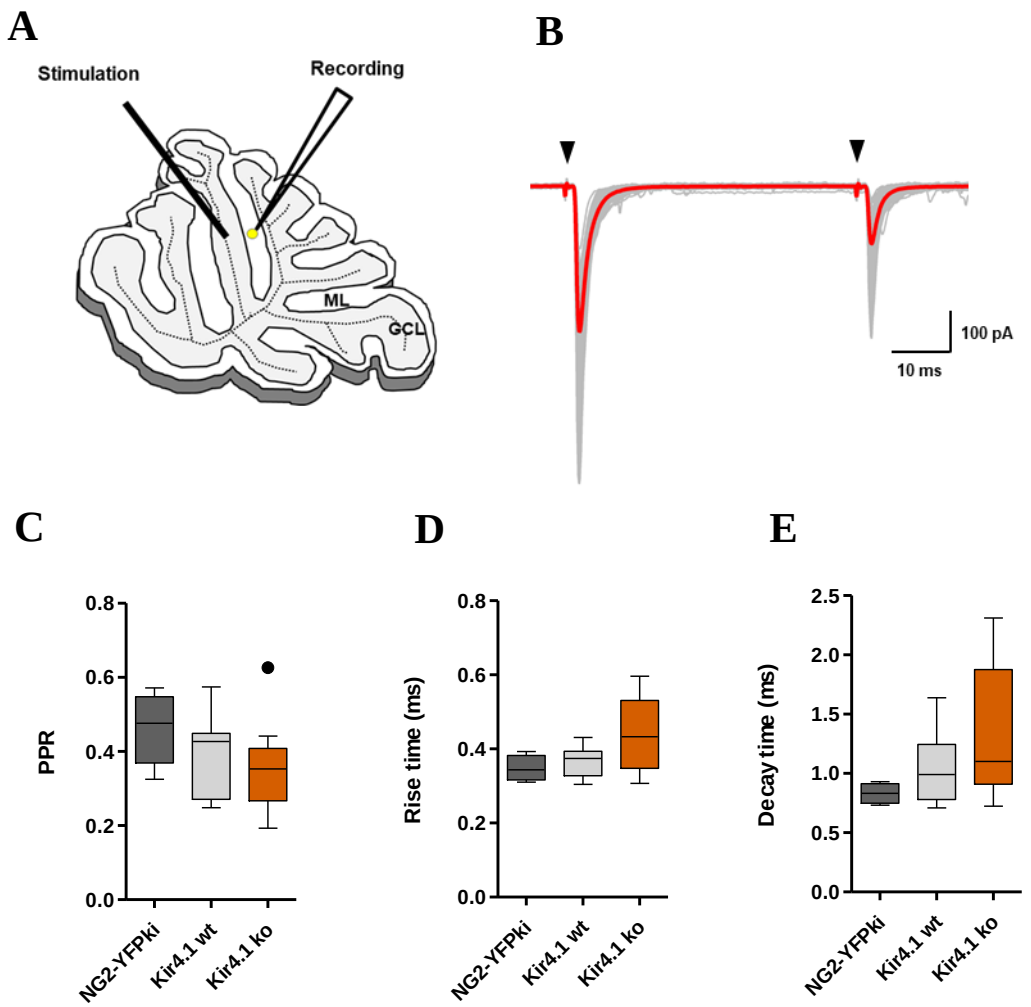

Fig. 5.28: Characteristics of eEPSCs in cerebellar NG2 glia during climbing fiber stimulation.
A) Position of stimulation and recording electrode in slices of the cerebellar vermis. Fluorescent NG2 glia (yellow circle) were recorded in the molecular layer (ML) upon climbing fiber stimulation in the granule cell layer (GCL). **B)** Average time course (red) of EPSCs of a NG2 glia to paired pulse stimulation of climbing fibers (CF) (inter-stimulus interval of 50 ms; holding potential of -80 mV). Stimulation pulse is indicated by black triangles. **C)** Paired pulse ratio (PPR), **D)** rise time and **E)** the decay time constant were not different between NG2 glia of NG2-EYFPki mice (NG2-EYFPki) and recombined NG2 glia of Kir4.1 flox mice (Kir4.1 wt, Kir4.1 ko). Kruskal-Wallis test with post-hoc Dunn´s test. NG2-EYFPki, n = 4; Kir4.1 wt cells, n = 6; Kir4.1 ko cells, n = 5. Data is presented as tukey box-plots with median (central line), quartiles (25% and 75%; box) and percentiles (1.5 times the interquartile range).

Table 11: Properties of climbing fiber induced EPSCs of cerebellar NG2 glia.
PPR, paired pulse ratio. Data is given as median and interquartile range (quartile 25% – quartile 75%). Number of cells is given in square brackets.

	NG2-EYFPki	Kir4.1 wt	Kir4.1 ko
PPR	0.48 (0.37 – 0.55) [4]	0.43 (0.27 – 0.45) [6]	0.35 (0.27 – 0.41) [5]
Rise time (ms)	0.34 (0.32 – 0.38) [4]	0.37 (0.33 – 0.39) [6]	0.43 (0.35 – 0.53) [5]
Decay time (ms)	0.83 (0.75 – 0.91) [4]	0.99 (0.78 – 1.24) [6]	1.10 (0.91 – 1.88) [5]

5.10.4 Effect of Kir4.1 ko on NG2 glia proliferation in the cerebellar cortex

According to the results of the previous experiment described in section 5.4, Kir4.1 did not seem to play a dominant role in initiating NG2 glia proliferation in the hippocampus, as the number of recombined NG2 glia being proliferating was similar between control and Kir4.1 flox mice 8 weeks after tamoxifen induced deletion of Kir4.1. To investigate the role of Kir4.1 on the proliferation of cerebellar NG2 glia fixed sections of the cerebellar vermis were stained for the Ki67. Co-staining for the reporter protein EYFP was performed to identify recombined NG2 glia. In the molecular layer of the cerebellum the proportion of recombined NG2 glia proliferating ($Ki67^+EYFP^+$ cells) was similar in Kir4.1 flox mice (7.78 ± 3.95%) and control (3.57 ± 2.53%) (Fig. 5.29 A, B; Table 12). In total about 2 cells per mm^2 were proliferating in both mouse lines (Fig. 5.29 C; Table 12). Likewise, in the cerebellar granule cell layer no difference was detected neither in the number of recombined NG2 glia being Ki67 positive nor in the total number of proliferating cells (Fig. 5.30; Table 12).

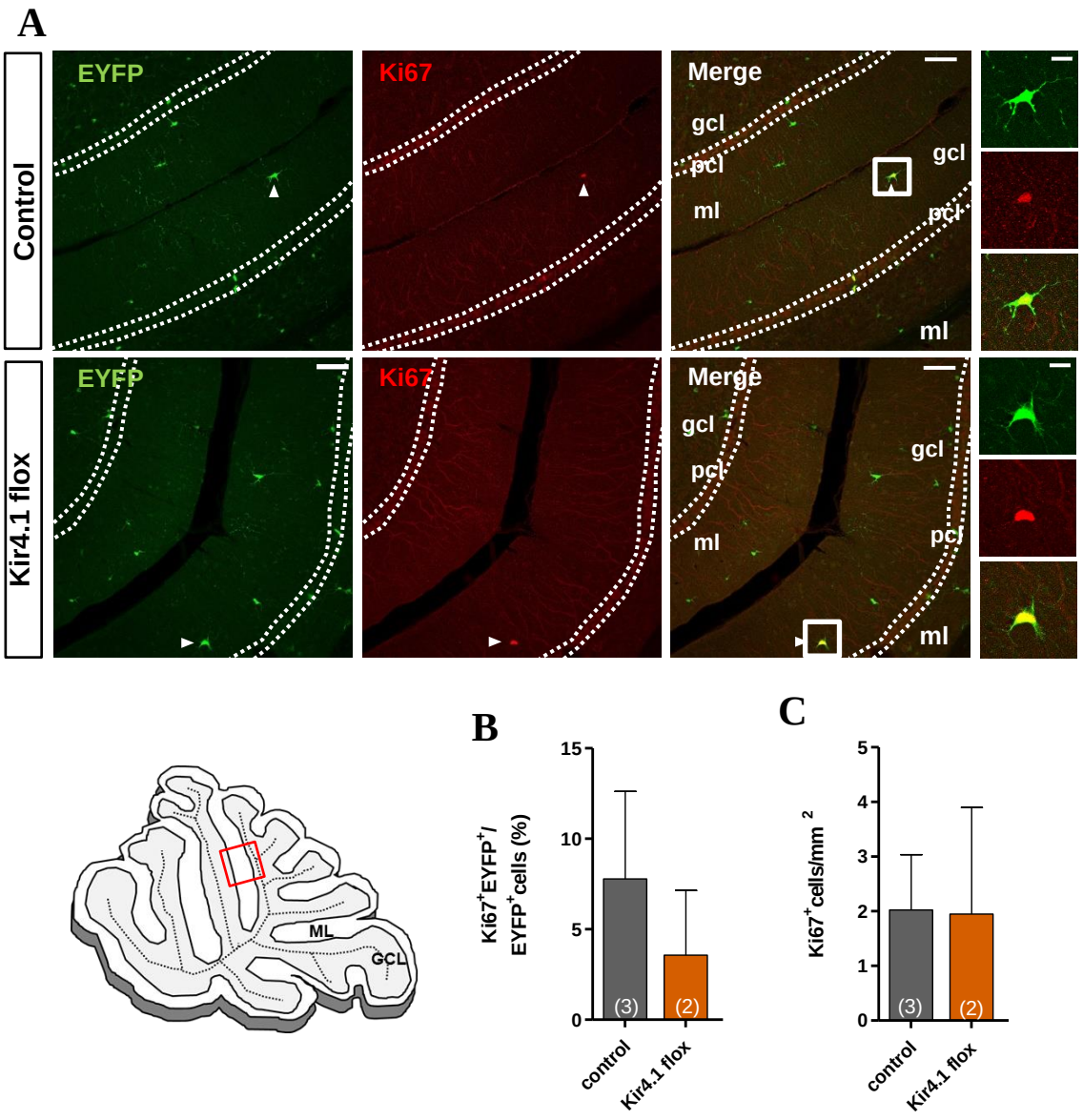

Fig. 5.29: Proliferation of NG2 glia in the cerebellar molecular layer is unaltered in Kir4.1 flox mice. **A)** Sagittal sections of the cerebellar vermis of control and Kir4.1 flox mice immunostained with EYFP (green) and nuclei antibody Ki67 (red). Double labeling of $EYFP^+$ and $Ki67^+$ cells is indicated by arrowheads. Boxed areas are shown at higher magnification on the right. Scale bar 60 µm and 15 µm (insets). Red square in the scheme of the cerebellar vermis marks the region analyzed. **B)** The proportion of $Ki67^+EYFP^+$ cells among all $Ki67^+$ cells and **C)** the density of $Ki67^+$ cells was similar in control and Kir4.1 flox mice. Mean ± SEM. t-test. GCL, granule cell layer; PCL, Purkinje cell layer; ML, molecular layer. Number of mice is given in parenthesis in the bar graphs.

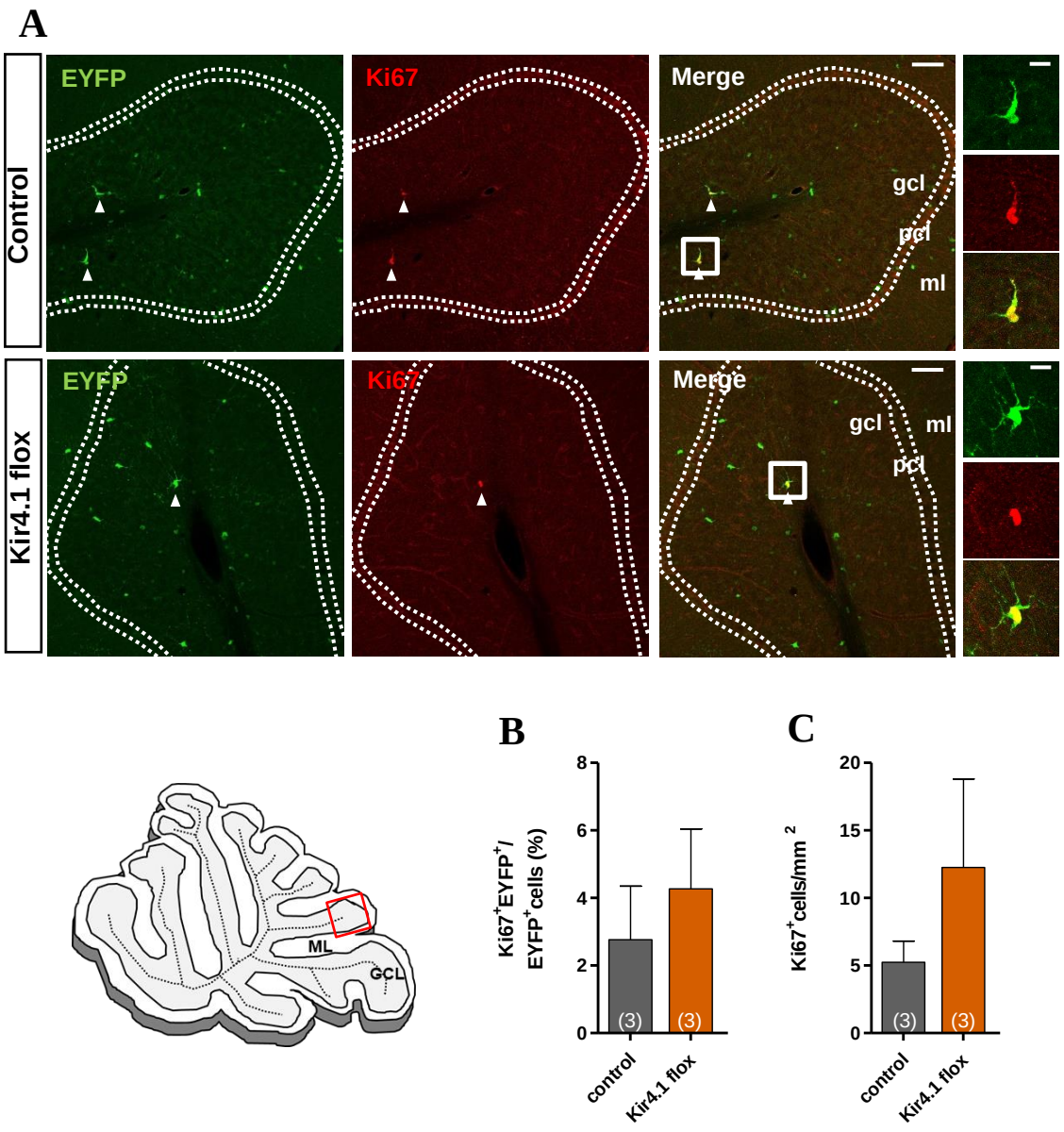

Fig. 5.30: Proliferation of NG2 glia in the cerebellar granule cell layer is not affected in Kir4.1 flox mice.

A) Sagittal sections of the cerebellar vermis of control and Kir4.1 flox mice immunostained with EYFP (green) and nuclei antibody Ki67 (red). Double labeling of $EYFP^+$ and $Ki67^+$ cells is indicated by arrowheads. Boxed areas are shown at higher magnification on the right. Scale bar 60 µm and 15 µm (insets). Red square in the scheme of the cerebellar vermis marks the region analyzed. **B)** Proportion of $Ki67^+EYFP^+$ cells among all $Ki67^+$ cells and **C)** the total number of $Ki67^+$ cells was similar in control and Kir4.1 flox mice. Mean ± SEM. t-test. GCL, granule cell layer; PCL, Purkinje cell layer; ML, molecular layer. Number of mice is given in parenthesis in the bar graphs.

Table 12: Proliferating cells in cerebellar vermis of control and Kir4.1 flox mice.
Percentage of proliferating recombined cells NG2 glia ($Ki67^+EYFP^+$ cells) among all recombined NG2 glia ($EYFP^+$ cells). The density of proliferating cells was determined per mm^2. Mean ± SEM. GCL, granule cell layer; PCL, Purkinje cell layer; ML, molecular layer. Number of mice is given in parenthesis.

Quantification	Mouse line	ML	GCL
$Ki67^+EYFP^+$/ $EYFP^+$cells (%)	Control	7.78 ± 3.95 (3)	2.77 ± 1.29 (3)
	Kir4.1 flox	3.57 ± 2.53 (2)	4.27 ± 1.44 (3)
$Ki67^+$ cells/mm^2	Control	2.02 ± 0.83 (3)	5.25 ± 1.28 (3)
	Kir4.1 flox	1.95 ± 1.38 (2)	12.25 ± 5.35 (3)

5.10.5 Effect of Kir4.1 on NG2 glia differentiation into oligodendrocytes in the cerebellar cortex

In contrast to the findings that a global or GFAP promoter restricted ko of Kir4.1 affected the development of myelinating oligodendrocytes (Djukic et al., 2007; Neusch et al., 2001), the NG2 glia restricted deletion of Kir4.1 described in this study did not affect the differentiation of hippocampal NG2 glia into mature oligodendrocytes (section 5.5). To investigate the effect of a NG2 glia specific ko of Kir4.1 on NG2 glia differentiation in the cerebellum, fixed sections of the cerebellar vermis were stained for the oligodendrocyte marker GSTpi and the reporter protein EYFP. Interestingly, in the molecular layer of mice lacking Kir4.1 in NG2 glia, 23.65 ± 5.11% of all recombined NG2 glia differentiated into oligodendrocytes ($EYFP^+GSTpi^+$), compared to only 4.63 ± 2.00% in sections of control mice ($p = 0.04$) (Fig. 5.31 A, B; Table 13). The densitiy of GSTpi positive cells was similar between groups (4.13 ± 0.83 to 11.56 ± 3.64 cells per mm^2) (Fig. 5.31 C; Table 13). In the cerebellar granule cell layer the proportion of oligodendrocytes originating from recombined NG2 glia as well as the density of $GSTpi^+$ oligodendrocytes was similar between control and Kir4.1 deficient mice (Fig. 5.32; Table 13). Generally, comparing both cerebellar subregions the proportion of double positive cells ($GSTpi^+EYFP^+$ cells) and the density of $GSTpi^+$ oligodendrocytes was higher in the granule cell layer than in the molecular layer. These observations indicate that the deletion of Kir4.1 from NG2 glia triggered NG2 glia differentiation into oligodendrocytes in the molecular layer but not in the granule cell layer. Overall, these results provide further evidence about the heterogeneity of NG2 glia properties between sublayers of single brain regions.

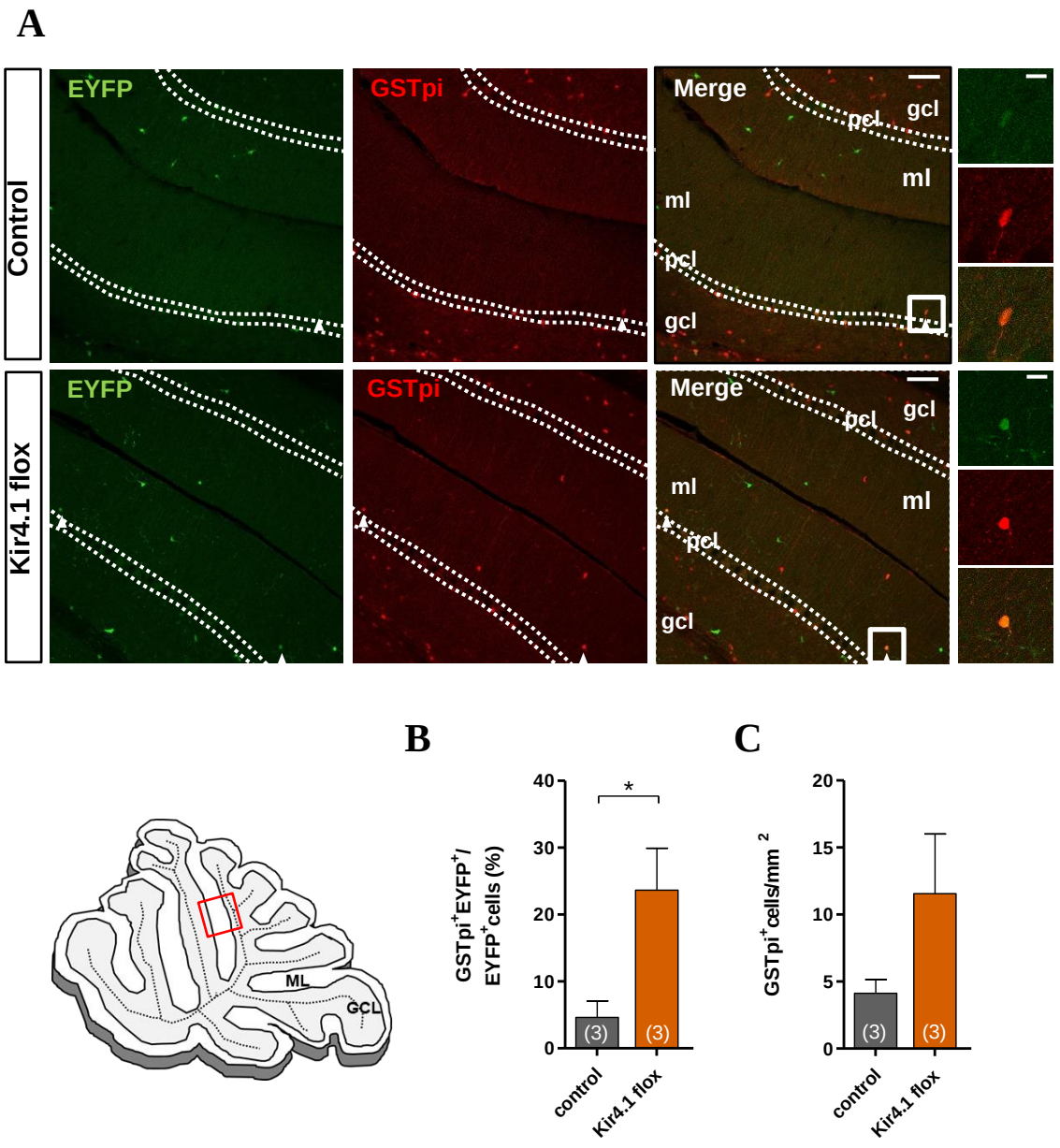

Fig. 5.31: Differentiation of recombined NG2 glia in the cerebellar molecular layer is increased in Kir4.1 flox mice. A) Sagittal sections of the cerebellar vermis of control and Kir4.1 flox mice immunostained with EYFP (green) and the oligodendrocyte marker GSTpi (red). Double labeling of EYFP+ and GSTpi$^+$ cells is indicated by arrowheads. Boxed areas are shown at higher magnification on the right. Scale bar 60 µm and 15 µm (insets). Red square in the scheme of the cerebellar vermis marks the region analyzed. **B)** The proportion of recombined NG2 glia (EYFP$^+$) that differentiate into oligodendrocytes (EYFP$^+$ GSTpi$^+$cells) was increased in Kir4.1 flox mice (2-sample t-test). **C)** The density of GSTpi$^+$ cells was similar in control and Kir4.1 flox mice. Mean ± SEM. t-test. GCL, granule cell layer; PCL, Purkinje cell layer; ML, molecular layer. Number of mice is given in parenthesis in the bar graphs.

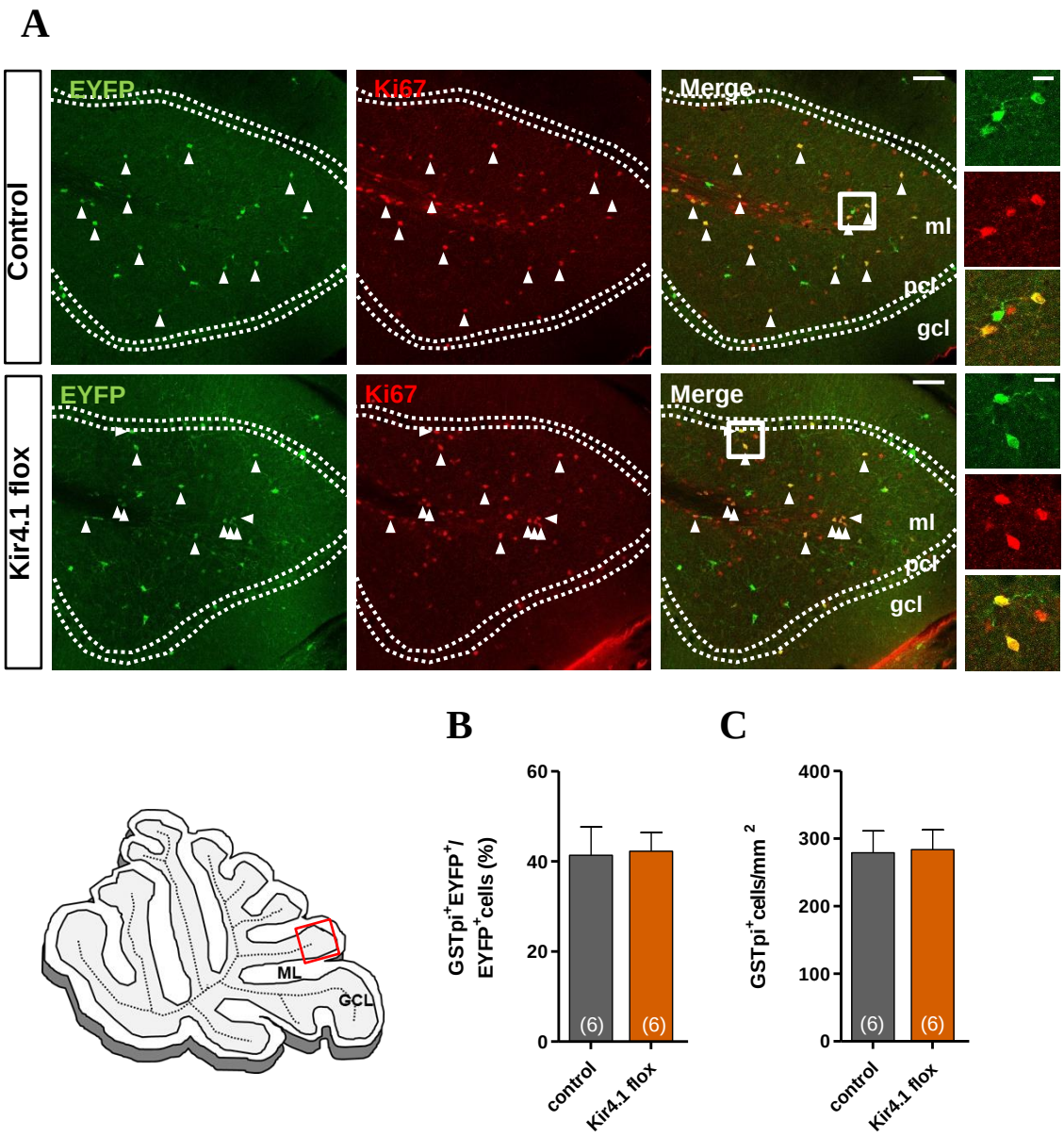

Fig. 5.32: Differentiation of NG2 glia in the cerebellar granule cell layer is unaffected in Kir4.1 flox mice.

A) Sagittal sections of the cerebellar vermis of control and Kir4.1 flox mice immunostained with EYFP (green) and the oligodendrocyte marker GSTpi (red). Double labeling of $EYFP^+$ and $GSTpi^+$ cells is indicated by arrowheads. Boxed areas are shown at higher magnification on the right. Scale bar 60 µm and 15 µm (insets). Red square in the scheme of the cerebellar vermis marks the region analyzed. **B)** The proportion of recombined NG2 glia ($EYFP^+$) that differentiate into oligodendrocytes ($EYFP^+$ $GSTpi^+$cells) and the **C)** the density of $GSTpi^+$ cells was similar in control and Kir4.1 flox mice. Mean ± SEM. t-test. GCL, granule cell layer; PCL, Purkinje cell layer; ML, molecular layer. Number of mice is given in parenthesis in the bar graphs.

Table 13: Cerebellar GSTpi$^+$ oligodendrocytes of control and Kir4.1 flox mice.
Percentage of recombined NG2 glia (EYFP$^+$ cells) that differentiated into oligodendrocytes (GSTpi$^+$EYFP$^+$ cells) among all recombined NG2 glia. The density of oligodendrocytes was determined per mm^2. Mean ± SEM. Asterik indicates statistical difference between genotpyes within a cerebellar layer. GCL, granule cell layer; PCL, Purkinje cell layer; ML, molecular layer Number of mice is given in parenthesis.

Quantification	Mouse line	ML	GCL
GSTpi$^+$EYFP$^+$ / EYFP$^+$cells (%)	Control	4.63 ± 2.00 (3)*	41.37 ± 5.74 (6)
	Kir4.1 flox	23.65 ± 5.11 (3)	42.25 ± 3.80 (6)
GSTpi$^+$ cells/mm^2	Control	4.13 ± 0.83 (3)	279.09 ± 29.43 (6)
	Kir4.1 flox	11.56 ± 3.64 (3)	283.72 ± 26.86 (6)

5.10.6 Beam walk paradigm

To assess cerebellar function of mice lacking Kir4.1 in NG2 glia, the beam walk test was performed. In this test control and Kir4.1 flox mice were placed on rods with different diameters to test for their motor- and coordination abilities. The time (latency) needed to cross the rod and to enter the goal box at the end of the rod was measured. On rods with a diameter of 28 mm and 14 mm mice lacking the Kir4.1 channel in NG2 glia completed the task significantly faster than control mice ($p = 0.03$ for 28 mm and $p = 0.03$ for 14 mm) (Fig. 5.33 A, B). Neither were differences found between male and female mice of either genotype nor was there an interaction between sex and genotype. On a rod of 8 mm diameter the performance between control and Kir4.1 flox mice and between male and female mice was similar (Fig. 5.33 C). However, statistical analysis revealed an interaction between sex and genotype ($p < 0.01$) indicating that the genotype differently affected the ability of male and female mice to walk on the rod. Taken together, the results obtained from the beam walking test led to the assumption that in mice lacking Kir4.1 channels in NG2 glia motor coordination was improved.

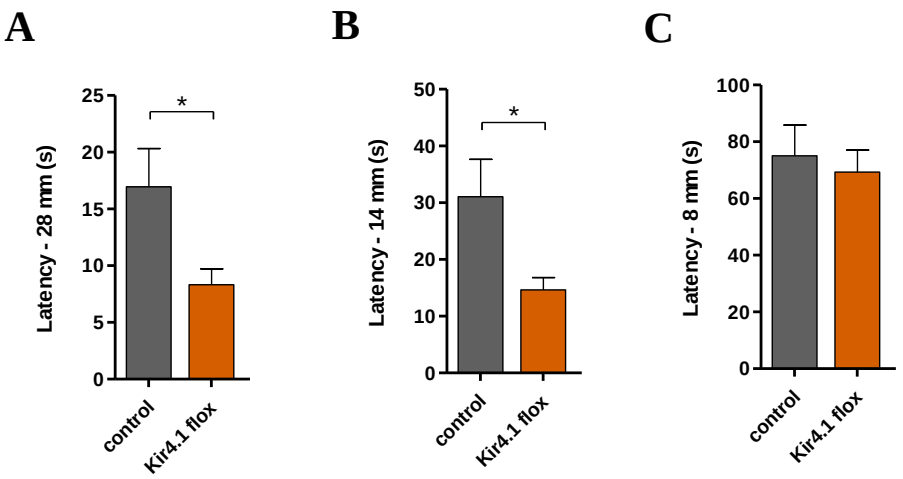

Fig. 5.33: Beam walking paradigm
In the beam walking test mice need to balance on rods of different diameter. Kir4.1 flox mice were reaching the goal box at the end of a **A)** 28 mm and **B)** 14 mm rod significantly faster than control mice. **C)** On a rod with 8 mm diameter the performance of control and Kir4.1 flox mice were similar. control, 17 mice; Kir4.1 flox, 19 mice. Mean ± SEM.

5.11 AMPA receptor knockout in NG2 glia: Triple GluA flox mice

For a different approach to investigate the impact of NG2 glia and neuron-NG2 glia signaling in the brain, a mouse line was established in which AMPA receptors expressed by NG2 glia are targeted for deletion. In these mice, the AMPA receptor subunits GluA1 (GluR1), GluA2 (GluR2) and GluA4 (GluR4), that mainly compose the AMPA receptors in NG2 glia (Seifert et al., 1997), are flanked by loxP sites (triple GluA flox mice). Similar to Kir4.1 flox mice, the expression of the recombinase CreER^{T2} is controlled by the NG2 glia promoter to ensures an NG2 glia specific ko. CreER^{T2} activity that leads to the recombination and subsequent deletion of all three subunits was induced by intraperitoneal application of the estrogen analogue tamoxifen.

5.11.1 Passive membrane properties of triple GluA flox NG2 glia in the hippocampus

Triple GluA flox mice were started to be characterized in parallel to the Kir4.1 flox mouse line. Before the tamoxifen protocol was established as described in section 5.1.2, these mice were treated with the initial tamoxifen protocol of 1 mg tamoxifen per injection, with 2 injections per day for five consecutive days (Huang et al., 2014). NG2 glia in which the recombinase CreER^{T2} was active were identified by expression of the reporter protein EYFP (recombined NG2 glia). To investigate if the ko of AMPA receptors affected passive membrane properties of NG2 glia, the resting membrane potential, the membrane resistance

and the membrane capacitance were analyzed. Whole-cell patch-clamp recordings were performed on recombined NG2 glia of triple GluA flox mice and NG2 glia of NG2-EYFPki mice that were serving as control. NG2 glia of both mouse lines displayed similar resting membrane potentials between – 85 mV and -90 mV (Fig. 5.34 A; table 14). The membrane resistance and membrane capacitance (Fig. 5.34 B,C; table 14) was also not different comparing NG2 glia of NG2-EYFPki mice and triple GluA flox mice. Thus, the passive membrane properties were not altered in recombined NG2 glia of triple GluA flox mice.

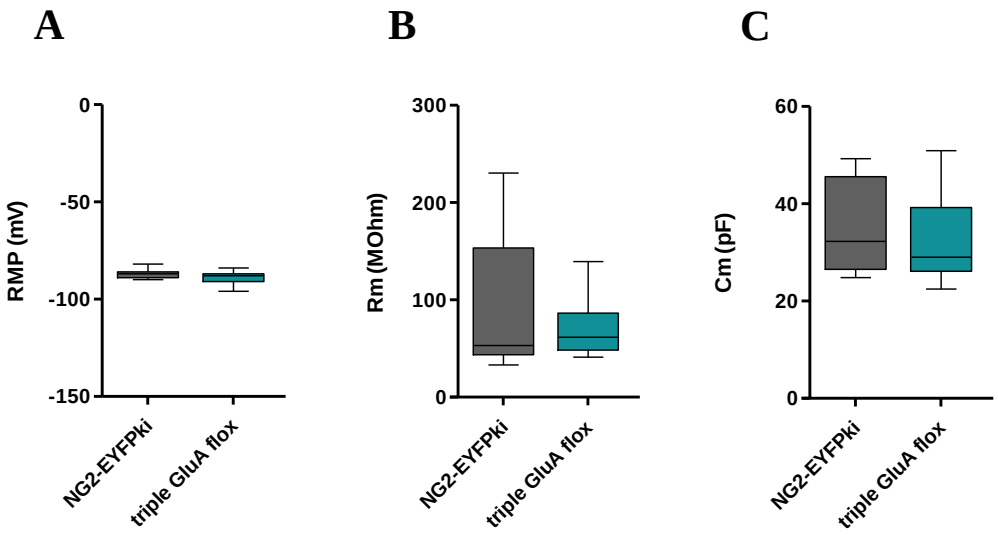

Fig. 5.34: Passive membrane properties of NG2 glia of NG2-EYFPki and triple GluA flox mice.
A) Resting membrane potential (RMP), **B)** membrane resistance (Rm) and **C)** membrane capacitance (Cm) were not different between NG2 glia of NG2-EYFPki mice and recombined NG2 glia of triple GluA flox mice (holding potential of -70 mV). NG2-EYFPki: n = 8; triple GluA flox: n = 11. Mann-Whitney U test. Data is presented as tukey box-plots with median (central line), quartiles (25% and 75%; box) and percentiles (1.5 times the interquartile range).

Table 14: Passive membrane properties of NG2 glia of NG2-EYFPki and triple GluA flox mice.
Holding potential of -70 mV. RMP, resting membrane potential; Rm, membrane resistance; Cm, membrane capacitance. Data is given as median and interquartile range (quartile 25% – quartile 75%). n, number of cells.

	NG2-EYFPki	Triple GluA flox
RMP (mV)	-87 (-89 - -86)	-88 (-91 - -87)
Rm (MOhm)	53.14 (43.65 – 153.36)	61.61 (48.27 – 86.28)
Cm (pF)	32.27 (26.53 – 45.59)	29.04 (26.53 – 39.23)
n	9	11

5.11.2 Characterization of kainte induced currents in hippocampal NG2 glia of triple GluA flox mice

To test if CreER^{T2} activity in recombined NG2 glia was able to delete the AMPA receptor subunits GluA1, GluA2 and GluA4 and thus, AMPA receptor mediated currents, the AMPA receptor agonist kainate (250 µM) was applied to the cells via focal pressure application (Fig. 5.35 A). Before application of kainate, voltage gated Na^+ channels, GABA receptors and K^+ channels were blocked by TTX (0.5 µM), quinine (200 µM) and picrotoxin (100 µM) to isolate the sole AMPA receptor mediated response. The maximal amplitude of the AMPA receptor current evoked upon kainate application was normalized to the respective membrane capacitance of the cell measured. Surprisingly, kainate application induced currents in recombined NG2 glia of both, NG2-EYFPki and triple GluA flox mice. The current density of kainate treated NG2 glia, measured at -70 mV, was between -15 pA/pF to -35 pA/pF similar in NG2-EYFPki mice and triple GluA flox mice (Fig. 5.35 B). Thus, despite CreER^{T2} activity, kainate induced receptor currents could be still detected in recombined NG2 glia of triple GluA flox mice.

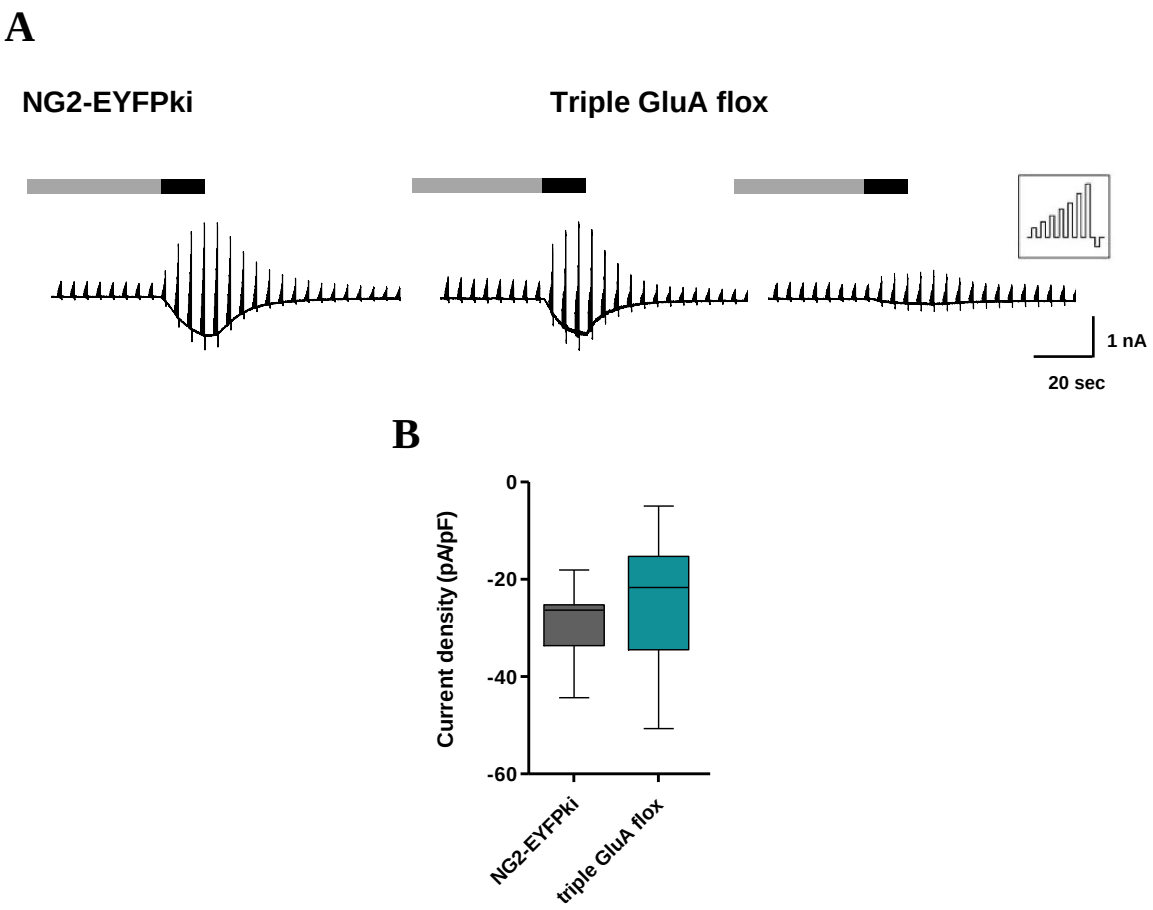

Fig. 5.35: Kainate induced receptor currents.
A) Example traces of NG2 glia of NG2-EYFPki mice and triple GluA flox mice during application of kainate (black bar). NG2 glia were patched in whole-cell configuration (holding potential of -70 mV) and clamped to different voltages (-40/-20/0/20/40/80/100/-100 mV; black peaks; see inset) every 3 s. K^+ channels, voltage gated Na^+ channels and GABA receptors were blocked by quinine (200 µM), TTX (0.5 µM) and picrotoxin (100 µM) (grey bar) before kainate (250 µM) was applied (black bar). **B)** Kainate induced current densities at -70 mV in NG2 glia of NG2-EYFPki mice and recombined NG2 glia of triple AMPA receptor mice were not different. t-test. NG2-EYFPki, n = 9 cells. Triple GluA flox, n = 12 cells. Data is presented as tukey box-plots with median (central line), quartiles (25% and 75%; box) and percentiles (1.5 times the interquartile range).

To estimate the characteristics of these receptor currents, the current-voltage (I-V) relation of kainate induced response were analyzed. Before, during and after kainate application, a voltage step protocol was applied that de- and hyperpolarized the cell between -100 mV to +80 mV (Fig. 5.28 A). Subtracting the voltage evoked currents before kainate application from those recorded during kainate application revealed the I-V relation of the pure kainate induced response that was then normalized to the smallest current measured during the voltage step protocol. In NG2 glia of NG2-EYFPki mice and in some recombined NG2 glia of triple GluA flox mice, the kainate induced response displayed a linear I-V relation (Fig. 5.36 A, B - left). In other recombined NG2 glia of triple GluA flox mice, the kainate induced current was close to zero between – 20 mV and +30 mV, progressively increasing again at more positive potentials (Fig. 5.36 B - right). This voltage dependent block of the receptor currents arises from polyamines like spermine that block the AMPA receptor channel pore from the intracellular site, preventing ion efflux and thus, leading to inwardly rectifying receptor currents (Bergles et al., 2000; Donevan and Rogawski, 1995; Kamboj et al., 1995b; Koh et al., 1995; Seifert et al., 2003). When the driving force is strong enough (membrane potentials more positive than +30 mV) spermine can pass the pore, allowing outward directed currents. To determine the rectification of the AMPA receptor currents in NG2-EYFPki mice and GluA flox mice, the rectification index (RI) was calculated (see section 4.4.8.2) by the current ratio of receptor currents at -70 mV, representing the resting potential where the block is low and AMPA receptor currents are inward directed and at +40 mV, the voltage at which the block is removed and the outward current starts to recover (Pellegrini-Giampietro, 2003). An index < 1 indicates inwardly rectifying receptor currents; > 1 outwardly rectifying currents. As during the whole-cell patch-clamp recording the cytoplasm is slowly dialyzed by the solution inside the patch-pipette, spermine (50 µM) was supplemented to the pipette solution to ensure the presence of this polyamines.

The rectification index of kainate induced receptor currents in NG2 glia of NG2-EYFPki mice indicated a linear rectification (RI = 1.01; n = 9). For recombined NG2 glia of triple GluA flox mice, that exhibited a reduced outward current at positive potentials, an RI = 0.55 (n = 12) was determined, indicating inwardly rectifying I-V relations, (Fig. 5.36 C). The reversal potential of kainate induced currents was with -2.7 mV and -3.6 mV similar in NG2 glia of NG2-EYFPki mice and recombined NG2-glia cells of triple GluA flox (Fig. 5.36 D).

In summary, these results showed that despite CreER^{T2} activity, single or multiple AMPA receptor subunits were still expressed by recombined NG2 glia of triple GluA flox mice. Differences in the I-V relation of kainate induced currents recorded in recombined NG2 glia of triple GluA flox mice compared to NG2 glia of NG2-EYFPki mice, indicate functional differences between AMPA receptors.

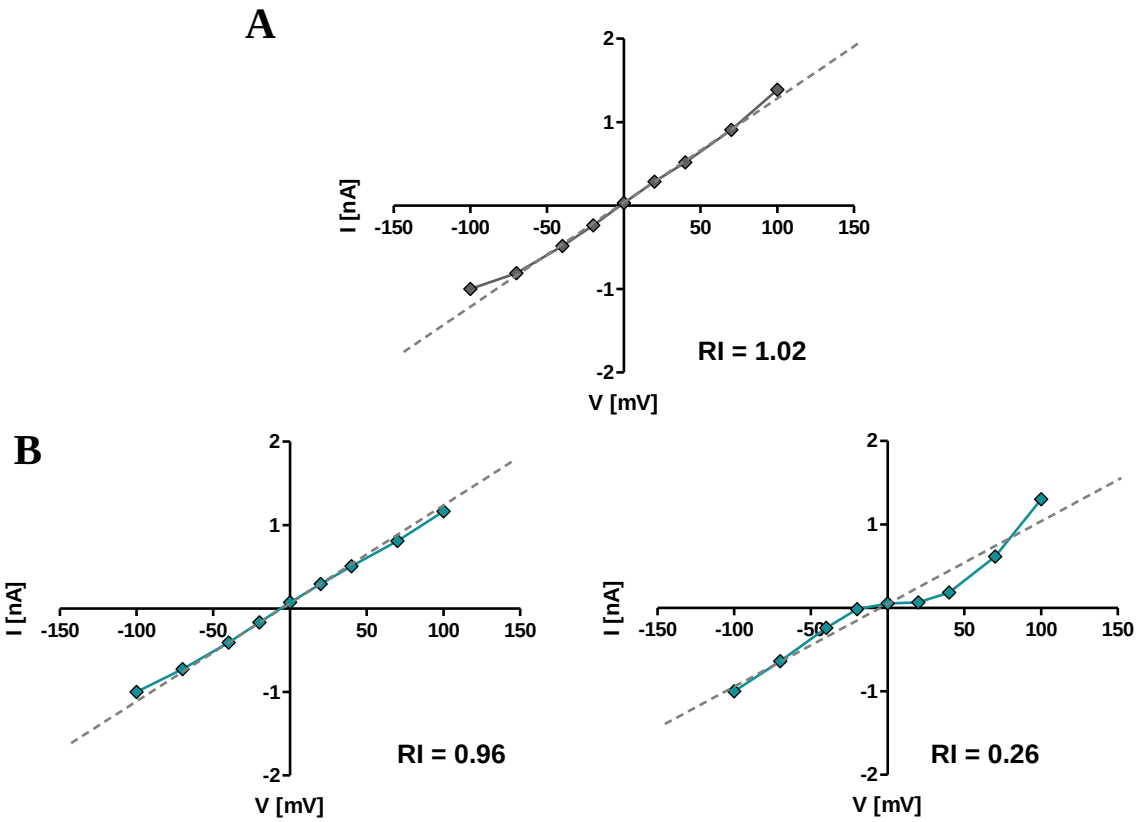

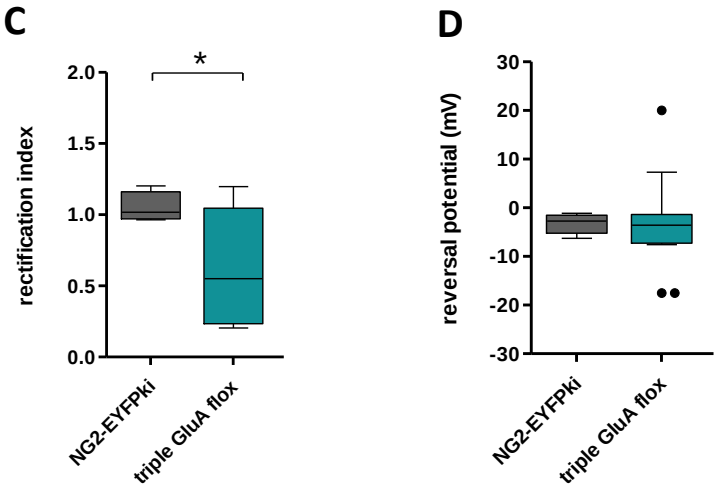

Fig. 5.36: Characteristics of AMPA receptors in NG2 glia.
A) Representative I-V relationships of kainate induced receptor currents in NG2 glia of NG2-EYFPki mice and **B)** recombined NG2 glia of triple GluA flox mice. Dashed line indicates linearity. The rectification index is mentioned respectively. In recombined NG2 glia of triple GluA flox mice, kainate induced currents showed linear (left) or inward rectifying (right) I-V relations. NG2 glia of NG2-EYFPki mice displayed a linear I-V relation. **C)** The rectification index determined for recombined NG2 glia of triple GluA flox mice revealed inward rectification (RI < 1) of kainate induces responses compared to the linear rectification (RI = 1) of kainate induced currents in NG2 glia of NG2-EYFPki mice ($p = 0.02$). **D)** The reversal potential was not different between groups. Mann-Whitney U test. NG2-EYFP, n = 9 cells; triple GluA flox, n = 12 cells. Data is presented as tukey box-plots with median (central line), quartiles (25% and 75%; box) and percentiles (1.5 times the interquartile range). Outliers are shown as dots. RI, rectification index.

5.11.3 Single-cell TR-PCR analysis of AMPA receptor subunits of triple GluA flox NG2 glia

Despite $CreER^{T2}$ activity, indicated by expression of the reporter protein EYFP, receptor mediated currents could be evoked in NG2 glia of triple GluA flox mice upon application of the AMPA/kainate receptor agonist kainate (Fig. 5.10.2). To determine whether these currents were mediated by the targeted AMPA receptor subunits GluA1, GluA2 and GluA4, samples of cells were tested on molecular level for the presence of AMPA receptor subunit mRNA with single cell RT-PCR (performed by Dr. Gerald Seifert). After application of kainate, the recorded cells were harvested and single cell RT-PCR was performed (Fig. 5.37). The analysis confirmed that mRNA for AMPA receptor subunits were still present. In cell number 1 mRNA coding for GluA2 and in cell number 2 and 3, mRNA for GluA3 were found. In cell number 4 mRNA of GluA2 and GluA3 was detected. Surprisingly in 3 out of 4 cells analyzed, mRNA coding for the AMPA receptor subunit GluA3 was detected. This led to the speculation that a compensatory upregulation of the GluA3 subunit took place upon deletion of other AMPA receptor subunits. Taken together, these results provided evidence

that the deletion of the subunits GluA1, GluA2, and GluA4 were not sufficient to completely abolish AMPA receptor mediated currents. All four receptor subunits seemed to be required to be targeted by CreER^{T2} mediated recombination and subsequent deletion to establish a total ko of AMPA receptors in NG2 glia.

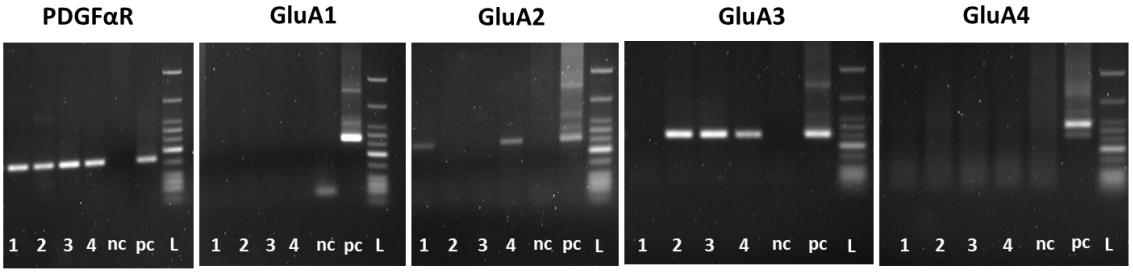

Fig. 5.37: Presence of AMPA receptor subunit mRNA in triple Glua flox NG2 glia
Agarose gels of single cell RT-PCR products. Single cell RT-PCR was performed with four recombined NG2 glia harvested from slices of triple GluA flox mice subsequent to pharmacological analysis. Recombined NG2 glia of triple GluA flox mice (cell # 1 - 4) were analysed for the presence of mRNA coding for the AMPA receptor subunits GluA1, 2, 3 and 4. To prove NG2 glia identity, the presence of PDGRα mRNA, a marker for NG2 glia, was tested. Gel electrophoretic analysis revealed the presence of single AMPA receptor subunits, including GluA3 in recombined NG2 glia. nc, negative control; pc, positive control; L, low molecular weight DNA ladder.

5.12 AMPA receptor knockout in NG2 glia: Quadruple GluA flox mice

In light of the results obtained from the triple GluA flox mouse line a successful deletion of functional AMPA receptors in NG2 glia required the establishment of a mouse line with all four genes coding for the AMPA receptor subunits being flanked by the recognitions sites, enabling CreER^{T2} mediated recombination to take place. This quadruple GluA flox mouse line was generated by breeding triple GluA flox mice with mice inheriting the gene coding for the AMPA receptor subunit GluA3 flanked by loxP sites (GluA3 flox). As this breeding generated in the first generation mice with all four AMPA receptor subunits being heterozygote for the loxP site, further breedings were necessary to obtain quadruple GluA flox mice.

To investigate the deletion of AMPA receptors in quadruple GluA flox mice after tamoxifen treatment, whole-cell patch-clamp recordings of recombined NG2 glia of the hippocampus were performed and kainate applied as decribed in section 5.11.2. The first recordings in recombined NG2 glia of quadruple GluA flox mice were promising as only a tiny residual kainate induced current was observed (Fig. 5.38). The question about the identity of these currents and the impact of an NG2 glia specific ko of AMPA receptors on NG2 glia proliferation and differentiation as well as its influence on myelination and neuronal network

function were started to be answered by Stefan Hardt, a medical doctorate student of the Institute of cellular Neurosciences.

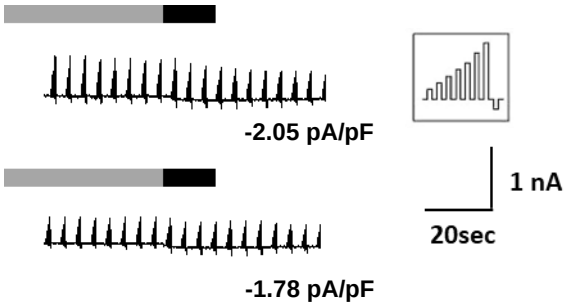

Fig. 5.38: Lack of kainate induced AMPA receptor mediated currents in quadruple GluA flox mice. Current traces of two recombined NG2 glia of quadruple GluA flox mice during application of kainate (black bar). Cells were patched in whole-cell configuration (holding potential of -70 mV) and clamped to different voltages (-40/-20/0/20/40/80/100/-100 mV; black peaks; see inset) every 3 s. K^+ channels, voltage gated Na^+ channels and GABA receptors were blocked by quinine (200 µM), TTX (0.5 µM) and picrotoxin (100 µM) (grey bar) before kainate (250 µM) was additionally applied (black bar). The current density at -70 mV is mentioned obove the respective current.

6 Discussion

NG2 glia receive direct synaptic input from GABAergic and glutamatergic neurons. But the role of these glial cells, especially in grey matter and the impact of this neuronal input are not well understood. In the present study, a mouse line based on the Cre/loxP system was used to specifically alter NG2 glia properties and to investigate consequences of dysfunctional NG2 glia on neuronal activity and animal behavior. As a target for the NG2-CreER^{T2} mediated ko, the gene encoding for the prominently expressed inwardly rectifying K^+ channel Kir4.1 was chosen.

In the hippocampus the deletion of Kir4.1 from adult NG2 glia resulted in drastic changes of the passive membrane properties of these cells further altering their excitability upon neuronal input. Consequences of the ko spread onto neuronal level, increasing the release probability of vesicles at the Schaffer collateral - NG2 glia synapse and weakening LTP at CA3 and CA1 synapses. On behavioral level the NG2 glia specific deletion of Kir4.1 even altered memory performance of ko mice.

6.1 Kir4.1 determines NG2 glia properties

In adult NG2 glia, Kir4.1 channels represent one of the most prominently expressed ion channels, that carry with more than 80% the main K^+ inward current at rest (Song et al., 2018). Genetic ablation of Kir4.1 from adult NG2 glia via CreER^{T2} mediated recombination, as presented in this study, successfully deleted these Kir4.1 mediated K^+ currents in more than 75% of all recombined NG2 glia, indicated by a conductance at -130 mV of < 6 pA/mV (Kir4.1 ko cells). However, a minor $BaCl_2$ sensitive current remained in NG2 glia deprived of Kir4.1. Barium (Ba^{2+}) is a non-selective K^+ channel blocker that inhibits different K^+ channels in a concentration dependent manner (Hibino et al., 2010; Lesage et al., 1996; Nwaobi et al., 2016; Seifert et al., 2009; Song et al., 2018; Zhou et al., 2009). To specifically block Kir channels, a submilimolar concentration of 100 µM was used, as described in other studies (Jansen et al., 2005; Seifert et al., 2009; Song et al., 2018). Despite Kir4.1 mediating the main K^+ conductance in NG2 glia, RNA sequencing revealed the expression of multiple Kir subunits like Kir5.1, Kir3.1, Kir2.1 and Kir6.1 in NG2 glia. However, the transcript level

of these subunits was much lower compared to the level of Kir4.1 mRNA (Kir4.1 - 83 FPKM (fragments per kilobase of transcript per million mapped reads) > Kir5.1 - 7 FPKM < other). TWIK1 channels, showing a higher transcript level then Kir5.1 (24 FPKM) could have also contributed to the remaining K^+ conductance (Larson et al., 2016; Zhang et al., 2014). It was demonstrated that TWIK1 channels, members of the two-pore domain channel family, show a similar Ba^{2+} sensitivity at 100 µM (Lesage et al., 1996). Even though functional analysis of TWIK1 expression could not confirm an impact of these channels on the electrophysiological characteristics of NG2 glia (Maldonado et al., 2013), evidence for their existence on transcript level exist (Larson et al., 2016). The potential contribution of TWIK1 and other Kir channels channels to the K^+ background conductance in NG2 glia, might have been masked so far, due to the massive influx of K^+ trough Kir4.1 channels. Deletion of Kir4.1, as shown in the present study, might have revealed a minor impact of TWIK1 on K^+ currents. The major K^+ inward conductance in NG2 glia, however, was confirmed to be mediated by Kir4.1 channels.

The relevance of Kir4.1 not only in setting cellular membrane properties but also to shape functional properties of glial cells, was proven by various studies, in which Kir4.1 was pharmacologically or genetically deleted. Deletion of this channel from Müller cells (Kofuji et al., 2000), astrocytes and cells of the oligodendrocyte lineage (Djukic et al., 2007; Neusch et al., 2001) had extensive consequences on K^+ buffering, regulation of neuronal activity and myelination. For adult NG2 glia, however, the potential role of Kir4.1 in regulating cell function is not known so far. During development, inwardly rectifying K^+ channels are upregulated in NG2 glia, setting the membrane potential close to the K^+ equilibrium potential and lowering the membrane resistance of these cells (Kressin et al., 1995). Consequently, the deletion of Kir4.1 from adult NG2 glia resulted in a depolarized resting membrane potential and drastic increase of the membrane resistance, turning NG2 glia into high ohmic cells. Studies, using a mouse line with a PDGFRα driven $CreER^{T2}$ expression to delete Kir4.1 specifically from NG2 glia, confirmed these findings (Larson et al., 2018; Song et al., 2018). In its role as a key determinant for NG2 glia membrane properties, its relevance in controlling NG2 glia excitability upon neuronal input was investigated in mEPSP recordings. According to Ohm´s law (V = I * R), a given *current I* will evoke an increase in *voltage V* if the *resistance R* is increased. As the strength of the transmitter mediated depolarization should therefore correspond to the membrane resistance (*R*), the response (*V*) upon neuronal input (*I*) was expected to be increased. Indeed, recording of mEPSPs that occur upon spontaneous fusion of vesicles with the presynapse in absence of action potentials revealed a much stronger and long-lasting depolarisation in cells lacking Kir4.1. Similar results were obtained from NG2 glia when Kir4.1 was blocked by $BaCl_2$ (Chan et al., 2013b) or upon current injection in

Müller cells lacking Kir4.1 (Kofuji et al., 2000). These findings support the idea, that Kir channels limit the temporal window of mEPSP while controling the EPSP amplitude and kinetics (Chan et al., 2013b). In NG2 glia lacking Kir4.1, these restrictions are canceled, resulting in the observed changes in mEPSP rise time, decay time and amplitude. The prolonged depolarization further enables temporal summation of subsequent mEPSP, that could additionally extend the duration and ampliude of the depolarization. This raises the question about the functional consequence of this highly excitable state. Interestingly, an upregulation of Kir channel expression and concomitant changes in passive membrane properties and excitability do also occur during the maturation process of dentate gyrus granule cells (Esposito, 2005; Mongiat et al., 2009). Similarly to low expression of Kir4.1 in juvenile NG2 glia, channels of the Kir2.x family (Kir2.1, Kir2.2, Kir2.3 and Kir2.4) are only weakly expressed in young granule cells (Kukley and Dietrich, 2009; Young et al., 2009). Consequently, the resulting high membrane resistance triggers the generation of action potentials already upon small synaptic currents (Mongiat et al., 2009). This efficient and reliable transduction of synaptic input into a postsynaptic response, is a key mechanism to compensate for the fact, that young neurons have only a low number of synaptic contacts. Mature neurons, by contrast, are highly innervated. The membrane resistance of mature neurons is, however, much lower, setting the threshold for the generation of action potentials higher than in young neurons. In the end, the spiking probability of these low ohmic cells with a high innervation (mature neurons) is similar to high ohmic cells with a low innervation (young neurons) (Mongiat et al., 2009). Granule cells of different developmental stages and characteristics are thus integrated perfectly into the network.

To estimate the connectivity of NG2 glia in control and Kir4.1 flox mice, the inter-event interval of mEPSPs was determined. Interestingly, the inter-event interval was increased for mEPSPs recorded in Kir4.1 ko cells compared to Kir4.1 wt cells, suggesting a lower connectivity of Kir4.1 ko cells. This observation could display a loss of synaptic contacts or redistribution of synapses from Kir4.1 ko cells to Kir4.1 wt cells, a regulatory mechanism to counterbalance the higher excitability of Kir4.1 ko cells similar to the situation described for juvenile dentate gyrus granule cells. So far, a reduction of synapses contacting NG2 glia was observed during development. Studies reported an age dependent decline of mEPSC frequency (Passlick et al., 2016) and the retraction of NG2 glia processes in adult mice (Rivera et al., 2016) that were assumed to correlate with a reduced number of contact sites. Some studies also suggested that mEPSP frequency is linked to the probability of vesicles to be released from the presynaptic terminal (Cho and Askwith, 2008; Prange and Murphy, 1999; Zucker and Regehr, 2002). The release probability at the neuron - NG2 glia synapse

was evaluated by paired pulse stimulation of Schaffer collaterals. At both, Kir4.1 wt and Kir4.1 ko synapses, the release probability was increased (see section 6.2). Consequently, the frequency of mEPSP in NG2 glia of the Kir4.1 flox mice should have been higher than in control. But this was not the case. Other publications already argued about the relationship between release probability, representing the evoked release of vesicles, and mEPSP that occur in absence of action potentials. It was claimed that the mechanisms underlying evoked and spontaneous release were regulated independently (Kavalali, 2015; Ramirez and Kavalali, 2011). Spontaneous release is thought to depend more on the basal Ca^{2+} concentration in the cell than evoked release and that even different vesicle pools exist that are released either spontaneously or due to stimulation. It should also be taken into account that mEPSPs represent the release of single vesicles from the synapse, whereas induced release recruit multiple vesicles and synapses at the same time (Kavalali et al., 2011). Importantly, for the interpretation of the results it has to be considered that the baseline of mEPSP, representing the resting membrane potential of the cell, was instable in Kir4.1 ko cells. Compared to Kir4.1 wt and control, mEPSP recordings of Kir4.1 ko cells showed fluctuation of a few mV. This demonstrates the necessity of Kir4.1 to set the membrane potential to a certain value and to restrain these fluctuations. Due to the rather unstable membrane potential, mEPSPs of smaller amplitudes might have been masked and not being taken into account for the subsequent mEPSP analysis. Consequently, the number of events recorded in Kir4.1 ko cells might have been underestimated. Recording of miniature excitatory postsynaptic **currents** (mEPSCs) instead, in which the membrane potential is clamped by the patch-clamp amplifier, would be more precise to answer the question about the connectivity of adult NG2 glia in mice lacking Kir4.1.

As both, glutamatergic and GABAergic input leads to a depolarization of NG2 glia (Jabs et al., 2005; Kukley et al., 2008; Lin and Bergles, 2004b; Mangin et al., 2008), the contribution of GABAergic input on mEPSP was prevented by application of GABA receptor blocker picrotoxin. Surprisingly, in Kir4.1 wt cells an increased inter-event interval was observed in presence of the blocker. For NG2 glia of control mice and Kir4.1 ko cells such an effect was not observed. This might be due to an unequally distributed number of synapses formed by either GABAergic or glutamatergic neurons. However, it is difficult to estimate the proportion of glutamatergic and GABAergic synapses formed with NG2 glia. In hippocampal NG2 glia the number of glutamatergic synapses was estimated between 7 and 19 (Bergles et al., 2000). As the density of GABAergic input was expected to be 5-times less than Glutamatergic input (Sun and Dietrich, 2013), the number of GABAergic synapses in the hippocampus should be limited to only a few. Additionally to this small number of synaptic

contacts between neurons and NG2 glia, spontaneous release of vesicles onto NG2 glia is generally a rare event (Kukley et al., 2010; Lin and Bergles, 2004a; Passlick et al., 2016).

In summary, the inwardly rectifying K^+ channel Kir4.1 mediates the main K^+ conductance in adult NG2 glia. Its expression determines the passive membrane properties of these cells and their excitability upon neuronal input. Genetic deletion of this channel in adult NG2 glia caused a drastic increase of the membrane resistance and a depolarization of the membrane potential. Consequently, neuronal input resulted in strong and prolonged responses in Kir4.1 ko cells.

6.2 Increased release probability at neuron-NG2 glia synapses in Kir4.1 flox mice

The probability of vesicles being released from a synapse determines the way, how neuronal signals are processed. Facilitating synapses, characterized by a low release probability, are supposed to strengthen synaptic transmission. Upon paired stimuli, these synapses show a stronger response upon the second stimulus than on the first. Synapses with a high release probability, showing a higher response upon the first than on the second stimulus, are considered to attenuate transmission (Abbott and Regehr, 2004). The release probability of a synapse depends on different factors within the presynapse like the intracellular Ca^{2+} concentration (basal Ca^{2+} level and during neuronal activity), activity of voltage gated Ca^{2+} channels (VGCCs), availability and size of the readily releasable vesicle pool, receptor expression and number of active release sites (Deng and Klyachko, 2011; Fioravante and Regehr, 2011; Zucker and Regehr, 2002). In the hippocampus, the probability of vesicles to be released at the Schaffer collateral - NG2 glia synapse is low, similar to synapses at Schaffer collateral - CA1 pyramidal cells (Bergles et al., 2000; Passlick et al., 2016; Speed and Dobrunz, 2009). Interestingly, in mice lacking Kir4.1 in NG2 glia the associated paired pulse facilitation was significantly reduced, indicating an increase in release probability. Surprisingly, this increase did not only account for synapses between neurons and Kir4.1 ko cells, but also between neurons and Kir4.1 wt cells. Thus, ablation of Kir4.1 from NG2 glia seemed to affect the release probability at all neuron - NG2 glia synapses in Kir4.1 flox mice, not only at those synapses formed between neurons and NG2 glia lacking Kir4.1. Notably, a high release probability at neuron - NG2 glia synapses, leading to paired pulse depression, was demonstrated in studies focusing on GABAergic and not glutamatergic input onto NG2 glia. In the stratum radiatum of adult rats, paired pulse stimulation in presence of the AMPA receptor blocker NBQX, revealed paired pulse depression at the Schaffer collateral - NG2

glia synapse (Lin and Bergles, 2004a). Similar results were obtained in cortical nestin^{+}/NG2^{+} cells during inhibition of glutamatergic input (Tanaka et al., 2009). In the barrel cortex of juvenile mice, where NG2 glia receive primarily GABAergic input, the release probability was likewise increased (Velez-Fort et al., 2010). In this respect, a high release probability seems to be a characteristic of GABAergic signaling onto NG2 glia. Indeed, upon application of GABA receptor blocker picrotoxin the release probability at neuron - NG2 glia synapses in Kir4.1 flox mice decreased to control levels. The release probability at neuron - NG2 glia of control mice remained unaffected in presence or absence of picrotoxin. It seems that GABAergic synapses play a more dominant role in Kir4.1 flox mice than in control mice, interfering with Schaffer collateral signaling onto NG2 glia. Even though the application of minimal stimulation intensities during the paired pulse recording should have provided the excitation of only a few or even just one axon. The stimulation of multiple axons, meaning those from glutamatergic and GABAergic neurons, would have caused multiple responses to occur upon a single stimulus. Depending on the speed of signal transmission, these responses might be temporally dispersed. In the study of Jabs et al. 2005, however, glutamatergic and GABAergic mediated responses were simultaneously induced, in correlation to the applied stimulus. According to the decay time, the responses could be assigned to glutamatergic (1-2 ms) or GABAergic input (> 20 ms) (Jabs et al., 2005). The decay time of evoked EPSCs in NG2 glia (1-2 ms) seemed to be entirely glutamatergic. The variation of the decay times, however, appeared to be slightly higher in Kir4.1 ko and Kir4.1 wt cells. In presence of picrotoxin this variability was reduced, implying a contribution of GABAergic signals to evoked EPSCs. The activation of GABAergic neurons might arise from the electric field that is generated by the stimulation electrode. Thus, not only Schaffer collaterals but also interneurons might be recruited in parallel upon the applied stimulus. Why a contribution of GABAergic signaling was only detected at neuron - NG2 glia synapses in Kir4.1 flox mice, but not control mice, is not clear. A potential role could play a difference in the level of BDNF (brain derived neurotrophic factor). BDNF was shown to affect neuronal release probability and to play a regulatory role concerning the balance of glutamatergic and GABAergic activity (Asztely et al., 2000; Frerking et al., 1998; Olofsdotter et al., 2000; Tanaka et al., 1997). In a transgenic mouse model with a heterozygous deletion of BDNF (BDNF +/- ko mice), the reduced BDNF level led to an increase in the release probability at the interneuron - granule cell synapse in the dentate gyrus (Olofsdotter et al., 2000). If this holds true for the interneuron - NG2 glia synapse in the stratum radiatum of Kir4.1 flox mice, it is interesting that during paired field potential recordings of involving CA3 - CA1 synapses, a change of release probability was not detected. Aszteky et al., 2000, claimed that the effect of BDNF can not

only differ according to the type of postsynaptic cell, but does also depend on the type of the synaptic input (Asztely et al., 2000; Rutherford et al., 1998). In the study of Aszteky et al., 2000 the reduced level of BDNF in BDNF +/- ko mice affected differently the release probability of two glutamatergic pathways of the cortex, innervating granule cells of the dentate gyrus. At synapses between the medial perforant path and granule cell the high release probability was impaired, whereas the low release probability at synapses formed between lateral perforant path and granule cells was not affected (Asztely et al., 2000). Evidence for the expression and release of BDNF by NG2 glia in vivo is lacking so far. Until now, Tanaka et al. (2009) discovered that in the neocortex a population of NG2 glia expressing nestin, a stem cell intermediate filament (Lendahl et al., 1990), were able to produce and release BDNF (Tanaka et al., 2009). The secretion was triggered by long-term incubation (9h) of isolated nestin^{+} NG2 glia with GABA. The authors assumed that the GABA induced depolarization and subsequent Ca^{2+} signals in nestin^{+} NG2 glia triggered the expression of BDNF (Tanaka et al., 2009). A Ca^{2+} dependent production of BDNF was also shown in cultured hippocampal neurons (Balkowiec and Katz, 2002). A potential link between Kir4.1 and BDNF signaling was demonstrated by Kinoboshi et al. in 2007. In cultured astrocytes, the expression and release of BDNF was shown to be coupled to the activation of MAP/ERK pathway. This pathway was activated upon pharmacological blockage of Kir4.1 or its inhibition via siRNA (Kinboshi et al., 2017). Thus, deletion of Kir4.1 and the depolarized membrane potential of Kir4.1 ko cells might trigger the expression and release of BDNF and/or other factors in a Ca^{2+}- dependent manner. As not only the vesicular release at the Schaffer collateral - Kir4.1 ko cell synapses was altered, but also at sites of Kir4.1 wt cells, a potential release of modulatory factors from Kir4.1 ko cells would require the spillover to other neuron-NG2 glia terminals.

In conclusion, the high excitability of NG2 glia and their depolarized membrane potential might favor Ca^{2+} induced expression and release of factors that can modulate the release probability at neuron - NG2 glia synapses. This would require VGCCs which were shown to be functionally expressed by NG2 glia of different brain regions and developmental stages (Akopian et al., 1996; Fulton et al., 2010; Haberlandt et al., 2011; Pitman et al., 2019; Sun et al., 2016; Velez-Fort et al., 2010). Both, L-type (long-lasting) and T-type (transient) channels belonging to the family of high and low VGCCs were shown to be present in NG2 glia (Akopian et al., 1996; Fulton et al., 2010; Haberlandt et al., 2011b; Kandel et al., 2000)

However, the conditions under which these channels can be activated in NG2 glia are still discussed. Stimulation experiments mimicking synaptic transmission of neurons to NG2 glia revealed Ca^{2+} transients in NG2 glia processes that were spreading to the soma (Sun et al.,

2016). In contrast, another study investigating the role of VGCCs in juvenile NG2 glia of the hippocampus, however, could not detect somatic Ca^{2+} transients upon physiological stimuli (Haberlandt et al., 2011). Similar results were obtained from the barrel cortex of 3 and 4 week old mice (Velez-Fort et al., 2010). The threshold of -50 mV for T-type and -20 mV for L-type channels (Akopian et al., 1996; Gómez-Pinilla et al., 1998) seems to be too high for adult NG2 glia that are characterized by a resting membrane potential of -80 mV. Deletion of Kir4.1, as described in the present study, resulting in a more depolarized resting membrane potential and a high input resistance, might be facilitate for the activation of VGCCs in adult NG2 glia. The stronger depolarization upon vesicular release might additionally favor the opening of these channels. The intracellular Ca^{2+} concentration can further rise in the soma via the opening of intracellular Ca^{2+} stores (Ca^{2+} induced Ca^{2+} release) or through Ca^{2+} permeable AMPA receptors and metabotropic glutamate receptors (Haberlandt et al., 2011). In its role as an important downstream molecule, the rise of intracellular Ca^{2+} could lead to an altered regulation of gene expression. For neurons, Ca^{2+} signaling through L-type channels led to the activation of the transcription factor CREB that can affect the expression of various genes like BDNF (Kornhauser et al., 2002; Murphy et al., 1991; West et al., 2001). As CREB was shown to be express in NG2 glia (Sato-Bigbee et al., 1999), similar consequences might be possible in these cells.

6.3 Deletion of Kir4.1 in NG2 glia favors myelination

NG2 glia lacking Kir4.1 were drastically altered according to their passive membrane properties, excitability and neuronal input. The loss of Kir4.1 and the associated changes raised the question about the effect of Kir4.1 deletion on NG2 glia proliferation and their ability to differentiate into myelinating oligodendrocytes. That Kir4.1 has an impact on glial cell proliferation has been demonstrated in several studies. Reactive astrocytes in models of gliosis were highly proliferative, and these cells did not or rarely express Kir channels and were characterized by a depolarized resting membrane potential (Bordey et al., 2001; MacFarlane and Sontheimer, 2000). Blockade of Kir channels by $BaCl_2$ mimicked this effect and led to an increased proliferation of astrocytes (MacFarlane and Sontheimer, 2000). Studies performed in glioma cells, representing a population of highly proliferative cells, confirmed that overexpression of Kir4.1 in astrocytic tumors and the concomitant hyperpolarization of these cells reduced their proliferative activity. It was stated that the hyperpolarization triggered a change in the cell cycle phase, from the proliferative G2/M phase to the quiescent G1/G0 phase (Higashimori and Sontheimer, 2007). These findings led

to the assumption that the proliferation of NG2 glia devoid of Kir4.1 might be altered. However, this role of Kir4.1 in controlling NG2 glia proliferation in the hippocampus of adult mice could not be confirmed. In agreement with the study of Larson and colleagues in 2018, using a PDGFRα-Cre mediated deletion of Kir4.1 specifically in NG2 glia, proliferation of recombined NG2 glia were not altered. The authors speculated that NG2 glia might compensate for the Kir4.1 ko induced changes of the resting membrane potential by upregulation of other K^+ channels (Larson et al., 2018). A reduced function or expression of voltage gated K^+ channels (Kv channels) were also shown to prevent NG2 glia proliferation (Chittajallu et al., 2002). The impact of Kv channels on NG2 glia proliferation was demonstrated to be linked to cyclin-dependent kinase inhibitors $p27_{Kip1}$ and $p21_{CIP1}$. Upon Kv channel inhibition and membrane depolarization the levels of these kinase inhibitors were enhanced, resulting in a cell cycle arrest of NG2 glia in the G1/G0 phase (Ghiani et al., 1999). Studies that investigated the role of Kir4.1 on the generation of oligodendrocytes, reported dramatic effects especially in CNS white matter regions, when deleting Kir4.1 from glial cells at a prenatal stage. In mice carrying a null mutation of the Kir4.1 gene, oligodendrocyte development was disturbed with severe consequences: Hypomyelination and demyelination took place, that were accompanied by vacuolization of myelin, damage or even degeneration of axons further causing deficits in motor coordination and a 100% lethality of these mice at p24 (Neusch et al., 2001). Similar results were obtained, restricting the ko to cells with an active GFAP promoter, deleting Kir4.1 from astrocytes and cells of the oligodendrocyte lineage (Djukic et al., 2007).

Compared to white matter, however, grey matter regions like the hippocampus are only sparsely myelinated, with a majority of NG2 glia retaining their phenotype and not differentiating into oligodendrocytes (Dimou et al., 2008; Hildebrand et al., 1993; Meier et al., 2004; Nickel and Gu, 2018). The deletion of Kir4.1 specifically from NG2 glia in adult mice, as described in present study, did not alter the low proportion differentiating NG2 glia. This observation is consistent with the findings of Larson et al. (2018), inducing a ko of Kir4.1 under the PDGFRA Cre promoter at the age of p21. Thus, in the hippocampus of adult mice, Kir4.1 does not seem to play a role in regulating hippocampal NG2 glia differentiation into oligodendrocytes. In this regard, it is remarkable, that in hippocampal slices of mice devoid of Kir4.1, the immunoreactivity for the myelin protein MBP was enhanced in the stratum radiatum, stratum lacunosum moleculae and stratum moleculare of the dentate gyrus. This increase in the MBP signal points towards an increased myelination in these mice. Even though MBP is not the sole component of myelin, its strong impact on myelin thickness allows the use of MBP expression as an indirect measure for the extent of myelination (Shine

et al., 1990). The need of MBP for the formation of compact myelin was pointed out in a study using mouse line, carrying different mutations in the MBP gene. These mouse lines were characterized by a graded expression of the MBP gene (0% - 100%) that correlated with the MBP protein level. Myelin thickness was shown to change accordingly. After reaching a relative expression of 50% of the MBP gene, myelin thickness did, however, not further increase (Shine et al., 1990). In mice that lack most of the gene encoding MBP, so called shiverer mice, MBP protein was nearly absent and the number of myelinated axons was dramatically reduced (Bird et al., 1978; Dupouey et al., 1979; Kirschner and Ganser, 1980; Roach et al., 1983; Shine et al., 1990). These mice developed a shivering tremor from p12 on, that became more severe during age (Chernoff, 1981).

The source of the observed enhanced MBP signal in the hippocampus in the present study is not clear. An increased formation of myelinating oligodendrocytes can be excluded, as the number of oligodendrocytes was similar in Kir4.1 and control mice. This seems to be contra intuitive as changes in myelinations during development (intrinsic myelination) and during neuronal activity (adaptive myelination), observed in both, white matte and grey matter regions (Bechler et al., 2018; Timmler and Simons, 2019) were shown to be associated with an increased number of oligodendrocytes. Long-term studies of Hughes et al. (2018) and Hill et al (2018) demonstrated that in the cortical grey matter the number of oligodendrocytes increases in parallel with enhanced myelination during aging (Hill et al., 2018; Hughes et al., 2018). This increase in myelination was related to the formation of new internodes by new oligodendrocytes at sites where myelin was absent before. Once formed, myelin was shown to be stable for up to 230 days, only a minority of internodes was retracting or expanding over time (Hill et al., 2018). This was mirrored in a heterogeneous myelin pattern, with differences in myelin coverage and internode length (Hill et al., 2018). An increased number of internodes in parallel with an increase in the number oligodendrocyte were observed in the somatosensory cortex after exposure of mice to sensory enrichment (Hughes et al., 2018). A few studies, however, reported changes of grey matter myelination without alterations in the proportion of oligodendrocytes. In socially isolated mice, the myelin sheath thickness was shown to be reduced in the prefrontal cortex (a brain region functionally relevant for social behavior), while the density of oligodendrocytes was unaffected. However, a decline of MBP and MAG mRNA was detected (Liu et al., 2012; Makinodan et al., 2012). Changes of MBP and MAG transcripts were also observed in the present study in recombined NG2 glia of Kir4.1 flox mice. Semiquantitative analysis of FAC sorted recombined hippocampal NG2 glia revealed an upregulation of MBP and MAG mRNA. This is rather surprising, as NG2 glia are not able to actively myelinate axons and only express MAG and MBP on transcript

level but not on protein level (Ye et al., 2003). In vitro studies showed that compared to oligodendrocytes, the translation of MBP in NG2 glia is repressed in a Fyn kinase dependent manner (Schäfer et al., 2016; White et al., 2008).

But how does the transcript level MBP in recombined NG2 glia correlate with the enhanced protein level revealed by the increased immunoreactivity for MBP? A promising mechanism displays the transcellular communication between cells as described by Frühbeis et al. (2013). Using a MOG-Cre mouse line, restricting the expression of Cre to the oligodendrocyte lineage, the authors were tracking the sites of recombination of the reporter gene LacZ. Surprisingly, the expression of the reporter gene took not only place in oligodendrocytes but also in neurons of different brain regions (hippocampus, granule cell layer of the cerebellum and brain stem). The authors concluded that Cre was delivered to neurons via multi vesicular bodies (MVBs), found at the adaxonal loop, the innermost myelin tongue facing the axon. In primary oligodendrocyte culture, the authors proofed the secretion of these oligodendroglial MVB´s and the uptake of the released exosomes by neurons in a clathrin-dependent manner (Frühbeis et al., 2013). MVB´s are multivesicular endosomes that can release their cargo (exosomes) via fusion with the plasma membrane (Colombo et al., 2014). In culture, the ability of oligodendrocytes to secrete exosomes filled with myelin proteins like PLP, CNP, MBP and other molecules was demonstrated (Krämer-Albers et al., 2007). The release of the exosomes was shown to be triggered by Ca^{2+} influx through AMPA - and NMDA receptors in oligodendrocytes (Frühbeis et al., 2013; Krämer-Albers et al., 2007). Oli-neu cells, an immortalized cell line derived from oligodendroglia precursor cells (Jung et al., 1995), were also shown to express molecules involved in exosome biogenesis and release and to actively secrete exosomes (Hessvik and Llorente, 2018; Frühbeis et al., 2013). In Kir4.1 flox mice of the present study, the enhanced level of MBP mRNA in recombined NG2 glia and the potential rise of Ca^{2+} signals, might favor the release of MBP mRNA loaded exosomes from NG2 glia to oligodendrocyte. After internalization of the MBP transcripts, the MBP protein can be locally synthesized by free ribosomes and integrated into the myelin sheath (Aggarwal et al., 2011; Colman et al., 1982). In vitro studies demonstrated the transport of granules packed with MBP transcript from the cell nucleus along microtubules to the processes and further to the myelin compartments (Ainger et al., 1993; Carson et al., 1997). In situ hybridization confirmed the distribution of MBP in the nucleus of oligodendrocytes and within the myelin internodes in different CNS regions (Trapp et al., 1987).

To facilitate a fast and specific delivery of MBP packed exosomes to oligodendrocytes, a close vicinity of NG2 glia and oligodendrocytes would be necessary. So far, NG2 glia in the corpus callosum and optic nerve were observed to stay in close contact with nodes of Ranvier

(Butt et al., 1999; Serwanski et al., 2017). Serwanski et al., 2017 speculated on the role of these white matter NG2 glia as sensors for the state of myelin, that can react upon need and affect modulation and maintenance of the neighboring internodes (Serwanski et al., 2017). However, the situation for grey matter NG2 glia is not known. If a close vicinity of NG2 glia and oligodendrocytes exist in regions like the hippocampus that allows NG2 glia to modulate grey matter myelination via the release of exosomes containing MBP mRNA to oligodendrocytes, needs to be investigated. Noteworthy, the enhanced immunoreactivity of MBP might not necessarily relate to an increase in myelination (including myelin sheath thickness and/or internode length), but to an enhanced density of MBP proteins in the myelin sheath. In its role in compacting myelin sheaths, it restricts the size of the cytoplasmatic space between the myelin layers. A higher density of MBP would reduce this space even more. In turn, the capacitance of the myelin sheath would decrease, allowing a faster conduction of action potentials than before (Min et al., 2009; Rasminsky and Sears, 1972). In its role in limiting the size of the extracellular space, MBP further functions as a molecular sieve that restricts the concentration and type of molecules with large cytoplasmic domains in the myelin layers (Aggarwal et al., 2011). A higher density of MBP would result in a stronger compaction that would further restrict the presence of molecules in a size dependent manner. To preserve an optimal function of myelin, a balance of different myelin factors is necessary (Aggarwal et al., 2011; Min et al., 2009). MAG, a component of the non-compact parts of myelin (Nave, 2010a), was also upregulated in Kir4.1 flox mice, supporting a balance of compact and non-compact myelin to assure proper myelin function. However, in the end, it remains unclear if the density of MBP was enhanced, the myelin thickness was increased, the number of myelinated axons was raised or if the number and/or length of internodes along an axon was multiplied in Kir4.1 flox mice.

In summary, the data presented here showed, that the loss of Kir4.1 hippocampal NG2 glia in adult mice and the increased excitability of theses ko cells, did not trigger proliferation or differentiation. If it is not the strength of the postsynaptic response controlling these events, the question arises, how synaptic input might induce proliferation and differentiation of NG2 glia as observed in other studies (Fannon et al., 2015; Gallo et al., 1996; Gibson et al., 2014; Li et al., 2010; Mangin et al., 2012). The strong depolarization of NG2 glia lacking Kir4.1 upon neuronal input seemed, however, to be sufficient to trigger gene expression and to increase transcripts of MBP and MAG. A potential mechanism behind an activity induced increase of MBP and MAG transcripts could involve Ca^{2+} signaling trough VGCCs. Interestingly, in the cortex and corpus callosum of juvenile mice, VGCC signaling in NG2 glia was shown to be related to the initiation of differentiation and myelination (Cheli et al.,

2016). In the study of Cheli et al. in 2016, Cre mediated deletion of Cav1.2 (L-type VGCC) from NG2 glia was induced by tamoxifen in mice at the age of p4, p10 and p30. The ablation of Cav1.2 at a young age (p4 and p10), reduced the density myelinated fibers and the expression level of myelin proteins like MBP and MOG. Accordingly, the number of oligodendrocytes was reduced. These effects were, however, not observed in mice in which the deletion of Cav1.2 was initiated at p30. These findings might relate to the high membrane resistance and depolarized membrane potential of NG2 glia in young mice (Kressin et al., 1995) that could have facilitated VGCC activation. A potential regain of function for a VGCC mediated signaling in adult NG2 glia that affect myelination was shown in a cuprizone model, disrupting basal myelination in the corpus callosum and cortex of adult mice (Santiago González et al., 2017). If the VGCC mediated signaling was caused by a change in passive membrane properties of adult NG2 glia in the demyelinating model, stays elusive.

6.4 Altered memory performance in mice lacking Kir4.1 in NG2 glia

Deletion of Kir4.1 from NG2 glia did not only affect neuron - NG2 glia communication and myelination but did also alter neuronal network function and animal behavior. Surprisingly, field potential recordings at the CA3 - CA1 synapse revealed an impaired formation of LTP in mice lacking Kir4.1 in NG2 glia. Potential mechanisms underlying the weakened potentiation involve most likely the postsynaptic site. Changes involving the release probability on presynaptic site can be excluded as the analysis of paired stimuli did not reveal any differences between slices of control and Kir4.1 flox mice. The basal excitability of neurons in the hippocampus, determined by the input-output relation of stimulation intensity and the evoked field potentials, was also indistinguishable between control and Kir4.1 flox mice. Djukic and colleagues mentioned similar observations for the basal excitability of hippocampal neurons in mice with a ko of Kir4.1 under control of the GFAP promotor, affecting astrocytes and cells of the oligodendrocyte lineage. Hippocampal LTP, induced by a high frequency stimulus was, in contrast to the findings in the present study, increased (Djukic et al., 2007). The authors pointed towards the relevance of Kir4.1 expressed in astrocytes for K^+ buffering during high neuronal activity. K^+ homeostasis and glutamate clearance by astrocytes are important functions in regulating neuronal excitability (Rothstein et al., 1996; Sibille et al., 2014; Wallraff et al., 2006). The authors argued, that due to the impaired function of astrocytes lacking Kir4.1, the elevated K^+ level and impaired glutamate clearance contributed to the observed increase of LTP (Djukic et al., 2007).

As in the mouse model, used in the present study, LTP was shown to be reduced, an impaired K^+ homeostasis causing the observed effect on neuronal plasticity can be excluded. Furthermore, the mouse model used in the present study exclusively delete Kir4.1 from NG2 glia. That Kir4.1 expressed by NG2 glia contribute to the K^+ homeostasis during neuronal activity is rather unlikely. Despite the prominent expression of Kir4.1, the ability of NG2 glia in sensing K^+ and to be involved in K^+ buffering, as suggested by Maldonado et al. 2013 is not clear (Maldonado et al., 2013). Compared to astrocytes, NG2 glia are not coupled with one another (Wallraff et al., 2004; Wigley and Butt, 2009). The uptake and redistribution of K^+ through a network of cells is not possible (Wallraff et al., 2006). A potential uptake of K^+ and its storage would be thus limited (Maldonado et al., 2013).

Beside their role in K+ buffering and glutamate uptake, astrocytes are able to modulate synaptic transmission, including LTP, by the release of gliotransmitters like ATP and D-Serine (Chen et al., 2013). Evidence that also NG2 glia can affect neuronal signaling, was demonstrated by Sakry and colleagues in 2014. Here, excitatory postsynaptic potentials (EPSPs) of L2/3 pyramidal neurons of the somatosensory cortex were recorded after induction of LTP by high frequency stimulation. They observed that the proteoglycan NG2 can be shedded by the α-secretase ADAM10. The cleaved NG2 ectodomain impaired LTP in pyramidal neurons due its interaction and modulation of neuronal AMPA receptors (Sakry et al., 2014). As the NG2-CreER^{T2} mouse line, used in the present study, is based on a knock-in of CreER^{T2} on exon 1 of the NG2 gene, homo- or heterozygous expression of Cre led to a reduced or even complete loss of NG2 expression. However, investigating NG2-EYFPki mice that were homozygous, heterozygous or wt for the NG2 protein, did not reveal any consequences on LTP formation or its maintenance. It seems that the hippocampus and somatosensory cortex differ in their susceptibility for a NG2 proteoglycan mediated effect on LTP. Other potential mechanisms that can modulate neuronal transmission involves the potential release of neuromodulatory factors from NG2 glia in Kir4.1 flox mice. A role could thereby paly the previously mentioned BDNF (see section 6.2). BDNF was shown to be expressed and secreted isolated nestin$^+$ NG2 glia (Tanaka et al., 2009) and astrocytes (Ohno et al., 2018) is such a candidate. It was demonstrated that LTP in the CA1 region of the hippocampus is impaired in the absence of BDNF (BDNF -/- mice) or at low BDNF levels (BDNF +/- mice) (Korte et al., 1995; Patterson et al., 1996). The impaired potentiation was shown to be restored by viral re-expression of the BDNF gene (Korte et al., 1995) and/or the application of BDNF (Patterson et al., 1996). The neurotrophic FGF-2 (fibroblast growth factor), that is known to be expressed and released by astrocytes, neurons and microglia cells (Araujo and Cotman, 1992; Eckstein et al., 1991) is another neurotrophic factor that is

involved in various functions, including neuronal plasticity, learning and memory (Zechel et al., 2010). It was demonstrated that in presence of FGF-2, LTP at the CA3 - CA1 synapse in hippocampal slices was enhanced (Terlau and Seifert, 1990). An increase in FGF-2 mRNA level in the hippocampus was detected after training in the Morris water maze, a behavioral task that requires hippocampal activity (Gómez-Pinilla et al., 1998). Abe and Saito correlated in 1992 the effect of FGF-2 on LTP with the interaction of the FGF-2 with NMDA receptors. In the presence of the neurotrophic factor, the NMDA receptor mediated increase of the intracellular Ca^{2+} level , that is involved in LTP formation, was even more enhanced (Abe and Saito, 1992). The expression and release of FGF-2 by NG2 glia was reported in 2015, Birey and colleagues. In their study, pharmacological ablation of NG2 glia from the prefrontal cortex, caused an impaired glutamatergic neurotransmission and a reduction in the astrocytic glutamate uptake. FGF-2 secreted by NG2 glia were correlated to these changes, as FGF-2 was able to control neuronal AMPA receptor subunit trafficking to the membrane and astrocytic GLAST expression (Birey et al., 2015). If a similar mechanism might affect neuronal AMPA receptor density and function in Kir4.1 flox mice is not clear. Experiments focusing on AMPA receptor mediated signaling in neurons would be necessary to answer this question.

Unexpectedly, the impaired potentiation after the high frequency stimulus in hippocampal slices of Kir4.1 flox mice, did not translate into deficits in memory performance. In contrast, Kir4.1 flox mice showed an improved declarative memory in the novel object location recognition (NOLR) test. This negative correlation between CA3 - CA1 LTP and behavior was also described by other groups. Mice deficient of the transcriptional activator Fmr2 showed a delay - dependent conditioned fear impairment, while NMDA receptor dependent and independent LTP at the CA3 - CA1 synapse was enhanced (Gu et al., 2002). Similarly, in mice deficient of the postsynaptic density-95 protein, LTP was enhanced but the ability of mice for spatial learning was impaired. The authors explained the necessity of bidirectional modification at the postsynapse, meaning LTD and LTP, to occur. In absence of LTD, the capacity to store information is reduced, causing an impairment in memory performance (Migaud et al., 1998). Minichiello et al. 1999, promoted the idea of a threshold for LTP before behavioral changes become apparent. In their study, heterozygous ko of the BDNF receptor trkB impaired LTP with no effect on animal behavioral paradigms like the water maze test (spatial learning) and partial eight-arm radial maze (working memory, short-term memory). A homozygote ko, however, caused impairments in both, CA1 LTP and behavior (Minichiello et al., 1999). That only a strong defect in potentiation reveals deficits in learning and memory performance was also suggested by Qi et al., 1996, who analyzed the

consequences of mutations in PKA (Qi et al., 1996). Thus, despite the observed impaired potentiation at the CA3 - CA1 synapse in Kir4.1 flox mice of the present study, the residual potentiation might still fulfill the requirement for long-time storage of information. That the performance in the NOLR test was even improved in Kir4.1 flox mice might be due to altered myelination detected in these animals. The association of myelination with cognitive function was revealed in different studies. Deficits in myelination of the prefrontal cortex, as a result of social isolation (Makinodan et al., 2012) or the deletion of the myelin regulating factor *Myrf*, that affect the formation of new oligodendrocytes in grey and white matter (McKenzie et al., 2014; Xiao et al., 2016), were accompanied by deficits in learning and memory. The inability to form new oligodendrocytes and to modulate myelination was suspected to be the cause for mice to fail learning new skills like wheel running (McKenzie et al., 2014; Xiao et al., 2016). Vice versa, an increase in myelin thickness improved the acquisition of fear memory (Jeffries et al., 2016). These studies demonstrate the need for myelin plasticity to occur and that this "adjustment" of the myelin sheath is essential for learning and memory. This effect of myelin might be due to its role as an insulator that affects the speed of signal transmission (see above). Depending on the myelin thickness and internode distance, the velocity of signal conduction can be increased or decreased (Waxman, 1980). Thus, myelin coordinates and adjusts the time point when action potentials arrive at the presynapse. The temporal regulation of neuronal input has consequences on the synchronicity of neuronal firing and thus on neuronal circuit function (Salami et al., 2003; Seidl, 2014). In mice with impaired myelination, synaptic transmission was shown to be temporally dispersed. The resulting asynchronous firing behavior caused deficits in motor learning (Kato et al., 2019). The concept of spike time dependent plasticity proved the need for a precise timing of action potential to arrive at the presynapse to allow synaptic plasticity to occur (Dan and Poo, 2006; Shouval et al., 2010). Thus, it seems possible that the enhanced myelination in Kir4.1 flox mice resulted in a higher synchronicity of synaptic inputs that in turn facilitates information processing and cognitive function.

Importantly, despite the improved performance of Kir4.1 flox mice in the novel object location recognition test, a general improvement in the performances during memory tasks could not be observed. In other tests, based on working memory (Y-maze) and social memory (partner recognition test), control and Kir4.1 flox mice behaved similarly. It has to be considered that not only the hippocampus is involved in the execution of these types of memory paradigms. Dependent on the behavioral test, other brain regions are additionally involved. Thus, the prefrontal cortex contributes to short term memory performance in the Y-maze test (Albayram et al., 2016; Lynch, 2004). Other areas of the limbic system, like the

amygdala, play a role during the partner recognition test (Bilkei-Gorzo et al., 2014; Kogan et al., 2000). For the NOLR, that is based on information about the object itself (familiar or new) and its location, the medial temporal lobe including perirhinal, entorhinal and parahippocampal cortices are important (Squire and Dede, 2015). The ko of Kir4.1 from NG2 glia is abundant in the entire brain, but consequences of this ko on other brain regions than the hippocampus and their effect on memory performance are not clear. It also has to be considered that depending on the behavioral test, different parts of the hippocampus are involved. Braadbent and colleagues (2004) demonstrated that a bilateral lesion of 50% of the hippocampus impairs memory performance in the morris water maze, a test for spatial learning. Impairments in the novel object recognition test, a test for recognition memory, were only visible in lesions covering more than 75% of the hippocampus. Thus, spatial memory required more subregions of the hippocampus than recognition memory (Broadbent et al., 2004). In conclusion, changes occurring in the hippocampus upon deletion of Kir4.1 from NG2 glia might differently affect memory performance, with some behavioral tasks being more susceptible to the ko induced alternations than others.

The fact, that female mice showed a better social memory performance than male mice was previously reported by Markham and Juraska (2007). The authors referred to sexual dimorphic neuronal pathways like those systems responsible for vasopressin and oxytocin that alter animal behavior (Markham and Juraska, 2007). The vasopressin system, for example, is more prominent in males than in females, as males possess a higher density of vasopressin fibers than the other sex (De Vries and Panzica, 2006). Thus, injection of a vasopressin antagonists negatively affected social memory of male but not female mice (Bluthé and Dantzer, 1990). Depending on the behavioral paradigm the action of vasopressin and oxytocin were shown to affect the performance of animals in individual tasks (Engelmann et al., 1996; Engelmann et al., 2000; de Wied et al., 1993). It has to be taken into account, that this hormone system could be additionally altered by the application of tamoxifen. Due to the affinity of tamoxifen and its metabolites to bind to estrogen receptors (Borgna and Rochefort, 1981), not only $CreER^{T2}$ activity can be controlled but also the function of endogenous estrogen receptors. Studies involving long-term treatment of rats with tamoxifen (Azizi-Malekabadi et al., 2015) or its application shortly before or after the behavioral experiment (Chen et al., 2002), were shown to affect animal behavior, including learning and memory function. However, injection of a low-dose of tamoxifen in adult mice for only 5 consecutive days and the conduction of behavioral paradigms 3 days later, did not provide any evidence for the impact of tamoxifen on behavior (Rotheneichner et al., 2017). As in the present study a similar protocol was used (3 days of injection; experiments 3-4 weeks after)

to induce a CreER^{T2} mediated deletion of Kir4.1 in NG2 glia, effects of tamoxifen treatment itself on the performance of mice in behavior paradigms are very unlikely to occur.

In summary, it can be concluded that the deletion of Kir4.1 specifically from NG2 glia impaired LTP at hippocampal CA3 - CA1 synapses. The residual potentiation was, however, sufficient to transduce the neuronal signal into altered memory formation. The latter might have been due to a change in the myelination - dependent speed of signal transduction, enhancing synchronicity of neuronal inputs and thus, supporting cognitive functions.

6.5 NG2 glia driven deletion of Kir4.1 in the cerebellum

NG2 glia represent a highly heterogeneous cell population in the brain. Depending on the brain region and developmental state, differences in proliferation and myelination can be detected, as well as variations in ion channel expression and the response to neuronal activity (Spitzer et al., 2019; Viganò and Dimou, 2016). Consequently, the physiological impact of Kir4.1 on NG2 glia properties and behavior might differ accordingly between regions. Therefore, next to the hippocampus, consequences of the CreER^{T2} mediated Kir4.1 ko in NG2 glia were started to be investigated in the cerebellum. Similar to the observation in the hippocampus, the deletion of Kir4.1 from cerebellar NG2 glia caused dramatic changes in the passive membrane properties of these cells. The observed depolarized resting membrane potential and increased membrane resistance suggested a similarly altered excitability of NG2 glia lacking Kir4.1. Therefore, the spontaneous release of neurotransmitters would be expected to result in strong and long-lasting depolarizations in cerebellar Kir4.1 ko cells, as observed for those in the hippocampus. Evoked release of vesicles upon axonal stimulation, however, already showed striking differences between cerebellar and hippocampal NG2 glia. Minimal stimulation of climbing fibers, that are innervating NG2 glia in the molecular layer of the cerebellum, evoked currents between -30 pA and -900 pA. In the hippocampus, NG2 glia responses upon Schaffer collateral stimulation induced much smaller EPSCs, rarely exceeding 30 pA. These results are in line with previous studies investigating evoked EPSCs in cerebellar and hippocampal NG2 glia (Bergles et al., 2000; Jabs et al., 2005; Lin et al., 2005). The reason why cerebellar NG2 glia receive such a strong input seems to be due to the high release probability from climbing fibers. At both, climbing fiber - Purkinje cells synapses (Dittman and Regehr, 1998; Silver et al., 1998; Wadiche and Jahr, 2001) and climbing fiber - NG2 glia synapses (Lin et al., 2005), paired pulse stimulation revealed a strong response upon the first stimulus and a smaller response upon the second. This paired pulse depression is known to be indicative of a high probability of vesicles to be released

from these synapses (Debanne et al., 1996). In the cerebellum the high release probability was shown to correlate with an enhanced level of glutamate in the synaptic cleft. The accumulation of glutamate was caused by the simultaneous release of multiple vesicles from a single climbing fiber synapse onto the postsynaptic Purkinje cell (Wadiche and Jahr, 2001). The high concentration of this neurotransmitter in the synaptic cleft impedes the efficiency of neurotransmitter clearance and their fast reuptake into the presynapse to refill the readily releasable vesicle pool (Silver et al., 1998; Wadiche and Jahr, 2001). Consequently, the amount of transmitter released upon a subsequent second stimulus and the postsynaptic response are smaller. Additionally, the elevated glutamate level assures a high occupancy and activation of AMPA receptors, causing a strong postsynaptic current in Purkinje cells (Harrison and Jahr, 2003). A similar situation might be operative at climbing fiber – NG2 glia, triggering high EPSC amplitudes upon paired stimulation. The effect might be additionally amplified by the strong innervation of NG2 glia in the cerebellum. Compared to Schaffer collaterals in the hippocampus that form 7 to 19 synapses with NG2 glia (Bergles et al., 2000), each climbing fiber was estimated to form up to 70 contacts with NG2 glia in the cerebellum (Lin et al., 2005). Stimulation of one climbing fiber would thus initiate the release of multiple vesicles at multiple sites. If other differences between hippocampal and cerebellar NG2 glia exist that contribute to the high EPSP amplitude of NG2 glia in the molecular layer of the cerebellum, is not clear. Regarding AMPA receptors, modulatory subunits like TARPs and cornichons were described to impact receptor channel function (Jackson and Nicoll, 2011). Especially TARP-y2 was shown to have a strong effect on the channel conductance of AMPA receptors. In absence of TARP-y2, AMPA receptor mediated currents were decreased in Purkinje cells upon climbing fiber stimulation (Yamazaki et al., 2010). The authors of the latter study further claimed a mutual dependence of TARP expression and subunit composition of AMPA receptors. In mice lacking TARP-y2, the subunits GluA2 and GluA3 were less abundant. The Ca^{2+} permeability of AMPA receptors was however not affected in presence or absence TARP-y2 (Yamazaki et al., 2010). Whether differences in AMPA receptor subunit composition and modulatory subunits expression exist between AMPA receptors of cerebellar and hippocampal NG2 glia, needs to be determined. So far, TARP-y4 but not TARP-y2 was shown to be expression by glial cells (Tomita et al., 2003).

Generally, the deletion of Kir4.1 from cerebellar NG2 glia did not alter the high release probability at the climbing fiber – NG2 glia synapse. The strong paired pulse depression detected at these synapses was similar in NG2 glia of control and Kir4.1 flox mice. This observation is in contrast to the data obtained from the hippocampus. Here, the deletion of Kir4.1 from NG2 glia reduced the paired pulse facilitation at the Schaffer collateral - NG2

glia synapse, implying an increase of the release probability. As the release probability at climbing fiber – NG2 glia synapses was already high, the ko might not exert an additional or detectable shift toward higher release probabilities.

Concerning the effect of Kir4.1 ablation from NG2 glia on cerebellar function and animal behavior, the performance of control and Kir4.1 flox mice in the beam walking paradigm was evaluated. Interestingly, mice lacking Kir4.1 in NG2 glia showed an improved motor coordination. The cellular mechanism underlying this effect, including the activity and interplay of cerebellar neurons, remain to be investigated. A potential role of myelination affecting the performance of mice during the behavioral task, as suggested for the hippocampus related NOLR test, needs to be investigated. Studies investigating the role of myelination on motor emphasized the necessity of myelin for the synchronicity of signal transmission and learning of certain motoric abilities of mice (Kato et al., 2019). Similarly, Zheng et al. (2019) revealed a correlation between myelination in the motor cortex and improved motoric functions of mice (Zheng et al., 2019).

Surprisingly, in respect to a NG2 glia differentiation in the cerebellum, deletion of Kir4.1 from NG2 increased their differentiation into oligodendrocytes in the molecular layer but not granule cells layer. NG2 glia characteristics that drive the heterogeneous effect of Kir4.1 deletion in different cerebellar subregions, might involve differential expression of membrane receptors or ion channels that were shown to play a regulatory role for NG2 glia differentiation (Chen et al., 2018, 2009; Spitzer et al., 2019). Differences regarding the type and strength of synaptic input onto NG2 glia in the granule cells layer vs molecular layer might also affect differentiation. NG2 glia of the molecular layer were shown to be innervated by climbing fibers but to a minor part by parallel fibers (Lin et al., 2005). Less is known about neuron - NG2 glia signaling in the granule cell layer. In 2009, Wigley and Butt referred to *en passant* synapses formed between neurons and NG2 glia of this cerebellar subregion (Wigley and Butt, 2009). These could involve climbing fibers and mossy fibers that transverse the granule cell layer (Purves et al., 2001). Additionally, the interaction with astrocytes, Bergmann glia and interneurons might affect differentiation of NG2 glia of different cerebellar subregions (Wigley and Butt, 2009; Purves et al., 2001). NG2 glia proliferation was not altered between Kir4.1 flox and control mice and between cerebellar subregions.

6.6 Deletion of AMPA receptors in hippocampal NG2 glia

A different approach to investigate the impact of NG2 glia and neuron - NG2 glia signaling in the brain was based on the modification of AMPA receptors in NG2 glia. Glutamatergic

input was shown to control NG2 glia proliferation and their differentiation into myelinating oligodendrocytes (Gautier et al., 2015; Gibson et al., 2014; Li et al., 2010; Mangin et al., 2012). Consequences, of a complete deletion of AMPA receptors specifically in NG2 glia were started to be investigated in the present study. Based on the Cre/loxP system, the NG2 driven CreER^{T2} expression was used to specifically delete AMPA receptor subunits from NG2 glia upon tamoxifen injection in adult mice. AMPA receptors in NG2 glia were shown to be mainly composed of the subunits GluA1, GluA2 and GluA4 (Seifert et al., 2003). Despite the low expression level of GluA3, the present study revealed the necessity of a mouse model in which all 4 subunits are deleted by CreER^{T2} mediated recombination. Pharmacological and molecular analysis revealed that targeting GluA1, GluA2 and GluA4 but not GluA3 (triple GluA flox mice) was insufficient to delete AMPA receptor mediated signaling in NG2 glia. The assembly of receptors composed of GluA3 subunits solely (homomeric AMPA receptors) or in combination with other subunits (heteromeric AMPA receptors) that were present despite CreER^{T2} activity, accounted for the kainate evoked currents in NG2 glia. According to the inward rectifying I/V relation of the receptor response, deletion of the GluA2 subunit seemed to be most successful in the majority of NG2 glia of triple GluA flox mice. Only in absence of GluA2, AMPA receptors can be blocked in a voltage dependent manner by polyamines like spermine, thereby preventing outward directed currents. In presence of GluA2, the channel pore of AMPA receptors is more positively charged, repelling polyvalent cations like spermine, which averts the channel block (Donevan and Rogawski, 1995; Kamboj et al., 1995b; Koh et al., 1995; Pellegrini-Giampietro, 2003; Seifert et al., 2003). Surprisingly, in the study of Kougioumitzidou and colleagues (2017), dual or triple deletion of GluA2/GluA3 or GluA2/GluA3/GluA4 subunits in NG2 glia of the corpus callosum was already sufficient to diminish AMPA receptor mediated currents. Consequences on the survival of newly generated oligodendrocytes and a reduced number of myelinated axons were also reported in these mice (Kougioumtzidou et al., 2017). These results, however, refer to experiments performed in young mice at the age of p13-16. For an inducible deletion of AMPA receptor mediated signaling in adult NG2 glia, the ablation of all 4 AMPA receptor subunits seems to be required. First experiments performed in hippocampal slices of mice with a targeted deletion of GluA1, GluA2, GluA3 and GluA4 from NG2 glia (quadruple GluA flox mice), revealed an almost functional ko of AMPA receptors. Whether the occasionally observed tiny residual receptor currents in quadruple GluA flox mice are due to kainate receptors (Kukley and Dietrich, 2009), remains to be investigated.

7 Summary

NG2 glia represents the 4th type of CNS glial cells. In white matter, most of them differentiate into myelinating oligodendrocytes but in grey matter a majority retains their NG2 phenotype throughout life. Intriguingly, these glial cells are the only non-neuronal cell type, receiving direct synaptic input from glutamatergic and GABAergic neurons. However, the functional consequence of this highly temporally and spatially restricted way of communication with neurons is not yet understood. The present study aimed to elucidate the role of grey matter NG2 glia and to reveal whether/how these cells influence brain function. For this purpose, a NG2-CreER^{T2} knock-in mouse line was generated, enabling the deletion of the prominently expressed K^+ channel Kir4.1 specifically in NG2 glia upon tamoxifen administration. In its role as a key determinant of passive membrane properties, hippocampal NG2 glia devoid of Kir4.1 displayed depolarized resting potentials and a drastically increased membrane resistance. These changes promoted the excitability of these knockout cells as revealed by strong and long-lasting responses upon quantal transmitter release at the neuron-NG2 glia-synapse. NG2 glia-targeted deletion of the Kir4.1 gene further entailed an increase of myelin protein transcripts in recombined cells and an upregulation of MBP protein, a main component of myelin sheaths. On neuronal circuit level it could be shown that not only short-term plasticity at the Schaffer collateral - NG2 glia synapse was altered in mice lacking Kir4.1 in NG2 glia, but also long-term potentiation (LTP) at synapses formed between CA3 and CA1 pyramidal neurons. As LTP is considered a cellular basis for learning and memory, the impaired potentiation was expected to be apparent on the behavior level. Surprisingly, animal performance during the novel object location recognition memory task indicated an improved declarative memory of Kir4.1-deficient mice. The functional impact of Kir4.1 deletion on other brain regions still needs to be investigated. First experiments performed in the cerebellum imply a regionally diverse impact of Kir4.1 knockout in NG2 glia. Short term plasticity was unaltered at cerebellar climbing fiber - NG2 glia synapse, in contrast to the situation in the hippocampus. Differentiation of NG2 glia into oligodendrocytes was, however, increased in the cerebellar molecular layer but not in the cerebellar granule cells layer or in the hippocampus. On the behavioral level, mice with a NG2 glia-targeted Kir4.1-

deficiency showed improved motor coordination in the beam walk paradigm, a test of cerebellar function.

In summary the findings presented here, provide exciting insights into the ability of NG2 glia to influence neuronal plasticity and animal behavior. The K^+ channel Kir4.1 expressed in NG2 glia seems to have a key function in determining NG2 glia excitability and in driving intracellular processes that enable NG2 glia to provoke changes of myelination, neuronal circuit function and memory performance.

8 Perspectives

Deletion of the inwardly rectifying K^+ channel Kir4.1 specifically from NG2 glia was shown to represent a promising tool to elucidate the impact of NG2 glia in the brain. The targeted deletion of Kir4.1 altered membrane properties of NG2 glia and transferred these cells into a highly excitability state. It was hypothesized that under these conditions the activation of voltages gated Ca^{2+} channels (VGCCs) in the NG2 glia membrane might be facilitated, allowing Ca^{2+} to enter the cell. Experiments involving Ca^{2+} imaging would reveal these Ca^{2+} transients in the soma and/or processes. The rise of the intracellular Ca^{2+} level might in turn drive intracellular processes that enable NG2 glia to provoke changes on neuronal circuit function. This includes a Ca^{2+} dependent expression and secretion of neuromodulatory factors like FGF-2 and/or BDNF. These factors are thought to underlie the altered transmitter release probability observed at Schaffer-collateral NG2 glia synapses and the reduced LTP at CA3 – CA1 synapses. Semi-quantitative PCR of FAC sorted recombined NG2 glia from Kir4.1 deficient mice could clarify the existence and amount of these factors on the transcript level. Regarding the impairment of LTP at CA3 – CA1 synapses in mice lacking Kir4.1 in NG2 glia, the mechanisms behind needs to be clarified. As presynaptic changes were excluded to be the cause for the weakened potentiation, postsynaptic mechanisms need to be evaluated. This would include the analysis of AMPA receptor currents, as channel conductance and density of AMPA receptors are known to affect LTP (Benke et al., 1998; Penn et al., 2017; Shi et al., 1999).

The observation that the MBP signal was enhanced in hippocampal brain slices of Kir4.1-deficient mice indicates modifications of the myelin structure. These modifications might be linked to an increased density of MBP between the myelin layers that would provoke a higher compactness of the entire myelin sheath. An increase in myelin thickness or higher coverage of axons with myelin could also relate to the increased MBP signal. In this respect, electron microscopy (EM) would provide detailed information about the myelin structure, including the number of myelin wraps per axon and their individual width. As EM and its analysis is rather time consuming, expansion microscopy (ExM) would allow first hints about the distribution of the MBP signal. ExM is a technique introduced by Chen et al., in 2015 that enables the physical magnification (expansion) of a specimen, while keeping the anatomy of

the structures intact (Chen et al., 2015). The magnification enables super resolution of structures with a conventional microscope. Concerning the enhanced MBP signal in Kir4.1 deficient mice, this technique would permit a high resolution of individual structures that are labeled with the MBP antibody and the quantification of MBP within each of these structures. In the context of myelination, it would be of interest to understand how the enhanced level of MBP and MAG transcripts, that were detected in recombined NG2 glia of Kir4.1 flox mice, translate into the enhanced MBP signal in the myelin sheath. Morphological analysis of recombined NG2 glia would provide further information about i) the number of processes that can interact with oligodendrocytes and ii) the spatial relation of NG2 glia processes and oligodendrocytes, for a potential transfer of exosomes from NG2 glia to oligodendrocytes.

Generally, it has to be considered that NG2 glia represent a heterogeneous cell population. Differences, regarding the response upon synaptic input, as well as variations in the expression of ion channels and their capacity to proliferate and differentiate were described for different brain areas and developmental stages. Investigating the effect of Kir4.1 ko in distinct brain areas, might be of further help to understand the role of NG2 glia and the impact of neuron – NG2 glia signaling for different neuronal networks and brain functions.

Another approach to understand the physiological impact of NG2 glia and neuron – NG2 glia synapses involves the deletion of AMPA receptor mediated signaling specifically in NG2 glia. The previously introduced quadruple AMPA receptor ko mice allow to investigate the influence of glutamatergic signaling on NG2 glia characteristic and consequences on neuronal network function including the induction and maintenance of LTP. Experiments on the behavioral level would further elucidate the role of neuron - NG2 glia interactions in the modulation of brain function and behavior.

References

Abbott, L.F., and Regehr, W.G. (2004). Synaptic computation. Nature *431*, 796–803.

Abe, K., and Saito, H. (1992). Epidermal growth factor selectively enhances NMDA receptor-mediated increase of intracellular Ca 2+ concentration in rat hippocampal neurons. Brain Res. *587*, 102–108.

Abel, T., Nguyen, P. V., Barad, M., Deuel, T.A.S., Kandel, E.R., and Bourtchouladze, R. (1997). Genetic demonstration of a role for PKA in the late phase of LTP and in hippocampus-based long-term memory. Cell *88*, 615–626.

Aggarwal, S., Yurlova, L., Snaidero, N., Reetz, C., Frey, S., Zimmermann, J., Pähler, G., Janshoff, A., Friedrichs, J., Müller, D.J., et al. (2011). A size barrier limits protein diffusion at the cell surface to generate lipid-rich myelin-membrane sheets. Dev. Cell *21*, 445–456.

Aggarwal, S., Snaidero, N., Pähler, G., Frey, S., Sánchez, P., Zweckstetter, M., Janshoff, A., Schneider, A., Weil, M.T., Schaap, I.A.T., et al. (2013). Myelin Membrane Assembly Is Driven by a Phase Transition of Myelin Basic Proteins Into a Cohesive Protein Meshwork. PLoS Biol. *11*,e1001577.

Ainger, K., Avossa, D., Morgan, F., Hill, S.J., Barry, C., Barbarese, E., and Carson, J.H. (1993). Transport and localization of exogenous myelin basic protein mRNA microinjected into oligodendrocytes. J. Cell Biol. *123*, 431–441.

Akopian, G., Kressin, K., Derouiche, A., and Steinhäuser, C. (1996). Identified glial cells in the early postnatal mouse hippocampus display different types of Ca2+ currents. Glia *17*, 181–194.

Albayram, Ö., Passlick, S., Bilkei-Gorzo, A., Zimmer, A., and Steinhäuser, C. (2016). Physiological impact of CB1 receptor expression by hippocampal GABAergic interneurons. Pflugers Arch. Eur. J. Physiol. *468*, 727–737.

Albus, J.S. (1971). A theory of cerebellar function. Math. Biosci. *10*, 25–61.

Allen, N.J., and Barres, B.A. (2009). GlaNature.pdf. *457*, 675–677.

Andersen, P., Morris, R., Amaral, D., Bliss, T., and O'Keefe, J. (2006). The Hippocampus Book. Oxford University Press.

Araujo, D.M., and Cotman, C.W. (1992). Basic FGF in astroglial, microglial, and neuronal cultures: Characterization of binding sites and modulation of release by lymphokines and trophic factors. J. Neurosci. *12*, 1668–1678.

Asztely, F., Kokaia, M., Olofsdotter, K., Örtegren, U., and Lindvall, O. (2000). Afferent-specific modulation of short-term synaptic plasticity by neurotrophins in dentate gyrus. Eur. J. Neurosci. *12*, 662–669.

Attwell, D., Buchan, A.M., Charpak, S., Lauritzen, M., MacVicar, B.A., and Newman, E.A. (2010). Glial and neuronal control of brain blood flow. Nature *468*, 232–243.

Azizi-Malekabadi, H., Pourganji, M., Zabihi, H., Saeedjalali, M., and Hosseini, M. (2015). Tamoxifen antagonizes the effects of ovarian hormones to induce anxiety and depressionlike behavior in rats. Arq. Neuropsiquiatr. *73*, 132–139.

Balia, M., Vélez-Fort, M., Passlick, S., Schäfer, C., Audinat, E., Steinhäuser, C., Seifert, G., and Angulo, M.C. (2015). Postnatal down-regulation of the GABAA Receptor γ2 subunit in neocortical NG2 cells accompanies synaptic-to-extrasynaptic switch in the GABAergic transmission mode. Cereb. Cortex *25*, 1114–1123.

Balkowiec, A., and Katz, D.M. (2002). Cellular mechanisms regulating activity-dependent release of native brain-derived neurotrophic factor from hippocampal neurons. J. Neurosci. *22*, 10399–10407.

Baraban, M., Mensch, S., and Lyons, D.A. (2016). Adaptive myelination from fish to man. Brain Res. *1641*, 149–161.

Barria, A., Muller, D., Derkach, V., Griffith, L.C., and Soderling, T.R. (2007). Regulatory Phosphorylation of AMPA-Type Glutamate Receptors by CaM-KII During Long-Term Potentiation Regulatory Phosphorylation of AMPA-Type Glutamate Receptors by CaM-KII During Long-Term Potentiation. Media *2042*, 2042–2045.

Baumann, N., and Pham-Dinh, D. (2001). Biology of oligodendrocyte and myelin in the mammalian central nervous system. Physiol. Rev. *81*, 871–927.

Bechler, M.E., Swire, M., and ffrench-Constant, C. (2018). Intrinsic and adaptive myelination—A sequential mechanism for smart wiring in the brain. Dev. Neurobiol. *78*, 68–79.

Benke, T.A., Luthl, A., Isaac, J.T.R., and Collingridge, G.L. (1998). Modulation of ampa receptor unitary conductance by synaptic activity. Nature *393*, 793–797.

Bennett, M.V.L., and Zukin, R.S. (2004). Electrical Coupling and Neuronal Synchronization in the Mammalian Brain. Neuron *41*, 495–511.

Bergles, D.E., and Richardson, W.D. (2016). Oligodendrocyte development and plasticity. Cold Spring Harb. Perspect. Biol. *8*, a020453.

Bergles, D.E., Roberts, J.D.B., Somogyl, P., and Jahr, C.E. (2000). Glutamatergic synapses on oligodendrocyte precursor cells in the hippocampus. Nature *405*, 187–191.

Bergles, D.E., Jabs, R., and Steinhäuser, C. (2010). Neuron-glia synapses in the brain. Brain Res. Rev. *63*, 130–137.

De Biase, L.M., Nishiyama, A., and Bergles, D.E. (2010). Excitability and Synaptic Communication within the Oligodendrocyte Lineage. J. Neurosci. *30*, 3600–3611.

Bilkei-Gorzo, A., Mauer, D., Michel, K., and Zimmer, A. (2014). Dynorphins regulate the strength of social memory. Neuropharmacology *77*, 406–413.

Bilkei-Gorzo, A., Albayram, O., Draffehn, A., Michel, K., Piyanova, A., Oppenheimer, H., Dvir-Ginzberg, M., Rácz, I., Ulas, T., Imbeault, S., et al. (2017). A chronic low dose of Δ9-tetrahydrocannabinol (THC) restores cognitive function in old mice. Nat. Med. *23*, 782–787.

Bird, T.D., Farrell, D.F., and Sumi, S.M. (1978). Brain lipid composition of the shiverer mouse: (genetic defect in myelin development). J. Neurochem. *31*, 387–391.

Birey, F., Kloc, M., Chavali, M., Hussein, I., Wilson, M., Christoffel, D.J., Chen, T., Frohman, M.A., Robinson, J.K., Russo, S.J., et al. (2015). Genetic and Stress-Induced Loss of NG2 Glia Triggers Emergence of Depressive-like Behaviors through Reduced Secretion of FGF2. Neuron *88*, 941–956.

Bliss, T.V.P., and Lømo, T. (1973). Long-lasting potentiation of synaptic transmission in the dentate area of the anaesthetized rabbit following stimulation of the perforant path. J. Physiol. *232*, 331–356.

Bluthé, R.M., and Dantzer, R. (1990). Social recognition does not involve vasopressinergic neurotransmission in female rats. Brain Res. *535*, 301–304.

Bordey, A., Lyons, S.A., Hablitz, J.J., and Sontheimer, H. (2001). Electrophysiological characteristics of reactive astrocytes in experimental cortical dysplasia. J. Neurophysiol. *85*, 1719–1731.

Borgna, J.L., and Rochefort, H. (1981). Hydroxylated metabolites of tamoxifen are formed in vivo and bound to estrogen receptor in target tissues. J. Biol. Chem. *256*, 859–868.

Broadbent, N.J., Squire, L.R., and Clark, R.E. (2004). Spatial memory, recognition memory, and the hippocampus. Proc. Natl. Acad. Sci. U. S. A. *101*, 14515–14520.

Bushong, E.A., Martone, M.E., Jones, Y.Z., and Ellisman, M.H. (2002). Protoplasmic astrocytes in CA1 stratum radiatum occupy separate anatomical domains. J. Neurosci. *22*, 183–192.

Butt, A.M., and Kalsi, A. (2006). Inwardly rectifying potassium channels (Kir) in central nervous system glia: A special role for Kir4.1 in glial functions. J. Cell. Mol. Med. *10*, 33-44.

Butt, A.M., Duncan, A., Hornby, M.F., Kirvell, S.L., Hunter, A., Levine, J.M., and Berry, M. (1999). Cells expressing the NG2 antigen contact nodes of ranvier in adult CNS white matter. Glia *26*, 84–91.

Butt, A.M., Hamilton, N., Hubbard, P., Pugh, M., and Ibrahim, M. (2005). Synantocytes: The fifth element. J. Anat. *207*, 695–706.

Carson, J.H., Worboys, K., Ainger, K., and Barbarese, E. (1997). Translocation of myelin basic protein mRNA in oligodendrocytes requires microtubules and kinesin. Cell Motil. Cytoskeleton *38*, 318–328.

Chai, H., Diaz-Castro, B., Shigetomi, E., Monte, E., Octeau, J.C., Yu, X., Cohn, W., Rajendran, P.S., Vondriska, T.M., Whitelegge, J.P., et al. (2017). Neural Circuit-Specialized Astrocytes: Transcriptomic, Proteomic, Morphological, and Functional Evidence. Neuron *95*, 531-549.e9.

Chan, C.-F., Kuo, T.-W., Weng, J.-Y., Lin, Y.-C., Chen, T.-Y., Cheng, J.-K., Lien, C.-C., Chan, C.-F., Kuo, T.-W., Weng, J.-Y., et al. (2013a). Ba 2+ -and bupivacaine-sensitive background K + conductances mediate rapid EPSP attenuation in oligodendrocyte precursor cells. J Physiol *59119*, 4843–485819.

Chan, C.F., Kuo, T.W., Weng, J.Y., Lin, Y.C., Chen, T.Y., Cheng, J.K., and Lien, C.C. (2013b). Ba2+- and bupivacaine-sensitive background K+ conductances mediate rapid EPSP attenuation in oligodendrocyte precursor cells. J. Physiol. *591*, 4843–4858.

Cheli, V.T., Santiago González, D.A., Namgyal Lama, T., Spreuer, V., Handley, V., Murphy, G.G., and Paez, P.M. (2016). Conditional Deletion of the L-Type Calcium Channel Cav1.2 in Oligodendrocyte Progenitor Cells Affects Postnatal Myelination in Mice. J. Neurosci. *36*, 10853–10869.

Chen, D., Wu, C.F., Shi, B., and Xu, Y.M. (2002). Tamoxifen and toremifene cause impairment of learning and memory function in mice. Pharmacol. Biochem. Behav. *71*, 269–276.

Chen, F., Tillberg, P.W., and Boyden, E.S. (2015). Expansion microscopy. Science *347*, 543–548.

Chen, J., Tan, Z., Zeng, L., Zhang, X., He, Y., Gao, W., Wu, X., Li, Y., Bu, B., Wang, W., et al. (2013). Heterosynaptic long-term depression mediated by ATP released from astrocytes. Glia *61*, 178–191.

Chen, T.J., Kula, B., Nagy, B., Barzan, R., Gall, A., Ehrlich, I., and Kukley, M. (2018). In Vivo Regulation of Oligodendrocyte Precursor Cell Proliferation and Differentiation by the AMPA-Receptor Subunit GluA2. Cell Rep. *25*, 852-861.e7.

Chen, Y., Wu, H., Wang, S., Koito, H., Li, J., Ye, F., Hoang, J., Escobar, S.S., Gow, A., Arnett, H.A., et al. (2009). The oligodendrocyte-specific G protein-coupled receptor GPR17 is a cell-intrinsic timer of myelination. Nat. Neurosci. *12*, 1398–1406.

Chernoff, G.F. (1981). Shiverer: an autosomal recessive mutant mouse with myelin deficiency. J. Hered. *72*, 128.

Chittajallu, R., Chen, Y., Wang, H., Yuan, X., Ghiani, C.A., Heckman, T., McBain, C.J., and Gallo, V. (2002). Regulation of Kv1 subunit expression in oligodendrocyte progenitor cells and their role in G1/S phase progression of the cell cycle. Proc. Natl. Acad. Sci. *99*, 2350–2355.

Chittajallu, R., Aguirre, A., and Gallo, V. (2004). NG2-positive cells in the mouse white and grey matter display distinct physiological properties. J. Physiol. *561*, 109–122.

Cho, J.H., and Askwith, C.C. (2008). Presynaptic release probability is increased in hippocampal neurons from ASIC1 knockout mice. J. Neurophysiol. *99*, 426–441.

Collingridge, G.L., Kehl, S.J., and McLennan, H. (1983). Excitatory amino acids in synaptic transmission in the Schaffer collateral-commissural pathway of the rat hippocampus. J. Physiol. *334*, 33–46.

Colman, D.R., Kreibich, G., Frey, A.B., and Sabatini, D.D. (1982). Synthesis and incorporation of myelin polypeptides into CNS myelin. J. Cell Biol. *95*, 598–608.

Colombo, M., Raposo, G., and Théry, C. (2014). Biogenesis, Secretion, and Intercellular Interactions of Exosomes and Other Extracellular Vesicles. Annu. Rev. Cell Dev. Biol. *30*, 255–289.

Cox, B.C., Liu, Z., Lagarde, M.M.M., and Zuo, J. (2012). Conditional gene expression in the mouse inner ear using cre-loxP. JARO - J. Assoc. Res. Otolaryngol. *13*, 295–322.

Czeh, M., Gressens, P., and Kaindl, A.M. (2011). The yin and yang of microglia. Dev. Neurosci. *33*, 199–209.

D'Angelo, E., Mapelli, L., Casellato, C., Garrido, J.A., Luque, N., Monaco, J., Prestori, F., Pedrocchi, A., and Ros, E. (2016). Distributed Circuit Plasticity: New Clues for the Cerebellar Mechanisms of Learning. Cerebellum *15*, 139–151.

Dan, Y., and Poo, M.M. (2006). Spike timing-dependent plasticity: From synapse to perception. Physiol. Rev. *86*, 1033–1048.

Davies, P.C.W. (1989). A brief history of time. Contemp. Phys. *30*, 135–136.

Debanne, D., Guérineau, N.C., Gähwiler, B.H., and Thompson, S.M. (1996). Paired-pulse facilitation and depression at unitary synapses in rat hippocampus: Quantal fluctuation affects subsequent release. J. Physiol. *491*, 163–176.

Degen, J., Dublin, P., Zhang, J., Dobrowolski, R., Jokwitz, M., Karram, K., Trotter, J., Jabs, R., Willecke, K., Steinhäuser, C., et al. (2012). Dual reporter approaches for identification of Cre efficacy and astrocyte heterogeneity. FASEB J. *26*, 4576–4583.

Deng, P.Y., and Klyachko, V.A. (2011). The diverse functions of short-term plasticity components in synaptic computations. Commun. Integr. Biol. *4*, 543–548.

Denker, A., and Rizzoli, S.O. (2010). Synaptic vesicle pools: An update. Front. Synaptic Neurosci. *2*, 1–12.

Derkach, V., Barria, A., and Soderling, T.R. (1999). Ca2+/calmodulin-kinase II enhances channel conductance of alpha-amino-3-hydroxy-5-methyl-4-isoxazolepropionate type glutamate receptors. Proc. Natl. Acad. Sci. U. S. A. *96*, 3269–3274.

Diers-Fenger, M., Kirchhoff, F., Kettenmann, H., Levine, J.M., and Trotter, J. (2001). AN2/NG2 protein-expressing glial progenitor cells in the murine CNS: Isolation, differentiation, and association with radial glia. Glia *34*, 213–228.

Dimou, L., Simon, C., Kirchhoff, F., Takebayashi, H., and Gotz, M. (2008). Progeny of Olig2-Expressing Progenitors in the Gray and White Matter of the Adult Mouse Cerebral Cortex. J. Neurosci. *28*, 10434–10442.

Dittman, J.S., and Regehr, W.G. (1998). Calcium dependence and recovery kinetics of presynaptic depression at the climbing fiber to Purkinje cell synapse. J. Neurosci. *18*, 6147–6162.

Djukic, B., Casper, K.B., Philpot, B.D., Chin, L.-S., and McCarthy, K.D. (2007). Conditional Knock-Out of Kir4.1 Leads to Glial Membrane Depolarization, Inhibition of Potassium and Glutamate Uptake, and Enhanced Short-Term Synaptic Potentiation. J. Neurosci. *27*, 11354–11365.

Donevan, S.D., and Rogawski, M.A. (1995). Intracellular polyamines mediate inward rectification of Ca2+-permeable a-amino-3-hydroxy-5-methyl-4- isoxazolepropionic acid receptors. Neurobiology *92*, 9298–9302.

Douglas, R.M., and Goddard, G. V. (1975). Long-term potentiation of the perforant path-granule cell synapse in the rat hippocampus. Brain Res. *86*, 205–215.

Dupouey, P., Jacque, C., Bourre, J.M., Cesselin, F., Privat, A., and Baumann, N. (1979). Immunochemical studies of myelin basic protein in shiverer mouse devoid of major dense line of myelin. Neurosci. Lett. *12*, 113–118.

Eccles, B.Y.J.C., Llinas, R., and Sasaki, K. (1966). The excitatory synaptic action of climbing fibres on the Purkinje cells of the cerebellum. J Physiol. *182*, 268–296.

Eckstein, F., Woodward, W.R., and Nishu, R. (1991). Differential Localization and Possible Functions of aFGF and bFGF in the Central and Peripheral Nervous Systems. Ann. N. Y. Acad. Sci. *638*, 348–360.

Engelmann, M., Wotjak, C.T., Neumann, I., Ludwig, M., and Landgraf, R. (1996). Behavioral consequences of intracerebral vasopressin and oxytocin: Focus on learning and memory. Neurosci. Biobehav. Rev. *20*, 341–358.

Esposito, M.S. (2005). Neuronal Differentiation in the Adult Hippocampus Recapitulates Embryonic Development. J. Neurosci. *25*, 10074–10086.

Etxeberria, A., Hokanson, K.C., Dao, D.Q., Mayoral, S.R., Mei, F., Redmond, S.A., Ullian, E.M., and Chan, J.R. (2016). Dynamic Modulation of Myelination in Response to Visual Stimuli Alters Optic Nerve Conduction Velocity. J. Neurosci. *36*, 6937–6948.

Fannon, J., Tarmier, W., and Fulton, D. (2015). Neuronal activity and AMPA-type glutamate receptor activation regulates the morphological development of oligodendrocyte precursor cells. Glia *63*, 1021–1035.

Feil, R., Wagner, J., Metzger, D., and Chambon, P. (1997). Regulation of Cre Recombinase Activity by Mutated Estrogen Receptor Ligand-Binding Domains. Biochem. Biophys. Res. Commun. *237*, 752–757.

Fields, R.D. (2014a). Myelin - More than insulation. Science *344*, 264–266.

Fields, R.D. (2014b). Myelin formation and remodeling. Cell *156*, 15–17.

Fink, L., Seeger, W., Ermert, L., Hänze, J., Stahl, U., Grimminger, F., Kummer, W., and Bohle, R.M. (1998). Real-time quantitative RT-PCR after laser-assisted cell picking. Nat. Med. *14*, 1329-33.

Fioravante, D., and Regehr, W.G. (2011). Short-term forms of presynaptic plasticity. Curr. Opin. Neurobiol. *21*, 269–274.

Ford, M.C., Alexandrova, O., Cossell, L., Stange-Marten, A., Sinclair, J., Kopp-Scheinpflug, C., Pecka, M., Attwell, D., and Grothe, B. (2015). Tuning of Ranvier node and internode properties in myelinated axons to adjust action potential timing. Nat. Commun. *6*, 1–14.

Frerking, M., Malenka, R.C., and Nicoll, R.A. (1998). Brain-derived neurotrophic factor (BDNF) modulates inhibitory, but not excitatory, transmission in the CA1 region of the hippocampus. J. Neurophysiol. *80*, 3383–3386.

Frey, M.C., Sprengel, R., and Nevian, T. (2009). Activity Pattern-Dependent Long-Term Potentiation in Neocortex and Hippocampus of GluA1 (GluR-A) Subunit-Deficient Mice. J. Neurosci. *29*, 5587–5596.

Frey, U., Krug, M., Reymann, K.G., and Matthies, H. (1988). Anisomycin, an inhibitor of protein synthesis, blocks late phases of LTP phenomena in the hippocampal CA1 region in vitro. Brain Res. *452*, 57–65.

Fröhlich, B. (2016). Microcircuits of the Hippocampus. In: Network Neuroscience, First Edition. Academic Press. pp. 97-106

Fröhlich, N., Nagy, B., Hovhannisyan, A., and Kukley, M. (2011). Fate of neuron-glia synapses during proliferation and differentiation of NG2 cells. J. Anat. *219*, 18–32.

Frühbeis, C., Fröhlich, D., Kuo, W.P., Amphornrat, J., Thilemann, S., Saab, A.S., Kirchhoff, F., Möbius, W., Goebbels, S., Nave, K.A., et al. (2013). Neurotransmitter-Triggered Transfer of Exosomes Mediates Oligodendrocyte-Neuron Communication. PLoS Biol. *11*, e1001604.

Fukunaga, K., Stoppini, L., Miyamoto, E., and Muller, D. (1993). Long-term potentiation is associated with an increased activity of Ca2+/calmodulin-dependent protein kinase II. J. Biol. Chem. *268*, 7863–7867.

Fulton, D., Paez, P.M., Fisher, R., Handley, V., Colwell, C.S., and Campagnoni, A.T. (2010). Regulation of L-type Ca++ currents and process morphology in white matter oligodendrocyte precursor cells by golli-myelin proteins. Glia *58*, 1292–1303.

Fünfschilling, U., Supplie, L.M., Mahad, D., Boretius, S., Saab, A.S., Edgar, J., Brinkmann, B.G., Kassmann, C.M., Tzvetanova, I.D., Möbius, W., et al. (2012). Glycolytic oligodendrocytes maintain myelin and long-term axonal integrity. Nature *485*, 517–521.

Gallo, V., Zhou, J.M., McBain, C.J., Wright, P., Knutson, P.L., and Armstrong, R.C. (1996). Oligodendrocyte progenitor cell proliferation and lineage progression are regulated by glutamate receptor-mediated K+ channel block. J. Neurosci. *16*, 2659–2670.

Gao, Z., Van Beugen, B.J., and De Zeeuw, C.I. (2012). Distributed synergistic plasticity and cerebellar learning. Nat. Rev. Neurosci. *13*, 619–635.

Gautier, H.O.B., Evans, K.A., Volbracht, K., James, R., Sitnikov, S., Lundgaard, I., James, F., Lao-Peregrin, C., Reynolds, R., Franklin, R.J.M., et al. (2015). Neuronal activity regulates remyelination via glutamate signalling to oligodendrocyte progenitors. Nat. Commun. *6*, 8518.

Ge, W.-P., Zhou, W., Luo, Q., Jan, L.Y., and Jan, Y.N. (2009). Dividing glial cells maintain differentiated properties including complex morphology and functional synapses. Proc. Natl. Acad. Sci. U. S. A. *106*, 328–333.

Geiger, J.R.P., Melcher, T., Koh, D.S., Sakmann, B., Seeburg, P.H., Jonas, P., and Monyer, H. (1995). Relative abundance of subunit mRNAs determines gating and Ca2+ permeability of AMPA receptors in principal neurons and interneurons in rat CNS. Neuron *15*, 193–204.

Gerdes, J., Lemke, H., Baisch, H., Wacker, H.H., Schwab, U., and Stein, H. (1984). Cell cycle analysis of a cell proliferation-associated human nuclear antigen defined by the monoclonal antibody Ki-67. J. Immunol. *133*, 1710–1715.

Ghiani, C.A., Yuan, X., Eisen, A.M., Knutson, P.L., DePinho, R.A., McBain, C.J., and Gallo, V. (1999). Voltage-activated K+ channels and membrane depolarization regulate accumulation of the cyclin-dependent kinase inhibitors p27(Kip1) and p21(CIP1) in glial progenitor cells. J. Neurosci. *19*, 5380–5392.

Gibson, E.M., Purger, D., Mount, C.W., Goldstein, A.K., Lin, G.L., Wood, L.S., Inema, I., Miller, S.E., Bieri, G., Zuchero, J.B., et al. (2014). Neuronal activity promotes oligodendrogenesis and adaptive myelination in the mammalian brain. Science *344*, 1252304.

Glasser, M.F., and Van Essen, D.C. (2011). Mapping Human Cortical Areas In Vivo Based on Myelin Content as Revealed by T1- and T2-Weighted MRI. J. Neurosci. *31*, 11597–11616.

Glowatzki, E., Fakler, G., Brandle, U., Rexhausen, U., Zenner, H.P., Ruppersberg, J.P., and Fakler, B. (1995). Subunit-dependent assembly of inward-rectifier K+ channels. Proc. R. Soc. B Biol. Sci. *261*, 251–261.

Gómez-Pinilla, F., So, V., and Kesslak, J.P. (1998). Spatial learning and physical activity contribute to the induction of fibroblast growth factor: Neural substrates for increased cognition associated with exercise. Neuroscience *85*, 53–61.

Greco, V., and Guo, S. (2010). Compartmentalized organization: a common and required feature of stem cell niches? Development *137*, 1586–1594.

Gu, H., Marth, J.D., Orban, P.C., Mossmann, H., and Rajewsky, K. (1992). Deletion of a DNA Polymerase beta Gene Segment in T Cells Using Cell Type-Specific Gene Targeting Type deletion. Science *265*, 103–106.

Gu, Y., McIlwain, K.L., Weeber, E.J., Yamagata, T., Xu, B., Antalffy, B.A., Reyes, C., Yuva-Paylor, L., Armstrong, D., Zoghbi, H., et al. (2002). Impaired Conditioned Fear and Enhanced Long-Term Potentiation in Fmr2 Knock-Out Mice. J. Neurosci. *22*, 2753–2763.

Haberlandt, C., Derouiche, A., Wyczynski, A., Haseleu, J., Pohle, J., Karram, K., Trotter, J., Seifert, G., Frotscher, M., Steinhäuser, C., et al. (2011). Gray matter NG2 cells display multiple Ca2+-signaling pathways and highly motile processes. PLoS One *6*, e17575.

Harrison, J., and Jahr, C.E. (2003). Receptor occupancy limits synaptic depression at climbing fiber synapses. J. Neurosci. *23*, 377–383.

Henneberger, C., Papouin, T., Oliet, S.H.R., and Rusakov, D.A. (2010). Long-term potentiation depends on release of d-serine from astrocytes. Nature *463*, 232–236.

Heuser, J.E., and Reese, T. (1973). Evidence for recycling synaptic vesicle membrane during neurotransmitter release at the frog neuromuscular junction. J Cell Biol *57*, 315–344.

Hibino, H., Inanobe, A., Furutani, K., Murakami, S., Findlay, I., and Kurachi, Y. (2010). Inwardly Rectifying Potassium Channels: Their Structure, Function, and Physiological Roles. Physiol. Rev. *90*, 291–366.

Higashi, K., Fujita, A., Inanobe, A., Tanemoto, M., Doi, K., Kubo, T., and Kurachi, Y. (2001). An inwardly rectifying K^+ channel, Kir4.1, expressed in astrocytes surrounds synapses and blood vessels in brain. Am. J. Physiol. Physiol. *281*, C922–C931.

Higashimori, H., and Sontheimer, H. (2007). Role of Kir4 . 1 Channels in Growth Control of Glia. *1679*, 1668–1679.

Hildebrand, C., Remahl, S., Persson, H., and Bjartmar, C. (1993). Myelinated nerve fibres in the CNS. Prog. Neurobiol. *40*, 319–384.

Hill, R.A., Li, A.M., and Grutzendler, J. (2018a). Lifelong cortical myelin plasticity and age-related degeneration in the live mammalian brain. Nat. Neurosci. *21*, 683–695.

Hille, B. (1992). Potassium Channels and Chloride Channels. In: Ionic Channels in Excitable Membranes, Third Edition. Sunderland, Massachusetts, Sinauer

Hoess, R.H., Ziese, M., and Sternberg, N.A.T. (1982). P1 site-specific recombination: Nucleotide sequence of the. *79*, 3398–3402.

Holland, P.M., Abramson, R.D., Watson, R., and Gelfand, D.H. (1991). Detection of specific polymerase chain reaction product by utilizing the $5' \rightarrow 3'$ exonuclease activity of Thermus aquaticus DNA polymerase. Proc. Natl. Acad. Sci. U. S. A. *88*, 7276–7280.

Hollmann, M. (1994). Cloned Glutamate Receptors. Annu. Rev. Neurosci. *17*, 31–108.

Hollmann, M., Hartley, M., and Heinemann, S. (1991). Ca2+ permeability of KA-AMPA - gated glutamate receptor channels depends on subunit composition. Science *252*, 851–853.

Huang, W., Zhao, N., Bai, X., Karram, K., Trotter, J., Goebbels, S., Scheller, A., and Kirchhoff, F. (2014). Novel NG2-CreERT2 knock-in mice demonstrate heterogeneous differentiation potential of NG2 glia during development. Glia *62*, 896–913.

Hughes, E.G., Orthmann-Murphy, J.L., Langseth, A.J., and Bergles, D.E. (2018). Myelin remodeling through experience-dependent oligodendrogenesis in the adult somatosensory cortex. Nat. Neurosci. *21*, 696–706.

Hume, R.I., Dingledine, R., and Heinemann, S.F. (1991). Identification of a site in glutamate receptor subunits that controls calcium permeability. Science *253*, 1028–1031.

Ishii, M., Horio, Y., Tada, Y., Hibino, H., Inanobe, a, Ito, M., Yamada, M., Gotow, T., Uchiyama, Y., and Kurachi, Y. (1997). Expression and clustered distribution of an inwardly rectifying potassium channel, KAB-2/Kir4.1, on mammalian retinal Müller cell membrane: their regulation by insulin and laminin signals. J. Neurosci. *17*, 7725–7735.

Ito, M., and Kano, M. (1982). Long-lasting depression of parallel fiber-Purkinje cell transmission induced by conjunctive stimulation of parallel fibers and climbing fibers in the cerebellar cortex. *33*, 253–258.

Jabs, R., Pivneva, T., Hüttmann, K., Wyczynski, A., Nolte, C., Kettenmann, H., and Steinhäuser, C. (2005). Synaptic transmission onto hippocampal glial cells with hGFAP promoter activity. J. Cell Sci. *118*, 3791–3803.

Jackson, A.C., and Nicoll, R.A. (2011). The Expanding Social Network of Ionotropic Glutamate Receptors: TARPs and Other Transmembrane Auxiliary Subunits. Neuron *70*, 178–199.

Jansen, L.A., Uhlmann, E.J., Crino, P.B., Gutmann, D.H., and Wong, M. (2005). Epileptogenesis and reduced inward rectifier potassium current in tuberous sclerosis complex-1-deficient astrocytes. Epilepsia *46*, 1871–1880.

Janzer, R.C., and Raff, M.C. (1987). Astrocytes induce blood-brain barrier properties in endothelial cells. Nature *325*, 253–257.

Jeffries, M.A., Urbanek, K., Torres, L., Wendell, S.G., Rubio, M.E., and Fyffe-Maricich, S.L. (2016). ERK1/2 Activation in Preexisting Oligodendrocytes of Adult Mice Drives New Myelin Synthesis and Enhanced CNS Function. J. Neurosci. *36*, 9186–9200.

Jung, M., Krämer, E., Grzenkowski, M., Tang, K., Blakemore, W., Aguzzi, A., Khazaie, K., Chlichlia, K., von Blankenfeld, G., Kettenmann, H., et al. (1995). Lines of Murine Oligodendroglial Precursor Cells Immortalized by an Activated neu Tyrosine Kinase Show Distinct Degrees of Interaction with Axons In Vitro and In Vivo. Eur. J. Neurosci. *7*, 1245–1265.

Kacem, K., Lacombe, P., Seylaz, J., and Bonvento, G. (1998). Structural organization of the perivascular astrocyte endfeet and their relationship with the endothelial glucose transporter: A confocal microscopy study. Glia *23*, 1-10

Kalsi, A.S., Greenwood, K., Wilkin, G., and Butt, A.M. (2004). Kir4.1 expression by astrocytes and oligodendrocytes in CNS white matter: A developmental study in the rat optic nerve. J. Anat. *204*, 475–485.

Kamboj, S.K., Swanson, G.T., and Cull-Candy, S.G. (1995a). Intracellular spermine confers rectification on rat calcium-permeable AMPA and kainate receptors. J. Physiol. *486*, 297–303.

Kamboj, S.K., Swanson, G.T., and Cull-Candy, S.G. (1995b). Intracellular spermine confers rectification on rat calcium-permeable AMPA and kainate receptors. J. Physiol. *486*, 297–303.

Kandel, E. R., Schwartz, J. H., Jessel, T. M. (2000). Principles of neural science. Fourth edition. McGraw-Hill Companies.

Kang, S.H., Fukaya, M., Yang, J.K., Rothstein, J.D., and Bergles, D.E. (2010). NG2+ CNS glial progenitors remain committed to the oligodendrocyte lineage in postnatal life and following neurodegeneration. Neuron *68*, 668–681.

Karram, K., Goebbels, S., Schwab, M., Jennisen, K., Seifert, G., Steinhäuser, C., Nave, K.A., and Trotter, J. (2008). NG2-expressing cells in the nervous system revealed by the NG2-EYFP-knock in mouse. Genesis *46*, 743–757.

Kato, D., Wake, H., Lee, P.R., Tachibana, Y., Ono, R., Sugio, S., Tsuji, Y., Tanaka, Y.H., Tanaka, Y.R., Masamizu, Y., et al. (2019). Motor learning requires myelination to reduce asynchrony and spontaneity in neural activity. Glia *68*,193-210.

Katz, B., and Miledi, R. (1968). The role of calcium in neuromuscular facilitation. J. Physiol. *195*, 481–492.

Kavalali, E.T. (2015). The mechanisms and functions of spontaneous neurotransmitter release. Nat. Rev. Neurosci. *16*, 5–16.

Kavalali, E.T., Chung, C.H., Khvotchev, M., Leitz, J., Nosyreva, E., Raingo, J., and Ramirez, D.M.O. (2011). Spontaneous neurotransmission: An independent pathway for neuronal signaling? Physiology *26*, 45–53.

Kinboshi, M., Mukai, T., Nagao, Y., Matsuba, Y., Tsuji, Y., Tanaka, S., Tokudome, K., Shimizu, S., Ito, H., Ikeda, A., et al. (2017). Inhibition of inwardly rectifying potassium (Kir) 4.1 channels facilitates brain-derived neurotrophic factor (BDNF) expression in astrocytes. Front. Mol. Neurosci. *10*, 1–12.

Kirschner, D.A., and Ganser, A.L. (1980). Compact myelin exists in the absence of basic protein in the shiverer mutant mouse. Nature *283*, 207–210.

Kleschevnikov, A.M., Sokolov, M. V, Kuhnt, U., Dawe, G.S., Stephenson, J.D., and Voronin, L.L. (1997). Changes in paired-pulse facilitation correlate with induction of long- term potentiation in area CA1 of rat hippocampal slices. Neuroscience *76*, 829–843.

Knierim, J.J. (2015). The hippocampus. Curr. Biol. *25*, R1116–R1121.

Knutson, P., Ghiani, C.A., Zhou, J.M., Gallo, V., and McBain, C.J. (1997). K+ channel expression and cell proliferation are regulated by intracellular sodium and membrane depolarization in oligodendrocyte progenitor cells. J. Neurosci. *17*, 2669–2682.

Kofuji, P., and Newman, E.A. (2004). Potassium buffering in the central nervous system. Neuroscience *129*, 1045–1056.

Kofuji, P., Ceelen, P., Zahs, K.R., Surbeck, L.W., Lester, H.A., and Newman, E.A. (2000). Genetic Inactivation of an Inwardly Rectifying Potassium Channel (Kir4.1 Subunit) in Mice: Phenotypic Impact in Retina. J. Neurosci. *20*, 5733–5740.

Kogan, J.H., Frankland, P.W., and Silva, A.J. (2000). Long-term memory underlying hippocampus-dependent social recognition in mice. Hippocampus *10*, 47–56.

Koh, D.S., Burnashev, N., and Jonas, P. (1995). Block of native Ca(2+)-permeable AMPA receptors in rat brain by intracellular polyamines generates double rectification. J. Physiol. *486*, 305–312.

Kornhauser, J.M., Cowan, C.W., Shaywitz, A.J., Dolmetsch, R.E., Griffith, E.C., Hu, L.S., Haddad, C., Xia, Z., and Greenberg, M.E. (2002). CREB transcriptional activity in neurons is regulated by multiple, calcium-specific phosphorylation events. Neuron *34*, 221–233.

Korte, M., Carrolltt, P., Wolf, E., Brem, G., Thoenent, H., and Bonhoeffer, T. (1995). brain-derived neurotrophic. *92*, 8856–8860.

Kougioumtzidou, E., Shimizu, T., Hamilton, N.B., Tohyama, K., Sprengel, R., Monyer, H., Attwell, D., and Richardson, W.D. (2017). Signalling through AMPA receptors on oligodendrocyte precursors promotes myelination by enhancing oligodendrocyte survival. Elife *6*, 1–31.

Krämer-Albers, E.M., Bretz, N., Tenzer, S., Winterstein, C., Möbius, W., Berger, H., Nave, K.A., Schild, H., and Trotter, J. (2007). Oligodendrocytes secrete exosomes containing major myelin and stress-protective proteins: Trophic support for axons? Proteomics - Clin. Appl. *1*, 1446–1461.

Kressin, K., Kuprijanova, E., Jabs, R., Seifert, G., and Steinhäuser, C. (1995). Developmental regulation of Na+ and K+ conductances in glial cells of mouse hippocampal brain slices. Glia *15*, 173–187.

Kukley, M., and Dietrich, D. (2009). Kainate receptors and signal integration by NG2 glial cells. Neuron Glia Biol. *5*, 13-20.

Kukley, M., Kiladze, M., Tognatta, R., Hans, M., Swandulla, D., Schramm, J., and Dietrich, D. (2008). Glial cells are born with synapses. FASEB J. *22*, 2957–2969.

Kukley, M., Nishiyama, A., and Dietrich, D. (2010). The Fate of Synaptic Input to NG2 Glial Cells: Neurons Specifically Downregulate Transmitter Release onto Differentiating Oligodendroglial Cells. J. Neurosci. *30*, 8320–8331.

Kuner, T., Beck, C., Sakmann, B., and Seeburg, P.H. (2001). Channel-lining residues of the AMPA receptor M2 segment: Structural environment of the Q/R site and identification of the selectivity filter. J. Neurosci. *21*, 4162–4172.

Larson, V.A., Zhang, Y., and Bergles, D.E. (2016). Electrophysiological properties of NG2+ cells: Matching physiological studies with gene expression profiles. Brain Res. *1638*, 138–160.

Larson, V.A., Mironova, Y., Vanderpool, K.G., Waisman, A., Rash, J.E., Agarwal, A., and Bergles, D.E. (2018). Oligodendrocytes control potassium accumulation in white matter and seizure susceptibility. Elife *7*, 1–33.

Laule, C., Vavasour, I.M., Kolind, S.H., Li, D.K.B., Traboulsee, T.L., Moore, G.R.W., and MacKay, A.L. (2007). Magnetic Resonance Imaging of Myelin. Neurotherapeutics *4*, 460–484.

Lee, K.H., Mathews, P.J., Reeves, A.M.B., Choe, K.Y., Jami, S.A., Serrano, R.E., and Otis, T.S. (2015). Circuit mechanisms underlying motor memory formation in the cerebellum. Neuron *86*, 529–540.

Lee, Y., Morrison, B.M., Li, Y., Lengacher, S., Farah, M.H., Hoffman, P.N., Liu, Y., Tsingalia, A., Jin, L., Zhang, P.W., et al. (2012). Oligodendroglia metabolically support axons and contribute to neurodegeneration. Nature *487*, 443–448.

Lemon, J. (2016). The analysis of event rates using intervals. Quant. Methods Psychol. *10*, 68–76.

Lendahl, U., Zimmerman, L.B., and McKay, R.D.G. (1990). CNS stem cells express a new class of intermediate filament protein. Cell *60*, 585–595.

Lesage, F., Guillemare, E., Fink, M., Duprat, F., Lazdunski, M., Romey, G., and Barhanin, J. (1996). weakly inward rectifying K+. EMBO J. *15*, 1004–1011.

Li, Q., Brus-Ramer, M., Martin, J.H., and McDonald, J.W. (2010). Electrical stimulation of the medullary pyramid promotes proliferation and differentiation of oligodendrocyte progenitor cells in the corticospinal tract of the adult rat. Neurosci. Lett. *479*, 128–133.

Lin, S.C., and Bergles, D.E. (2004a). Synaptic signaling between GABAergic interneurons and oligodendrocyte precursor cells in the hippocampus. Nat. Neurosci. *7*, 24–32.

Lin, S.C., and Bergles, D.E. (2004b). Synaptic signaling between neurons and glia. Glia *47*, 290–298.

Lin, S.C., Huck, J.H.J., Roberts, J.D.B., Macklin, W.B., Somogyi, P., and Bergles, D.E. (2005). Climbing fiber innervation of NG2-expressing glia in the mammalian cerebellum. Neuron *46*, 773–785.

Lisman, J., Yasuda, R., and Raghavachari, S. (2012). Mechanisms of CaMKII action in long-term potentiation. Nat. Rev. Neurosci. *13*, 169–182.

Liu, J., Dietz, K., Deloyht, J.M., Pedre, X., Kelkar, D., Kaur, J., Vialou, V., Lobo, M.K., Dietz, D.M., Nestler, E.J., et al. (2012). Impaired adult myelination in the prefrontal cortex of socially isolated mice. Nat. Neurosci. *15*, 1621–1623.

Livak, K.J., Flood, S.J.A., Marmaro, J., Giusti, W., and Deetz, K. (1995). Oligonucleotides with fluorescent dyes at opposite ends provide a quenched probe system useful for detecting PCR product and nucleic acid hybridization. Genome Res. *4*, 357–362.

Lu, W., Shi, Y., Jackson, A.C., Bjorgan, K., During, M.J., Sprengel, R., Seeburg, P.H., and Nicoll, R.A. (2009). Subunit Composition of Synaptic AMPA Receptors Revealed by a Single-Cell Genetic Approach. Neuron *62*, 254–268.

Luque, N.R., Garrido, J.A., Naveros, F., Carrillo, R.R., D'Angelo, E., and Ros, E. (2016). Distributed Cerebellar Motor Learning: A Spike-Timing-Dependent Plasticity Model. Front. Comput. Neurosci. *10*, 1–22.

Lynch, M.A. (2004). Long-term potentiation and memory. Philos. Trans. R. Soc. B Biol. Sci. *358*, 643–647.

Lynch, G., Larson, J., Kelso, S., Barrionuevo, G., and Schottler, F. (1983). Intracellular injections of EGTA block induction of hippocampal long-term potentiation. Nature *305*, 719–721.

Macdermott, A.B., Mayer, M.L., Westbrook, G.L., Smith, S.J., and Barker, J.L. (1986). NMDA-receptor activation increases cytoplasmic calcium concentration in cultured spinal cord neurones. Nature *321*, 519–522.

MacFarlane, S.N., and Sontheimer, H. (2000). Changes in ion channel expression accompany cell cycle progression of spinal cord astrocytes. Glia *30*, 39–48.

Makinodan, M., Rosen, K.M., Ito, S., and Corfas, G. (2012). A critical period for social experience-dependent oligodendrocyte maturation and myelination. Science *337*, 1357–1360.

Maldonado, P.P., Velez-Fort, M., Levavasseur, F., and Angulo, M.C. (2013). Oligodendrocyte Precursor Cells Are Accurate Sensors of Local K+ in Mature Gray Matter. J. Neurosci. *33*, 2432–2442.

Malinow, R., Schulman, H., and Tsien, R.W. (1989). Inhibition of postsynaptic PKC or CaMKII blocks induction but not expression of LTP. Science *245*, 862–866.

Mangin, J.-M., Kunze, A., Chittajallu, R., and Gallo, V. (2008). Satellite NG2 Progenitor Cells Share Common Glutamatergic Inputs with Associated Interneurons in the Mouse Dentate Gyrus. J. Neurosci. *28*, 7610–7623.

Mangin, J.-M., Li, P., Scafidi, J., and Gallo, V. (2012). Experience-dependent regulation of NG2 progenitors in the developing barrel cortex. Nat. Neurosci. *15*, 1192–1194.

Markham, J.A., and Juraska, J.M. (2007). Social recognition memory: Influence of age, sex, and ovarian hormonal status. Physiol. Behav. *92*, 881–888.

Marr, D. (1969). A theory of cerebellar cortex. J. Physiol. *202*, 437–470.

Mayer, M.L., Westbrook, G.L., and Guthrie, P.B. (1984). Voltage-dependent block by Mg 2+ of NMDA responses in spinal cord neurones. Nature *309*, 261–263.

McKenzie, I.A., Ohayon, D., Li, H., De Faria, J.P., Emery, B., Tohyama, K., and Richardson, W.D. (2014). Motor skill learning requires active central myelination. Science *346*, 318–322.

McNaughton, B.L. (1982). Long-term synaptic enhancement and short-term potentiation in rat fascia dentata act through different mechanisms. J. Physiol. *324*, 249–262.

Mei, F., Christin Chong, S.Y., and Chan, J.R. (2013). Myelin-based inhibitors of oligodendrocyte myelination: Clues from axonal growth and regeneration. Neurosci. Bull. *29*, 177–188.

Meier, S., Bräuer, A.U., Heimrich, B., Nitsch, R., and Savaskan, N.E. (2004). Myelination in the hippocampus during development and following lesion. Cell. Mol. Life Sci. *61*, 1082–1094.

Metzger, D., Clifford, J., Chiba, H., and Chambon, P. (1995). Conditional site-specific recombination in mammalian cells using a ligand-dependent chimeric Cre recombinase. Proc Natl Acad Sci U S A *92*, 6991–6995.

Meyer, N., Richter, N., Fan, Z., Siemonsmeier, G., Pivneva, T., Jordan, P., Steinhäuser, C., Semtner, M., Nolte, C., and Kettenmann, H. (2018). Oligodendrocytes in the Mouse Corpus Callosum Maintain Axonal Function by Delivery of Glucose. Cell Rep. *22*, 2383–2394.

Migaud, M., Charlesworth, P., Dempster, M., Webster, L.C., Watabe, A.M., Makhinson, M., He, Y., Ramsay, M.F., Morris, R.G.M., Morrison, J.H., et al. (1998). Enhanced long-term potentiation and impairedlearninginmicewithmutant postsynaptic density-95 protein. 433–439.

Milstein, A.D., Zhou, W., Karimzadegan, S., Bredt, D.S., and Nicoll, R.A. (2007). TARP Subtypes Differentially and Dose-Dependently Control Synaptic AMPA Receptor Gating. Neuron *55*, 905–918.

Min, Y., Kristiansen, K., Boggs, J.M., Husted, C., Zasadzinski, J.A., and Israelachvili, J. (2009). Interaction forces and adhesion of supported myelin lipid bilayers modulated by myelin basic protein. Proc. Natl. Acad. Sci. U. S. A. *106*, 3154–3159.

Minichiello, L., Korte, M., Wolfer, D., Kühn, R., Unsicker, K., Cestari, V., Rossi-Arnaud, C., Lipp, H.P., Bonhoeffer, T., and Klein, R. (1999). Essential role for TrkB receptors in hippocampus-mediated learning. Neuron *24*, 401–414.

Mitew, S., Gobius, I., Fenlon, L.R., McDougall, S.J., Hawkes, D., Xing, Y.L., Bujalka, H., Gundlach, A.L., Richards, L.J., Kilpatrick, T.J., et al. (2018). Pharmacogenetic stimulation of neuronal activity increases myelination in an axon-specific manner. Nat. Commun. *9*, 1–16.

Mongiat, L.A., Espósito, M.S., Lombardi, G., and Schinder, A.F. (2009). Reliable activation of immature neurons in the adult hippocampus. PLoS One *4*, e5320.

Morris, R.G.M., Anderson, E., Lynch, G.S., and Baudry, M. (1986). Selective impairment of learning and blockade of long-term potentiation by an N-methyl-D-aspartate receptor antagonist, AP5. Nature *319*, 774–776.

Mount, C.W., and Monje, M. (2017). Wrapped to Adapt: Experience-Dependent Myelination. Neuron *95*, 743–756.

Murphy, T.H., Worley, P.F., and Baraban, J.M. (1991). L-type voltage-sensitive calcium channels mediate synaptic activation of immediate early genes. Neuron *7*, 625–635.

Nagamatsu, S., Sawa, H., Kamada, K., Nakamichi, Y., Yoshimoto, K., and Hoshino, T. (1993). Neuron-specific glucose transporter (NSGT): CNS distribution of GLUT3 rat glucose transporter (RGT3) in rat central neurons. FEBS Lett. *334*, 289–295.

Nave, K.A. (2010a). Myelination and support of axonal integrity by glia. Nature *468*, 244–252.

Nave, K.A. (2010b). Myelination and the trophic support of long axons. Nat. Rev. Neurosci. *11*, 275–283.

Neusch, C., Rozengurt, N., Jacobs, R.E., Lester, H.A., and Kofuji, P. (2001). Kir4.1 potassium channel subunit is crucial for oligodendrocyte development and in vivo myelination. J. Neurosci. *21*, 5429–5438.

Neves, G., Cooke, S.F., and Bliss, T.V.P. (2008). Synaptic plasticity, memory and the hippocampus - a neural network aproach to causality. Nat. Rev. Neurosci. *9*, 65–75.

Nichols, C.G., and Lopatin, A.N. (2002). Inward Rectifier Potassium Channels. Annu. Rev. Physiol. *59*, 171–191.

Nickel, M., and Gu, C. (2018). Regulation of central nervous system myelination in higher brain functions. Neural Plast. *2018*, 1-12.

Nimmerjahn, A., Kirchhoff, F., and Helmchen, F. (2005). Neuroscience: Resting microglial cells are highly dynamic surveillants of brain parenchyma in vivo. Science *308*, 1314–1318.

Nishiyama, A. (2013) Physiological Properties of NG2+ Glial Cells. In: Neuroglia, third edition (Kettenmann H, Ransom BR, eds). New York: Oxford University Press.

Nishiyama, A., Komitova, M., Suzuki, R., and Zhu, X. (2009). Polydendrocytes (NG2 cells): Multifunctional cells with lineage plasticity. Nat. Rev. Neurosci. *10*, 9–22.

Nowak, L., Bregestovski, P., Ascher, P., Herbet, A., and Prochiantz, A. (1984). Magnesium gates glutamate-activated channels in mouse central neurones. Nature *307*, 462–465.

Nwaobi, S.E., Cuddapah, V.A., Patterson, K.C., Randolph, A.C., and Olsen, M.L. (2016). The role of glial-specific Kir4.1 in normal and pathological states of the CNS. Acta Neuropathol. *132*, 1-21.

Ohno, Y., Kinboshi, M., and Shimizu, S. (2018). Inwardly rectifying potassium channel kir4.1 as a novel modulator of BDNF expression in astrocytes. Int. J. Mol. Sci. *19*, 1-18.

Oliver, D., Baukrowitz, T., and Fakler, B. (2000). Polyamines as gating molecules of inward-rectifier K+ channels. Eur. J. Biochem. *267*, 5824–5829.

Olofsdotter, K., Lindvall, O., and Asztély, F. (2000). Increased synaptic inhibition in dentate gyrus of mice with reduced levels of endogenous brain-derived neurotrophic factor. Neuroscience *101*, 531–539.

Orkand, R.K., Nicholls, J.G., and Kuffler, S.W. (1966). Effect of nerve impulses on the membrane potential of glial cells in the central nervous system of amphibia. J. Neurophysiol. *29*, 788–806.

Osterstock, G., Le Bras, B., Arulkandarajah, K.H., Le Corronc, H., Czarnecki, A., Mouffle, C., Bullier, E., Legendre, P., and Mangin, J.M. (2018). Axoglial synapses are formed onto pioneer oligodendrocyte precursor cells at the onset of spinal cord gliogenesis. Glia *66*, 1678–1694.

Palmer, C.L., Cotton, L., and Henley, J.M. (2005). The molecular pharmacology and cell biology of α-amino-3-hydroxy-5- methyl-4-isoxazolepropionic acid receptors. Pharmacol. Rev. *57*, 253–277.

Paolicelli, R.C., Bolasco, G., Pagani, F., Maggi, L., Scianni, M., Panzanelli, P., Giustetto, M., Ferreira, T.A., Guiducci, E., Dumas, L., et al. (2011). Synaptic pruning by microglia is necessary for normal brain development. Science *333*, 1456–1458.

Passlick, S., Trotter, J., Seifert, G., Steinhäuser, C., and Jabs, R. (2016). The NG2 Protein Is Not Required for Glutamatergic Neuron-NG2 Cell Synaptic Signaling. Cereb. Cortex *26*, 51–57.

Patterson, S.L., Abel, T., Deuel, T.A.S., Martin, K.C., Rose, J.C., and Kandel, E.R. (1996). Recombinant BDNF rescues deficits in basal synaptic transmission and hippocampal LTP in BDNF knockout mice. Neuron *16*, 1137–1145.

Pellegrini-Giampietro, D.E. (2003). An activity-dependent spermine-mediated mechanism that modulates glutamate transmission. Trends Neurosci. *26*, 9–11.

Pellerin, L., and Magistretti, P.J. (1994). Glutamate uptake into astrocytes stimulates aerobic glycolysis: A mechanism coupling neuronal activity to glucose utilization. Proc. Natl. Acad. Sci. U. S. A. *91*, 10625–10629.

Penn, A.C., Zhang, C.L., Georges, F., Royer, L., Breillat, C., Hosy, E., Petersen, J.D., Humeau, Y., and Choquet, D. (2017). Hippocampal LTP and contextual learning require surface diffusion of AMPA receptors. Nature *549*, 384–388.

Pereda, A.E. (2014). Electrical synapses and their functional interactions with chemical synapses. Nat. Rev. Neurosci. *15*, 250–263.

Peters, A. (1964). Observations on the connexions between myelin sheaths ang glias cells in the optic nerves of young rats. J. Anat. *98*, 125–134.

Picard, D. (1994). Regulation of protein function through expression of chimaeric proteins. Curr.Opin.Biotechnol. *5*, 511–515.

Pitman, K.A., Ricci, R., Gasperini, R., Beasley, S., Macarena Pavez, J., Charlesworth, L.F., and Young, K.M. (2019). The voltage gated calcium channel CaV1.2 promotes adult oligodendrocyte progenitor cell survival in the mouse corpus callosum but not motor cortex. Glia *in press*, 1–17.

Poopalasundaram, S., Knott, C., Shamotienko, O.G., Foran, P.G., Dolly, J.O., Ghiani, C.A., Gallo, V., and Wilkin, G.P. (2000). Glial heterogeneity in expression of the inwardly rectifying K(+) channel, Kir4.1, in adult rat CNS. *372*, 362–372.

Prange, O., and Murphy, T.H. (1999). Correlation of miniature synaptic activity and evoked release probability in cultures of cortical neurons. J. Neurosci. *19*, 6427–6438.

Purves, D., Augustine, G. J., Fitzpatrick, D., Hall, W. C., LaMantia, A., McNamara, J. O., and Williams, S. M. (2004). Neuroscience. Third edition. Sinauer Associates.

Qi, M., Zhuo, M., Skålhegg, B.S., Brandon, E.P., Kandel, E.R., Mcknight, G.S., and Idzerda, R.L. (1996). Impaired hippocampal plasticity in mice lacking the Cβ1 catalytic subunit of cAMP-dependent protein kinase. Proc. Natl. Acad. Sci. U. S. A. *93*, 1571–1576.

Ramirez, D.M.O., and Kavalali, E.T. (2011). Differential regulation of spontaneous and evoked neurotransmitter release at central synapses. Curr. Opin. Neurobiol. *21*, 275–282.

Rasminsky, M., and Sears, T.A. (1972). Internodal conduction in undissected demyelinated nerve fibres. J. Physiol. *227*, 323–350.

Ramón y Cajal, S. (1909). Histologie du système nerveux de l'homme & des vertébrés (Paris : Maloine). Reviewed by Burwell, R.D and Agster, K. L. (2008). Anatomy of the Hippocampus and the Declarative Memory System. In: Learning and Memory: A Comprehensive Reference. (J. Byrne, eds.) Oxford: Elsevier, pp. 47-66.

Raymond, J.L., Lisberger, S.G., and Mauk, M.D. (1996). The cerebellum: A neuronal learning machine? Science *272*, 1126–1131.

Readhead, C., Popko, B., Takahashi, N., David Shine, H., Saavedra, R.A., Sidman, R.L., and Hood, L. (1987). Expression of a myelin basic protein gene in transgenic shiverer mice: Correction of the dysmyelinating phenotype. Cell *48*, 703–712.

Rivera, A., Chacon De La Rocha, I., Neville, R., and Butt, A.M. (2016). Pathophysiology of Ng2-Glia: a 'Chicken and Egg' Scenario of Altered Neurotransmission and Disruption of NG2-Glial Cell Function. Opera Medica Physiol. *2*, 27–33.

Rivka Sherman-Gold (eds) (2012). The Axon Guide. Electrophysiology and Biophysics Laboratory Techniques. 3rd edition. Molecular Devices

Rizzoli, S.O., and Betz, W.J. (2005). Synaptic vesicle pools. Nat. Rev. Neurosci. *6*, 57–69.

Roach, A., Boylan, K., Horvath, S., Prusiner, S.B., and Hood, L.E. (1983). Characterization of cloned cDNA representing rat myelin basic protein: Absence of expression in brain of shiverer mutant mice. Cell *34*, 799–806.

Rotheneichner, P., Romanelli, P., Bieler, L., Pagitsch, S., Zaunmair, P., Kreutzer, C., König, R., Marschallinger, J., Aigner, L., and Couillard-Després, S. (2017). Tamoxifen activation of cre-recombinase has no persisting effects on adult neurogenesis or learning and anxiety. Front. Neurosci. *11*, 1–8.

Rothstein, J.D., Dykes-Hoberg, M., Pardo, C.A., Bristol, L.A., Jin, L., Kuncl, R.W., Kanai, Y., Hediger, M.A., Wang, Y., Schielke, J.P., et al. (1996). Knockout of glutamate transporters reveals a major role for astroglial transport in excitotoxicity and clearance of glutamate. Neuron *16*, 675–686.

Rouach, N., Koulakoff, A., Abudara, V., Willecke, K., and Giaume, C. (2008). Astroglial metabolic networks sustain hippocampal synaptic transmission. Science *322*, 1551–1555.

Rutherford, L.C., Nelson, S.B., and Turrigiano, G.G. (1998). BDNF has opposite effects on the quantal amplitude of pyramidal neuron and interneuron excitatory synapses. Neuron *21*, 521–530.

Sakry, D., Neitz, A., Singh, J., Frischknecht, R., Marongiu, D., Binamé, F., Perera, S.S., Endres, K., Lutz, B., Radyushkin, K., et al. (2014). Oligodendrocyte Precursor Cells Modulate the Neuronal Network by Activity-Dependent Ectodomain Cleavage of Glial NG2. PLoS Biol. *12*, e1001993.

Salami, M., Itami, C., Tsumoto, T., and Kimura, F. (2003). Change of conduction velocity by regional myelination yields constant latency irrespective of distance between thalamus and cortex. Proc. Natl. Acad. Sci. *100*, 6174–6179.

Santiago González, D.A., Cheli, V.T., Zamora, N.N., Lama, T.N., Spreuer, V., Murphy, G.G., and Paez, P.M. (2017). Conditional deletion of the L-type calcium channel Cav1.2 in NG2 positive cells impairs remyelination in mice. J. Neurosci. *37*, 1787–17.

Sato-Bigbee, C., Pal, S., and Chu, A.K. (1999). Different neuroligands and signal transduction pathways stimulate CREB phosphorylation at specific developmental stages along oligodendrocyte differentiation. J. Neurochem. *72*, 139–147.

Sauer, B. (1998). Inducible Gene Targeting in Mice Using the Cre/loxSystem. Methods *14*, 381–392.

Schafer, D.P., Lehrman, E.K., Kautzman, A.G., Koyama, R., Mardinly, A.R., Yamasaki, R., Ransohoff, R.M., Greenberg, M.E., Barres, B.A., and Stevens, B. (2012). Microglia sculpt postnatal neural circuits in an activity and complement-dependent manner. Neuron *74*, 691–705.

Schäfer, I., Müller, C., Luhmann, H.J., and White, R. (2016). MOBP levels are regulated by Fyn kinase and affect the morphological differentiation of oligodendrocytes. J. Cell Sci. *129*, 930–942.

Scherrer, L.C., Picard, D., Massa, E., Harmon, J.M., Simons, S.S., Yamamoto, K.R., and Pratt, W.B. (1993). Evidence that the Hormone Binding Domain of Steroid Receptors Confers Hormonal Control on Chimeric Proteins by Determining Their Hormone-Regulated Binding to Heat-Shock Protein 90. Biochemistry *32*, 5381–5386.

Schonewille, M., Gao, Z., Boele, H.J., Vinueza Veloz, M.F., Amerika, W.E., Šimek, A.A.M., De Jeu, M.T., Steinberg, J.P., Takamiya, K., Hoebeek, F.E., et al. (2011). Reevaluating the Role of LTD in Cerebellar Motor Learning. Neuron *70*, 43–50.

Schwartzkroin, P.A., and Wester, K. (1975). Long-lasting facilitation of a synaptic potential following tetanization in the in vitro hippocampal slice. Brain Res. *89*, 107–119.

Schwenk, J., Harmel, N., Zolles, G., Bildl, W., Kulik, A., Heimrich, B., Chisaka, O., Jonas, P., Schulte, U., Fakler, B., et al. (2009). Functional proteomics identify cornichon proteins as auxiliary subunits of AMPA receptors. Science *323*, 1313–1319.

Scoville, W.B., and Milner, B. (1957). Loss of Recent Memory After Bilateral Hippocampal Lesions. J. Neurol. Neurosurg. Psychiatry *20*, 11–21.

Seidl, A.H. (2014). Regulation of conduction time along axons. Neuroscience *276*, 126–134.

Seifert, G., Becker, A., and Steinhäuser, C. (2002).Combining Patch-Clamp Techniques with RT-PCR. In: Patch-Clamp Analysis. Advanved Techniques. (Walz, W., Boulton, A. A., Baker, G. B., eds). Neuromethods, volume 35, p301-330. Totowa, New Jersey: Human Press.

Seifert, G., Rehn, L., Weber, M., and Steinhäuser, C. (1997). AMPA receptor subunits expressed by single astrocytes in the juvenile mouse hippocampus. Mol. Brain Res. *47*, 286–294.

Seifert, G., Weber, M., Schramm, J., and Steinhäuser, C. (2003). Changes in splice variant expression and subunit assembly of AMPA receptors during maturation of hippocampal astrocytes. Mol. Cell. Neurosci. *22*, 248–258.

Seifert, G., Huttmann, K., Binder, D.K., Hartmann, C., Wyczynski, A., Neusch, C., and Steinhauser, C. (2009). Analysis of Astroglial K+ Channel Expression in the Developing Hippocampus Reveals a Predominant Role of the Kir4.1 Subunit. J. Neurosci. *29*, 7474–7488.

Serwanski, D.R., Jukkola, P., and Nishiyama, A. (2017). Heterogeneity of astrocyte and NG2 cell insertion at the node of ranvier. J Comp Neurol. *525*, 535-552.

Shi, S.-H., Hayashi, Y., Petralia, R.S., Zaman, S.H., Wenthold, R.J., Svoboda, K., and Malinow, R. (1999). Rapid Spine Delivery and Redestribution of AMPA Receptors After Synaptic NMDA Receptor Activation. Science *284*, 1811–1816.

Shine, H.D., Readhead, C., Popko, B., Hood, L., and Sidman, R.L. (1990). Myelin basic protein and myelinogenesis: morphometric analysis of normal, mutant and transgenic central nervous system. Prog Clin Biol Res *336*, 81–92.

Shouval, H.Z., Wang, S.S.H., and Wittenberg, G.M. (2010). Spike timing dependent plasticity: A consequence of more fundamental learning rules. Front. Comput. Neurosci. *4*, 1–13.

Sibille, J., Pannasch, U., and Rouach, N. (2014). Astroglial potassium clearance contributes to short-term plasticity of synaptically evoked currents at the tripartite synapse. J. Physiol. *592*, 87–102.

Silva, A.J., Stevens, C.F., Tonegawa, S., and Wang, Y. (1992a). Deficient hippocampal long-term potentiation in α-calcium-calmodulin kinase II mutant mice. Science *257*, 201–206.

Silva, A.J., Paylor, R., Wehner, J.M., and Tonegawa, S. (1992b). Impaired spatial learning in α-calcium-calmodulin kinase II mutant mice. Science *257*, 206–211.

Silver, R.A., Momiyama, A., and Cull-Candy, S.G. (1998). Locus of frequency-dependent depression identified with multiple-probability fluctuation analysis at rat climbing fibre - Purkinje cell synapses. J. Physiol. *510*, 881–902.

Simon, C., Götz, M., and Dimou, L. (2011). Progenitors in the adult cerebral cortex: Cell cycle properties and regulation by physiological stimuli and injury. Glia *59*, 869–881.

Sokolov, M. V., Rossokhin, A. V., Behnisch, T., Reymann, K.G., and Voronin, L.L. (1998). Interaction between paired-pulse facilitation and long-term potentiation of minimal excitatory postsynaptic potentials in rat hippocampal slices: A patch-clamp study. Neuroscience *85*, 1–13.

Sommer, B., Köhler, M., Sprengel, R., and Seeburg, P.H. (1991). RNA editing in brain controls a determinant of ion flow in glutamate-gated channels. Cell *67*, 11–19.

Song, F., Hong, X., Cao, J., Ma, G., Han, Y., Cepeda, C., Kang, Z., Xu, T., Duan, S., Wan, J., et al. (2018). Kir4.1 channels in NG2-glia play a role in development, potassium signaling, and ischemia-related myelin loss. Commun. Biol. *1*, 1–9.

Sontheimer, H., Black, J.A., and Waxman, S.G. (1996). Voltage-gated Na+ channels in gila: Properties and possible functions. Trends Neurosci. *19*, 325–331.

Speed, H.E., and Dobrunz, L.E. (2009). Developmental changes in short-term facilitation are opposite at temporoammonic synapses compared to schaffer collateral synapses onto CA1 pyramidal cells. Hippocampus *19*, 187–204.

Spitzer, S.O., Sitnikov, S., Kamen, Y., Evans, K.A., Kronenberg-Versteeg, D., Dietmann, S., de Faria, O., Agathou, S., and Káradóttir, R.T. (2019). Oligodendrocyte Progenitor Cells Become Regionally Diverse and Heterogeneous with Age. Neuron *101*, 459-471.e5.

Squire, L.R. (2004). Memory systems of the brain: A brief history and current perspective. Neurobiol. Learn. Mem. *82*, 171–177.

Squire, L., and Zola-Morgan, S.M. (1991). The medial temporal lobe memory system. Science *253*, 1380–1386.

Squire, L.R., and Dede, A.J.O. (2015). Conscious and unconscious memory systems. Cold Spring Harb. Perspect. Med. *5*, a021667.

Srinivas, S., Watanabe, T., Lin, C.S., William, C.M., Tanabe, Y., Jessell, T.M., and Costantini, F. (2001). Cre reporter strains produced by targeted insertion of EYFP and ECFP into the ROSA26 locus. BMC Dev. Biol. *1*, 1–8.

Stallcup, W.B. (1981). The NG2 antigen, a putative lineage marker: Immunofluorescent localization in primary cultures of rat brain. Dev. Biol. *83*, 154–165.

Steinhäuser, C., Kressin, K., Kuprijanova, E., Weber, M., and Seifert, G. (1994). Properties of voltage-activated Na+ and K+ currents in mouse hippocampal glial cells in situ and after acute isolation from tissue slices. Pflügers Arch. Eur. J. Physiol. *428*, 610–620.

Sternberg, N., and Hamilton, D. (1981). Bacteriophage Pl Site-specific Recombination. J. Mol. Biol. *150*, 467–486.

Sun, W., and Dietrich, D. (2013). Synaptic integration by NG2 cells. Front. Cell. Neurosci. *7*, 1–13.

Sun, W., Matthews, E.A., Nicolas, V., Schoch, S., and Dietrich, D. (2016). NG2 glial cells integrate synaptic input in global and dendritic calcium signals. Elife *5*, e16262.

Swanson, G.T., Kamboj, S.K., and Cull-Candy, S.G. (1997). Single-channel properties of recombinant AMPA receptors depend on RNA editing, splice variation, and subunit composition. J. Neurosci. *17*, 58–69.

Takano, T., Tian, G.F., Peng, W., Lou, N., Libionka, W., Han, X., and Nedergaard, M. (2006). Astrocyte-mediated control of cerebral blood flow. Nat. Neurosci. *9*, 260–267.

Takayama, F., Hayashi, Y., Wu, Z., Liu, Y., and Nakanishi, H. (2016). Diurnal dynamic behavior of microglia in response to infected bacteria through the UDP-P2Y 6 receptor system. Sci. Rep. *6*, 1–10.

Tanaka, T., Saito, H., and Matsuki, N. (1997). Inhibition of GABA(A) synaptic responses by brain-derived neurotrophic factor (BDNF) in rat hippocampus. J. Neurosci. *17*, 2959–2966.

Tanaka, Y., Tozuka, Y., Takata, T., Shimazu, N., Matsumura, N., Ohta, A., and Hisatsune, T. (2009). Excitatory GABAergic activation of cortical dividing glial cells. Cereb. Cortex *19*, 2181–2195.

Tani, H., Dulla, C.G., Farzampour, Z., Taylor-Weiner, A., Huguenard, J.R., and Reimer, R.J. (2014). A local glutamate-glutamine cycle sustains synaptic excitatory transmitter release. Neuron *81*, 888–900.

Tasaki, I. (1939). The Electro-Saltatory Transmission of the Nerve Impulse and the Effect of Narcosis Upon the Nerve Fiber. Am. J. Physiol. Content *127*, 211–227.

Terlau, H., and Seifert, W. (1990). Fibroblast Growth Factor Enhances Long-term Potentiation in the Hippocampal Slice. Eur. J. Neurosci. *2*, 973–977.

Thach, W.T. (2017). Somatosensory receptive fields of single units in cat cerebellar cortex. J. Neurophysiol. *30*, 675–696.

Timmler, S., and Simons, M. (2019). Grey matter myelination. Glia *67*, 2063–2070.

Tomassy, G.S. (2014). Distinct Profiles of Myelin Distribution. Science *344*, 319–324.

Tomita, S., Chen, L., Kawasaki, Y., Petralia, R.S., Wenthold, R.J., Nicoll, R.A., and Bredt, D.S. (2003). Functional studies and distribution define a family of transmembrane AMPA receptor regulatory proteins. J. Cell Biol. *161*, 805–816.

Tong, X., Ao, Y., Faas, G.C., Nwaobi, S.E., Xu, J., Haustein, M.D., Anderson, M.A., Mody, I., Olsen, M.L., Sofroniew, M. V., et al. (2014). Astrocyte Kir4.1 ion channel deficits contribute to neuronal dysfunction in Huntington's disease model mice. Nat. Neurosci. *17*, 694–703.

Trapp, B.D., Moench, T., Pulley, M., Barbosa, E., Tennekoon, G., and Griffin, J. (1987). Spatial segregation of mRNA encoding myelin-specific proteins. Proc. Natl. Acad. Sci. U. S. A. *84*, 7773–7777.

Traynelis, S.F., Wollmuth, L.P., McBain, C.J., Menniti, F.S., Vance, K.M., Ogden, K.K., Hansen, K.B., Yuan, H., Myers, S.J., and Dingledine, R. (2010). Glutamate receptor ion channels: Structure, regulation, and function. Pharmacol. Rev. *62*, 405–496.

Tsien, J.Z., Chen, D.F., Gerber, D., Tom, C., Mercer, E.H., Anderson, D.J., Mayford, M., Kandel, E.R., and Tonegawa, S. (1996). Subregion- and cell type-restricted gene knockout in mouse brain. Cell *87*, 1317–1326.

Vautrin, J., and Barker, J.L. (2003). Presynaptic quantal plasticity: Katz's original hypothesis revisited. Synapse *47*, 184–199.

Velez-Fort, M., Maldonado, P.P., Butt, A.M., Audinat, E., and Angulo, M.C. (2010). Postnatal switch from synaptic to extrasynaptic transmission between interneurons and NG2 cells. J Neurosci. *30*, 6921–6929.

Verdoorn, T.A., Burnashev, N., Monyer, H., Seeburg, P.H., and Sakmann, B. (1991). Structural determinants of ion flow through recombinant glutamate receptor channels. Science *252*, 1715–1718.

Viganò, F., and Dimou, L. (2016). The heterogeneous nature of NG2-glia. Brain Res. *1638*, 129–137.

Virchow R (1856) Die Cellularpathologie in ihrer Begründung auf physiologische and pathologische Gewebelehre. Zwanzig Vorlesungen gehalten während der Monate Februar, März und April 1858 im pathologischen Institut zu Berlin. Berlin: August. Hirschwald, p. 440.

Volianskis, A., Collingridge, G.L., and Jensen, M.S. (2013). The roles of STP and LTP in synaptic encoding. PeerJ *1*, e3, 1-13.

Volterra, A., and Meldolesi, J. (2005). Astrocytes, from brain glue to communication elements: The revolution continues. Nat. Rev. Neurosci. *6*, 626–640.

De Vries, G.J., and Panzica, G.C. (2006). Sexual differentiation of central vasopressin and vasotocin systems in vertebrates: Different mechanisms, similar endpoints. Neuroscience *138*, 947–955.

Wadiche, J.I., and Jahr, C.E. (2001). Multivesicular release at climbing fiber-Purkinje cell synapses. Neuron *32*, 301–313.

Wake, H., Ortiz, F.C., Woo, D.H., Lee, P.R., Angulo, M.C., and Fields, R.D. (2015). Nonsynaptic junctions on myelinating glia promote preferential myelination of electrically active axons. Nat. Commun. *6*, 7844, 1-9.

Wallraff, A., Odermatt, B., Willecke, K., and Steinhäuser, C. (2004). Distinct types of astroglial cells in the hippocampus differ in gap junction coupling. Glia *48*, 36–43.

Wallraff, A., Köhling, R., Heinemann, U., Theis, M., Willecke, K., and Steinhäuser, C. (2006). The impact of astrocytic gap junctional coupling on potassium buffering in the hippocampus. J. Neurosci. *26*, 5438–5447.

Wang, W.Y., Tan, M.S., Yu, J.T., and Tan, L. (2015). Role of pro-inflammatory cytokines released from microglia in Alzheimer's disease. Ann. Transl. Med. *3*, 136.

Waxman, S.G. (1980). Determinants of conduction velocity in myelinated nerve fibers. Muscle Nerve *3*, 141–150.

Waxman, S.G., and Sims, T.J. (1984). Specificity in central myelination: evidence for local regulation of myelin thickness. Brain Res. *292*, 179–185.

West, A.E., Chen, W.G., Dalva, M.B., Dolmetsch, R.E., Kornhauser, J.M., Shaywitz, A.J., Takasu, M.A., Tao, X., and Greenberg, M.E. (2001). Calcium regulation of neuronal gene expression. Proc. Natl. Acad. Sci. U. S. A. *98*, 11024–11031.

White, R., Gonsior, C., Krämer-Albers, E.M., Stöhr, N., Hüttelmaier, S., and Trotter, J. (2008). Activation of oligodendroglial Fyn kinase enhances translation of mRNAs transported in hnRNP A2-dependent RNA granules. J. Cell Biol. *181*, 579–586.

Whitlock, J.R. (2006). Learning Induces Long-Term Potentiation in the Hippocampus. Science *313*, 1093–1097.

de Wied, D., Diamant, M., and Fodor, M. (1993). Central nervous system effects of the neurohypophyseal hormones and related peptides. Front. Neuroendocrinol. *14*, 251–302.

Wigley, R., and Butt, A.M. (2009). Integration of NG2-glia (synantocytes) into the neuroglial network. Neuron Glia Biol. *5*, 21–28.

Williams, K.A., Deber, C.M., and Klrschner, O.A. (1993). The structure and function of central nervous system myelin. Crit. Rev. Clin. Lab. Sci. *30*, 29–64.

Wilson, S.S., Baetge, E.E., and Stallcup, W.B. (1981). Antisera specific for cell lines with mixed neuronal and glial properties. Dev. Biol. *83*, 146–153.

Wright, A., and Vissel, B. (2012). The essential role of AMPA receptor GluA2 subunit RNA editing in the normal and diseased brain. Front. Mol. Neurosci. *5*, 34

Xiao, L., Ohayon, D., McKenzie, I.A., Sinclair-Wilson, A., Wright, J.L., Fudge, A.D., Emery, B., Li, H., and Richardson, W.D. (2016). Rapid production of new oligodendrocytes is required in the earliest stages of motor-skill learning. Nat. Neurosci. *19*, 1210–1217.

Yamazaki, M., Fukaya, M., Hashimoto, K., Yamasaki, M., Tsujita, M., Itakura, M., Abe, M., Natsume, R., Takahashi, M., Kano, M., et al. (2010). TARPs γ-2 and γ-7 are essential for AMPA receptor expression in the cerebellum. Eur. J. Neurosci. *31*, 2204–2220.

Ye, P., Bagnell, R., and D'Ercole, A.J. (2003). Mouse NG2+ oligodendrocyte precursors express mRNA for proteolipid protein but not its DM-20 variant: a study of laser microdissection-captured NG2+ cells. J. Neurosci. *23*, 4401–4405.

Young, C.C., Stegen, M., Bernard, R., Müller, M., Bischofberger, J., Veh, R.W., Haas, C.A., and Wolfart, J. (2009). Upregulation of inward rectifier K+ (Kir2) channels in dentate gyrus granule cells in temporal lobe epilepsy. J. Physiol. *587*, 4213–4233.

Young, K.M., Psachoulia, K., Tripathi, R.B., Dunn, S.J., Cossell, L., Attwell, D., Tohyama, K., and Richardson, W.D. (2013). Oligodendrocyte dynamics in the healthy adult CNS: Evidence for myelin remodeling. Neuron *77*, 873–885.

Zechel, S., Werner, S., Unsicker, K., and Von Bohlen Und Halbach, O. (2010). Expression and functions of fibroblast growth factor 2 (FGF-2) in hippocampal formation. Neuroscientist *16*, 357–373.

Zhang, Y., Chen, K., Sloan, S.A., Bennett, M.L., Scholze, A.R., O'Keeffe, S., Phatnani, H.P., Guarnieri, P., Caneda, C., Ruderisch, N., et al. (2014). An RNA-Sequencing Transcriptome and Splicing Database of Glia, Neurons, and Vascular Cells of the Cerebral Cortex. J. Neurosci. *34*, 11929–11947. see also Database on: https://web.stanford.edu/group/barres_lab/brain_rnaseq.html

Zheng, J., Sun, X., Ma, C., Li, B.M., and Luo, F. (2019). Voluntary wheel running promotes myelination in the motor cortex through Wnt signaling in mice. Mol. Brain *12*, 1–10.

Zhou, M., Xu, G., Xie, M., Zhang, X., Schools, G.P., Ma, L., Kimelberg, H.K., and Chen, H. (2009). TWIK-1 and TREK-1 are potassium channels contributing significantly to astrocyte passive conductance in rat hippocampal slices. J. Neurosci. *29*, 8551–8564.

Zucker, R. (1989). Short-Term Synaptic Plasticity. Annu. Rev. Neurosci. *12*, 13–31.

Zucker, R.S., and Regehr, W.G. (2002). Short-Term Synaptic Plasticity. Annu. Rev. Physiol. *64*, 355–405.

Selected conference abstracts

Dysfunction of grey matter NG2 glial cells affects neuronal plasticity and behaviour. (***Talk***)
Timmermann A, Boehlen A, Skubal M Jabs, R, Bilkei-Gorzo A, Zimmer A, Kirchhoff F, Seifert G, Steinhäuser C.
Meeting of the DFG priority programme "Functional specialisations of neuroglia as critical determinants of brain activity (SPP 1757), Düsseldorf, Germany (2019)

NG2 glia-specific gene knockout as a tool to understand the impact of neuron-glia synaptic signalling. (***Poster***)
Timmermann A, Boehlen A, Skubal M Jabs, R, Bilkei-Gorzo A, Zimmer A, Kirchhoff F, Seifert G, Steinhäuser C.
13th Meeting of the German Neuroscience Society, Göttingen, Germany (2019)

NG2 glia-specific gene knockout as a tool to understand the impact of neuron-glia synaptic signalling. (***Poster & Lightning talk***)
Timmermann A, Boehlen A, Skubal M, Jabs R, Bilkei-Gorzo A, Zimmer A, Kirchhoff F. Seifert G, Steinhäuser, C.
4th Bonn Brain^3 Meeting, Bonn, Germany (2018)

NG2 glia-specific gene knockout as a tool to understand the impact of neuron-glia synaptic signalling. (***Poster***)
Timmermann A, Boehlen A, Skubal M, Jabs R, Kirchhoff F. Seifert G, Steinhäuser C.
XIII European Meeting on Glial Cells in Health and Disease, Edinburgh, United Kingdom (2017)

NG2 glia-specific gene knockout as a tool to understand the impact of neuron-glia synaptic signalling. (***Poster***)
Timmermann A, Skubal A, Kirchhoff F, Seifert G, Steinhäuser C.
10th FENS (Forum of Neuroscience), Copenhagen, Denmark (2016)

NG2 cell specific gene knockout as a tool to understand the impact of neuron-glia synaptic signalling. (***Talk***)
Timmermann A, Kirchhoff F, Seifert G, Steinhäuser C.
BIGS Neuroscience Student Symposium, Nideggen, Germany (2015)

Temporal and spatial control of an NG2 cell specific gene knockout
Timmermann A, Schmitz C, Kirchhoff F, Seifert G, Steinhäuser C. (***Poster***)
THEME Graduate School Student Symposium, Nideggen, Germany (2014)

Publications

Claus L, Philippot C, Griemsmann S, **Timmermann A**, Jabs R, Henneberger C, Kettenmann H, Steinhäuser C (2018) Barreloid Borders and Neuronal Activity Shape Panglial Gap Junction-Coupled Networks in the Mouse Thalamus. Cereb Cortex 28:213-222.

Recabal A, Elizondo-Vega R, Philippot C, Salgado M, López S, Palma A, Tarifeño-Saldivia E, **Timmermann A**, Seifert G, Caprile T, Steinhäuser C, García-Robles MA (2018) Connexin-43 Gap Junctions Are Responsible for the Hypothalamic Tanycyte-Coupled Network. Front Cell Neurosci 12:406.

Wefers AK, Haberlandt C, Tekin NB, Fedorov DA, **Timmermann A**, van der Want JJL, Chaudhry FA, Steinhäuser C, Schilling K, Jabs R. (2017) Synaptic input as a directional cue for migrating interneuron precursors. Development. 15;144(22):4125-4136.

Awards and Honors

IPID4all grant	DAAD, University of Bonn; Conference Participation grant for XIII European Meeting on Glial Cells in Health and Disease, Edinburgh, United Kingdom (2017)
Poster Award	Meeting of the International Graduate School THEME (2014)